THE UNIVERSITY
of EDINBURGH

Protein Nanopores as a Platform for Transmembrane Nanodevices

Dominic Francis Cairns-Gibson

THE UNIVERSITY *of* EDINBURGH

Thesis presented for the degree of

Doctor of Philosophy

The University of Edinburgh

2022

Declaration

I declare that this thesis has been composed entirely by myself.

I confirm that a substantial volume of the research presented herein has been performed by myself, and any contributions from other researchers have been outlined at the beginning of each chapter and indicated in relevant figure captions.

I declare that this work has not been submitted for any other degree or professional qualification.

Signature: Date: 14th September 2022

Dominic Cairns-Gibson

Table of Contents

Acknowledgements

I would like to thank Prof Scott Cockroft, as I would not be writing this thesis without his unique and insightful mentorship. Throughout a global pandemic, he has offered endless support and it has been a privilege to be a member of his group. Even if he does have an odd liking for Fray Bentos pies.

A great deal of thanks is owed to Dr Stefan Borsley, who welcomed me to the group as a naive master student and taught me all there is to know about nanopores. Dr Marius Haugland and Dr Rebecca Burns were both there in those early days to welcome me to the group as a friend. It has been a pleasure to see Marius begin his academic career, and I wish him all the best with his nanopore endeavours. Becky has been a teacher, friend and mentor all rolled into one. I had the absolute job of working with one of my closest friends for so many years and she has been a shining light of the Cockroft group.

In no particular order, I would like to thank the rest of the Cockroft group. I have been so fortunate to be in the company of such an incredible group of people. Dr Andrew West has been a constant source of sass, entertainment, and cocktail focused conversation. Dr Alex Elmi imparted invaluable computational and synthetic advice, along with terrible fashion advice. Ivan Smolair is perhaps the most joyful and mischievous person I have ever had the pleasure to meet. Louis Gravillier will always be our youngest group member, and I am waiting for the day when British food no longer appals you. Tim Spankie is a kind hearted computational wiz, and I cannot wait to see all the amazing things you compute – even if I understand absolutely none of it. Dan Edwards, thank you so much for your friendship and support in the nanopore lab. Few other people will understand the trials and tribulations of α-HL and I am so glad that I got to share that experience with you. Dr Krzysztof Bak has helped enormously in the short time we had together, and now the nanopore legacy is passed to him.

Throughout my PhD I have enjoyed becoming an involved member of the School of Chemistry, and I have met so many fantastic people. Thank you to Dr Jenny Bos and Dr Anna-Maria Maciejuk for introducing me to the world of public outreach and shaping my future career. Thank you to Dr Jean O'Donoghue for your expert training in Equality, Diversity and Inclusion, and for your support throughout my degree. The technical staff have been a phenomenal team throughout my outreach and teaching endeavours. Thank you Kirsty, Jen and Craig for putting up with all of my nonsense and always being there to help.

Last but not least, I would like to thank my family. My dad, Frank, has always supported me in whatever I done and has worked so hard to ensure I could lead the best life possible. My brother, David, has done his very best to keep me grounded and always asks "how is uni going?". My Aunt Liz and Uncle Frank have been a cornerstone in my life and I do not know where I would be without them. My partner, Dominik, has been there for me throughout it all. You have supported me throughout the PhD and I am so privileged to have the life we have together.

Finally, I thank the University of Edinburgh and the various funding bodies that have made my PhD possible.

Abstract

Nanopore sensing has seen vast development over the past four decades. The technique originally looked to use electrophysiological methods to study native protein channels. However, it is now possible to exploit these proteins for sensing applications. Herein, we explore methods for covalent and non-covalent modification of a biological nanopore to achieve new functionality.

Chapter 1 summarises the history of nanopore technology; from its inception as a method for studying native channels, to its deployment in nanopore sensing. To achieve effective sensing, native proteins have undergone a broad range of chemical modification to achieve enhanced functionality. This chapter explores the amalgamation of biological and solid-state nanopores.

Chapter 2 seeks to the monitor the binding and catalytic turnover of substrates within a single cucurbituril molecule captured within a protein nanopore. Previous work has shown that cucurbiturils and cyclodextrins can transiently interact with an α-hemolysin channel. Capture of a single cucurbituril within a protein nanopore was achieved, and the dwell time of the binding events was optimised. Following this, it was demonstrated that observations of the catalysed Diels-Alder could be made at the single-molecule level. However, further optimisation of the resolution would be required to elucidate mechanistic information.

Chapter 3 presents methods for *in situ* chemical functionalisation of a biological nanopore. Here, the focus is upon the chemical modification of a wild-type protein thereby to circumventing the need for mutagenesis. Three target residues are discussed: lysine, methionine and tyrosine. Successful modification was achieved at both the lysine and methionine sites of α-hemolysin. While some provisional success was recorded with tyrosine, the modifications were not reproducible.

Chapter 4 introduces preliminary work towards the development of transmembrane molecular machines. This utilises the lysine modification discussed in Chapter 2 to covalently attach established synthetic molecular machines to the channel. Molecular switches, motors and pumps were all explored. Some success was achieved attaching the molecular machines to a protein channel. However, issues with pore stability limited the progress and true machine-like behaviour was not observed.

Lay summary

Life is a series of compartmentalised systems. Each of these is separated by a boundary: the macroscopically tangible barrier of skin to the microscopic cell membrane and beyond. Without these membranes, we would be little more than the primordial ooze of 4 billion years ago. However, each of these systems does not exist in isolation. Transmembrane channels facilitate the transport of substrate between the intracellular and extracellular environment. These architectures are sophisticated in their design, with selective permeability and selectivity.

To achieve life as we know it, molecules and ions must be moved across these membrane barriers and away from equilibrium. Nature has developed a sophisticated array of systems that are capable of achieving this. However, we as chemists are only beginning to scratch the surface of what is possible. Utilising transmembrane protein channels, it is hoped that novel methods of traversing the membrane may be achieved.

Chapter 1 discusses the existing literature on methods to chemical and biologically functionalise transmembrane nanopores. **Chapter 2** looks at the application of a non-covalent host trapped within the nanopore to achieve new functionality. Successful utilisation of nanopore technology would open doors to new methods to observe reaction mechanisms at the single molecule level. **Chapter 3** demonstrates new methods to chemically modify protein nanopores. This provides a means of generating novel pores with bespoke functionalities. Finally, **Chapter 4** explores the application of such modification techniques to work towards transmembrane molecular machines. Molecular machines, such as ATP-synthase, are vital for life and the creation of artificial machines from a nanopore template would provide a powerful method for emulating biology. It is hoped that this may culminate in a transmembrane machine that is capable of working away from equilibrium.

Abbreviations

α-HL	α-hemolysin
AAC	1,3 dipolar azide-alkyne cycloadditions
ATP	Adenosine triphosphate
aq.	Aqueous
BODIPY	Boron dipyrromethene
CB[5]	Curcurbit[5]uril
CB[6]	Curcurbit[6]uril
CB[7]	Curcurbit[7]uril
CB[n]	Curcurbit[n]uril
CD	Cyclodextrin
ClyA	Cytolysin A
CuAAC	Cu(I)-catalysed azide-alkyne [3+2] cycloaddition
DB24C8	Dibenzo-24-crown-8
DBU	1,8-Diazabicyclo[5.4.0]undec-7-ene
DCM	Dichloromethane
DMAP	4-Dimethylaminopyridine
DMSO	Dimethyl sulfoxide
DNA	Deoxyribose nucleic acid
dsDNA	Double stranded-DNA
DTT	Dithiothreitol
EDC	1-ethyl-3-(3-dimethylaminopropyl)carbodiimide
EOF	Electro osmotic Force
h	Hours

HPTS	8-hydroxypyrene-1,3,6-trisulfonic acid
FraC	fragaceatoxin C
KPi	Potassium phosphate dibasic
Lys	Lysine
Met	Methionine
mRNA	Messenger ribose nucleic acid
MspA	*Mycobacterium smegmatis* porin A
mV	Millivolt
pA	Picoamp
PEG	Polyethyleneglycol
PTAD	4-Phenyl-1,2,4-triazole-3,5-dione
PTM	Post-translational modification
RNA	Ribose nucleic acid
RT	Room temperature
s	Seconds
SNR	Signal-to-Noise ratio
ssDNA	Singlestranded deoxyribose nucleic acid
SLS	Sodium lauryl sulfate
SPAAC	Strain-promoted azide-alkyne cycloaddition
SuFEx	Sulphur (VI) fluoride exchange
Sulfo-NHS	N-Hydroxysulfosuccinimide
SC_4	Sulfonato-calix[4]arene
THF	Tetrahydrofuran
TESPMA	Triethoxysilylpropylmaleamic acid

TRIS	2-amino-2-hydroxymethylpropane-1,3-diol
Tyr	Tyrosine
UV	Ultraviolet
V^{2+}-Az	4, 4′-dipyridinium-azobenzene
WT	Wild type

Publications

Functionalised nanopores: chemical and biological modifications.

D. F. Cairns-Gibson, and S. L. Cockroft*. ***Chem. Sci.***, **2022**, ***13***, 1869-1882.

Switchable foldamer ion channels with antibacterial activity.

A. D. Peters, S. Borsley, F. della Sala, D. F. Cairns-Gibson, M. Leonidou, J. Clayden, G. F. S. Whitehead, I. J. Vitórica-Yrezábal, E. Takano, J. Burthem, S. L. Cockroft, and S. J. Webb*. ***Chem. Sci.***, **2020**, ***11***, 7023-7030.

Synthetically diversified protein nanopores: resolving click reaction mechanisms.

M. M. Haugland, S. Borsley, D. F. Cairns-Gibson, A. Elmi, and S. L. Cockroft*. *ACS Nano,* **2019,** *13* (4), 4101-4110.

Chapter 1

Converging biological and chemical functionalisation in nanopore technologies

Abstract

Nanopore technology has established itself as a powerful tool for single-molecule studies. It is a relatively modern technique that originated in the electrophysiological experiments of Neher and Sakmann. By analysing changes in the ion current flow through a single transmembrane channel, a wealth of molecular information can be elucidated. Early studies primarily saw nanopore technology applied for sensing applications, but on-going developments have diversified the remit of the technique. Nanopores can be synthetic, solid-state, or biological in origin, but recent work has seen these boundaries blurred through the development of hybrid-functionalised pores. The modification of existing pores and the construction of novel synthetic pores has been an enticing goal for creating systems with tailored properties and functionality. Here, we explore the functionalisation of nanopores. Furthermore, we look at how these functionalised channels have far-reaching implications for the development of transmembrane molecular machines.

Excerpts of the chapter published as:
Functionalised nanopores: chemical and biological modifications. D. F. Cairns-Gibson, and S. L. Cockroft*. ***Chem. Sci*., 2022, *13*,** 1869-1882.

1.1 Introduction

Nanopore technology is an eminent single-molecule technique. However, it is not alone in its ability to probe the atomic domain. To date, X-ray crystallography has afforded researchers with the clearest image of the nanoscale, but advancements in microscopy have made the capabilities of the two techniques comparable.[1] Indeed, it is now possible to achieve Ångstrom-level resolution with electron microscopy.[2] While techniques such as atomic force microscopy or fluorescence labelling have been used for single-molecule studies, they often involve the fixing of molecules or the incorporation of probes that can interfere with the reactivity of the system.[3]

While the information generated by nanopore sensing is arguably more ambiguous than that of microscopy or crystallography, it holds a key advantage in that single-molecule interactions can be observed in real-time and in dynamic solution-phase systems. The technique has been broadly applied for sensing applications and single-molecule studies, and more recently used to probe real-time reaction mechanisms. Herein, we explore the emergence of the technique and how functionalisation of nanopores has furthered its remit.

1.2 Fundamentals of Nanopore Technology

Origins of Nanopore Technology

Nanopore technology relies on the Coulter principle, which states that passage of an analyte through a channel will reduce the measured current proportional to the dimensions of the analyte.[4] The Coulter counter, from which this principle is derived, was initially developed to analyse red blood cells (**Figure 1.1**). Over time, the resolution of the technique improved to the point that

studies can now be conducted at the single-molecule level. From this, the foundations of patch clamp electrophysiology were laid.

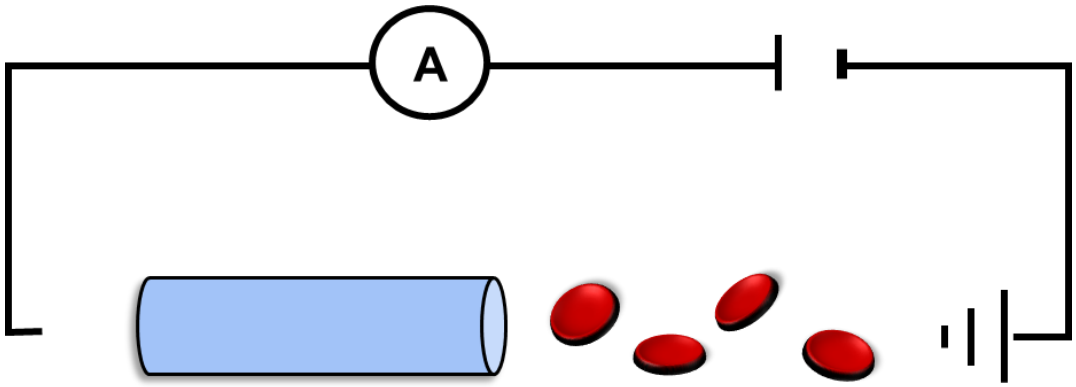

Figure 1.1: Cartoon representation of a Coulter Counter. Under an applied electric field, particles moving through a microchannel will cause an augmentation of the resistance of the fluid. This is observed through variations in the measured current.

During patch clamp electrophysiology, a micropipette containing a counter electrode and electrolyte solution is sealed against a small section of the cell membrane.[5] If this 'patch' of membrane contains a single ion channel, then the application of a voltage across the membrane results in a measurable flow of ions through the channel (**Figure 1.2**). The opening and closing of single ion channels in membrane patches could be monitored in real time as sub-picoamp changes to the current flow. In order to work with such small voltages and currents, a patch clamp amplifier was required.[6] This breakthrough, arguably the first ever single-molecule biophysics technique, led to Neher and Sakmann being awarded the 1991 Nobel Prize in Physiology or Medicine for their contributions to the understanding of ion channel function.[7]

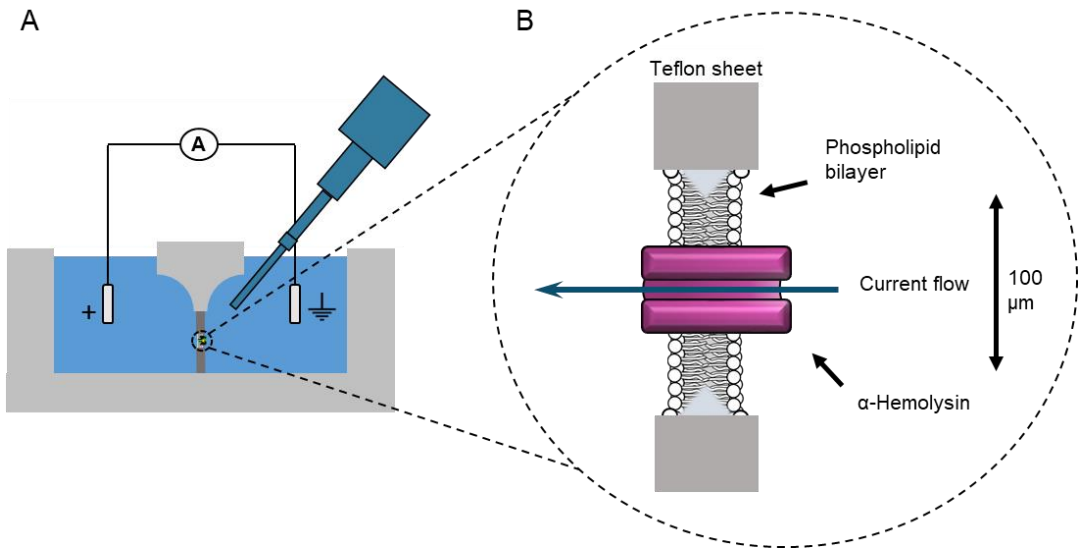

Figure 1.2: A) Schematic of a typical electrophysiological cell for nanopore experiments. Two buffered wells are separated by a Teflon sheet, and joined by a single aperture of approximately 100 µm. An artificial lipid bilayer is formed across this aperture. Using a micropipette, a single protein channel is inserted into the bilayer. Using a patch clamp, a potential is applied. B) Enhanced representation of the aperture (not drawn to scale). The single protein channel is inserted into the lipid bilayer and allows a current to pass between the two buffered wells.

In contrast to the original intention of single-channel electrophysiology to monitor the dynamics of channel opening and closing, nanopore sensing instead seeks to exploit biological transmembrane proteins with stable open channels. The central principle of nanopore sensing is that the entry of an analyte molecule into a nanopore reduces the ability of ions to flow through the channel. In an unobstructed channel, a consistent free-pore current (I_o) will be observed (**Figure 1.3A**). Under the same conditions, I_o will be of the same magnitude across channels and will scale with the applied potential. As blockages of the pore occur, a drop in current to a new level (I_b) will be observed that will be related to size and charge properties of the molecule causing the blockage (**Figure 1.3B**).[8-9] Generally, the magnitude of the blockage will be reported as the ratio I_b/I_o to account for slight variations across channels. Since patch clamp amplifiers can record ion currents with high sensitivity (<0.1 pA) on the >100 kHz timescale, nanopore sensing can reveal information about the dynamics of molecular interactions and reactions

occurring within the pore. By virtue of being a single-molecule technique, the ordering of events, short-lived intermediates, and the temporal distribution of events can be resolved, which would otherwise be obscured in bulk ensemble measurements.

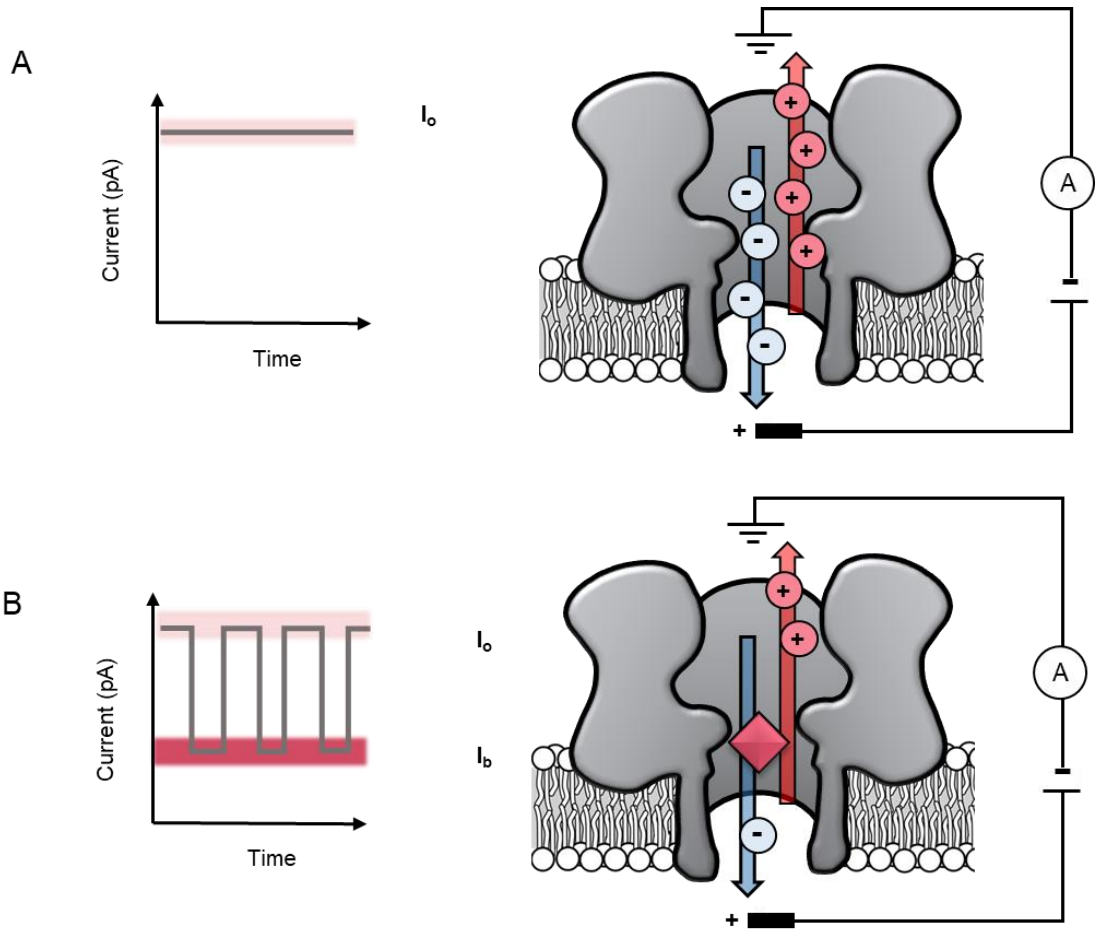

Figure 1.3: In a system with a membrane-bound biological pore, a consistent free pore current (I_o) will be observed when a constant potential is applied. The only variances will result from signal noise. As depicted, an applied positive potential will result in a positive current flow. A negative applied potential will result in a negative current. B) As an analyte enters the pore there is a reduction in current (I_b) that is related to the size and charge of the molecule. From this, information on reaction kinetics and mechanisms can be elucidated.

In a development of this method by Branton, Deamer, and Kasianowicz, a small potential (voltage-clamp) or current (current-clamp) was applied across a membrane bound transmembrane protein, α-hemolysin (α-HL), separating two buffered wells, which results in proportional output current or voltage

respectively.[9] While the term does appear sporadically in the literature prior to 1996, it was in their seminal work that the term ‘nanopore’ was coined in relation to a protein channel for single-molecule sensing.

Early work by the trio sought to apply nanopores for characterising individual polynucleotides.[9] It was determined that single channel measurements could be used to determine the length of polynucleotides. From this, it was speculated that nanopore technology could be used to determine other characteristics of DNA or RNA, and even read full sequences. However, much refinement of the technique was needed before this was possible. Through subsequent development, advances were made in sensing[10] and sequencing applications.[8] α-HL, a heptameric toxin protein (**Figure 1.4**), was selected as the channel for these early studies, and has remained a workhorse of the technique.[9]

Biological Nanopores

α-HL is a pore-forming protein that has been demonstrated extensively to insert into an artificial lipid bilayer for use in nanopore experiments (**Figure 1.4**).[9, 11-12] The protein is secreted naturally by *Staphylococcus aureus* bacteria to lyse cells, thus bringing about cell death.[13] α-HL exists as a monomer in solution but will self-assemble to form a heptameric, membrane-spanning protein.[14] In rare incidences, the protein will insert as a hexamer.[15] α-Hemolysin is stable at temperatures of up to 100 °C[16] and will tolerate a wide range of pH values (pH 3 - 11).[17]

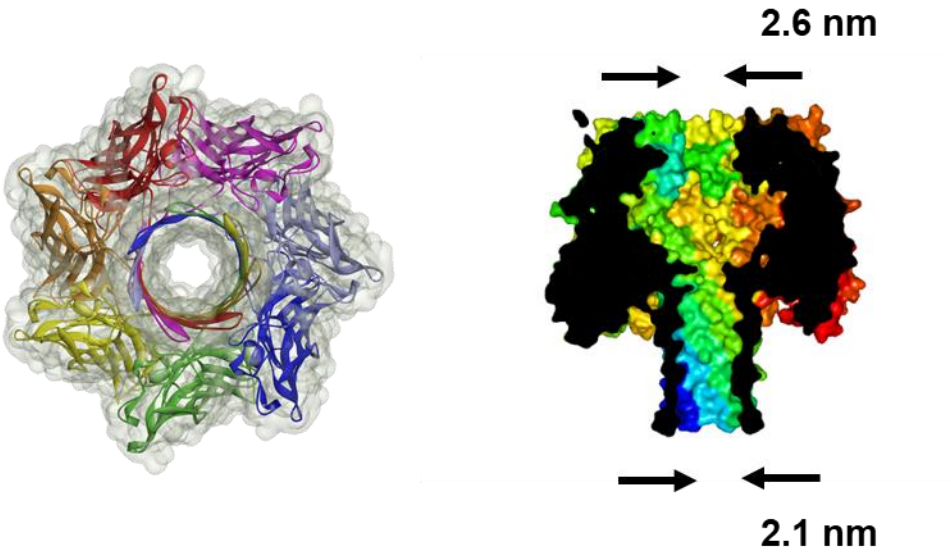

Figure 1.4: Crystal structure of α-HL with a top down (left) and side of cross-section (right) view. Each colour represents one of the seven sub-units of the heptameric structure.[12]

Biological nanopores are sourced from nature and numerous proteins have been repurposed for nanopore technologies (**Figure 1.5**).[10, 18] While these proteins can be used in their wild-type form, there has been growing interest in developing mutant or functionalised pores for a specific function.[19] Aerolysin has a similar β-barrel tertiary structure as the membrane-spanning region α-HL but offers a more consistent and narrower pore diameter.[20] *Mycobacterium smegmatis* porin A (MspA) has a more cone-shaped geometry that concentrates to a narrow constriction site (**Figure 1.5**).[10, 21]

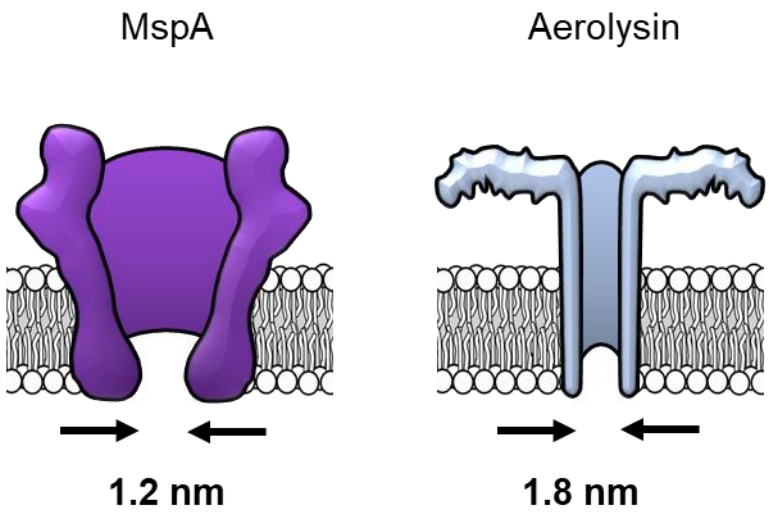

Figure 1.5: Representative structures of biological nanopores exploited in single-molecule investigations.[10, 21 20]

As previously mentioned, one of the primary pursuits of nanopore technology has been to achieve fast and affordable DNA sequencing. The sequencing of the human genome was a herculean, not to mention expensive task, but two decades later gene sequencing can be accessed *via* hand held devices such as Oxford Nanopore's MinIon for as little as $1000.[22] The Minion is comprised of an array of protein nanopores inserted in a stabilised membrane embedded in a solid-state framework.[23] While Branton and Deamer speculated from early on that nanopore technology could be applied for sequencing, the reality of achieving this has not been simple. The rate of translocation through the pore is incredibly rapid and has, until recently, been too fast to resolve single nucleobases.[3, 9]

Several intuitive methods to slow the translocation of single-stranded DNA (ssDNA) through nanopores have been explored, such as reducing the system temperature and increasing viscosity.[24-25] Such methods were effective in reducing the speed of DNA translocation by an order of magnitude; however, a greater reduction in speed would be desirable to achieve the resolution required to discern individual nucleotides. Moreover, there are limitations of

these techniques that must be considered. The temperature minimum will be dictated by the freezing point of the buffer, while the viscosity of the solution can only be varied to a certain degree until it starts to affect other factors, such as conductance and solubility. In addition, lower temperatures reduce the hydrophobic effect, which may negatively affect protein folding or membrane stability.[26] Indeed, greater success in enhancing the resolution of DNA has been observed by the use of nucleic acid manipulating enzymes,[27] and the addition of molecular adaptors to the nanopore channel *via* site-directed mutagenesis.[28]

Beyond Biological Channels

To this point, all discussion has been of biological nanopores, but other classes of nanopores have been developed. Broadly speaking, nanopores can be split into three categories: biological, solid-state, and synthetic. To date, biological and solid-state nanopores have been the most widely exploited, largely due to their availability and relative ease of fabrication. Synthetic pores, on the other hand, are vastly more challenging in their design but their development opens doors to entirely bespoke systems. The primary focus of this section will be on solid-state and biological nanopores. More detailed accounts of synthetic channels are given in other published works.[29-30]

The turn of the 21st century saw patch clamp amplifiers being used with so-called solid-state nanopores constructed from inorganic materials and nanotubes.[31-32] Solid-state nanopores are formed in materials such as silicon oxide or nitride *via* a top-down approach, where the pore is bored into the material with either a laser or electron beam.[31] The pore formed can be tuned to specific geometries and sizes with nanometer precision, typically with a diameter in the 1-20 nm range.[33,34] Since effective single-molecule sensing requires the diameter of the nanopore to be slightly larger than the analyte molecule, diameters on the lower end of this scale are often desired.[33] Solid-

state nanopores tend to be significantly more thermally and chemically stable than their biological counterparts.[35] However, due to the etching methods used in their production, solid-state nanopores cannot be reproduced with atomically precise dimensions and can be difficult to functionalise or modify.[36] This lack of atomic precision, combined with the use of relatively inert materials, often means that solid-state nanopores lack specific handles for synthetic modification.

In contrast, biological nanopores are less robust, but have atomically precise dimensions encoded by the protein sequences and present numerous handles for chemical and genetic modification. Not only the stability and size must be considered. Solid-state and biological channels can have drastically difference sources of signal noise and signal-to-noise ratios (SNR).[37] Research is now turning to the amalgamation of the biological and synthetic nanopores to gain access to the 'best of both worlds' (**Figure 1.6**).

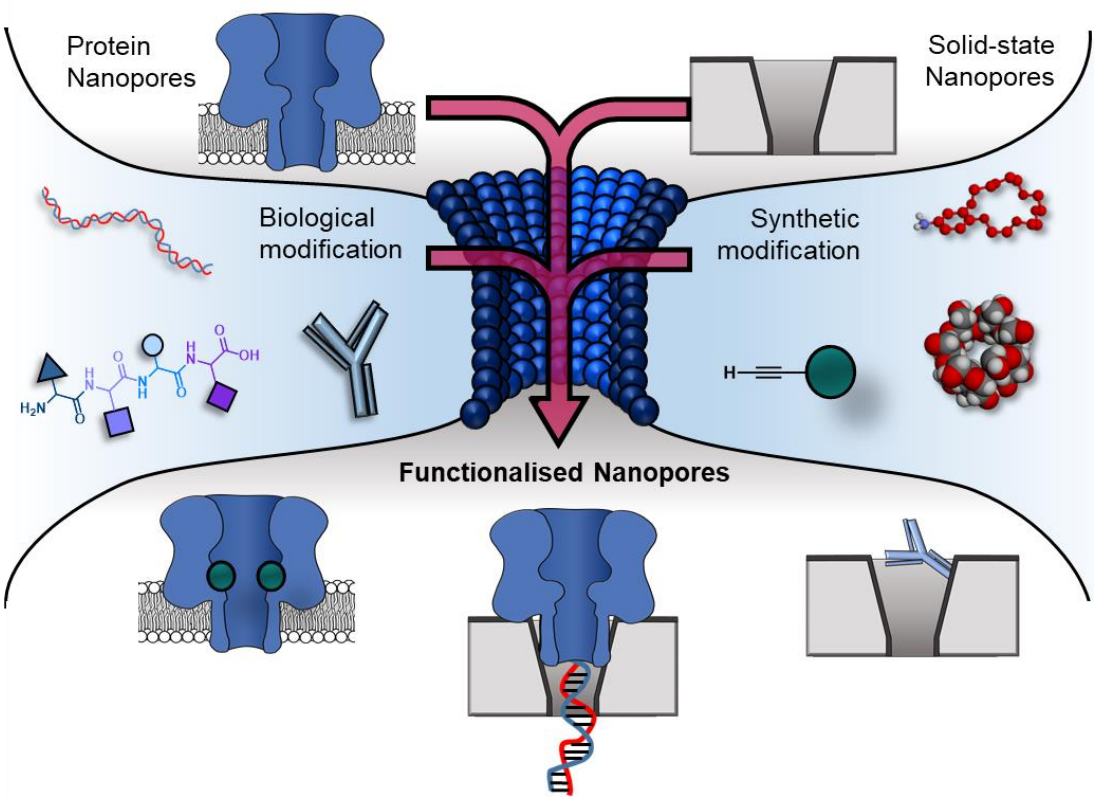

Figure 1.6: The incorporation of biological and synthetic modifications into biological and solid-state nanopores with enhanced functionality. Modification with biomolecules such as DNA, peptides and antibodies can endow otherwise inert solid-state nanopores with the ability to engage in specific (bio)molecular interactions. Meanwhile, biological pores can be modified with synthetic components such as crown ethers, cyclodextrins and reactive small molecules, enabling new modes of detection and the real-time observation of molecular interactions and chemical reactions at the single-molecule level. Similarly, biological and solid-state nanopores can themselves be combined to yield hybrid nanopores with increased robustness and stability.

In recent years, there has been an emergence of nanopore technologies that draw inspiration from solid-state and biological pores. As with many disciplines, nanopore technologies no longer exist in discrete categories and this coalescence of techniques gives rise to systems with more bespoke functionalities.

1.3 Functionalisation of Nanopores

Functionalisation of Solid-State Nanopores with Biomolecules

Solid-state nanopores are typically constructed from robust, but relatively inert matrices derived from silicon or other inorganic materials.[34] Unlike their biological counterparts, the absence of atomically precise dimensions and positioned functional groups render most solid-state nanopores incapable of engaging in specific molecular recognition processes. However, one of the major challenges in early nanopore studies using biological pores was the poor membrane stability. Challenges to pore stability can be overcome by utilising the reliable framework of solid-state pores. The incorporation of biomolecules with solid-state pores provides a means of mitigating the intrinsic limitations and challenges of both biological and solid-state nanopores.

One approach to introducing reactive handles into solid-state pores is to functionalise the surface with a more reactive material. For example, Rant and co-workers showed that solid-state silicon nitride nanopores could be coated with a thin gold film to enable functionalisation with a self-assembled thiol monolayer (blue in **Figure 1.7**).[38] The combination of the gold treatment and monolayer assembly reduced the diameter of the nanopore channel to 12-39 nm, thereby making the nanopore a suitable size for the detection of individual protein molecules. Alkane-thiols modified with nitrilotriacetic acid ligands (purple in **Figure 1.7**) were included during monolayer formation. In the presence of Ni^{2+}, the nitrilotriacetic groups could bind His_6-tagged proteins, which allowed stochastic sensing of protein association/dissociation by monitoring ion currents flowing through the nanopore. By increasing the number of nitrilotriacetic acid head groups in the synthetic linker to three, the authors found that they were able to bind His_6-tagged proteins for hour-long durations. This robust anchoring further enabled the detection of protein-protein interactions between the anchored protein (red in **Figure 1.7**) and

immunoglobulin G antibodies (orange in **Figure 1.7**). Hence, the authors demonstrated the construction of a selective single-molecule biosensor *via* the biochemical modification of a previously inert solid-state nanopore. Reliable and rapid biosensing systems such as this are invaluable tools, particularly in research and clinical settings. Future developments may see a wider range of proteins being detected, potentially for early detection of disease or high sensitivity analyte detection in the field.

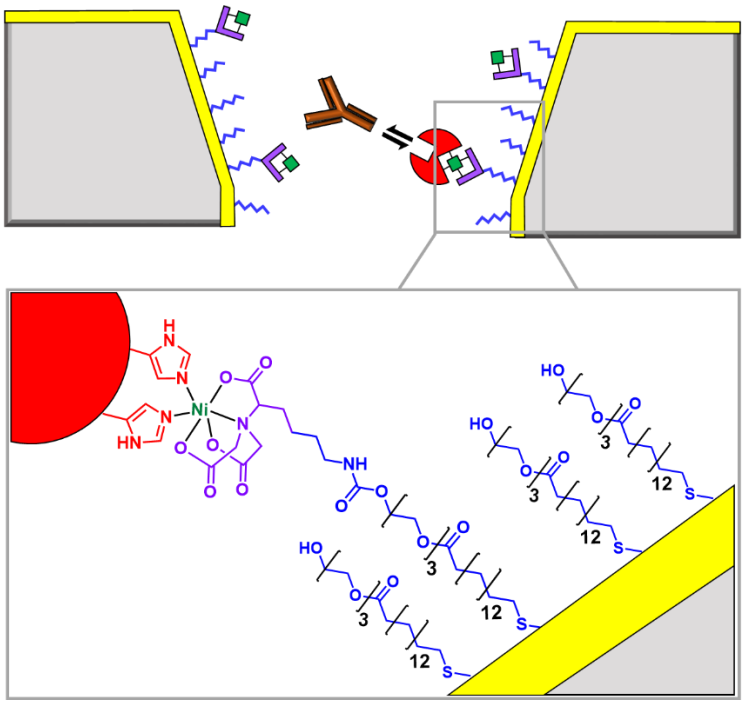

Figure 1.7: Cross section of a silicon nitride solid-state nanopore coated in a thin gold film. Synthetic nitrilotriacetic acid receptors (purple) were anchored to the gold surface within a self-assembled monolayer (blue). These receptors were then able to bind His_6-tagged protein molecules (red) *via* Ni^{2+} chelation. By increasing the number of nitrilotriacetic acid groups in the receptor, protein molecules could be bound for hour-long durations enabling the further detection of protein-protein interactions, such as immunoglobulin antibody (orange) recognition of the red protein.

Non-covalent modification can be employed as a useful strategy for modifying the surface properties of a solid-state nanopore, thereby instilling new functionality.[36] A demonstration of this approach was the addition of a lipid bilayer to a solid-state pore to enhance protein sensing capabilities. Mayer and co-workers demonstrated that lipid-coated solid-state nanopores can be used

to fingerprint the approximate shape and charge characteristics of individual protein molecules.[39] As a single protein molecule translocates the pore, it will rotate and perturb the ion flow, such that proteins with different sizes and shapes give rise to characteristic ion current 'fingerprints' (**Figure 1.8A**). The fluid lipid bilayer prevents non-specific adhesion of the protein, allowing the Brownian rotation of the protein to be better studied. To achieve sufficient time resolution of the translocation events, a range of protein tethers were embedded into the lipid bilayer (**Figure 1.8B**). The flexibility and length of the tether permitted free rotation of the protein in the pore, such that all orientations could be accessed. An elegant analysis of the magnitude and distribution of the ion current fingerprints enabled the shape and volume of several different proteins to be elucidated. Meanwhile, the net charge of the protein could be determined from the dwell times of the translocation events.

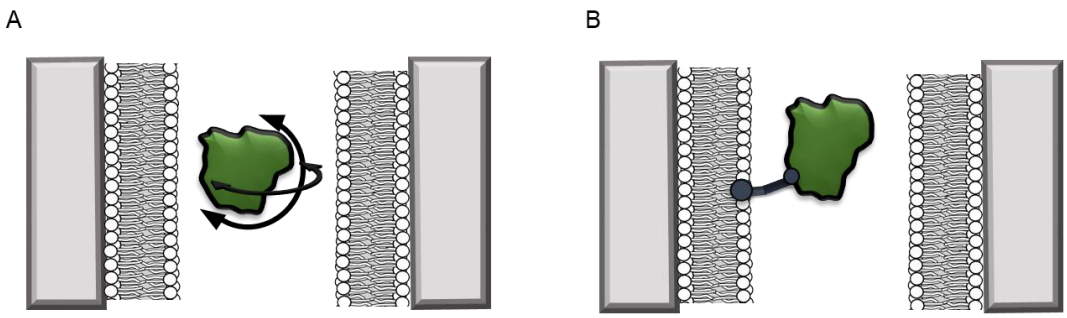

Figure 1.8: A) A silicon nitride nanopore functionalised with synthetic lipids (99.2 mol% 1-palmitoyl-2-oleoyl-*sn*-glycero-3-phosphocholine (POPC) and 0.8 mol% 1,2-dipalmitoyl-*sn*-glycero-3-phosphoethanolamine-*N*-(lissamine rhodamine B sulphonyl)) enabled the shape and size of different proteins to be determined from ion current fluctuations as they tumbled through the nanopore. B) The incorporation of tethers into the lipid bilayer capable of binding the target protein further slowed the rotational dynamics to enable the physical characteristics of the translocating protein to be revealed in even greater detail.[39-40]

In subsequent work, Mayer and co-workers demonstrated a tether-free method for the analysis of proteins as they translocated lipid-coated solid-state pores.[40] A more sophisticated experimental set-up brought about a 40% reduction in the current noise, which in turn enhanced the signal-to-noise ratio and alleviated the need to further slow the translocation of the protein with a tether.

Lipid-functionalised solid-state nanopores have the potential for a wide scope of applications beyond protein fingerprinting. Many conventional biophysical methods require labelling or modification to study proteins and few techniques allow the study of native wild-type proteins. Labelling can influence structure and activity, meaning that some caution is required when interpreting results obtained using labelled proteins. Hence, such ambiguity can be avoided since lipid-functionalised solid-state nanopores enable native proteins to be studied in biologically relevant buffers.

As solid-state nanopore technology has developed, the potential of biomimetic pores has been realised. Siwy and co-workers, fabricated a potassium ion selective solid-state nanopore using surface functionalisation.[41] The authors modified a silicon nitride-coated pore with triethoxysilylpropylmaleamic acid (TESPMA) as a reactive handle for further functionalisation (**Figure 1.9A**). The terminal carboxylic acid of TESPMA was activated with 1-ethyl-3-(3-dimethylaminopropyl)carbodiimide (EDC), allowing functionalisation of the pore with a crown ether *via* an amide linkage (**Figure 1.9A**). Functionalisation with only crown ether (**Figure 1.9B**) afforded the pore notable potassium ion selectivity. Potassium ion selectivity decreased exponentially with an increase in pore diameter and was non-existent for pores with diameters > 3 nm. When a pore with an appropriate diameter was used, transit of potassium ions was facilitated due to binding/unbinding of the crown-ether modification. Drawing inspiration from biological voltage-gated ion channels, the authors theorised that appending single-stranded DNA to the membrane surface might provide a means of further modulating ion selectivity (**Figure 1.9C**). They hypothesised that the high negative charge density on one side of the pore would promote the passage of positively charged ions but would have no effect on the selectivity. This was indeed shown to be the case, and significantly higher potassium ion transport was observed when the membrane was additionally modified with DNA.

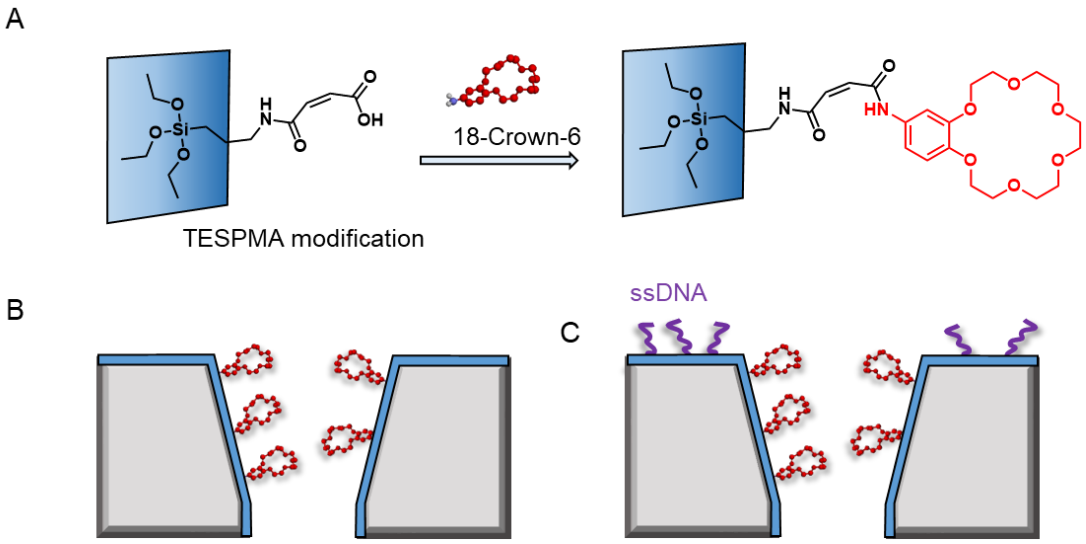

Figure 1.9: A) A solid-state silicon pore was coated with silicon nitride (blue). This allowed the surface to be functionalised with TESPMA, adding a reactive handle onto which further modifications could be attached. B) 18-Crown-6 (red) coupled to the pore *via* EDC coupling to the TESPMA. C) Additional single-stranded DNA (ssDNA, purple) modification on one side of a silicon nitride membrane further modulated the ion selectivity of the nanopore.

Solid-state nanopores are an attractive platform for sensing and single molecule studies, due to their chemical robustness and stability. By the addition of a reactive coating or lipid membrane to the surface, new functionality or reactive handles can be imparted. By taking inspiration from, and co-opting, biology, sophisticated channels with novel functionality can be created. Clearly, we have only sampled some of the possibilities enabled by modification of solid-state pores with biologically derived molecules, and synthetic chemical modification further broadens the horizons.[36, 42]

Engineered Protein Nanopores and Site-specific Modification

Side-chain modification of native transmembrane proteins has long been used to gain insight into their structure and activity.[43-46] The use of native biological protein pores has seen much success in sensing applications; however, it is undoubtedly advantageous to adapt the pore structure to suit different applications. A vast range of modifications involving mutagenesis, protein

manipulation and *in situ* chemical modification have been demonstrated,[47] and only select examples are presented here.

Mutagenesis has been a widely applied method of modifying proteins, as a high degree of control and selectivity can be achieved. An excellent example comes from Maglia and co-workers who used Cytolysin A (ClyA) channels to study the post-translational ubiquitination of a protein.[48] The authors selected the E2 Ubc4 enzyme from *Saccharomyces cerevisiae* for their investigation due to its ability to self-ubiquitinate. Moreover, single E2 enzyme molecules can be trapped within ClyA under an applied transmembrane potential due to it being small enough to enter the pore, but too large to translocate through the 3.3 nm wide constriction of the pore (**Figure 1.10**).

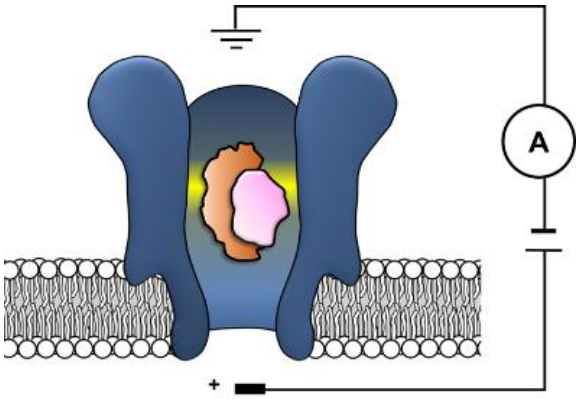

Figure 1.10: Cytolysin A (ClyA) was engineered with a ring of hydrophobic tryptophan residues (yellow band) in place of glutamine residues within the lumen of the pore. This increased the hydrophobicity of the pore and increased the dwell time such that the binding of individual E2 enzyme molecules (orange) could be resolved. Captured E2 enzymes that were post-translationally modified with ubiquitin (pink) gave distinct ion current traces compared to the unmodified E2 enzyme (orange).[48]

The authors used a genetically engineered ClyA pore in which a ring of glutamine residues were mutated to tryptophan residues on the inner surface of the pore (yellow band in **Figure 1.10**). This mutation was found to be particularly important for increasing the dwell time of captured E2 protein molecules by increasing the hydrophobicity of the pore interior. By using these pores, the authors were able to resolve different isomeric E2-ubiquitin

conjugates and monitor the ubiquitination of E2 enzymes in real-time. Real-time measurements particularly those that can be conducted in biologically relevant conditions, are invaluable for the study of fundamental protein interactions.

Maglia, Bayley and co-workers have also introduced charged residues into the beta barrel of an α-HL channel to slow the translocation of ssDNA (**Figure 1.11A**) [49] A range of homo- and hetero-heptameric α-HL mutants with varying numbers of positive charges within the channel were produced and found to influence the kinetics of ssDNA translocation (**Figure 1.11B**).

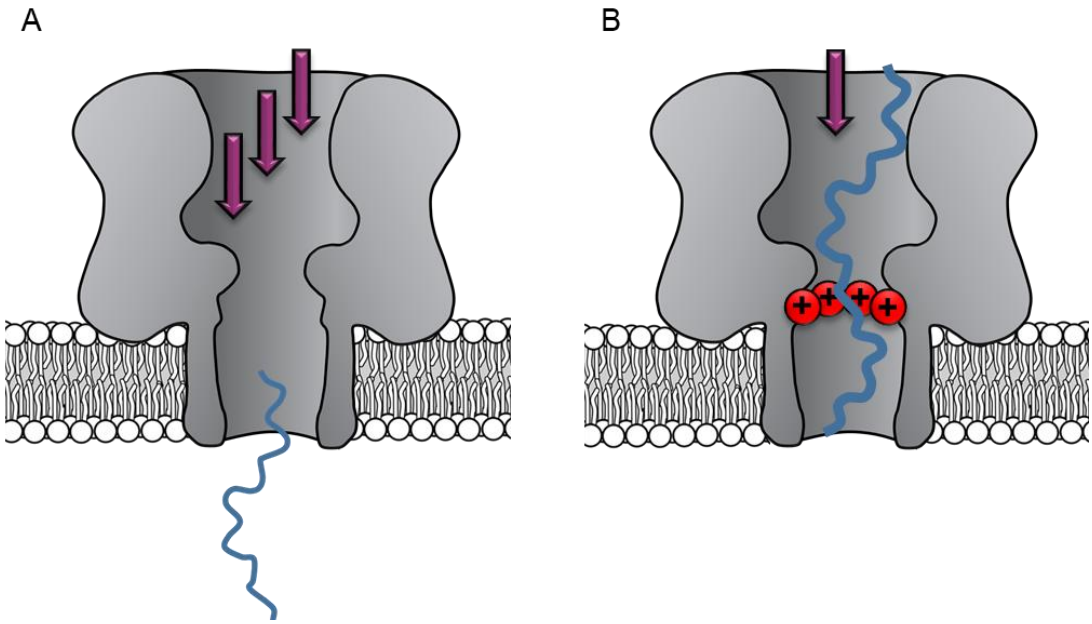

Figure 1.11: A) Translocation of DNA (blue) is incredibly rapid through a wild-type pore, such that little information of the sequence could be elucidated. B) Translocation of ssDNA molecules through a protein channel is slowed due to attractive interactions between the negatively charged DNA and positively charged arginine resides engineered into the pore.[49]

However, these charged mutations also greatly reduced the flow of ions through the channel, resulting in near-complete blockage of the ion current during ssDNA translocation. Such poor signal-to-noise ratios therefore rendered the pores unsuitable for DNA sequencing applications that rely on an ion current readout. Nonetheless, an effective strategy for slowing the

translocation of ssDNA was demonstrated, and the authors proposed that similar channels might be exploited in combination with other means of nucleotide readout where slower movement of DNA is required.

The aforementioned example highlights one of the limitations of modifying residues within a protein channel, since varying the charges within a nanopore can affect ion currents and the associated electro-osmotic flow.[50-51] Nonetheless, such changes can be exploited to attain beneficial characteristics. For example, the Luchian group demonstrated that pH-tuning enabled balancing of the electro-osmotic force against the usually dominant electrophoretic force.[52] The fine balancing of these forces then enabled a single charged peptide to be captured within the pore. Similarly, varying the pH and the charged residues within the Fragaceatoxin C (FraC) nanopore has enabled the detection of differently charged peptides that would otherwise not enter the pore.[51]

As illustrated by the two preceding examples, genetic engineering of nanopores has largely relied upon the 20 canonical amino acids to tune functionality. However, non-natural amino acids can also be introduced into genetically engineered pores,[53-55] provided channel stability can be maintained,[56-57] and any additional technical challenges can be overcome.[58] However, examples of the incorporation of non-natural amino acids to a protein nanopore is far less common than their canonical counterparts. Future work may see greater extent of incorporation of non-natural amino acids, as these could provide unique channels with novel functionality.

The manipulation of protein channels is not limited to mutagenesis as amino acids can act as reactive handles onto which further modification may be achieved *via* bioconjugation.[58] While chemical modification of membrane-spanning proteins has long been used to gain insight into the structure and activity of transmembrane proteins,[43-46] the modification of protein nanopores to add new functionality has been a more contemporary pursuit. Early

examples include the modification of α-HL cysteine mutants with ssDNA,[59-60] and a photocleavable group that blocked pore assembly until it was removed by UV light.[61] However, these approaches do not exist in isolation; the combination of genetic engineering and bioconjugation provides a powerful strategy for incorporating reactive handles in desired positions.[47, 58] As there are no naturally occurring cysteine residues with the α-HL protein, introducing cysteine residues affords absolute control of the positioning of the reactive site.[12]

The Bayley group have made extensive use of the powerful pairing of cysteine mutagenesis and the subsequent chemical modification of α-HL nanopores. In 2001, they examined the viability of using chemical modification reactions to probe the internal three-dimensional structure of a transmembrane channel.[62] α-HL was used as a model protein since the crystal structure of the assembled protein is already known.[12] Seven homoheptameric mutants were produced to position rings of cysteine residues in different locations within the channel of the nanopore channel. The approximate location of the constriction site at the mid-point of the nanopore was determined by analysing the relative rate of disulfide exchange when each of the mutant nanopores reacted with monomethoxypoly(ethylene glycol)-*o*-pyridyl disulfide polymers of differing lengths. In addition, larger blockages in the ion current were observed when reactions occurred at the narrowest points in the channel, providing further insight into the internal dimensions of the transmembrane ion channel.

The ability to assemble heteroheptameric α-HL mutants provides additional control over chemical modification. Indeed, α-HL nanopores assembled with a single cysteine in just one of the seven constituent proteins have been particularly fruitful (**Figure 1.12**). Since the assembly of single-mutant pores requires mixing the mutant and wild-type proteins, a means of separating the desired single mutant heptameric assembly from assemblies with zero or more than one mutant protein is required (**Figures 1.12B – 1.12C**).

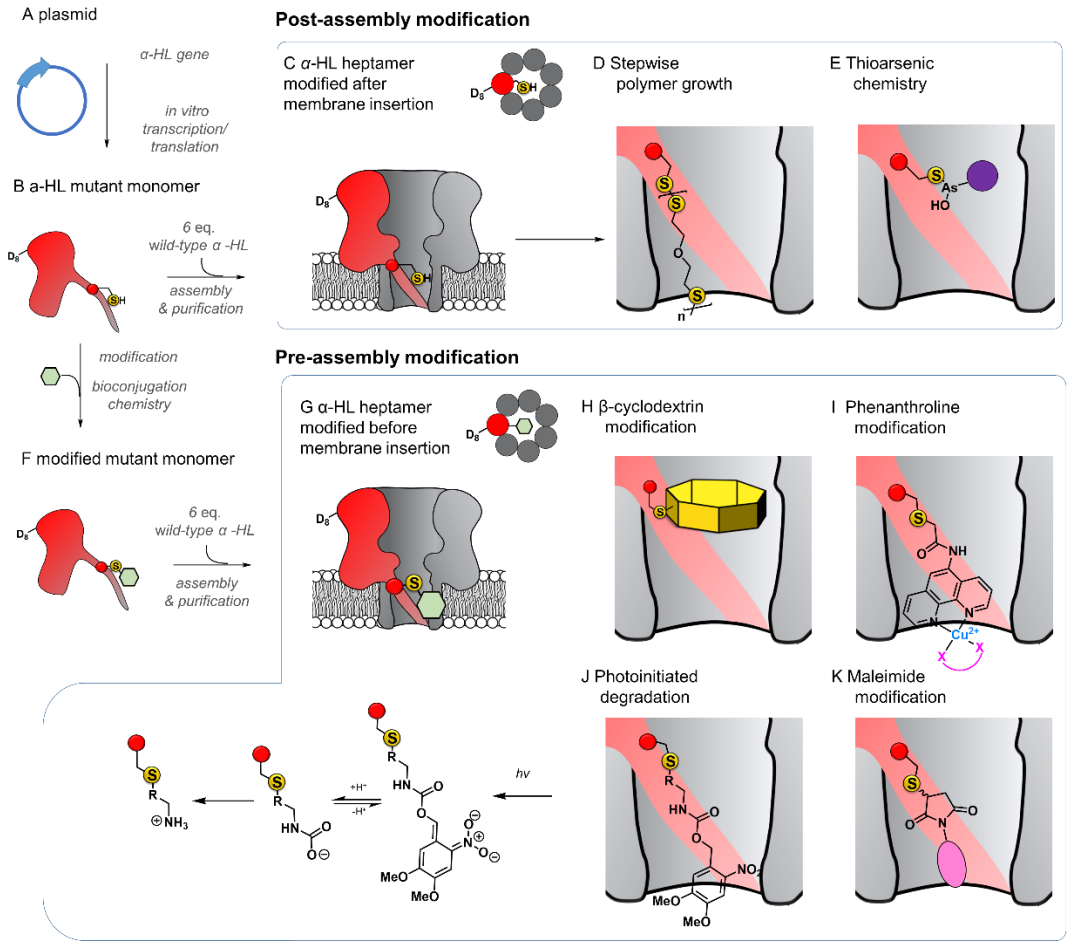

Figure 1.12: Production of α-HL homoheteroheptameric nanopores modified at a single cysteine residue before (bottom panel) or after nanopore assembly (top panel). A) α-hemolysin monomers synthesised using in vitro transcription/translation from a plasmid encoding the mutant protein. B) The mutant protein monomer contains an octa-aspartic acid tail (D_8) at the C-terminus to enable separation by gel electrophoresis. C) A mutant pore containing a single cysteine residue modified after reconstitution in a lipid bilayer to monitor D) stepwise polymer growth arising from disulfide exchange reactions,[64] and E) reversible thioarsenic chemistry.[63, 65-67] F) to G) Cysteine mutant monomers have been functionalised with a wide range of modifications prior to assembly into heptameric nanopores, purification, and reconstitution in a lipid bilayer. H) Modification with β-cyclodextrin enabled the discrimination of individual nucleoside bases.[28, 68] I) Attachment of phenanthroline enabled the detection of chelating groups (pink) such as neurotransmitters[69] and amino acid enantiomers[70] in the presence of Cu(II). J) Photoinitiated degradation of a 3,4-dimethoxy-6-nitrobenzylcarbamate group bond to the pore.[71] K) A maleimide-based linker used to attach functional groups enabled attachment and monitoring of subsequent cycloaddition addition reactions involving tetrazine, cyclooctene, and cyclooctyne functional groups.[72]

Following assembly of a mixture of heptameric pores in rabbit red blood cell membranes, separation via gel electrophoresis is enabled by the additional

presence of a genetically encoded 8-residue aspartic acid tail on the C-terminus of the mutant monomer protein (D8 in Figure 1.12B).63 The isolated mutant protein can then be reconstituted in a lipid bilayer for nanopore experiments. For example, a single cysteine handle within such a mutant protein has been used to monitor the stepwise growth of a polymer chain (Figures 1.12C – 1.12D).64 When 5,5′-dithiobis-(2-nitrobenzoic acid) (DTNA) and (mercaptoethyl)-ether were placed on opposite sides of a suspended lipid bilayer containing a single cysteine mutant pore, sequential disulfide exchange reactions occurring within the channel to form a polymer chain could be monitored by the progressive blockage of the ion channel current.

The same mutant nanopore has also been used to probe the formation of the thioarsenic bonds at the single-molecule level (**Figure 1.12E**).[63] By measuring the durations of the events and the concentration dependency, the kinetics of bond formation and disassociation were determined. Later work used a similar approach to probe pyramidal inversion of thioarsenic chiral centres[65] and multi-component reaction networks.[66]

Taking the approach a step further, the Bayley group have constructed α-HL nanopores containing one mutant protein that contains a track of up to six cysteine footholds along the membrane-spanning β-barrel (**Figure 1.13A**).[67, 73] The first such study exploited the reversible thioarsenic chemistry introduced above to create a molecule capable of walking along the cysteine track. The walking occurred *via* alternating intra- and inter-molecular As-S bond-making/breaking reactions *via* a hand-over-hand mechanism, reminiscent of the way in which dynein and kinesin motor proteins walk along microtubules. The thioarsenic walker was found to stochastically walk towards a thermodynamic sink position, but more recent work based on disulfide exchange has developed a molecular hopper in which the direction of movement along the cysteine track could be controlled (**Figures 1.13B – 1.13C**).[73] A trapavidin-biotin complex served as a bulky stopper to enable

capture of the loading molecule within the nanopore, while the length of the carrier linker was tuned to target loading (*via* disulfide exchange) onto the desired cysteine residue within the pore (**Figure 1.13C**). The externally applied transmembrane voltage could then be used to control the direction of hopping since the electric field exerts a force on the negatively charged single-stranded DNA (ssDNA) cargo.

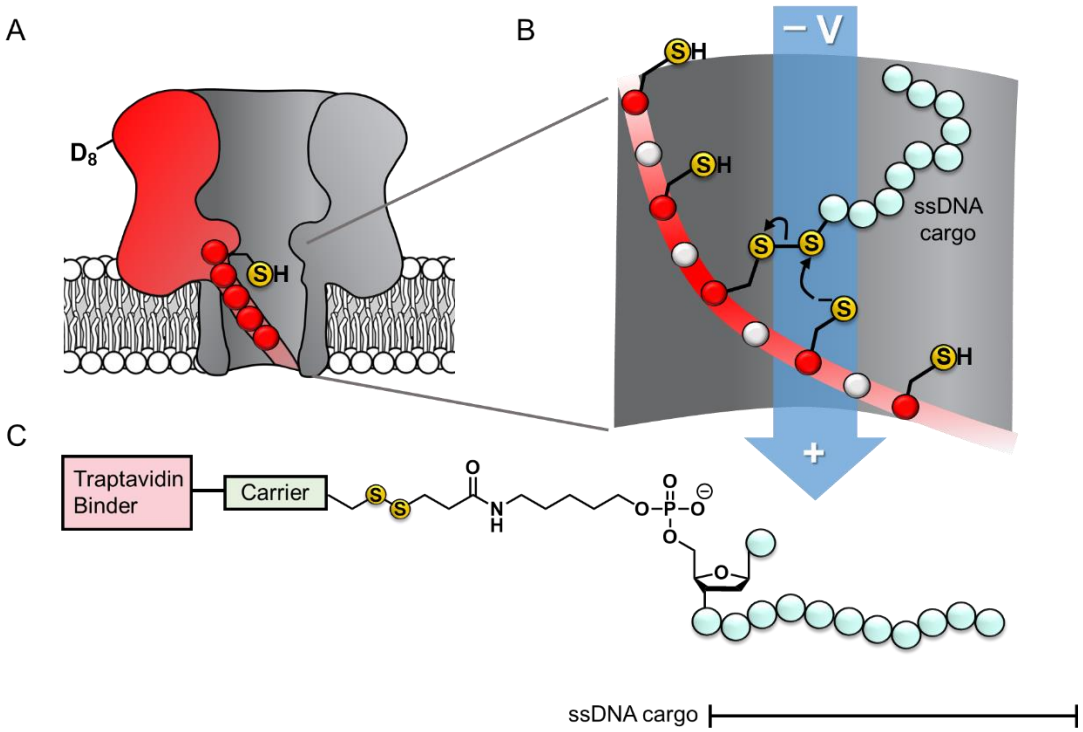

Figure 1.13: A) A cysteine track (red) was incorporated into a single residue of an α-HL channel. B) The molecular hopper (pale blue) was terminated with a thiol group, allowing a disulfide bond to form between the hopper and the pore. Due to steric restrictions, the hopper could only move backwards or forward one cysteine station at a time. Moving multiple stations and formation of disulfide bonds between residues of the pore was disallowed. C) The molecular hopper is bound *via* a disulfide bond to a carrier, and at the other end to a DNA cargo.[73]

In a more recent application of this work, the Bayley group have demonstrated that single nucleobase variations in a DNA sequence can be detected using the chemical stepping of the molecular hopper.[74] The incorporation of a molecular track has created a system with machine-like properties. This highlights the capability of nanopore technology to observe molecular

interactions and reactions at the single molecule level. While some caveats must be taken as the systems studied experience an applied potential, nanopore technologies can provide invaluable insight into reaction mechanisms and pathways.

Contrasting with the approach of modifying cysteine residues after assembly into heptameric nanopores (*i.e.* **Figures 1.12A – E and 1.13**), singly modified α-HL nanopores may also be generated by functionalising cysteine mutant monomers prior to assembly and purification (**Figures 1.12B, F – K**). The Bayley group have modified cysteine-mutant α-HL monomers with a diverse selection of synthetic groups and found that this does not prevent assembly into the desired singly functionalised heteroheptameric nanopores (**Figures 1.12H – K**). For example, β-cyclodextrin has been covalently attached to α-HL monomers prior to assembly to generate a nanopore capable of continuous read-out of molecular recognition events occurring within the β-cyclodextrin cavity, and even found capable of discriminating the bases of individual nucleosides (**Figure 1.12H**).[68-69] Phenanthroline-modified nanopores have also been generated using the pre-assembly modification approach (**Figure 1.12I**). The presence of copper(II) as a bridging chelating agent enabled the binding and resolution of different neurotransmitters[69] and amino acid enantiomers based on changes in the ion current.[70] The same pre-assembly modification strategy has also been used to assemble α-HL nanopores modified with a single azobenzene unit to observe light-induced configurational switching between *E* and *Z* isomers.[75]

The ability to readily modify α-HL has facilitated its use as a nanoreactor to observe chemical reactions at the single-molecule level. Monitoring ion currents allows reactions to be monitored down to the high microsecond timescale, thereby enabling the observation of transient intermediates. For example, a nanopore pre-modified with 3,4-dimethoxy-6-nitrobenzylcarbamate was observed to undergo photoinitiated degradation *via*

a multi-step process in which the kinetics of individual steps could be elucidated (**Figure 1.12J**).[71] Maleimide has also served as a useful reagent for the modification of cysteine-modified α-HL monomers (**Figure 1.12K**).[72] α-HL nanopores were pre-modified with three different maleimide linkers containing additional terminal sites for further bioconjugation; a tetrazine, a *trans*-cyclo-octene, and a cyclo-octyne. When these modified pores were reconstituted in a lipid bilayer, the ion current facilitated the observation of cycloaddition reactions with reagents added to the solution on one side of the membrane. Five different cycloaddition reaction combinations were examined, but no intermediates were observed on the timescale of the ion current recordings, meaning that the intermediates these reactions must have lifetimes of <80 μs. The Bayley group has also employed cysteine-maleimide bioconjugation to modify pre-assembled α-HL pores (*i.e.* **Figure 1.12**, top), rather than prior to assembly as in the preceding work.[76]

As is evident, extensive work has been carried out on the functionalisation of α-HL *via* mutagenesis. This can most likely be attributed to the relatively low cost and high availability of the protein, along with its comprehensive characterisation. However, a growing number of alternative pores have emerged in previous years. Aerolysin, for example, has a similar heptameric, β-barrel structure to α-hemolysin, albeit with a narrower diameter of 13.7 Å.[77] This makes aerolysin an attractive alternative to α-HL as enhanced signal-to-noise ratios can be achieved. A rational design approach has been used to produce a series of aerolysin single mutants, in which residues were substituted with alanine or tryptophan (to vary the size of the channel), or lysine, glutamine or glutamate (to vary the charge).[78] Experimental and simulation data showed that the translocation and capture of DNA and protein could be modulated by varying residues at the constriction points of the pore. Similarly, the Maglia group has shown that the introduction of charged residues has no effect on peptide retention in a fragaceatoxin (FraC) nanopore, whereas the

incorporation of an aromatic residue increased the peptide capture capabilities of the pore.[79]

Chemical functionalisation of protein nanopores is not limited to the modification of genetically engineered variants. Recent work has seen the *in-situ* modification of wild-type α-HL at both lysine and methionine residues.[80-81] α-HL presents several solvent-exposed lysine residues that could serve as potential sites for bioconjugation (**Figure 1.14A**).

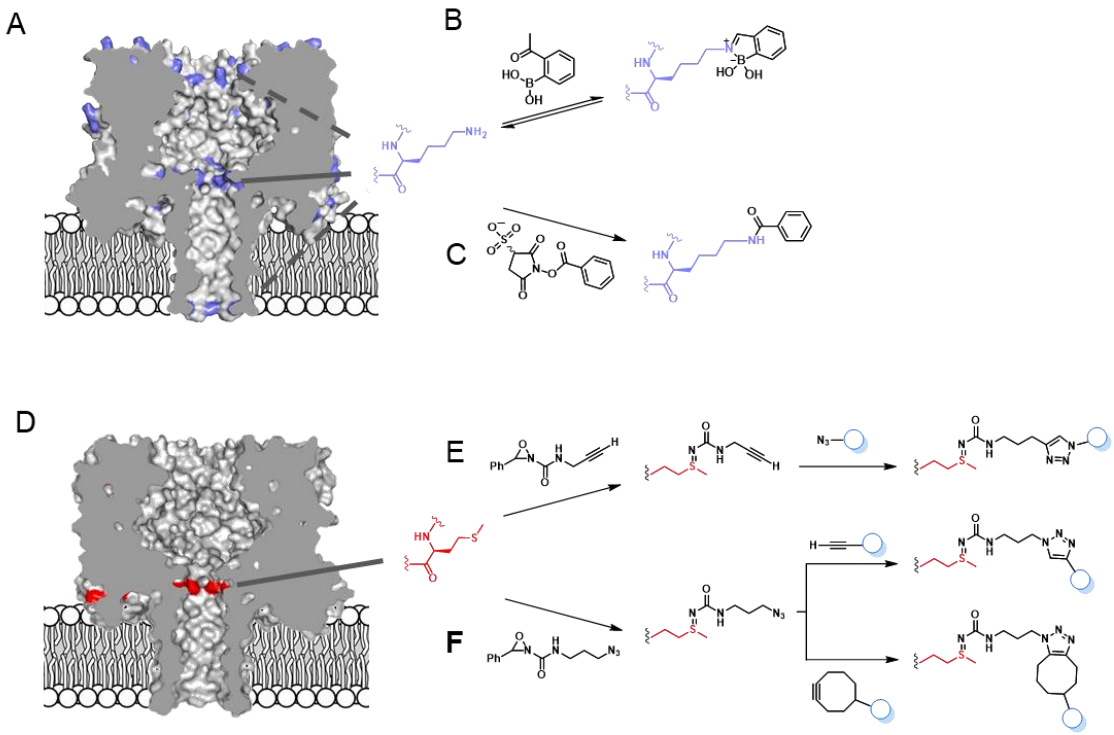

Figure 1.14: A) Locations of lysine residues in the α-hemolysin nanopore (blue). B) Reversible modification of lysine with a boronic acid was used to probe the reactivity of the solvent-exposed lysine residues. Only reactions occurring on the three rings of lysine residues on the interior of the channel were found to modulate the transmembrane ion current. The central ring of lysine residues were found to be the most reactive. C) Irreversible amide modification of lysine residues within the channel interior was achieved using 3-sulfo-*N*-succinimidyl benzoate sodium salt.[81] D) α-Hemolysin contains one solvent-exposed ring of seven methionine residues within the lumen of the nanopore. Methionine (red) irreversibly reacts with oxaziridines to yield nanopores functionalised with E) alkynes or F) azides, which can be further functionalised using click chemistry. Ion current changes also allowed short-lived reactive intermediates to be resolved and assigned.[80]

Initially, Borsley and Cockroft used reversible iminoboronate chemistry to map the reactivity of these residues (**Figure 1.14B**).[81] Ion current recordings revealed a surprisingly simple reactivity pattern that could be attributed to iminoboronate formation at one of the three rings of lysine residues lining the interior of the channel (Figure 1.14A), indicating that reactions occurring on any other external lysine residues did not influence the ion current. Moreover, the central-most ring of lysine residues was found to be substantially more reactive than the other lysine sites. Irreversible modification by amide bond formation was demonstrated using 3-sulfo-*N*-succinimidyl benzoate sodium salt (**Figure 1.14C**).

The same group went on to selectively modify methionine residues in wild-type α-HL using a similar *in situ* approach (**Figures1.14D – F**).[80] Methionine is a highly desirable target for protein modification as it is one of the least common canonical amino acids and is rarely solvent exposed due to its high hydrophobicity, meaning that a higher degree of selectivity can be achieved. Indeed, α-HL presents only one solvent-exposed methionine residue in each of its subunits within the transmembrane channel (**Figure 1.14D**). Bioorthogonal azide and alkyne groups were introduced into α-HL using oxaziridine reagents originally developed by Toste (**Figures 1.14E – F**).[82] Subsequent click reactions enabled the decoration of the alkyne- and azide-modified pores with a range of substrates, including an acid, a base, a nucleotide and even a single-stranded DNA oligonucleotide (**Figure 1.14E**).[80] Notably, characteristic ion current traces were observed during the Cu(I)-catalysed azide-alkyne [3+2] cycloaddition (CuAAC) modifications of the alkyne-modified nanopore. A series of experiments in which the Cu(I) concentration and applied potential was varied enabled the complete assignment of all the observed ion current levels, including short-lived copper-bound reaction intermediates. The Bayley group similarly investigated CuAAC reactions in α-HL channels in earlier work, but using the more challenging strategy of incorporating an unnatural alkyne amino acid.[55]

DNA Nanopores

The pursuit of single-molecule DNA sequencing has been a major driver in the development of nanopore technologies. Detection of specific oligonucleotides has a range of applications, particularly for the detection of disease and gene abnormalities involving single-nucleotide polymorphism. Both solid-state[83] and biological nanopores [59-60] have been modified with DNA for the detection of complementary counter strands. Even single-nucleotide mismatches within an otherwise fully complementary stand could be detected using ion currents.[59-60, 84] Bashir[83] and Mussi[84] used 1,4-phenylene diisothiocyanate to cross-link amino-terminated DNA to solid-state nanopores coated with (3-aminopropyl)trimethoxysilane (**Figure 1.15**).

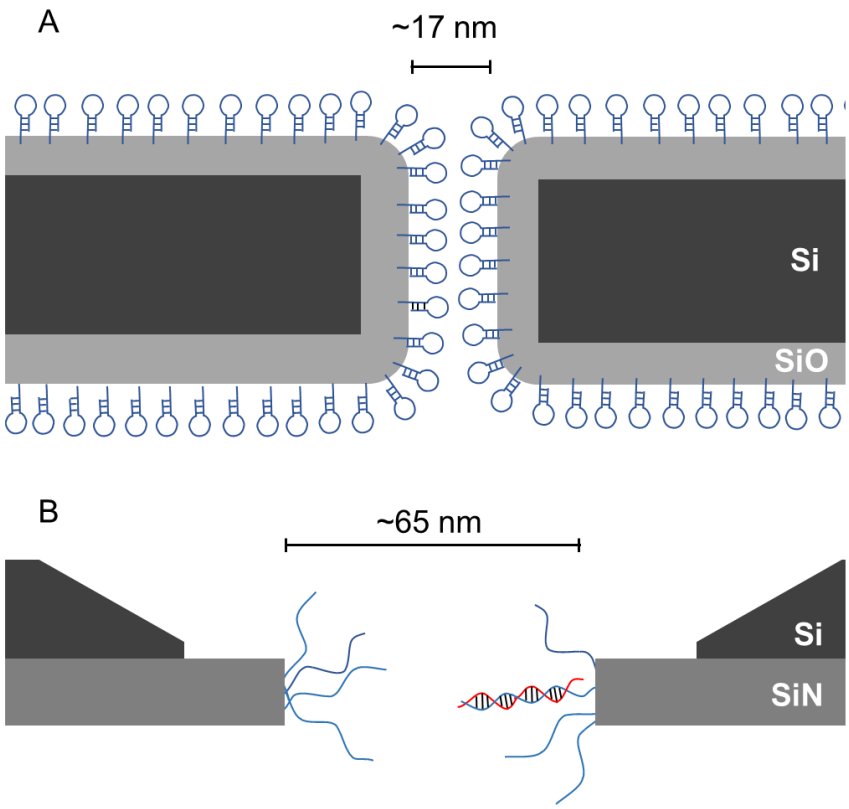

Figure 1.15: Solid-state nanopores modified using 1,4-phenylene diisothiocyanate as a cross-linking agent to attach amino-terminated (A) DNA hairpins [83] and (B) single-stranded DNA.[85] The passage of complementary strands through such pores was slowed, resulting in prolonged ion current drops.

Meanwhile, Howorka and Bayley used pre-assembly cysteine modification (**Figure 1.12G**) to attach single-stranded DNA to α-HL protein nanopores (**Figure 1.16A**).[59-60] Bayley and Dekker subsequently used DNA-modified α-HL to enable electrophoretic capture in a solid-state nanopore.[86] Post-assembly modification was employed (**Figure 1.12C**) to attach a thiol-terminated 12-mer DNA sequence to a cysteine residue within an extended loop at the β-barrel opening. The 12-mer oligonucleotide acted as a handle for hybridisation to a 2 kb double-stranded plasmid DNA with a complementary sticky end (blue/green in **Figure 1.16B**).

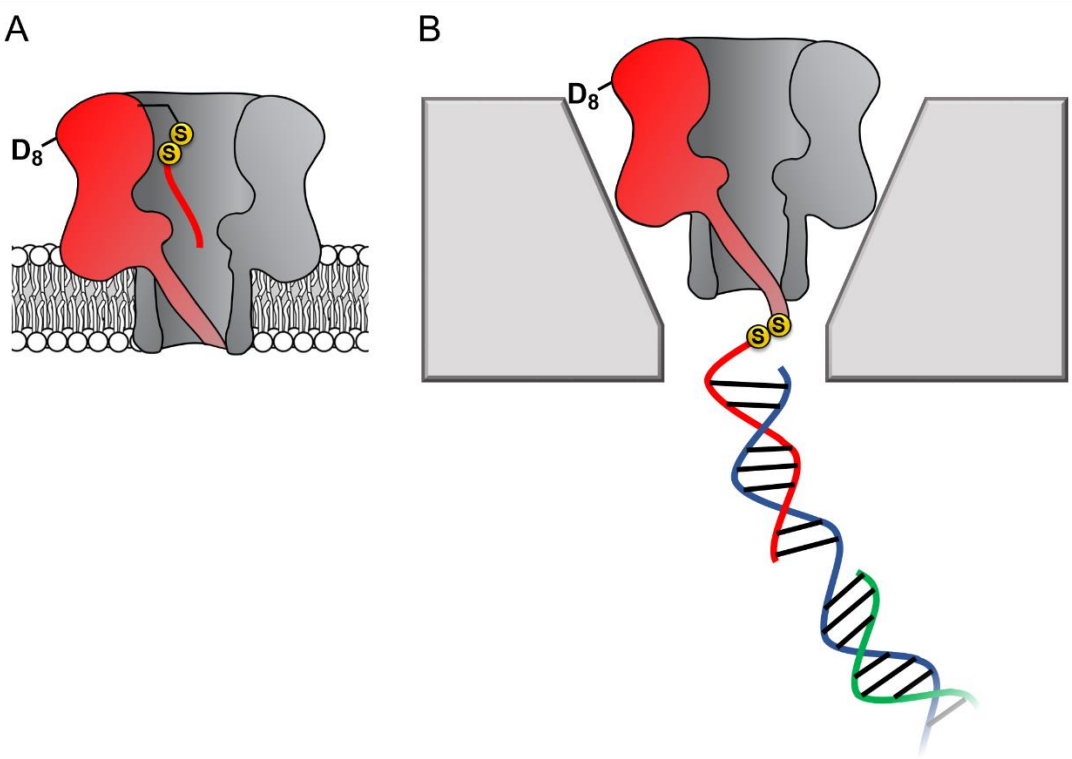

Figure 1.16: A) Membrane-spanning α-hemolysin nanopore modified with an 8-mer single-stranded DNA *via* a disulfide linkage.[59-60] B) α-hemolysin modified with a 2kb DNA tether enabled threading and capture of the protein nanopore within a solid-state nanopore.[86]

Under an applied potential, the negatively charged DNA tail guided the α-HL into a solid-state pore that was large enough to accommodate the narrow β-barrel of α-HL, but too small for the cap domain to pass though, thereby

trapping the protein. Ion-current traces of the nanopore within a nanopore showed that free single-stranded DNA molecules were still able to transit through the α-HL channel. The insertion of the biological nanopore into a solid-state one draws benefits from both approaches. The solid-state components provide enhanced stability, with the hybrid pores lasting for several days, which is generally unobtainable using lipid-membrane systems. Meanwhile, the biological component provides atomically precise dimensions and the potential for further functionalisation that would otherwise be difficult for a typical solid-state pore. Such developments herald the wider application of solid-state/biological hybrid nanopores.

In addition to decorating existing nanopores with simple oligonucleotides, larger DNA origami constructs can also be used to tune the properties of solid-state pores. The pairing of DNA origami and nanopore technology has been explored in numerous contexts.[87] DNA origami can be fabricated into precise and intricate structures through the utilisation of molecular self-assembly.[88] DNA nanoplates are an example of one of the many architectures possible. Dietz has shown that nanoplates can be captured at the entrance of solid-state nanopores to enhance their function and give greater control over the dimensions of the pore (**Figure 1.17 A – B**).[89] Like the preceding example presented in **Figure 1.16B**, the loop of DNA in **Figure 1.17A** enables the DNA origami nanoplates to be captured and held in place by the applied voltage. The nanoplate approach constitutes an interesting platform for developing biological-synthetic hybrid nanopores with enhanced sensing capabilities. In the absence of the nanoplate, the addition of the small protein streptavidin caused fleeting transient blockades in the ion current as it entered the SiN nanopore. However, once the DNA nanoplate was in place, prolonged translocation events were detected. The addition of the much larger immunoglobulin G gave no translocation events when the nanoplate was in place, demonstrating size-selective capabilities of the portal within the DNA nanoplate. In addition to having tuneable size selectivity, DNA nanoplates

were constructed that position a DNA “bait” sequence at the opening of the pore (**Figure 1.17A**). When the target “prey” sequence hybridises with the bait sequence this or slows the passage of the analyte of interest for detection purposes.

A major advantage of DNA origami is its extreme flexibility, allowing complex 3D architectures to be fabricated. Alongside the DNA nanoplate, Dietz and Dekker have demonstrated that DNA nanospheres can be captured within a lipid-coated solid-state nanopore under an applied potential (**Figure 1.17C**).[90] The DNA sphere was permeable to ions, so a total blockage of ions was not observed.

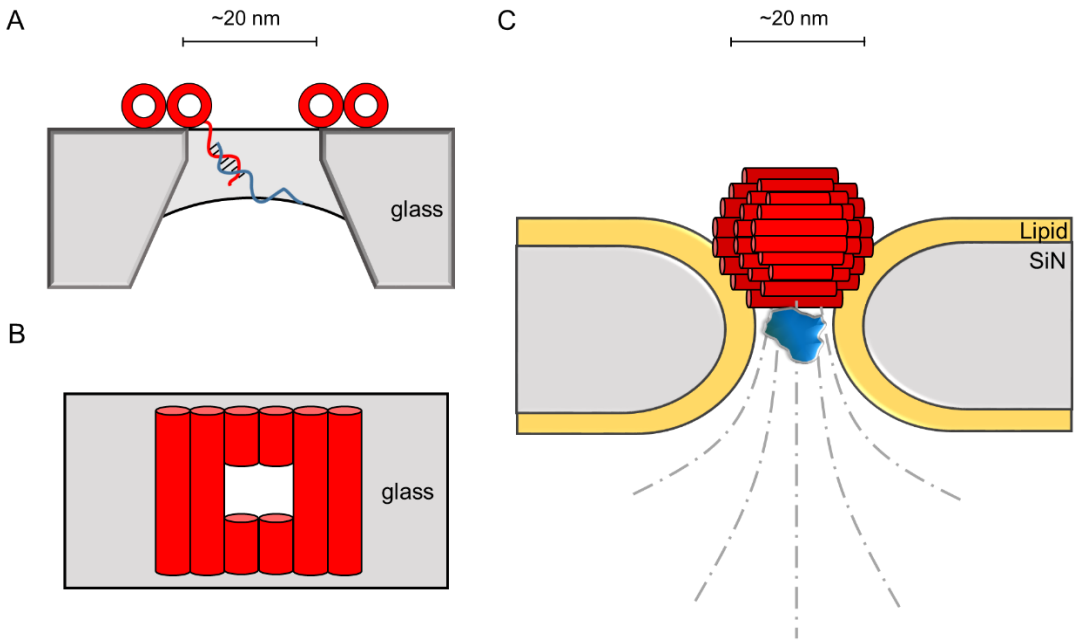

Figure 1.17: A) Single-stranded DNA was used to guide the voltage-driven capture of a DNA-origami nanoplate (red cylinders) at the opening of a SiN nanopore. Nanoplates containing a terminal single-stranded DNA strand could be used to detect the binding of complementary sequences.[89] B) Top-down view of the nanoplate. The size of the opening can be controlled by the design of the sequences used to assemble the nanoplate.[89] C) Voltage-driven capture of a DNA nanosphere (red) in lipid-coated SiN nanopore enabled the electro-osmotic trapping and detection of several different proteins (blue).[90]

In this case, an electro-osmotic hydrodynamic flow facilitated long-duration trapping of protein molecules. Proteins varying in size and mass were trapped.

Not only did each protein give a distinct signal, but differences in the orientation and conformations of the individual proteins could be resolved. This presents a novel approach where a lipid-functionalised nanopore, further functionalised with DNA origami exhibits enhanced protein trapping and identification properties. Future development of this work may lead to significant advancements in label-free protein analysis. The combination of DNA nanotechnology and solid-state nanopores provides platforms with wide-reaching biosensing applications, as a near limitless range of modifications are accessible through DNA assembly and existing synthetic DNA modifications.

Synthetic Protein nanopores

The functionalisation of existing biological and solid-state nanopores has drastically reshaped the remit and application of the nanopore approaches. Nanopore electrophysiology has evolved from a technique used to study pores themselves, to a method that is sensitive enough to resolve single amino acid and nucleotide variations.[74, 91]

Modification of existing protein channels has been demonstrated to produce a range of bespoke pores with novel functionality. However, the future may see entirely synthetic protein pores being fabricated with a specific function in mind. While this would circumvent the issues of protein instability that come with extensive modification, developing artificial proteins is not without its own challenges, as protein tertiary structures can be difficult to predict.[92] Even if successful protein design and structure is achieved in an aqueous environment, there is no guarantee that the protein will insert into a lipid bilayer while retaining its tertiary structure and the integrity of the membrane. Nonetheless, progress has been made towards the development of *de novo* protein architectures for nanopore applications. For example, Woolfson and Bayley have demonstrated the design and construction of a self-assembled α-

helical transmembrane protein based on the structure of Wza, an *Escherichia coli* polysaccharide transporter (**Figure 1.18A**).[93]

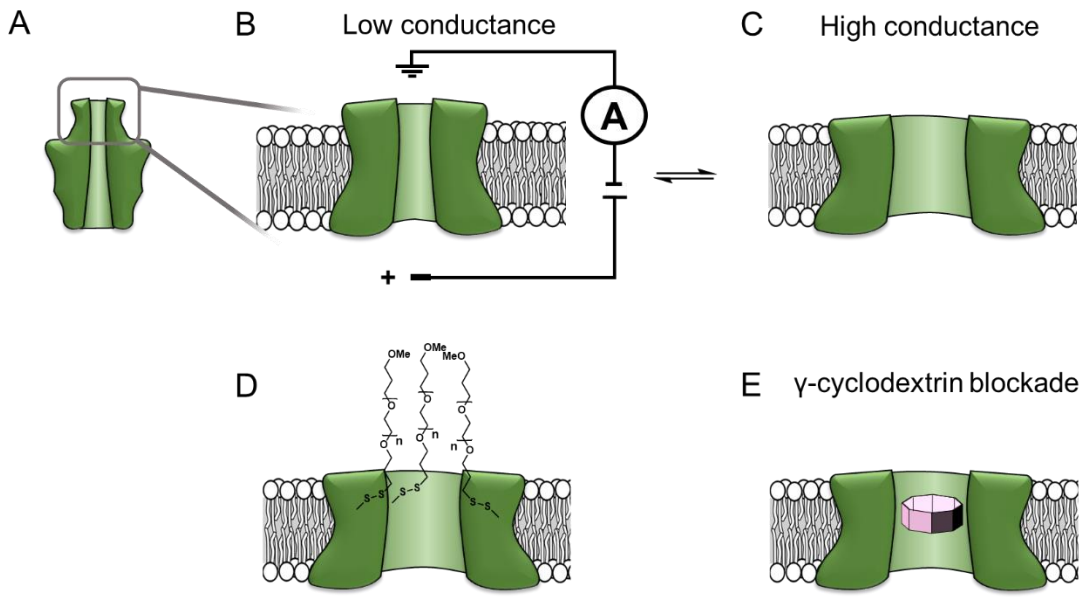

Figure 1.18: A) The amino acid sequence of the membrane-spanning D4 domain of *E. coli* Wza protein was used for consensus sequence searching in BLAST. B) The evolutionarily conserved, 35-amino acid consensus sequence (cWza) was then synthesised using solid-phase peptide synthesis and found to form pores that were much more stable than those assembled from the original BLAST query sequence (Wza). C) Ion currents revealed the cWza pores to be in conformational exchange between low and high conductance states. D) Nanopores constructed using a cysteine-containing peptide were modified with polyethylene glycol groups (PEG) *via* disulfide bond formation. The disulfide bonds were subsequently cleaved using dithiothreitol (DTT) revealing ≤ eight steps in the ion current to return to the unmodified form, thereby confirming the octameric nature of the pore. E) Octasaccharide β-cyclodextrin derivatives were found both to bind to and template the formation of the octameric semi-synthetic cWza pores.

An initial BLAST search (http://blast.ncbi.nlm.nih.gov/) was performed using the membrane-spanning residues of the Wza sequence as the input query to reveal an evolutionarily well-conserved consensus sequence from 94 hits. This 35-residue peptide sequence (cWza) was synthesised by solid-phase peptide synthesis. Ion current recordings indicated that the peptide formed discrete transmembrane channels, which (based on crystallographic evidence) were expected to assemble as an octamer in the lipid bilayer (**Figure 1.18B**). The

channels were also seen to undergo reversible conformational changes between a low-conductance state and a high-conductance state (**Figure 1.18B-C**). This channel, therefore, does not afford the same structural rigidity and reproducibility as a biological pore such as α-HL. However, the semi-synthetic cWza pore was remarkably more stable than the original Wza query sequence, which only formed noisy and unstable pores. The orientation of the peptides within the membrane and the octameric nature of the pore was confirmed using several clever experiments. Firstly, ion currents showed that polyethyleneglycol (PEG) pyridyl-disulfide derivatives reacted most readily with pores assembled from cysteine-mutant peptides when they were added to one side of the bilayer. Secondly, the addition of dithiothreitol (DTT) to the same side of the membrane reopened the pore in a stepwise manner by cleaving the PEG-disulfide bonds, but this always occurred with eight or fewer steps (**Figure 1.18C-D**). A pyridyl-disulfide derivatised octasaccharide, γ-cyclodextrin could also be used to template the formation of cysteine-mutant pores, with the addition of DTT resulting in the release of the cyclodextrin (**Figure 1.18 C-E).** In addition, the binding of amine-derivatised hexa-, hepta- and octa-saccharides (α, β and γ-cyclodextrin, respectively) was compared (**Figure 1.18E**). The work presents an exciting premise for the development of custom-designed protein channels.

While pore-forming sections of larger proteins have been exploited as monodisperse channels for nanopore sensing, multiple proteins can also be combined in a modular fashion to attain functional nanpores. The Maglia group genetically modified α-HL with loop sequences from the GroES protein that bind the GroEL chaperonin protein (**Figure 1.19A**).[94] The modified pore was found to retain pore-forming ability while also being able to bind a single-ring version of the GroEL chaperonin protein. Remarkably, GroEL-assisted protein folding by the GroES nanopore was found to be on par with the native GroES-GroEL co-chaperonin complex. This presents a novel concept where protein pores with a specific function can be fabricated *via* a bottom-up approach from

pre-existing components. In this case, the use of α-HL as a scaffold to construct multi-protein assemblies provides a promising approach for the assembly of novel functionalised pores.

Building on this precedent, the Maglia group went on to demonstrate the assembly of another modular nanopore constructed from several different proteins (**Figure 1.19B**).[95] The channel was constructed from the genetically encoded fusion of three proteins; a membrane spanning β-barrel derived from *Bacillus anthracis*, part of the proteasome activator 28α (REG), and the α-subunit of the 20S proteasome from *Thermoplasma acidophilum*. By replacing the disordered region of REG with the transmembrane β-barrel a synthetic multi-component nanopore was constructed. The multi-protein assembly retained the ability to insert into a lipid bilayer and form a stable channel. However, at voltages beyond +20 mV the channel tended to gate. Interestingly, the isolated β-barrel domain would not insert into the membrane by itself, meaning that the larger protein framework was required to maintain integrity. The outermost α-subunit of the assembly retained its ability to reversibly bind an unfoldase enzyme from *T. acidophilum* (orange, **Figure 1.19B**). Remarkably, the complete assembly enabled ATP-driven unfolding and proteolytic digestion of green fluorescent protein as it was threaded through the nanopore (depending on whether a proteolytically active or inactive variant of the proteasome–nanopore was used). While single amino acid detection based on the resulting ion currents was not demonstrated, this may become a possibility in future work. Indeed, the authors propose that single amino acid resolution might be achieved by engineering a similar system with a smaller pore diameter. While further work is required for single-molecule fingerprinting, this modular approach for incorporating enzymatic nanomachinery from biology into transmembrane nanopores presents an exciting new direction.

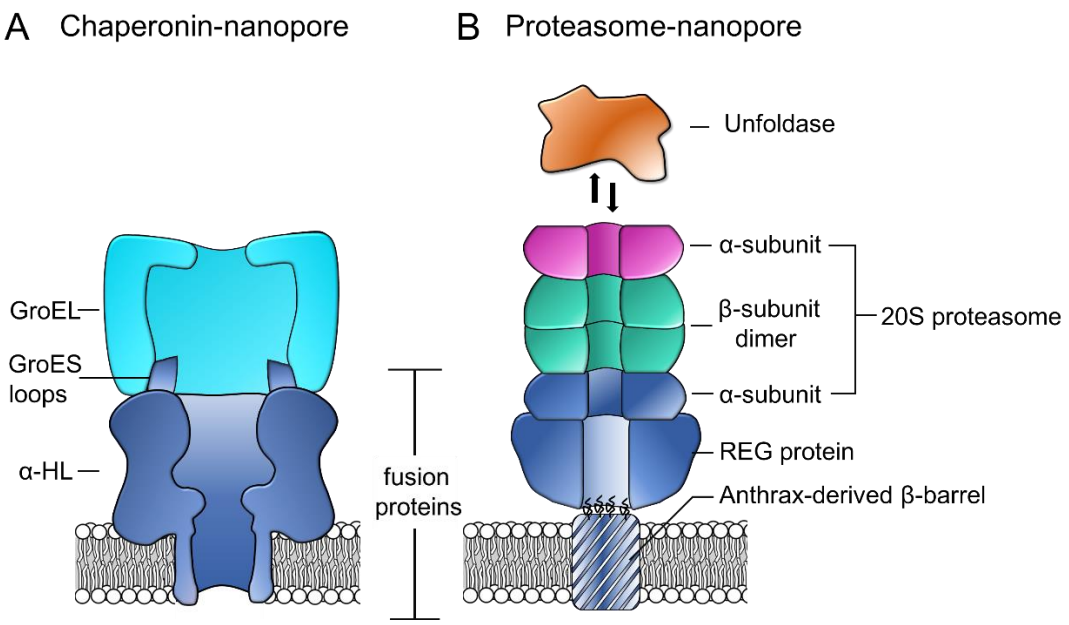

Figure 1.19: A) Chimeric protein nanopore formed by the genetic fusion of α-HL and loops from the GroES co-chaperonin protein (dark blue). The fused GroES loops endows the fusion protein with the ability to bind a single-ring variant of the GroEL protein-folding chaperonin protein (turquoise). The chimeric protein formed stable channels in membranes, while also catalysing protein refolding in the presence of ATP and GroEL.[94] B) Representation of a proteasome nanopore formed by the fusion of three proteins. The anthrax-derived β-barrel was genetically fused to both a REG protein and an α-subunit of a 20S proteasome (dark blue). The rest of the 20S proteasome was assembled non-covalently by the back-to-back stacking of two β-subunits (teal) and an additional α-subunit (purple). The whole assembly was furthermore capable of binding an unfoldase (orange), which could catalyse the unfolding and translocation of proteins into the proteosome nanopore. The whole assembly was shown to be capable of coupling protein translocation and degradation when assembled using a proteolytically active proteasome.[95]

This work presents an exciting premise for the development of custom-designed, bio-inspired protein channels for use in nanopore technologies. While entirely synthetic nanopores have seen limited application in the technique, they propose a likely alternative to biological and solid-state channels in the future, due to the high degree of modulation possible. However, until that is achieved, other techniques can afford a similar degree of control in the channel structure that can be exploited.

Outlook for Functionalised Nanopores

Early ventures in nanopore research saw the adoption of naturally occurring transmembrane protein channels as nanoscale sensors. In the intervening years, the incorporation of non-native functionalities, reactive handles, and molecular adaptors has helped to realise this potential.[28, 48, 80] Notably, the incorporation of a cysteine residue by site-directed mutagenesis to α-HL has been applied for a broad scope of applications. The modification of protein nanopores *via* site-directed mutagenesis has focused on the incorporation of the 20 canonical amino acids. In contrast, unnatural amino acids have rarely been used to modify protein nanopores.[53-55] This may be due to the increased technical challenge and difficulty in predicting protein structure that comes with the use of unnatural amino acids.[56-58] It may also be that the ability to directly modify,[80-81] or to pair conventional mutagenesis with post-translational modification[58] renders the more challenging use of unnatural amino acids unnecessary. Indeed, cysteine modification of nanopores has proven to be particularly powerful when paired with bioconjugation reactions.[47] Nonetheless, future advances in synthetic molecular biology may lead to greater exploitation of unnatural amino acids to access their diverse chemical functionalities and properties.

While the functionalisation and amalgamation of biological and solid-state pores has proved fruitful, the design of *de novo* synthetic channels provides the potential for gaining unrivalled control over channel properties.[29, 96-97] The stability and channel-forming abilities of synthetic nanopores are rapidly improving by exploiting, adapting, or taking inspiration from biomolecules. The design of stable entirely synthetic channels remains challenging, meaning that the modification or re-engineering of existing proteins presents a more accessible alternative. For example, a consensus sequence from the membrane-spanning region Wza proteins was generated to construct a semi-synthetic protein-based membrane-spanning channel.[93]

The incorporation of reactive handles into biological and solid-state nanopores has led to huge advances in the field. Many of these have focused on enhancing the sensing capabilities of nanopores. However, these reactive handles present huge potential for the future of the technique. By exploiting these reactive sites, biological nanopores can be transformed into a platform for transmembrane nanodevices.

1.4 Nanopore as a Platform for Molecular Machines

While the nomenclature may be more contemporary, molecular machines are by no means a modern concept. Many of the vital processes for life rely on a delicately balanced molecular machinery to carry out essential processes. The term ‘molecular machine’ describes a system that takes energy, be that chemical, light, or kinetic, and converts it into useful work to complete a task.[98] A wide range of machines have been described, such as motors, rotors, and switches. However, the exact definition of what constitutes a machine is contentious. Many of the observations of tasks are rooted in macroscopic motions and steeped in dated definitions.[99] In recent years, the language around molecular machinery had become more standardised, and clearer definitions have emerged. A notable distinction is that between a molecular switch and motor.[99-100] A molecular switch will move between two kinetically trapped states; the *cis* or *trans* isomer of an azobenzene or docking stations of a rotaxane. Therefore, any work done must subsequently be undone to return to the original state. Contrastingly, a motor can autonomously cycle through states, passing through the original state without the input work having to be undone. As such, molecular switches are often described as having machine-like properties, whereas a motor is a truly autonomous molecular machine.[98]

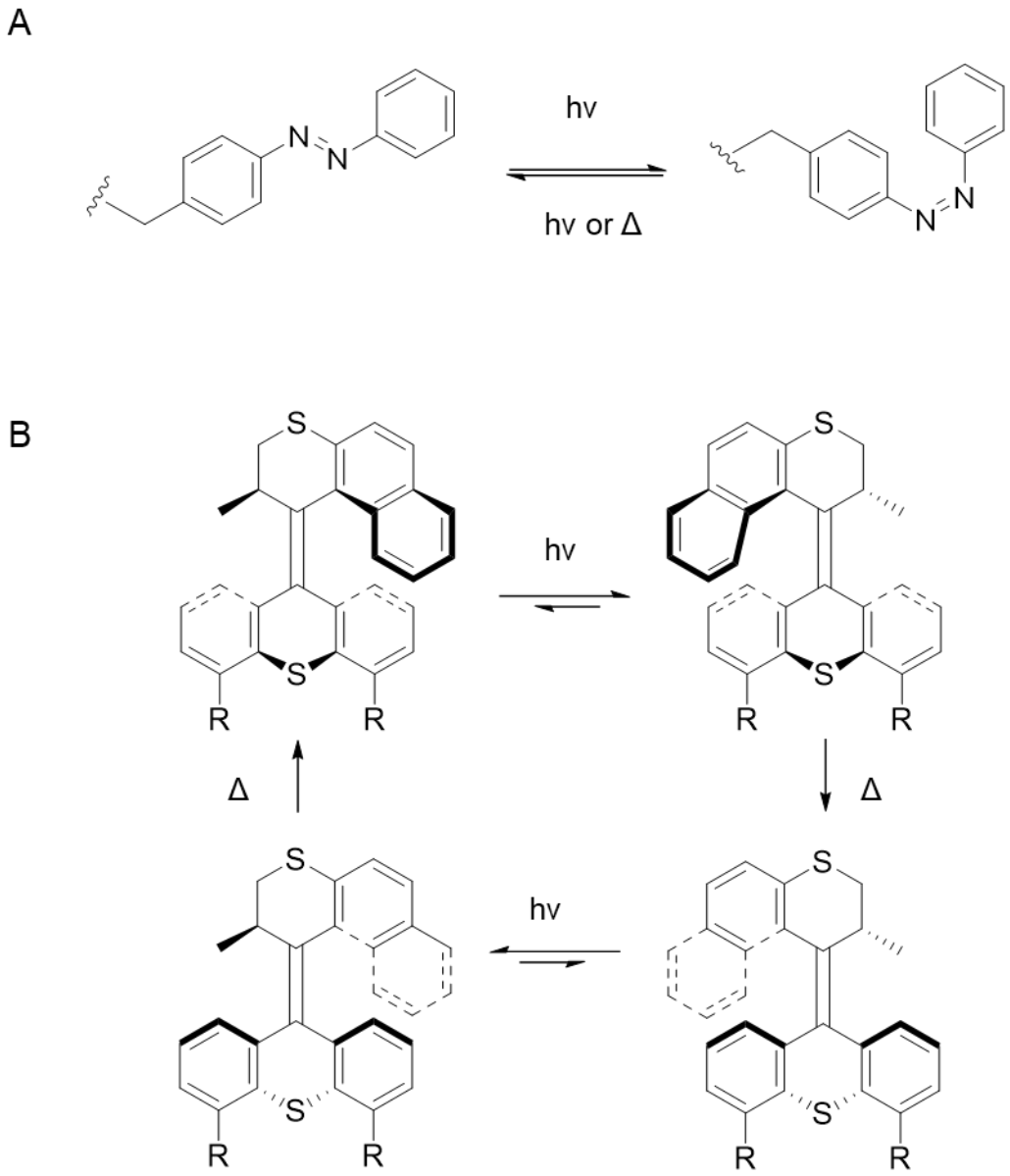

Figure 1.20: A) The azobenzene switch. Upon irradiation with UV light, the molecule will undergo *cis/trans* isomerisation between two kinetically trapped states. B) Feringa-style motor. Upon irradiation with UV light, this molecule will rotate through discrete kinetic states and then return to the initial conformation.[101]

Figure 1.20 shows examples that represent comparatively simple chemical systems that have been artificially derived. However, countless complex molecular machines exist in nature.

Biological Molecular Machines

Biological life is a complex cacophony of interconnected compartmentalised systems.[102] While the exact origins of life remain elusive, several theories such as the RNA world hypothesise the origins of life.[103-104] Haldane's 1929 theory of a primordial soup suggested that the earliest modicums of life sprung from a 'hot dilute soup' of organic molecules.[105] Now controversial at points, it is still believed that early life relied on basic pH and redox potentials to work against Brownian motion.[106] As life developed, more complex systems emerged that were capable of moving ions and molecules across membranes, including against concentration gradients.

Adenosine triphosphate (ATP) synthase has evolved as a membrane-bound, highly complex architecture consisting of several proteins that work in unison (**Figure 1.21**).[98] The axle of the synthase is threaded through an F_0 motor, which is embedded in the membrane. In essence, it is an electrically powered motor, which draws its power from a proton gradient across the membrane: as protons flow through the assembly, the motor rotates. The membrane bound F_0 region is connected by a stator to the F_1 motor. As the F_0 motor rotates, it forces the F_1 motor to spin, thus creating a generator, which provides the driving force for the mechanochemical synthesis of ATP from ADP and inorganic phosphate. ATP synthase is an incredibly efficient machine – in one day the average person will turn over more than their entire body weight in ATP, which will then be broken down and recycled.[107] The machine also displays versatility of purpose and can work in reverse; the chemically driven F_1 motor can take ATP and generate a proton gradient.

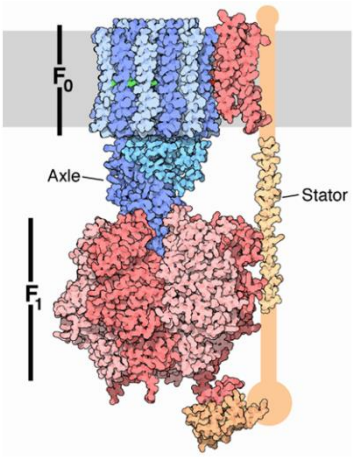

Figure 1.21: Structure of ATP synthase. Image credit to David Goodsell, The Scripps Research Institute, California.

The ribosome is arguably an even more impressive molecular machine. Found in virtually all living cells, it produces the proteins on which life is built.[108-109] It is capable of assembling huge numbers of amino acids, following an mRNA template, to synthesise proteins far longer than a synthetic chemist could achieve. The ribosome is not a single structure, but a symphony of specialised RNA strands and small proteins that come together to carry out translation. While many artificial molecular machines have been synthesised, chemists are yet to match the functionality and complexity of biology.

Artificial Molecular Machines

The 2016 Nobel Prize in chemistry was a landmark occasion, when this prestigious award went to Ben Feringa, Fraser Stoddart, and Jean-Pierre Sauvage for their work on molecular machines.[110] This was one of the relatively unusual occasions where a Chemistry Nobel Prize was awarded to an area with no established practical application. However, it is foreseen that molecular machines will have boundless application – we just need to work out what these are. From motors to muscles to the molecular elevator, a huge range of machine-like molecular systems has been synthesised.[111-113] Unlike

their biological counterparts, artificial molecular machines are still in their early stages of development.

Artificial molecular machines such as the nanocar are capable of taking energy, in this instance a flow of electrons or photons, to induce a conformational change about the rotatable bonds and in turn bring about directional motion (**Figure 1.22**).[114]

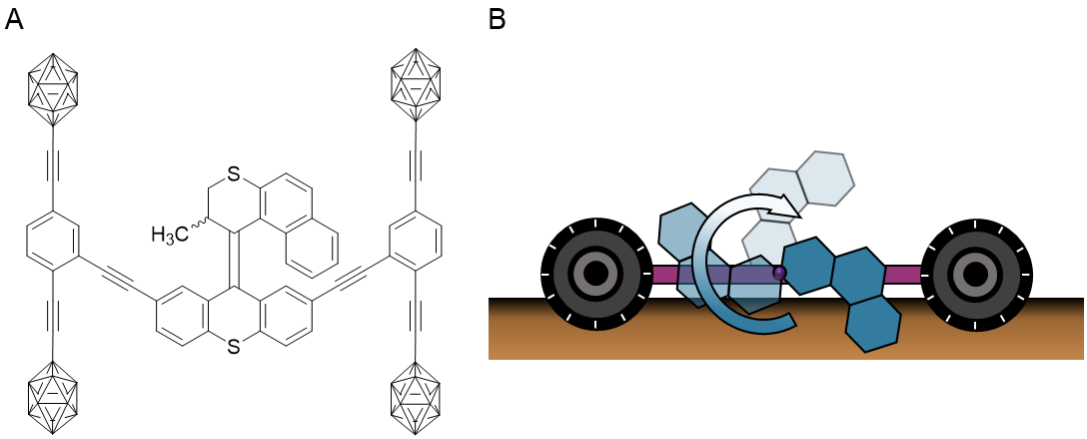

Figure 1.22: A) Structure of nanocar. The central structure is based on a Feringa style rotary motor. The body is joined by two rigid axles to four *p*-carborane wheels. B) Proposed cartoon representation of how the nanocar achieves motion. As the molecular motor (blue) undergoes photoinduced isomerisation it will rotate about the ridged axel (purple). The action of the motor against the surface would then propel the car forwards.[114]

The system has become so well developed that there are now nanocar races: the cars are raced along a 100 nm track using scanning tunnelling microscopy.[115] While this is undoubtedly an astonishing feat of chemistry and engineering, it is a prime example of a highly complex system with negligible useful work output and limited practical applications. Nonetheless, the development of light-driven molecular machines is highly desirable as they may be used bioorthogonally to living systems and provide non-invasive means of modulating the body's natural chemistries.[116-117]

Other artificial systems are being developed that arguably have a greater potential to be developed into true molecular machines with practical

applications. For example, David Leigh has been a pioneer in developing hugely intricate and synthetically sophisticated systems that emulate certain biological characteristics, a prime example of which being the development of an artificial ribosome (**Figure 1.22**).[118] The machine functions by passing a macrocycle along a molecular axle in a rotaxanated system. As the macrocycle moves between stations, the functionalised peptide thread can pick up amino acids to extend the peptide chain.

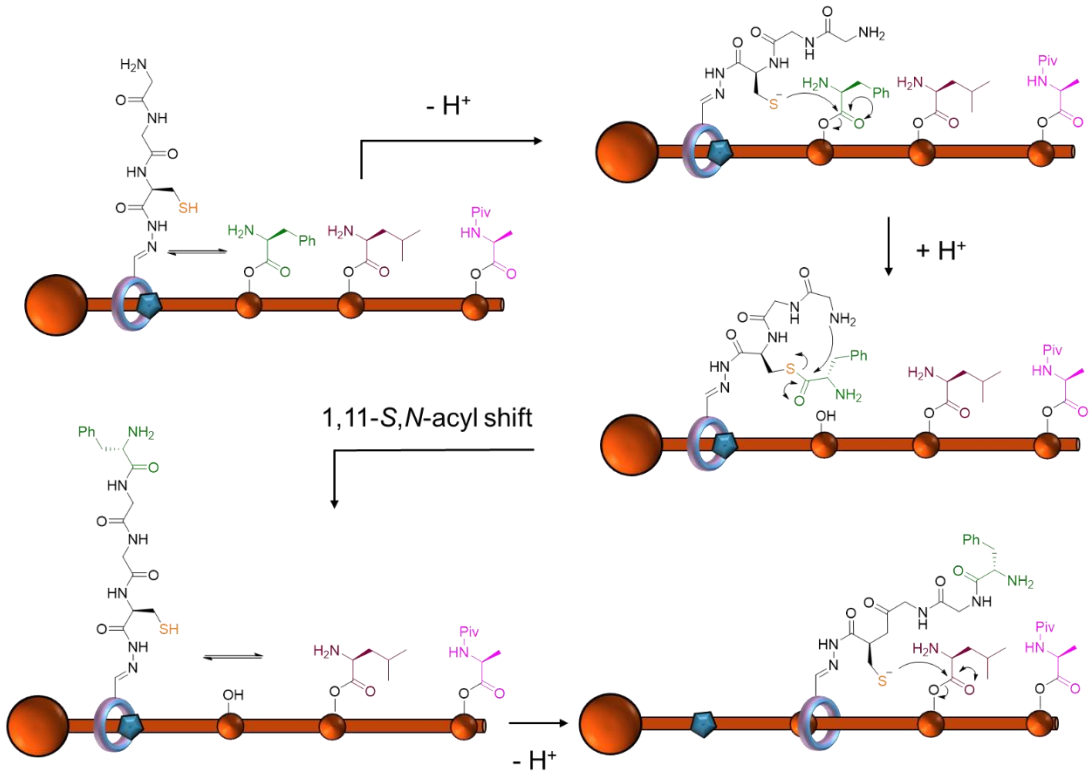

Figure 1.23: Synthetic pathway of the artificial small-molecule molecular machine. The macrocycle works its way along the molecular axle and picks up amino acids as it goes.[118]

Artificial molecular machines are a rapidly growing area with boundless potential. In the literature, a majority of artificial machine-like systems are demonstrated in the bulk.[100, 119] In contrast, in order to carry out their transport properties, biological molecular machines are often membrane bound.[120] However, that is not to say that molecular machinery must be membrane

bound to be effective. Myosins are a powerful class of motor proteins that work in partnership with actin tracks to bring about mechanical motion in humans.[121]

To extract useful work and develop artificial transmembrane devices, it is advantageous to create membrane-bound artificial systems.[122] The amalgamation of molecular machines and nanopore technology is expected to allow for further exploration of the potential of machine-like systems and even lead to the development of transmembrane molecular machines.

Membrane-bound Molecular Machines

Life relies on the existence of membrane-bond compartmentalised systems that are joined by ion channels and transporter proteins. To better study these systems, synthetic lipid bilayers have been fabricated and deployed in numerous studies.[123] In turn, research has sought to develop membrane-bound artificial molecular machines. Machines such as the artificial ribosome in the previous section, all exist in the bulk. However, there are advantages to the construct of membrane bound systems. Many biological machines, including ion transporters, are membrane bound. By replication of these systems, there lies potential treatment for channelopathies. Beyond biological systems, the movement of ions against a concentration gradient is the fundamental principle behind a voltaic cell. Therefore, the development of artificial membrane bound molecular machines has the exciting potential to realise biological batteries.

There are several examples in the literature of man-made molecular machines acting at a lipid bilayer. For example, using a Feringa-style rotary motor (**Figure 1.20**), the a machine that would physically adhere to the surface of a membrane (**Figure 1.24**) has been designed[124] Upon activation with UV light, nanomechanically induced entry into vesicles was triggered through rotation of the machine. Initial studies focused on observation of the release of boron dipyrromethene (BODIPY) from synthetic lipid vesicles. However, the group

progressed to using phase modulation nanoscopy to observe the release of BODIPY from live cells.

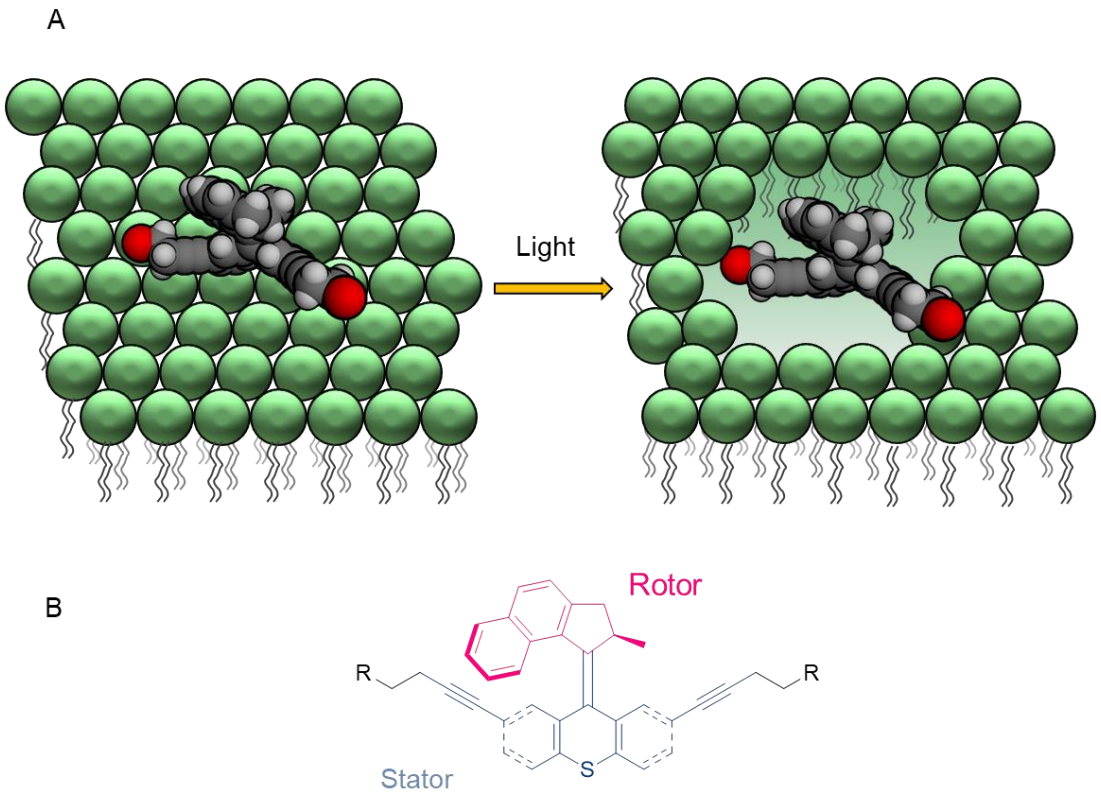

Figure 1.24: A) Representation of a solitary rotor molecule (grey) adhered to a bilayer (green). Under ambient light conditions, the motor will sit benignly on the surface of the bilayer. However, upon irradiation with UV light, nanomechanical action will disrupt in the bilayer, which ultimately ruptures the membrane. B) Core structure of the molecular machine, showing the rotor (pink) and the stator (blue) components. Each arm of the stator (R) can be functionalised with a range of peptides and fluorophores.[124]

While undoubtedly an astonishing feat, this rotor system does not provide a means of transport across the membrane. Indeed, the process would ultimately lead to cell death through lysis of the membrane. An alternative approach has been developed by Barboiu and Giuseppone. The ability of crown ethers to form ion permeable transmembrane channels has been established for several decades.[125] However, this relies on passive ion transport. By functionalising 18-crown-6 macrocycles with a Feringa-style rotary motor, the authors presented a molecular system that would

incorporated into a lipid bilayer. Upon irradiation with light, a marked acceleration in the transport of alkali metal ions was observed (**Figure 1.25A**).[126]

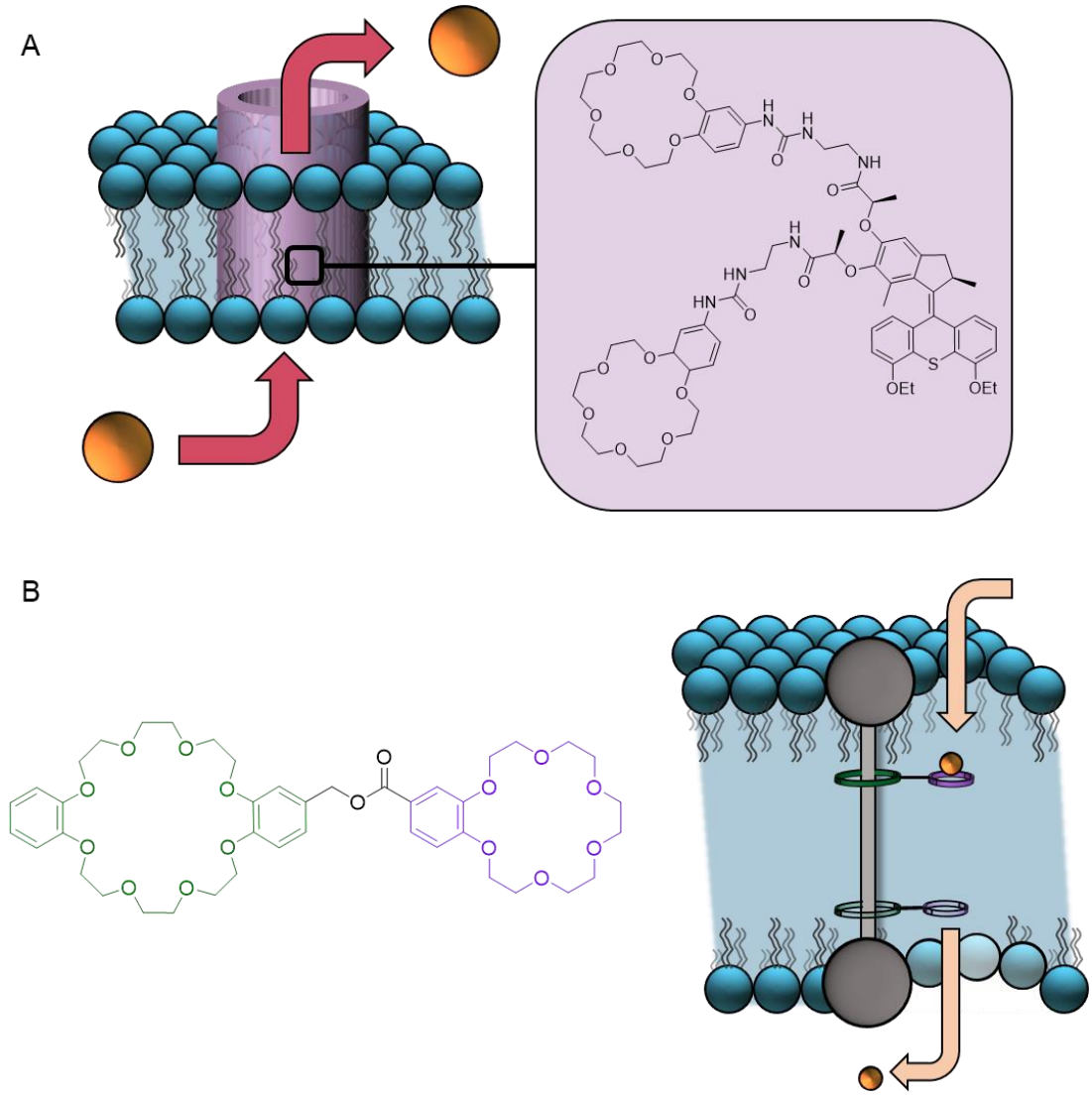

Figure 1.25: A) (left) Representation of an artificial transmembrane channel formed by 18-crown-6 functionalised rotary motors. The artificial channel (purple) spans the bilayer (blue) and allows passive diffusion of alkali metal ions (orange). (Right) The structure of the constituent molecules of the channel is shown in the enlargement. Upon irradiation with UV light, the ion transport is accelerated across the membrane.[126] B) (Left) Structure of the molecular shuttle. The dibenzo-24-crown-8 macrocycle ring component (green) tethers the shuttle to the rotaxane thread and the benzo-18-crown-6 (purple) acts as a carrier for K^+. (Right) representation of how the rotaxane axle (grey) spans the bilayer. The molecular shuttle will move between stations of the axle and accelerate passage of ions.[127]

Two compounds were synthesised: the rotary motor shown in **Figure 1.25** and a control compound, where the vital photoactuating double bond was replaced with an episulfide moiety. A 8-hydroxypyrene-1,3,6-trisulfonic acid (HPTS) fluorescence assay was deployed to monitor the transport of alkali metal ions. HPTS was encapsulated within a vesicle at pH 6.4, where the majority of the probe was in the protonated form and absorbed at 450 nm. The bulk solution was then basified with NaOH to pH 7.4, creating a pH gradient. As the intravesicular pH equalised to the bulk, HPTS was deprotonated to HPTS−. In turn, the absorption profile changed and the probe now absorbed at 405 nm. By monitoring the relative fluorescence intensity (I_{450}/I_{405}) the metal ion concentration inside the vesicle could be indirectly determined. In the absence of the motor, it was found that there was virtually no variation in the intensity over time for Na^+, K^+, or Rb^+ with or without UV irradiation. However, once the channel forming motor was introduced a steady increase was observed, with the larger metal ions passively entering the vesicle more rapidly. Upon irradiation with UV light (365 nm for 330 s) a marked increase was observed in the uptake of all metals into the vesicle. Upon analysis, it was determined that up to a 400% increase in ion uptake was achieved upon irradiation with UV light.

Rotatory motors are not the only means of forming a transmembrane machine. A rotaxane-based membrane-bound machine has enabled an elegant use of supramolecular chemistry to transport substrates across the membrane (**Figure 1.25B**).[127] The Tian group synthesised an amphiphilic rotaxane axis with a tetraethylene glycol group at each terminal end to tether it into the bilayer. On to this, a dibenzo-24-crown-8 (DB24C8) macrocycle ring was threaded that would shuttle stochastically along the axis of the rotaxane. To achieve ion transport, the K^+ benzo-18-crown-6 was tethered to the DB24C8 *via* a short ester linker. As the macrocycle shuttled along the axle, K^+ was transported across the bilayer. These systems demonstrate the recent advances in the development of constructs with characteristics that emulate the capabilities of

biological machines. However, these membrane bound machines rely on their own inherent pore forming capabilities. By exploiting naturally occurring pore forming proteins, membrane spanning machine-like systems can be devised without the added challenges of encoding channel forming properties.

An emerging direction of research is the combination of molecular machines with nanopore technology. This is of potential for several reasons. Notably, actions of the machine could be observed in real time, leading to a greater understanding of the operation of artificial machines. In addition, these membrane bound systems may present a means of harnessing the energy produced by the machine.

Pore forming toxin proteins such as α-HL form stable open channels, which are essential for their application in nanopore technologies. In nature, however, channel gating is a vital property for cell signalling that mediates the transport of ions across a membrane.[128] The application of the machine-like properties of a molecular switch in combination with supramolecular chemistry has led to the development of a voltage gated α-HL channel.[129] Under standard conditions, α-HL will rarely exhibit channel gating. However, when sulfonato-calix[4]arene (SC_4) was introduced to the *trans* side of the channel (**Figure 1.26A**) at voltages more negative than -70 mV large current blockages were observed. Based on the size of SC_4, these blockages were significantly larger than expected, leading the authors to conclude that the calixarene was forming a host-guest complex with charged residues within the lumen of the pore and inducing gating events. Upon the induction of a competitive guest, 4,4′-dipyridinium-azobenzene (V^{2+}-Az) (**Figure 1.26B**) in the *trans* isomers these gating events all but ceased. However, irradiation at λ = 365 nm induced the *cis* conformer and disrupted the host-guest relationship between V^{2+}-Az and SC_4 (**Figure 1.26C**). This reinstated the gating events of α-HL. By utilisation of a photo-driven molecular switch, a native protein channel was instilled with

controllable voltage gating properties. This presents an exciting precedent for protein channels to be repurposed to emulate other biological processes.

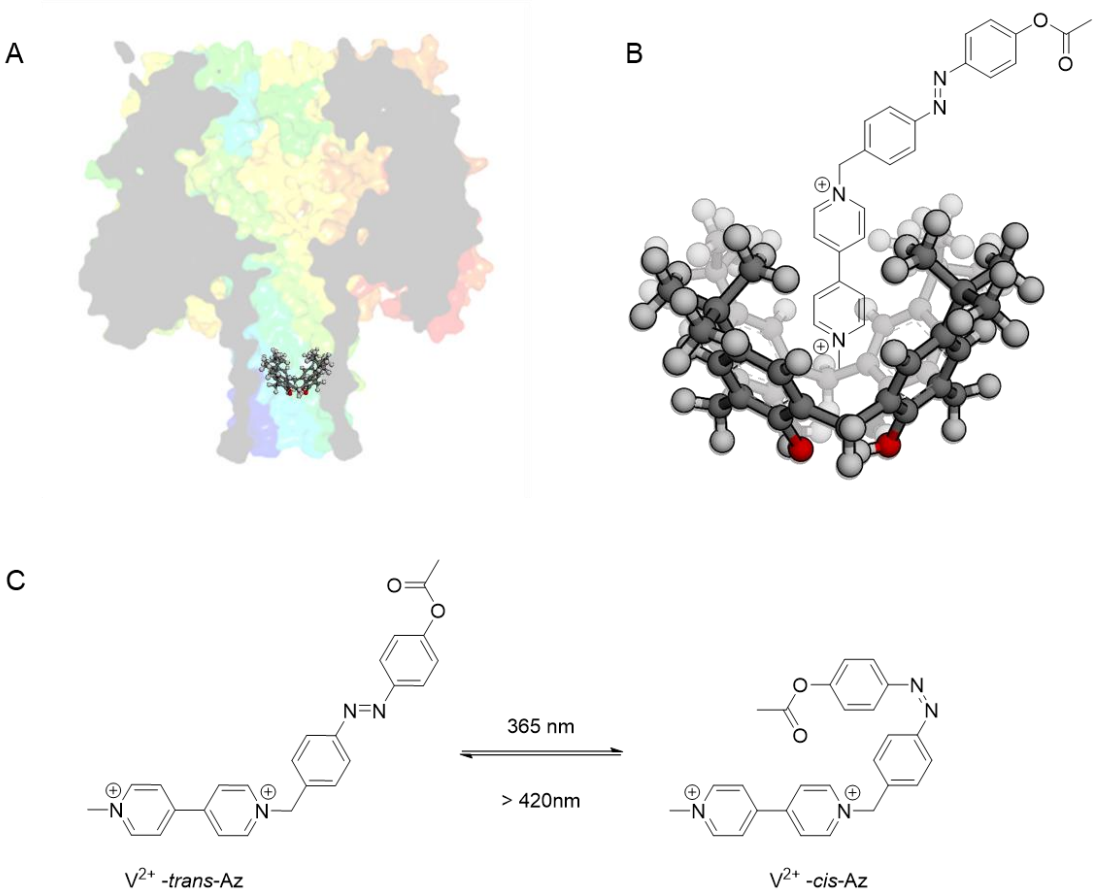

Figure 1.26: A) SC_4 sitting within the trans side of α-HL. B) V^{2+}-trans-Az sits within the cavity of SC_4 and acts as a competitive binder. In turn, this prevents the interaction of SC_4 with the protein channel. C) Photo induced isomerisation of V^{2+}-Az to the *cis* isomer. This disrupts the binding of V^{2+}-Az and SC_4 and reinstates the gating events.

Larger architectures within the pore may also be applied to develop a machine-like system. By attaching an azobenzene switch to a poly(dA)$_4$ ssDNA strand *via* a *D*-threoninol linker, a so-called molecular train was formed (**Figure 1.27**).[130] Under an applied potential, this molecular train will translocate through an aerolysin channel formed in a lipid bilayer. Upon irradiation with UV light (λ = 365 nm) for 15 minutes the bound molecular switch entered into the *cis* conformation, leading to a lower steric hindrance and more rapid translocation. With isomerisation to the *trans* state *via* irradiation at λ > 450 nm,

the steric hindrance of the DNA construct increased and the translocation of the train slowed. This photo-controlled construct presents a system with machine-like qualities within a protein nanopore. While the practical applications of this are limited at present, systems like this give a tantalising foresight into the development of biological logic systems. Indeed, DNA logic systems are becoming more prevalent in the literature and there is future potential for DNA computing systems.[131-132]

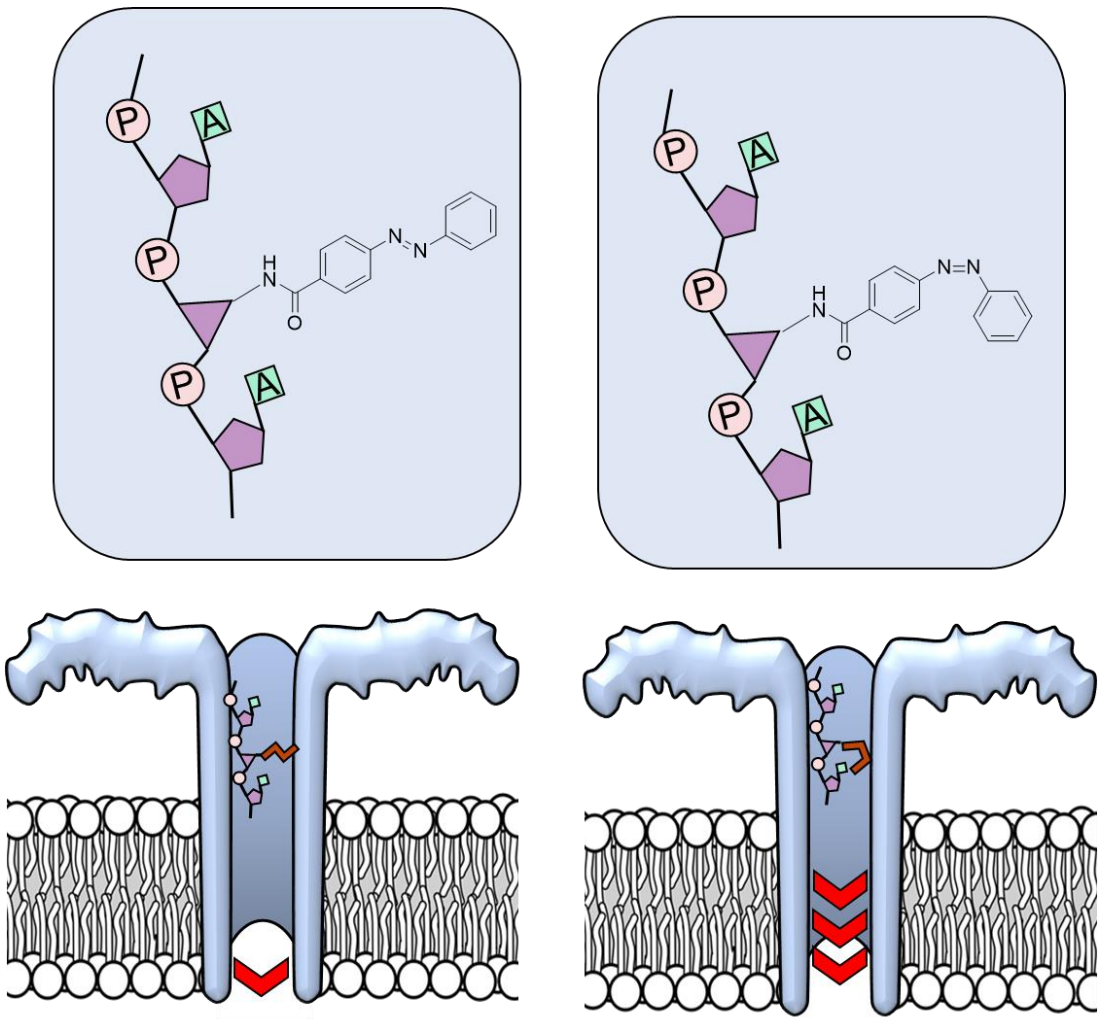

Figure 1.27: An azobenzene moiety is bound to a poly(dA) DNA strand. In the *trans* conformation (left) the molecule is more sterically hindered as it passes through an aerolysin channel (blue) This results in a slower translocation event with a greater I_b/I_o. Upon irradiation with UV light, the azobenzene will enter the *cis* conformation. Translocation events then become more rapid and with a lower I_b/I_o. This is indicative that the steric barrier has been removed and demonstrates a control over translocation of DNA.

An example of a molecular machine being used in parallel with nanopore technology comes from the Cockroft group. Using α-HL as a framework, Watson and Cockroft constructed a system capable of reciprocating nanomechanical motion (**Figure 1.28**).[133]

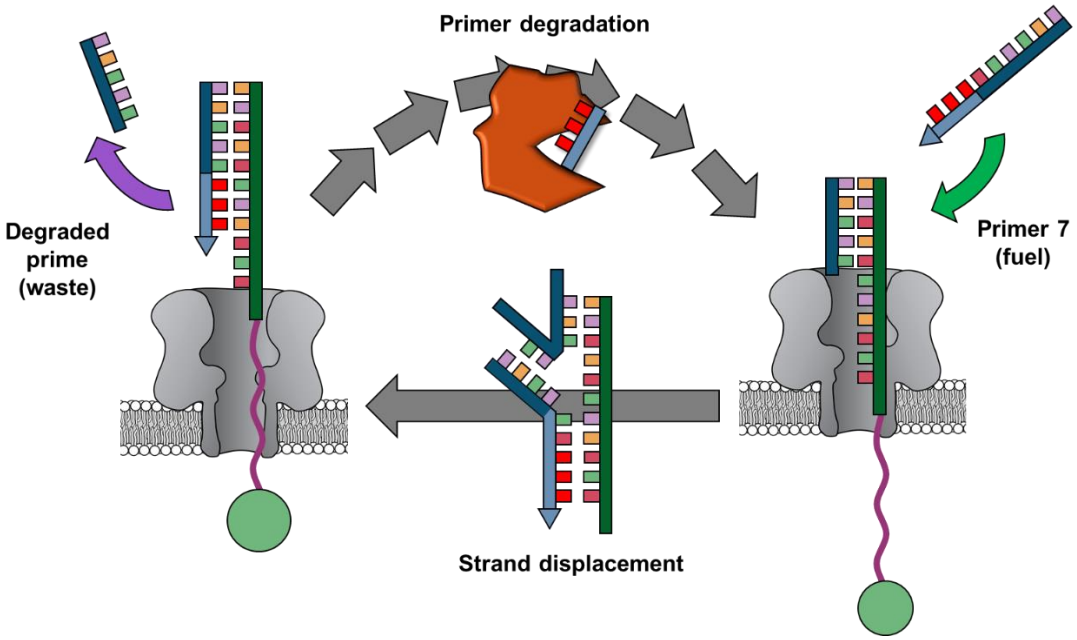

Figure 1.28: Under an applied voltage of -140 mV a DNA-PEG copolymer strand with a streptavidin cap was threaded through an α-HL nanopore. The PEG (purple) was used as a linker between the streptavidin (green) and the DNA (dark blue). The voltage was then decreased to -28 mV to allow the complementary primer strand (dark blue/light blue) to anneal. As both the streptavidin and dsDNA are too large to traverse the channel, this creates a pseudo rotaxane. An enzyme (orange) then degrades a section of the primer (red bases). This pulls the DNA strand through the channel in the direction of the applied potential and reveals a toehold binding site on the thread strand. A complementary primer 7 fuel strand is then able to anneal to the DNA thread strand. As each base pairing occurs, the DNA thread strand is pulled out of the channel in a ratchet mechanism against the applied potential. This action displaces the primer strand (dark blue), which is discarded as waste. The process begins again once the primer 7 fuel strand has fully annealed.

By monitoring stepwise changes in the observed current, the authors were able to conceptualise the mechanical motion of the machine. Under a negative applied potential, a streptavidin capped DNA-PEG copolymer was threaded through the *trans* opening of α-HL. The voltage was then made less negative to allow the complementary primer present in the *cis* well to anneal to the

threaded DNA strand. The resulting double-stranded DNA was then too large to pass back through the protein channel, creating a mechanically interlocked system. Under a positive applied potential, it was observed that enzyme-catalysed degradation, followed by strand displacement, drove a stepwise ratchet mechanism against the applied potential.

As highlighted by the authors, this presents a machine with striking similarities to biological systems: the machine consists of an interlocked architecture that uses a chemical fuel to work away from equilibrium. While it exhibits some characteristics of a molecular pump, it is yet to match the full potential of what biology has to offer.

The given examples have all relied on a sophisticated application of supramolecular chemistry in order to achieve machine-like systems. Examples of molecular machines covalently bound to a nanopore framework are, to the author's knowledge, sparse in the literature, apart from work from the Bayley group that has demonstrated the application of a modified α-HL channel as a platform for a molecular walker (Figure 1.13). However, the full potential of nanopores as frameworks for molecular machines is yet to be realised.

1.5 Conclusions

Nanopore technologies are becoming important tools for a range of single-molecule applications, with examples of nanopores being used to study proteins, bacteria, and viruses. [38, 134] Nanopores have also been used to probe chemical reactivity and kinetics at the single-molecule level.[80, 135] Future advancements in nanopore technology will require further adaptations of the technique. Research is now turning to the amalgamation of the biological and synthetic to create enhanced systems; solid-state nanopores have been functionalised with biological elements, while biological pores have been subjected to synthetic and chemical modification. Similarly, the stability and

channel-forming ability of synthetic nanopores are improving by exploiting, adapting or taking inspiration from biological macromolecules.

The development of solid-state nanopore sensors followed shortly after the initial exploitation of biological pore proteins. Solid-state nanopores present more robust, but relatively inert, frameworks for nanopore technology. On the other hand, biological proteins lack this stability, but present with anatomically precise dimensions and reactive handles. Mirroring the strategies of modifying biological nanopores, solid-state pores have been functionalised with biological molecules both to control the aperture size and to enhance molecular recognition capabilities.

Such modifications have progressed nanopore technology from being a tool for sensing, to a platform for the study of biophysics, reaction mechanisms and beyond.[27, 55, 72, 80, 136-137] Hybrid nanopore systems in handheld devices can provide rapid and sensitive diagnostic information and could prove vital in future healthcare applications. Indeed, Oxford Nanopore's MinIon was deployed during the SARS-CoV-2 pandemic for genome analysis.[138] Whether we see a growing number of chemically modified biological pores, biologically modified solid-state pores, or biologically inspired wholly synthetic pores in the future, the full potential of the technology is only just beginning to be explored.

A particularly exciting avenue research may take is the application of protein nanopores as a platform for transmembrane nanodevices. While limited in the literature, there are examples of artificial molecular machines being used in tangent with nanopore technology. This presents a powerful means of observing the action of molecular machines in real time at the single molecule level. In addition, as protein nanopores are embedded in a lipid bilayer, they provide an excellent framework for transmembrane machines.

1.6 References

1. Higgins, M. K.; Lea, S. M., On the state of crystallography at the dawn of the electron microscopy revolution. *Curr. Opin. Struct. Biol.* **2017,** *46*, 95-101.

2. Frank, J., Advances in the field of single-particle cryo-electron microscopy over the last decade. *Nat. Protoc.* **2017,** *12* (2), 209-212.

3. Deamer, D. W.; Branton, D., Characterization of Nucleic Acids by Nanopore Analysis. *Acc. Chem. Res.* **2002,** *35* (10), 817-825.

4. Don, M., The Coulter Principle: Foundation of an Industry. *JALA: Journal of the Association for Laboratory Automation* **2003,** *8* (6), 72-81.

5. Sakmann, B.; Neher, E., Patch Clamp Techniques for Studying Ionic Channels in Excitable Membranes. *Annu. Rev. Physiol.* **1984,** *46* (1), 455-472.

6. Akeson, M.; Branton, D.; Kasianowicz, J. J.; Brandin, E.; Deamer, D. W., Microsecond Time-Scale Discrimination Among Polycytidylic Acid, Polyadenylic Acid, and Polyuridylic Acid as Homopolymers or as Segments Within Single RNA Molecules. *Biophys. J.* **1999,** *77* (6), 3227-3233.

7. Neher, E.; Sakmann, B., Single-channel currents recorded from membrane of denervated frog muscle fibres. *Nature* **1976,** *260* (5554), 799-802.

8. Deamer, D.; Akeson, M.; Branton, D., Three decades of nanopore sequencing. *Nat. Biotechnol.* **2016,** *34*, 518.

9. Kasianowicz, J. J.; Brandin, E.; Branton, D.; Deamer, D. W., Characterization of individual polynucleotide molecules using a membrane channel. *PNAS* **1996,** *93* (24), 13770-13773.

10. Ying, Y.-L.; Cao, C.; Long, Y.-T., Single molecule analysis by biological nanopore sensors. *Analyst* **2014,** *139* (16), 3826-3835.

11. Bakás, L.; Ostolaza, H.; Vaz, W. L.; Goñi, F. M., Reversible adsorption and nonreversible insertion of Escherichia coli alpha-hemolysin into lipid bilayers. *Biophys. J.* **1996,** *71* (4), 1869-1876.

12. Song, L.; Hobaugh, M. R.; Shustak, C.; Cheley, S.; Bayley, H.; Gouaux, J. E., Structure of Staphylococcal α-Hemolysin, a Heptameric Transmembrane Pore. *Science* **1996,** *274* (5294), 1859-1865.

13. Füssle, R.; Bhakdi, S.; Sziegoleit, A.; Tranum-Jensen, J.; Kranz, T.; Wellensiek, H. J., On the mechanism of membrane damage by Staphylococcus aureus alpha-toxin. *J. Cell Biol.* **1981,** *91* (1), 83-94.

14. Jayasinghe, L.; Miles, G.; Bayley, H., Role of the Amino Latch of Staphylococcal α-Hemolysin in Pore Formation. *J. Biol. Chem.* **2006,** *281* (4), 2195-2204.

15. Czajkowsky, D. M.; Sheng, S.; Shao, Z., Staphylococcal α-hemolysin can form hexamers in phospholipid bilayers. *J. Mol. Biol.* **1998,** *276* (2), 325-330.

16. Kang, X.-f.; Gu, L.-Q.; Cheley, S.; Bayley, H., Single Protein Pores Containing Molecular Adapters at High Temperatures. *Angew. Chem. Int. Ed.* **2005,** *44* (10), 1495-1499.

17. Gu, L.-Q.; Bayley, H., Interaction of the Noncovalent Molecular Adapter, β-Cyclodextrin, with the Staphylococcal α-Hemolysin Pore. *Biophys. J.* **2000,** *79* (4), 1967-1975.

18. Bayley, H., Piercing insights. *Nature* **2009,** *459* (7247), 651-652.

19. Qing, Y.; Tamagaki-Asahina, H.; Ionescu, S. A.; Liu, M. D.; Bayley, H., Catalytic site-selective substrate processing within a tubular nanoreactor. *Nat. Nanotechnol* **2019,** *14* (12), 1135-1142.

20. Podobnik, M.; Kisovec, M.; Anderluh, G., Molecular mechanism of pore formation by aerolysin-like proteins. *Philos Trans R Soc Lond B Biol Sci* **2017,** *372* (1726).

21. Derrington, I. M.; Butler, T. Z.; Collins, M. D.; Manrao, E.; Pavlenok, M.; Niederweis, M.; Gundlach, J. H., Nanopore DNA sequencing with MspA. *PNAS* **2010,** *107* (37), 16060.

22. Mikheyev, A. S.; Tin, M. M. Y., A first look at the Oxford Nanopore MinION sequencer. *Mol. Ecol. Resour.* **2014,** *14* (6), 1097-1102.

23. Lindsay, S., The promises and challenges of solid-state sequencing. *Nat. Nanotechnol* **2016,** *11* (2), 109-111.

24. Fologea, D.; Uplinger, J.; Thomas, B.; McNabb, D. S.; Li, J., Slowing DNA Translocation in a Solid-State Nanopore. *Nano Lett.* **2005,** *5* (9), 1734-1737.

25. Meller, A.; Nivon, L.; Brandin, E.; Golovchenko, J.; Branton, D., Rapid nanopore discrimination between single polynucleotide molecules. *PNAS* **2000,** *97* (3), 1079.

26. Schellman, J. A., Temperature, stability, and the hydrophobic interaction. *Biophys. J.* **1997,** *73* (6), 2960-2964.

27. Ma, L.; Cockroft, S. L., Biological Nanopores for Single-Molecule Biophysics. *ChemBioChem* **2009,** *11* (1), 25-34.

28. Wu, H.-C.; Astier, Y.; Maglia, G.; Mikhailova, E.; Bayley, H., Protein Nanopores with Covalently Attached Molecular Adapters. *J. Am. Chem. Soc.* **2007,** *129* (51), 16142-16148.

29. Sakai, N.; Matile, S., Synthetic Ion Channels. *Langmuir* **2013,** *29* (29), 9031-9040.

30. Gokel, G. W.; Carasel, I. A., Biologically active, synthetic ion transporters. *Chem. Soc. Rev.* **2007,** *36* (2), 378-389.

31. Li, J.; Stein, D.; McMullan, C.; Branton, D.; Aziz, M. J.; Golovchenko, J. A., Ion-beam sculpting at nanometre length scales. *Nature* **2001,** *412* (6843), 166-169.

32. Sun, L.; Crooks, R. M., Single Carbon Nanotube Membranes: A Well-Defined Model for Studying Mass Transport through Nanoporous Materials. *J. Am. Chem. Soc.* **2000,** *122* (49), 12340-12345.

33. Storm, A. J.; Chen, J. H.; Ling, X. S.; Zandbergen, H. W.; Dekker, C., Fabrication of solid-state nanopores with single-nanometre precision. *Nat. Mater* **2003,** *2* (8), 537-540.

34. Xue, L.; Yamazaki, H.; Ren, R.; Wanunu, M.; Ivanov, A. P.; Edel, J. B., Solid-state nanopore sensors. *Nat. Rev. Mater.* **2020**.

35. Oikonomopoulos, S.; Wang, Y. C.; Djambazian, H.; Badescu, D.; Ragoussis, J., Benchmarking of the Oxford Nanopore MinION sequencing for quantitative and qualitative assessment of cDNA populations. *Sci. Rep.* **2016,** *6* (1), 31602.

36. Pérez-Mitta, G.; Burr, L.; Tuninetti, J. S.; Trautmann, C.; Toimil-Molares, M. E.; Azzaroni, O., Noncovalent functionalization of solid-state nanopores via self-assembly of amphipols. *Nanoscale* **2016,** *8* (3), 1470-1478.

37. Fragasso, A.; Schmid, S.; Dekker, C., Comparing Current Noise in Biological and Solid-State Nanopores. *ACS Nano* **2020,** *14* (2), 1338-1349.

38. Wei, R.; Gatterdam, V.; Wieneke, R.; Tampé, R.; Rant, U., Stochastic sensing of proteins with receptor-modified solid-state nanopores. *Nat. Nanotechnol* **2012,** *7* (4), 257-263.

39. Yusko, E. C.; Bruhn, B. R.; Eggenberger, O. M.; Houghtaling, J.; Rollings, R. C.; Walsh, N. C.; Nandivada, S.; Pindrus, M.; Hall, A. R.; Sept, D.; Li, J.; Kalonia, D. S.; Mayer, M., Real-time shape approximation and fingerprinting of single proteins using a nanopore. *Nat. Nanotechnol* **2017,** *12* (4), 360-367.

40. Houghtaling, J.; Ying, C.; Eggenberger, O. M.; Fennouri, A.; Nandivada, S.; Acharjee, M.; Li, J.; Hall, A. R.; Mayer, M., Estimation of Shape, Volume, and Dipole Moment of Individual Proteins Freely Transiting a Synthetic Nanopore. *ACS Nano* **2019,** *13* (5), 5231-5242.

41. Acar, E. T.; Buchsbaum, S. F.; Combs, C.; Fornasiero, F.; Siwy, Z. S., Biomimetic potassium-selective nanopores. *Sci. Adv.* **2019,** *5* (2), eaav2568.

42. Wanunu, M.; Meller, A., Chemically Modified Solid-State Nanopores. *Nano Lett.* **2007,** *7* (6), 1580-1585.

43. Tokunaga, H.; Tokunaga, M.; Nakae, T., Permeability properties of chemically modified porin trimers from Escherichia coli B. *J. Biol. Chem.* **1981,** *256* (15), 8024-8029.

44. Darveau, R. P.; Hancock, R. E. W.; Benz, R., Chemical modification of the anion selectivity of the PhoE porin from the Escherichia coli outer membrane. *Biochim. Biophys. Acta* **1984,** *774* (1), 67-74.

45. Mindell, J. A.; Zhan, H.; Huynh, P. D.; Collier, R. J.; Finkelstein, A., Reaction of diphtheria toxin channels with sulfhydryl-specific reagents: observation of chemical reactions at the single molecule level. *PNAS* **1994,** *91* (12), 5272.

46. Krishnasastry, M.; Walker, B.; Braha, O.; Bayley, H., Surface labeling of key residues during assembly of the transmembrane pore formed by staphylococcal α-hemolysin. *FEBS Lett.* **1994,** *356* (1), 66-71.

47. Ayub, M.; Bayley, H., Engineered transmembrane pores. *Curr. Opin. Chem. Biol.* **2016,** *34*, 117-126.

48. Wloka, C.; Van Meervelt, V.; Van Gelder, D.; Danda, N.; Jager, N.; Williams, C. P.; Maglia, G., Label-Free and Real-Time Detection of Protein Ubiquitination with a Biological Nanopore. *ACS Nano* **2017,** *11* (5), 4387-4394.

49. Rincon-Restrepo, M.; Mikhailova, E.; Bayley, H.; Maglia, G., Controlled Translocation of Individual DNA Molecules through Protein Nanopores with Engineered Molecular Brakes. *Nano Lett.* **2011,** *11* (2), 746-750.

50. Yusko, E. C.; An, R.; Mayer, M., Electroosmotic Flow Can Generate Ion Current Rectification in Nano- and Micropores. *ACS Nano* **2010,** *4* (1), 477-487.

51. Huang, G.; Willems, K.; Soskine, M.; Wloka, C.; Maglia, G., Electro-osmotic capture and ionic discrimination of peptide and protein biomarkers with FraC nanopores. *Nat. Commun* **2017,** *8* (1), 935.

52. Asandei, A.; Schiopu, I.; Chinappi, M.; Seo, C. H.; Park, Y.; Luchian, T., Electroosmotic Trap Against the Electrophoretic Force Near a Protein Nanopore Reveals Peptide Dynamics During Capture and Translocation. *ACS Appl. Mater. Interfaces* **2016,** *8* (20), 13166-13179.

53. Banerjee, A.; Mikhailova, E.; Cheley, S.; Gu, L.-Q.; Montoya, M.; Nagaoka, Y.; Gouaux, E.; Bayley, H., Molecular bases of cyclodextrin adapter interactions with engineered protein nanopores. *PNAS* **2010,** *107* (18), 8165.

54. Beene, D. L.; Dougherty, D. A.; Lester, H. A., Unnatural amino acid mutagenesis in mapping ion channel function. *Curr. Opin. Neurobiol.* **2003,** *13* (3), 264-270.

55. Lee, J.; Bayley, H., Semisynthetic protein nanoreactor for single-molecule chemistry. *PNAS* **2015,** *112* (45), 13768.

56. Howorka, S., Building membrane nanopores. *Nat. Nanotechnol* **2017,** *12* (7), 619-630.

57. Zhang, J.; Cao, J.; Jia, W.; Zhang, S.; Yan, S.; Wang, Y.; Zhang, P.; Chen, H.-Y.; Li, W.; Huang, S., Mapping Potential Engineering Sites of Mycobacterium smegmatis porin A (MspA) to Form a Nanoreactor. *ACS Sens.* **2021**.

58. Spicer, C. D.; Davis, B. G., Selective chemical protein modification. *Nat. Commun* **2014,** *5* (1), 4740.

59. Howorka, S.; Movileanu, L.; Braha, O.; Bayley, H., Kinetics of duplex formation for individual DNA strands within a single protein nanopore. *PNAS* **2001,** *98* (23), 12996.

60. Howorka, S.; Cheley, S.; Bayley, H., Sequence-specific detection of individual DNA strands using engineered nanopores. *Nat. Biotechnol.* **2001,** *19* (7), 636-639.

61. Chang, C.-y.; Niblack, B.; Walker, B.; Bayley, H., A photogenerated pore-forming protein. *Chem. Biol.* **1995,** *2* (6), 391-400.

62. Movileanu, L.; Cheley, S.; Howorka, S.; Braha, O.; Bayley, H., Location of a Constriction in the Lumen of a Transmembrane Pore by Targeted Covalent Attachment of Polymer Molecules. *J. Gen. Physiol.* **2001,** *117* (3), 239-252.

63. Shin, S.-H.; Luchian, T.; Cheley, S.; Braha, O.; Bayley, H., Kinetics of a Reversible Covalent-Bond-Forming Reaction Observed at the Single-Molecule Level. *Angew. Chem. Int. Ed.* **2002,** *41* (19), 3707-3709.

64. Shin, S.-H.; Bayley, H., Stepwise Growth of a Single Polymer Chain. *J. Am. Chem. Soc.* **2005,** *127* (30), 10462-10463.

65. Shin, S.-H.; Steffensen, M. B.; Claridge, T. D. W.; Bayley, H., Formation of a Chiral Center and Pyrimidal Inversion at the Single-Molecule Level. *Angew. Chem. Int. Ed.* **2007,** *46* (39), 7412-7416.

66. Steffensen, M. B.; Rotem, D.; Bayley, H., Single-molecule analysis of chirality in a multicomponent reaction network. *Nat. Chem* **2014,** *6* (7), 603-607.

67. Pulcu, G. S.; Mikhailova, E.; Choi, L.-S.; Bayley, H., Continuous observation of the stochastic motion of an individual small-molecule walker. *Nat. Nanotechnol* **2015,** *10* (1), 76-83.

68. Clarke, J.; Wu, H.-C.; Jayasinghe, L.; Patel, A.; Reid, S.; Bayley, H., Continuous base identification for single-molecule nanopore DNA sequencing. *Nat. Nanotechnol* **2009,** *4* (4), 265-270.

69. Boersma, A. J.; Brain, K. L.; Bayley, H., Real-Time Stochastic Detection of Multiple Neurotransmitters with a Protein Nanopore. *ACS Nano* **2012,** *6* (6), 5304-5308.

70. Boersma, A. J.; Bayley, H., Continuous Stochastic Detection of Amino Acid Enantiomers with a Protein Nanopore. *Angew. Chem. Int. Ed.* **2012,** *51* (38), 9606-9609.

71. Luchian, T.; Shin, S.-H.; Bayley, H., Kinetics of a Three-Step Reaction Observed at the Single-Molecule Level. *Angew. Chem. Int. Ed.* **2003,** *42* (17), 1926-1929.

72. Qing, Y.; Pulcu, G. S.; Bell, N. A. W.; Bayley, H., Bioorthogonal Cycloadditions with Sub-Millisecond Intermediates. *Angew. Chem. Int. Ed.* **2018,** *57* (5), 1218-1221.

73. Qing, Y.; Ionescu, S. A.; Pulcu, G. S.; Bayley, H., Directional control of a processive molecular hopper. *Science* **2018,** *361* (6405), 908.

74. Qing, Y.; Bayley, H., Enzymeless DNA Base Identification by Chemical Stepping in a Nanopore. *J. Am. Chem. Soc.* **2021,** *143* (43), 18181-18187.

75. Loudwig, S.; Bayley, H., Photoisomerization of an Individual Azobenzene Molecule in Water: An On−Off Switch Triggered by Light at a Fixed Wavelength. *J. Am. Chem. Soc.* **2006,** *128* (38), 12404-12405.

76. Qing, Y.; Liu, M. D.; Hartmann, D.; Zhou, L.; Ramsay, W. J.; Bayley, H., Single-Molecule Observation of Intermediates in Bioorthogonal 2-Cyanobenzothiazole Chemistry. *Angew. Chem. Int. Ed.* **2020,** *59* (36), 15711-15716.

77. Iacovache, I.; De Carlo, S.; Cirauqui, N.; Dal Peraro, M.; Van Der Goot, F. G.; Zuber, B., Cryo-EM structure of aerolysin variants reveals a novel protein fold and the pore-formation process. *Nat. Commun* **2016,** *7* (1), 12062.

78. Cao, C.; Cirauqui, N.; Marcaida, M. J.; Buglakova, E.; Duperrex, A.; Radenovic, A.; Dal Peraro, M., Single-molecule sensing of peptides and nucleic acids by engineered aerolysin nanopores. *Nat. Commun* **2019,** *10* (1).

79. Lucas, F. L. R.; Sarthak, K.; Lenting, E. M.; Coltan, D.; Van Der Heide, N. J.; Versloot, R. C. A.; Aksimentiev, A.; Maglia, G., The Manipulation of the Internal Hydrophobicity of FraC Nanopores Augments Peptide Capture and Recognition. *ACS Nano* **2021,** *15* (6), 9600-9613.

80. Haugland, M. M.; Borsley, S.; Cairns-Gibson, D. F.; Elmi, A.; Cockroft, S. L., Synthetically Diversified Protein Nanopores: Resolving Click Reaction Mechanisms. *ACS Nano* **2019**.

81. Borsley, S.; Cockroft, S. L., In Situ Synthetic Functionalization of a Transmembrane Protein Nanopore. *ACS Nano* **2018,** *12* (1), 786-794.

82. Lin, S.; Yang, X.; Jia, S.; Weeks, A. M.; Hornsby, M.; Lee, P. S.; Nichiporuk, R. V.; Iavarone, A. T.; Wells, J. A.; Toste, F. D.; Chang, C. J., Redox-based reagents for chemoselective methionine bioconjugation. *Science* **2017,** *355* (6325), 597.

83. Iqbal, S. M.; Akin, D.; Bashir, R., Solid-state nanopore channels with DNA selectivity. *Nat. Nanotechnol* **2007,** *2* (4), 243-248.

84. Mussi, V.; Fanzio, P.; Repetto, L.; Firpo, G.; Scaruffi, P.; Stigliani, S.; Tonini, G. P.; Valbusa, U., DNA-functionalized solid state nanopore for biosensing. *Nanotechnology* **2010,** *21* (14), 145102.

85. Mussi, V.; Fanzio, P.; Repetto, L.; Firpo, G.; Stigliani, S.; Tonini, G. P.; Valbusa, U., "DNA-Dressed NAnopore" for complementary sequence detection. *Biosensors and Bioelectronics* **2011,** *29* (1), 125-131.

86. Hall, A. R.; Scott, A.; Rotem, D.; Mehta, K. K.; Bayley, H.; Dekker, C., Hybrid pore formation by directed insertion of α-haemolysin into solid-state nanopores. *Nat. Nanotechnol* **2010,** *5* (12), 874-877.

87. Hernández-Ainsa, S.; Keyser, U. F., DNA origami nanopores: developments, challenges and perspectives. *Nanoscale* **2014,** *6* (23), 14121-14132.

88. Castro, C. E.; Kilchherr, F.; Kim, D.-N.; Shiao, E. L.; Wauer, T.; Wortmann, P.; Bathe, M.; Dietz, H., A primer to scaffolded DNA origami. *Nat. Methods* **2011,** *8* (3), 221-229.

89. Wei, R.; Martin, T. G.; Rant, U.; Dietz, H., DNA Origami Gatekeepers for Solid-State Nanopores. *Angew. Chem. Int. Ed.* **2012,** *51* (20), 4864-4867.

90. Schmid, S.; Stömmer, P.; Dietz, H.; Dekker, C., Nanopore electro-osmotic trap for the label-free study of single proteins and their conformations. *Nat. Nanotechnol* **2021,** *16* (11), 1244-1250.

91. Brinkerhoff, H.; Kang, A. S. W.; Liu, J.; Aksimentiev, A.; Dekker, C., Multiple rereads of single proteins at single-amino acid resolution using nanopores. *Science* **2021,** *0* (0), eabl4381.

92. Thomson, A. R.; Wood, C. W.; Burton, A. J.; Bartlett, G. J.; Sessions, R. B.; Brady, R. L.; Woolfson, D. N., Computational design of water-soluble α-helical barrels. *Science* **2014,** *346* (6208), 485-488.

93. Mahendran, K. R.; Niitsu, A.; Kong, L.; Thomson, A. R.; Sessions, R. B.; Woolfson, D. N.; Bayley, H., A monodisperse transmembrane α-helical peptide barrel. *Nat. Chem* **2017,** *9* (5), 411-419.

94. Ho, C. W.; Van Meervelt, V.; Tsai, K. C.; De Temmerman, P. J.; Mast, J.; Maglia, G., Engineering a nanopore with co-chaperonin function. *Sci Adv* **2015,** *1* (11), e1500905.

95. Zhang, S.; Huang, G.; Versloot, R. C. A.; Bruininks, B. M. H.; de Souza, P. C. T.; Marrink, S.-J.; Maglia, G., Bottom-up fabrication of a proteasome–nanopore that unravels and processes single proteins. *Nat. Chem* **2021**.

96. Bickerton, L. E.; Johnson, T. G.; Kerckhoffs, A.; Langton, M. J., Supramolecular chemistry in lipid bilayer membranes. *Chem. Sci.* **2021,** *12* (34), 11252-11274.

97. Gokel, G. W.; Carasel, I. A., Biologically active, synthetic ion transporters. *Chem. Soc. Rev.* **2007,** *36* (2), 378-389.

98. Watson, M. A.; Cockroft, S. L., Man-made molecular machines: membrane bound. *Chem. Soc. Rev.* **2016,** *45* (22), 6118-6129.

99. Kay, E. R.; Leigh, D. A.; Zerbetto, F., Synthetic molecular motors and mechanical machines. *Angew. Chem. Int. Ed. Engl.* **2007,** *46* (1-2), 72-191.

100. Erbas-Cakmak, S.; Leigh, D. A.; McTernan, C. T.; Nussbaumer, A. L., Artificial Molecular Machines. *Chem. Rev.* **2015,** *115* (18), 10081-10206.

101. van Delden, R. A.; ter Wiel, M. K. J.; Pollard, M. M.; Vicario, J.; Koumura, N.; Feringa, B. L., Unidirectional molecular motor on a gold surface. *Nature* **2005,** *437* (7063), 1337-1340.

102. Urban, P. L., Compartmentalised chemistry: from studies on the origin of life to engineered biochemical systems. *New J. Chem.* **2014,** *38* (11), 5135-5141.

103. Bartel, D. P.; Unrau, P. J., Constructing an RNA world. *Trends Cell Biol.* **1999,** *9* (12), M9-M13.

104. Orgel, L. E., Some Consequences of the RNA World Hypothesis. *Origins Life Evol. Biosphere* **2003,** *33* (2), 211-218.

105. Tirard, S., J. B. S. Haldane and the origin of life. *J Genet* **2017,** *96* (5), 735-739.

106. Lane, N.; Allen, J. F.; Martin, W., How did LUCA make a living? Chemiosmosis in the origin of life. *Bioessays* **2010,** *32* (4), 271-280.

107. Cole, L. A., Chapter 10 - Adenosine Triphosphate Energetics. In *Biology of Life*, Cole, L. A., Ed. Academic Press: 2016; pp 65-77.

108. Spirin, A. S., Ribosome as a molecular machine. *FEBS Lett.* **2002,** *514* (1), 2-10.

109. de la Cruz, J.; Karbstein, K.; Woolford, J. L., Functions of Ribosomal Proteins in Assembly of Eukaryotic Ribosomes In Vivo. *Annu. Rev. of Biochem.* **2015,** *84* (1), 93-129.

110. Leigh, D. A., Genesis of the Nanomachines: The 2016 Nobel Prize in Chemistry. *Angew. Chem. Int. Ed.* **2016,** *55* (47), 14506-14508.

111. Badjić, J. D.; Balzani, V.; Credi, A.; Silvi, S.; Stoddart, J. F., A Molecular Elevator. *Science* **2004,** *303* (5665), 1845.

112. Bruns, C. J.; Stoddart, J. F., Rotaxane-Based Molecular Muscles. *Acc. Chem. Res.* **2014,** *47* (7), 2186-2199.

113. Leigh, D. A.; Wong, J. K. Y.; Dehez, F.; Zerbetto, F., Unidirectional rotation in a mechanically interlocked molecular rotor. *Nature* **2003,** *424* (6945), 174-179.

114. Morin, J.-F.; Shirai, Y.; Tour, J. M., En Route to a Motorized Nanocar. *Org. Lett.* **2006,** *8* (8), 1713-1716.

115. Rapenne, G.; Joachim, C., The first nanocar race. *Nat. Rev. Mater.* **2017,** *2*, 17040.

116. van Dijken, D. J.; Kovaříček, P.; Ihrig, S. P.; Hecht, S., Acylhydrazones as Widely Tunable Photoswitches. *J. Am. Chem. Soc.* **2015,** *137* (47), 14982-14991.

117. Velema, W. A.; Szymanski, W.; Feringa, B. L., Photopharmacology: Beyond Proof of Principle. *J. Am. Chem. Soc.* **2014,** *136* (6), 2178-2191.

118. Lewandowski, B.; De Bo, G.; Ward, J. W.; Papmeyer, M.; Kuschel, S.; Aldegunde, M. J.; Gramlich, P. M. E.; Heckmann, D.; Goldup, S. M.; D'Souza, D. M.; Fernandes, A. E.; Leigh, D. A., Sequence-Specific Peptide Synthesis by an Artificial Small-Molecule Machine. *Science* **2013,** *339* (6116), 189.

119. Balzani, V.; Credi, A.; Raymo, F. M.; Stoddart, J. F., Artificial Molecular Machines. *Angew. Chem. Int. Ed.* **2000,** *39* (19), 3348-3391.

120. Roux, B., *Molecular Machines*. World Scientific Publishing Company: 2011.

121. Squire, J. M., Muscle contraction: Sliding filament history, sarcomere dynamics and the two Huxleys. *Glob Cardiol Sci Pract* **2016,** *2016* (2), e201611.

122. Aprahamian, I., The Future of Molecular Machines. *ACS Cent. Sci.* **2020,** *6* (3), 347-358.

123. Mosgaard, L. D.; Heimburg, T., Lipid Ion Channels and the Role of Proteins. *Acc. Chem. Res.* **2013,** *46* (12), 2966-2976.

124. García-López, V.; Chen, F.; Nilewski, L. G.; Duret, G.; Aliyan, A.; Kolomeisky, A. B.; Robinson, J. T.; Wang, G.; Pal, R.; Tour, J. M., Molecular machines open cell membranes. *Nature* **2017,** *548* (7669), 567-572.

125. Meillon, J.-C.; Voyer, N., A Synthetic Transmembrane Channel Active in Lipid Bilayers. *Angew. Chem. Int. Ed.* **1997,** *36* (9), 967-969.

126. Wang, W.-Z.; Huang, L.-B.; Zheng, S.-P.; Moulin, E.; Gavat, O.; Barboiu, M.; Giuseppone, N., Light-Driven Molecular Motors Boost the Selective Transport of Alkali Metal Ions through Phospholipid Bilayers. *J. Am. Chem. Soc.* **2021,** *143* (38), 15653-15660.

127. Chen, S.; Wang, Y.; Nie, T.; Bao, C.; Wang, C.; Xu, T.; Lin, Q.; Qu, D.-H.; Gong, X.; Yang, Y.; Zhu, L.; Tian, H., An Artificial Molecular Shuttle Operates in Lipid Bilayers for Ion Transport. *J. Am. Chem. Soc.* **2018,** *140* (51), 17992-17998.

128. Terlau, H.; Stühmer, W., Structure and function of voltage-gated ion channels. *Naturwissenschaften* **1998,** *85* (9), 437-44.

129. Ying, Y.-L.; Zhang, J.; Meng, F.-N.; Cao, C.; Yao, X.; Willner, I.; Tian, H.; Long, Y.-T., A Stimuli-Responsive Nanopore Based on a Photoresponsive Host-Guest System. *Sci. Rep.* **2013,** *3* (1), 1662.

130. Ying, Y.-L.; Li, Z.-Y.; Hu, Z.-L.; Zhang, J.; Meng, F.-N.; Cao, C.; Long, Y.-T.; Tian, H., A Time-Resolved Single-Molecular Train Based on Aerolysin Nanopore. *Chem* **2018,** *4* (8), 1893-1901.

131. Bader, A.; Cockroft, S. L., Simultaneous G-Quadruplex DNA Logic. *Chem. Eur. J.* **2018,** *24* (19), 4820-4824.

132. Ogihara, M.; Ray, A., Simulating Boolean Circuits on a DNA Computer. *Algorithmica* **1999,** *25* (2), 239-250.

133. Watson, M. A.; Cockroft, S. L., An Autonomously Reciprocating Transmembrane Nanoactuator. *Angew. Chem. Int. Ed.* **2016,** *55* (4), 1345-1349.

134. McMullen, A.; de Haan, H. W.; Tang, J. X.; Stein, D., Stiff filamentous virus translocations through solid-state nanopores. *Nat. Commun* **2014,** *5* (1), 4171.

135. Ramsay, W. J.; Bell, N. A. W.; Qing, Y.; Bayley, H., Single-Molecule Observation of the Intermediates in a Catalytic Cycle. *J. Am. Chem. Soc.* **2018,** *140* (50), 17538-17546.

136. Li, M.; Rauf, A.; Guo, Y.; Kang, X., Real-Time Label-Free Kinetics Monitoring of Trypsin-Catalyzed Ester Hydrolysis by a Nanopore Sensor. *ACS Sens.* **2019,** *4* (11), 2854-2857.

137. Willems, K.; Van Meervelt, V.; Wloka, C.; Maglia, G., Single-molecule nanopore enzymology. *Philosophical Transactions of the Royal Society B: Biol. Sci.* **2017,** *372* (1726), 20160230.

138. Bull, R. A.; Adikari, T. N.; Ferguson, J. M.; Hammond, J. M.; Stevanovski, I.; Beukers, A. G.; Naing, Z.; Yeang, M.; Verich, A.; Gamaarachchi, H.; Kim, K. W.; Luciani, F.; Stelzer-Braid, S.; Eden, J.-S.; Rawlinson, W. D.; Van Hal, S. J.; Deveson, I. W., Analytical validity of nanopore sequencing for rapid SARS-CoV-2 genome analysis. *Nat. Commun* **2020,** *11* (1).

Chapter 2

Cucurbituril Catalysis at the Single-Molecule Level

Abstract

Supramolecular catalysis is a growing field that seeks to develop enzyme mimetics. While the catalytic capabilities of a wide range of supramolecular systems have been established, precise details of the mechanisms of these reactions are not always known. By application of nanopore technology, reaction mechanisms and kinetics can be elucidated on the single-molecule level. Herein, we explore CB[7]-catalysed Diels-Alder reactions using a protein nanopore. The binding events of CB[7] with an α-HL nanopore were first explored in a range of buffer conditions. It was determined that optimal binding for application as a molecular adapter occurred in a 2 M KCl buffer, as this provided well defined binding events with second long durations. Using this optimised system, an intramolecular Diels-Alder reaction was investigated. It was found that unique signals could be detected upon the addition of a Diels-Alder reagent.

Contributons: Work in this chapter was completed in colabration with Prof Oren Sherman, University of Cambridge. Initial samples of compunds were provided by Prof Sherman, and subsequent samples (except curcubiturils) were synthesised by DCG. All nanopore experimental work was performed by DCG.

2.1 Introduction

Catalysis is instrumental to life. The term was first coined in 1835 by Jöns Jacob Berzelius, but the murky history dates back further to pioneering works by Davy, Désormes, Clément and Fulhame.[1] Biocatalysts, otherwise known as enzymes, are complex protein molecules that catalyse reactions in biological systems. Extensive research effort has been directed towards the synthesis of artificial enzymes but these studies are in relatively rudimentary stages when compared with what nature has to offer. Due to the complex character of enzymes, it is often beneficial to study small-molecule analogues that emulate some of the characteristics of the active site of the enzyme.[2] Often these molecules fall in to the category of supramolecular catalysts, which themselves are garnering growing interest.[3]

Supramolecular chemistry is the study of how non-covalent interactions dictate the behaviour of molecular assemblies.[4] Jean-Marie Lehn was awarded the 1987 Nobel Prize in chemistry for his work in supramolecular chemistry – in particular for the development of cryptands.[5] While cryptands have seen extensive application in industrial processes, there are limited reports of catalytic applications. However, cyclodextrin (CD) and cucurbituril (CB[n]) hosts have been developed more recently and are among those exhibiting catalytic capabilities.[6]

Constrictive binding was a term coined in the early 1990s by Donald Cram.[7] It described a host-guest complex where a high-energy barrier to decomplexation provided a mechanical barrier to the dissociation of the molecules.[8] It was hypothesised that this created a system whereby there is a different phase inside the rigid host molecule compared to the bulk solution.[7] At the time, Cram suggested that this property could stabilise molecules that

would otherwise be too reactive to be in the bulk. It was later realised that rigid molecular containers could be used as enzyme mimetics. Much like their enzymatic counterparts, supramolecular catalysts rely on arranging and orientating reactive groups through non-covalent interactions into a proximity that favours bond making and breaking reactions.[9-10] Such pre-organisation can be considered as providing an entropic benefit to lower the activation energy of a reaction.

Similarly, protein nanopores present a confined space, which has led to the development of so-called 'nanoreactors'.[11-12] Within the cavity of the nanoreactor, reactions can be observed in real time at the single-molecule level.[13] However, there are often issues with compatibility when it comes to nanopore studies. If the analyte passes too rapidly through the channel, or is of an incomparable size, there will be insufficient temporal or special resolution for detection. In addition, many chemical reactions involve reagents that are insoluble in aqueous solvents required for biological nanopores. The utilisation of supramolecular host molecules as molecular adapters presents an elegant solution to these caveats.[14-16]

Cyclodextrins (CDs) are macrocyclic molecules first described by Villeiers over 100 years ago.[17] CDs have been established as enzyme mimetics, as their hydrophobic interior cavity can accommodate small molecules and catalyse reactions.[6] The Bayley group have established methods of covalently attaching CD to an α-HL nanopore for stochastic sensing and DNA sequencing (**Figure 2.1**).[16, 18] This involved the incorporation of a single cysteine mutant to an α-HL channel followed by synthetic modification (**Figure 1.12**, **Chapter 1**). As the modification of macrocycles can be somewhat challenging, cyclic peptides have also been used as molecular adapters.[19] While these can be more easily functionalised with tethering side groups, their application has had limited success. Covalent attachment provides a robust and long-lived system for sensing, but molecular adapters do not need to be covalently bond to the

pore to be effective. Indeed, non-covalent molecular adapters have unique benefits over their bound counterparts. β-CD has been demonstrated on several occasions as a non-covalent molecular adapter for sensing.[14, 20] More recently, the Maglia group established that enzymes could be reversibly trapped within a ClyA nanopore.[21] These proteins retained their ability to bind ligand molecules. While the trapping of enzymes is possible in larger nanopores such as ClyA, the smaller α-HL channel does not have the capacity to trap large proteins.

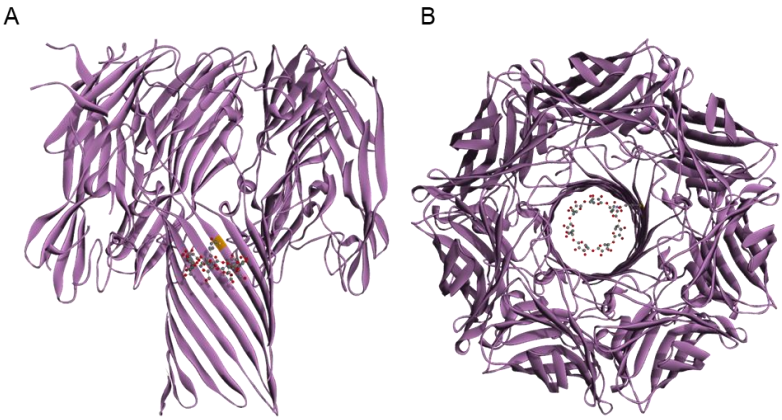

Figure 2.1: β-Cyclodextrin (β-CD) attached to an α-HL pore. This was achieved by the addition of a reactive linker to CD and the incorporation of a cysteine residue at position 113 of α-HL.[16] Attachment could also be achieved at mutant cysteine residues in positions 119, 121, 123, 135 and 137.[18] A) shows a side view and B) a top down view.

The application of non-covalently bound molecular adapters in a protein nanopore present several advantages. Namely, it circumvents the arduous requirement to modify and covalently attach molecules to the pore. In addition, it has the scope to create systems that are more versatile. Host-guest interactions will often be highly specific and if a single host is permanently bound then the remit of detectable analytes is restricted. By utilising non-covalent systems, the host can be more easily varied and a wider range of analytes can be detected. Of course, this must be caveated with the fact that non-covalent molecular adapters will most likely have a shorter dwell time

than their covalent counterparts. However, this may not always be detrimental if the dwell time of the binding event is sufficiently long lived.

While CDs have both been used as molecular adapters and have proven catalytic qualities, they often lack selectivity and high affinity for substrates.[22] Although this may not be disastrous in the industrial processes in which they are favoured, this lack of specificity is non-ideal for single-molecule studies. Therefore, alternative adapters have been explored. Cucurbiturils (CB[n]) are another well-established class of molecules with host-guest capabilities.[23-24] The macrocycles have been reported from as early as 1905, where it was understood that a condensation product was formed between glycoluril and formaldehyde.[25] However, it was not until 1981 that the first homologue was successfully crystallised and characterised to reveal the pumpkin-like shape that the molecule derives its name from.[26]. In addition to their capabilities for molecular recognition and formation of host-guest complexes, the macrocycles act as supramolecular catalysts by bringing reactive groups into close proximity and catalysing the reaction.[22, 27] This is often achieved through the energetically favoured encapsulation of a guest within the hydrophobic cavity of the molecule (**Figure 2.2**).

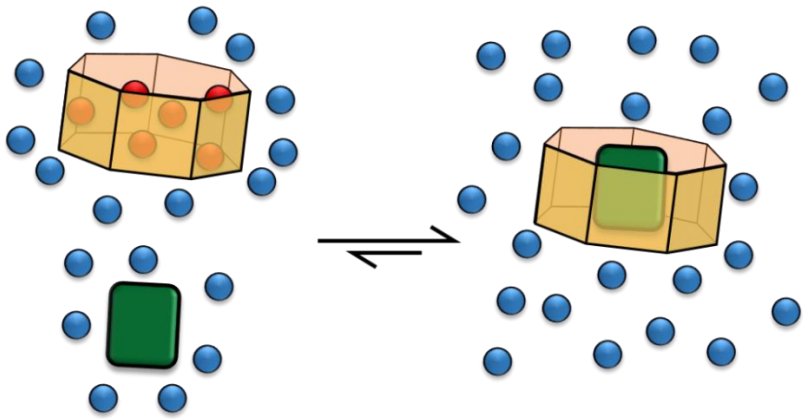

Figure 2.2: (Left) High-energy water inside the hydrophobic cavity is energetically disfavoured while the guest is solvated in the bulk solution. (Right) the guest is desolvated and forms a more stable host-guest complex with CB[n] and the previously high-energy water enters a favoured lower energy state in the bulk.

Previous applications of molecular adapters in nanopores have centred on sensing applications. Herein, we present an approach to utilise sensing and apply CB[7] as a molecular adapter for real-time observations of catalytic turnover.

2.2 Project Aims

Supramolecular catalysis is a growing field, yet the mechanisms by which it operates are not always fully understood. Nanopore technology has repeatedly been demonstrated to provide powerful insight into reaction mechanisms at the single-molecule level. Herein, we explore the exploitation of nanopore technology to study single-molecule catalysis.

The overarching aim of this project was to observe the catalytic turnover of an intramolecular Diels-Alder reaction at the single-molecule level. Through this, it was hoped to develop insight into the reaction pathway and develop a protocol by with other examples of supramolecular catalysis could be characterised. By extension, the project aimed to optimise of the capture of a supramolecular adapter in a protein nanopore for its utilisation in single-molecule catalysis.

2.3 Single-molecule sensing of cucurbituril

Cucurbituril as a Molecular Adapter

Cucurbiturils are macrocyclic hosts, which are synthesised by a condensation reaction between glycoluril and formaldehyde (**Figure 2.3A**).[24] The molecules range in size from the diminutive CB[5] to the comparatively cavernous CB[16] (**Figure 2.3**).[28-30] While the smaller homologues retain a relatively ridged structure, larger variants will exhibit some conformational distortion (**Figure 2.3**). Indeed, once the series surpasses CB[14], a twisted conformation is often adopted.[29, 31]

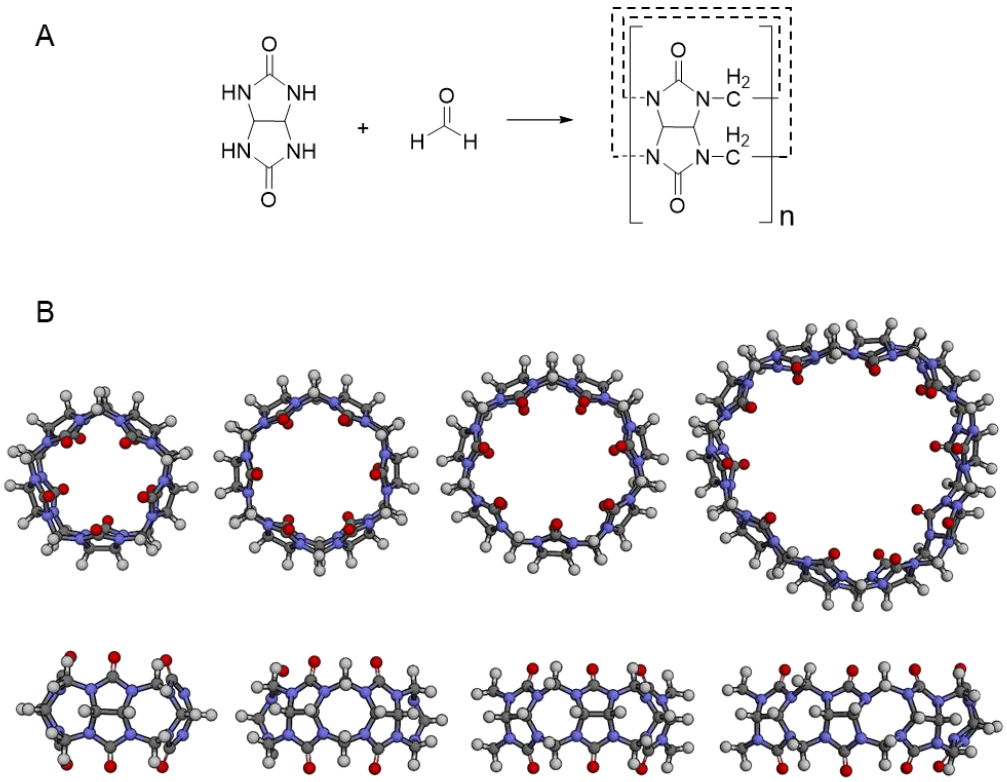

Figure 2.3: A) Scheme for the synthesis of CB[n] from glycoluril and formaldehyde. Depending on the conditions applied, there will be n-number of repeating units in the final product. B) Structures of CB[n] homologues. Equilibrium geometries at the ground state were calculated using Spartan 14 at PM3 (semi-empirical) and visualised using Discovery Studio Visualizer. CB[5], CB[6], and CB[7] (Left-to-right) all show a ridged and regular structure, whereas CB[10] (far right) exhibits signs of distortion.

CB[7] is an incredibly powerful host. It has previously been demonstrated that the host-guest complex between acriflavine and CB[7] boasts a K_a of 7.2×10^{17} M^{-1} in D_2O[32] – rivalling that of avidin-biotin.[33] A wide range of compounds will bind to CB[7] with high affinity (**Figure 2.4).** However, water solubility is often an issue with many of these compounds. This factor must be considered in the context of nanopore technology, as any system to be studied must exhibit a degree of water solubility.

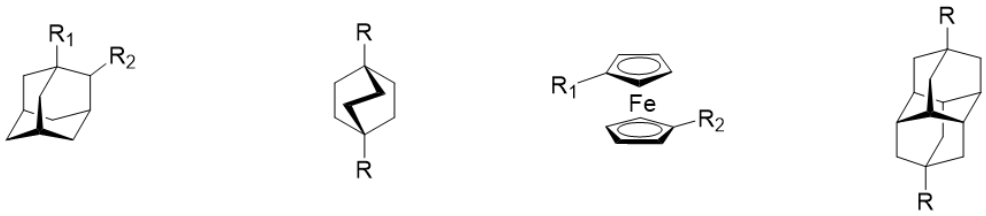

A			B		C			D	
	R_1	R_2		R		R_1	R_2		R
A1	-H	-H	B1	$-CH_2OH$	C1	-H	-H	D1	-H
A2	-OH	-H	B2	$-CH_2NH_3^+$	C2	$-CH_2OH$	-H	D2	NH_3^+
A3	$-NH_3^+$	-H			C3	$-CH_2NHMe_2^+$	-H	D3	$-NMe_3^+$
A4	-H	$-NH_3^+$			C4	$-CH_2NMe_3^+$	-H		
A5	$-CH_2NH_3^+$	-H			C5	$-CH_2NMe_3^+$	$-CH_2NMe_3^+$		
A6	$-NMe_3^+$	-H							

Figure 2.4: Examples of various tight binders of CB[7]. Adapted from [34].

In addition to being excellent hosts, CB[n] analogues are catalysts. While CB[5] is generally too small to act as a catalyst, other homologues have been used extensively. CB[6] and CB[7] have catalytic properties and are generally better suited to intramolecular reactions or reactions between small molecules. The larger CB[8] is can accommodate much bigger molecules and will favour bimolecular reactions.[35] Observations of the catalytic capabilities of cucurbituril

date back decades, with Mock and co-workers demonstrating that 1,3-dipolar azide-alkyne cycloadditions (AAC) could be catalysed by CB[6] (**Figure 2.5**).[36]

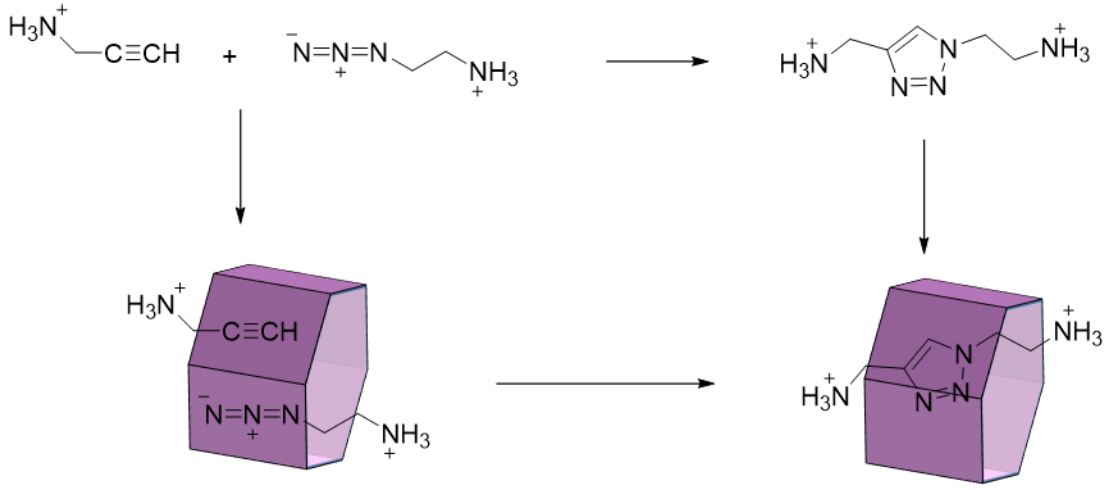

Figure 2.5: Intermolecular AAC reaction catalysed by CB[6] (purple). The alkyne and the azide are brought into proximity by the formation of a trimolecular host-guest complex. The preferential spatial arrangement and exclusion of water facilitates the click reaction.[36]

While a great deal of industrial and biological processes rely on the catalysis of intermolecular reactions, intramolecular reactions provide a more suitable model system for single molecule nanopore studies. Working in collaboration with Prof Oren Scherman, University of Cambridge, CB[7] was identified as a potential molecular adapter for used in nanopore studies. It has been established that in aqueous conditions, CB[7] catalyses the intramolecular Diels-Alder reaction (**Figure 2.6**) of a rage of substrates on a time scale suitable for nanopore studies.[37]

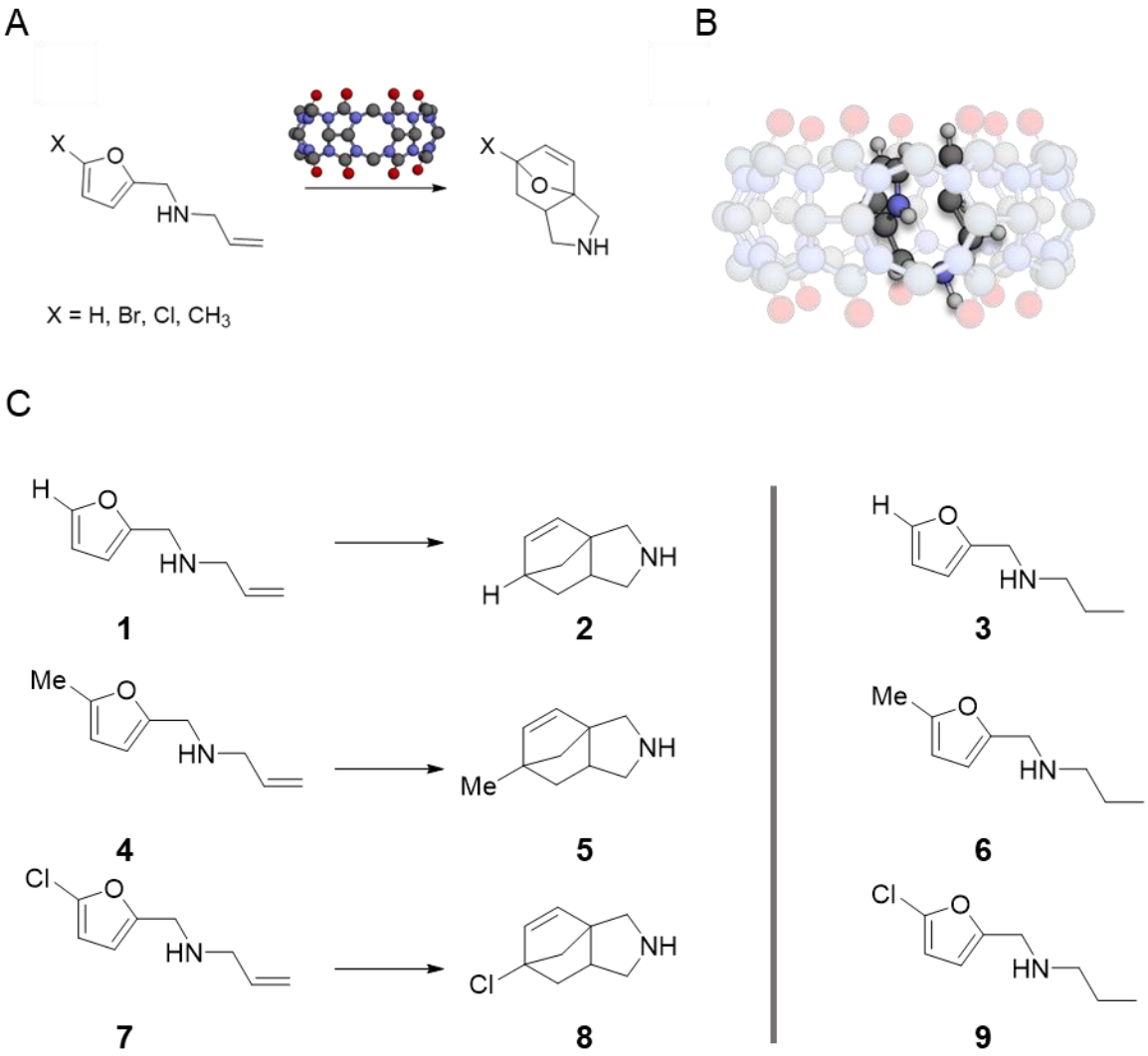

Figure 2.6: A) scheme for the intramolecular Diels-Alder catalysed by CB[7]. B) Representation of the bend Diels-Alder reagent in the cavity of CB[7] C) structures of Diels-Alder substrates (compounds **1, 4**, and **7**) and their corresponding products (compounds **2**, **5**, and **8**). Non-reactive analogues (**3**, **6**, and **9**) were also provided. These form a host-guest complex with CB[7] with a similar binding affinity, but are unable to undergo the Diels-Alder reaction.

Compounds **1** through **9** were initially obtained from the Schermann group, University of Cambridge and used for preliminary studies. Subsequent batches of compound **7** and **9** were synthesised by DCG as per the procedure in **Chapter 5**.

It was proposed that if CB[7] could be captured within the lumen of the protein then observations of the reaction at the single-molecule level could be achieved.

Computational assessment of CB[7] in a pore

A linchpin of nanopore studies is that the analyte must be of a suitable charge and size to enter into the lumen of the pore. Therefore, it was pertinent to assess whether CB[7] was capable of entering into the pore. For successful application of the CB[7] as a molecular adapter, it must be small enough to enter into either the *cis* or *trans* opening of the channel. However, for trapping to occur, the molecule must be large enough that it does not pass through the constriction site of the pore.

Limited examples exist in the literature of the addition of CB[7] to a protein nanopore, and generally rely on the association of CB[7] with a probe.[38] However, precedent has been set for the addition of CB[6] to the narrower *trans* side of α-HL, which gave regular but short-lived interaction of the macrocycle with the pore without the requirement of a probe.[15] While this is suited for sensing applications, as discrete levels for the host and the host-guest complex could be observed, the scope for the observation of reactions occurring within the CB[6] is limited. Due to the transient and short-lived nature of the events, only reactions that occur on a time scale shorter than the duration of the binding event could be observed. There is also a heighten possibility of partial reaction events being observed. Therefore, it is advantageous to achieve prolonged trapping of the macrocycle within the pore. As such, our studies hoped to see the successful addition and prolonged trapping of CB[7] to the *cis* side of the protein

To assess whether CB[7] was an appropriate size for nanopore studies with α-HL, computational modelling was used (**Figure 2.7**). While sophisticated computational models using molecular dynamics have been designed to study

membrane bound α-HL,[39] these are beyond the scope of this work. Here, more simplistic approaches were applied.

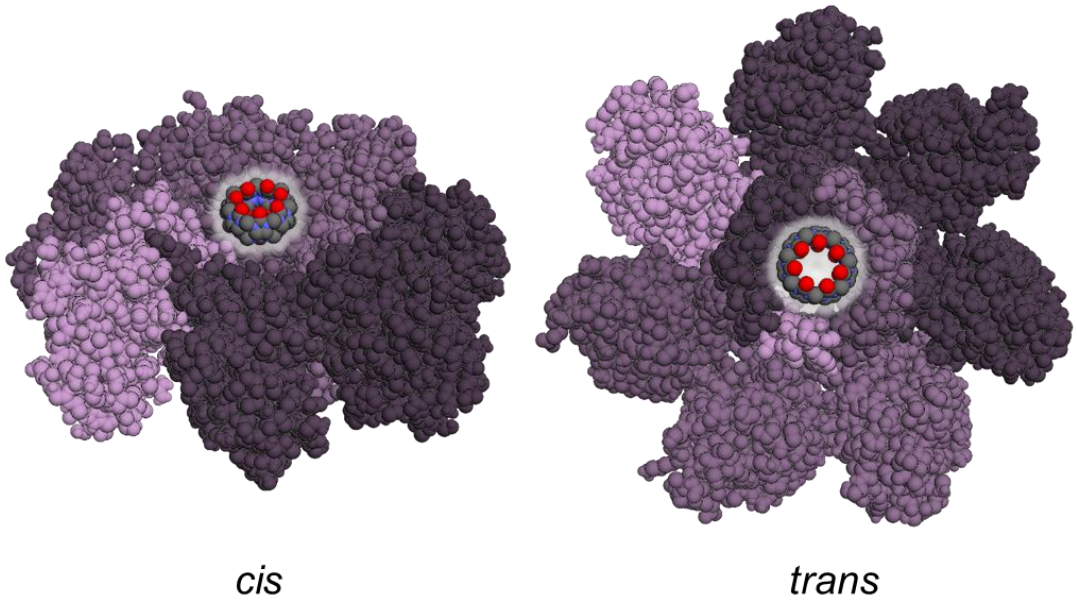

Figure 2.7: Truncated crystal structure showing the constriction site and CB[7]. The *cis* cap domain (left) and the β-barrel (right) are both large enough to accommodate CB[7]. However, CB[7] can be seen to be too large to easily pass through the constriction site.

Computational space-filling models (Discovery Studio Visualizer) indicated that CB[7] was a good candidate for the study as it had adequate size to become trapped in the pore. CB[7] has an outer calculated diameter of 1.6 Å.[34] Comparing this with α-HL, the macrocycle should be expected to be able to enter either the *cis* (2.5 Å) or *trans* (2.1 Å) side of the channel, but still be too large to pass through the 1.5 Å constriction site.[40] Similarly, CB[7] shares the same seven-fold symmetry as the heptameric protein nanopore itself, which should be anticipated to maximise interactions between the CB[7] and the nanopore. It was hoped that by trapping CB[7] in the nanopore, it would be possible to make real-time observations will be made of its catalytic turn over. This would then allow detailed mechanistic and kinetic studies to be conducted on the system.

Experimental examination of capture from the *cis* side

Initial attempts saw CB[7] added to the *cis* well of the pore in 1 M KCl buffer. Neutral macrocycle molecules, such as CB[7], are driven into biological nanopores by electroosmotic force (EOF). Due to the charge distribution, the propensity of a macrocycle to enter α-HL from the *trans* side is significantly higher than from the *cis*. Past prescient has, however, been set for the reliable capture of β-CD upon addition to the *cis* side of α-HL.[41] This was achieved by the substitution of charged residues at the mouth of the pore with neutral asparginine. It was hoped that by changing the macrocycle from β-CD to CB[7], it may be possible to achieve trapping from the *cis* side of the channel. This was desirable as the CB[7] would be lodged in the larger cap domain of the channel, which in turn could facilitate the coming together of the CB[7] and the Diels-Alder reagent.

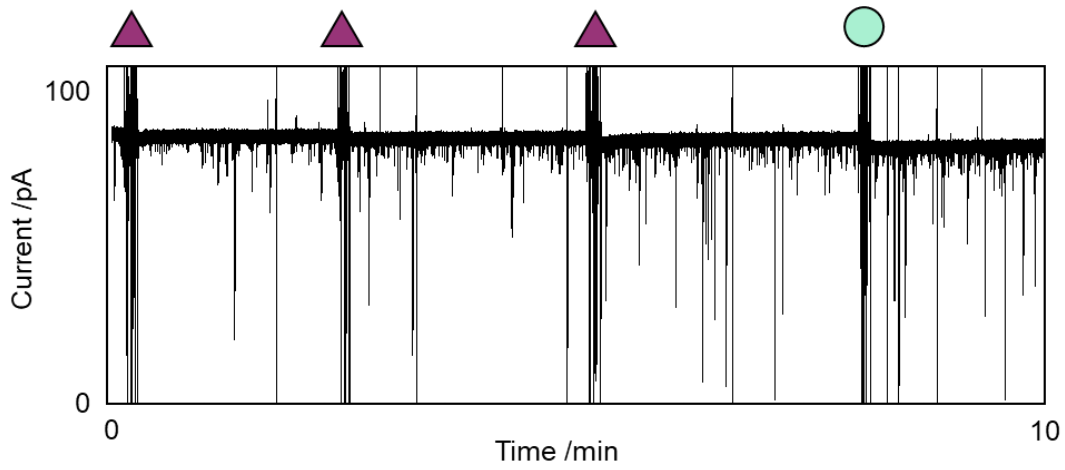

Figure 2.8: Addition of CB[7] to the *trans* well. Over several minutes, a large excess of CB[7] was added to the channel but no trapping events were observed. Purple triangles indicate the addition of 9.61 mM (stock) CB[7] in 20 µL aliquots. At the teal circle an addition of CB[7] (50 µL of 9.61 mM stock) was made. Subsequent additions increased the number of short-duration events, which suggests that the CB[7] was transiently interacting with the pore. A drift down in current was observed that could be attributed to the dilution of the well or instability of the Ag/AgCl electrodes. Initial well volume 600 µL. Buffer 1 M KCl, 30 mM K_2HPO_4, pH 8. Voltage +100 mV. Lowpass Bessel filter 100 kHz and output gain x50.

Following the standard procedure outlined in **Chapter 5, Section 5.1**, a single channel was formed. Over the course of tens of minutes, a large excess of CB[7] was added to the *cis* well. While some events were observed, these were fleeting and did not produce a consistent level (**Figure 2.8**).

Undeterred, it was sought to achieve longer duration binding events from the *cis* side. It was hypothesised that a higher salt concentration buffer may facilitate the driving of the macrocycle into the pore. An advantage of performing experiments in a higher salt concentration buffer is that ion current increases proportionally with concentration. In a 1 M KCl buffer solution, a free pore will give a consistent output current of approximately +100 pA under an applied potential of +100 mV. As the concentration is increased, a linear relationship was observed between the concentration and current under a consistent applied potential (**Figure 2.9**).

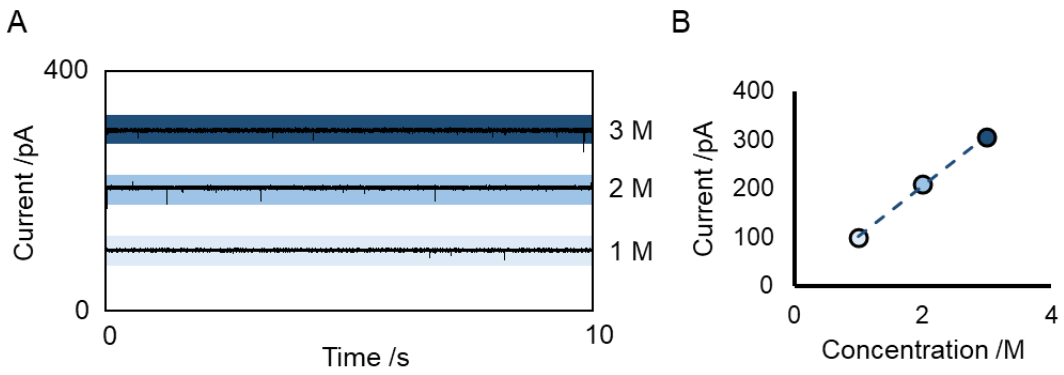

Figure 2.9: A) Comparison of output current trace at three different salt buffer concentrations for a free pore: 1 M, 2 M, and 3 M KCl. The lowest concentration (1 M KCl) is shown in pale blue and the highest concentration (3 M KCl) is down in dark blue. Voltage +100 mV. Lowpass Bessel filter 100 kHz and output gain x20. B) Plot of concentration against output current at a consistent applied voltage. There is a proportional increase in current with concentration.

In addition, the membrane becomes more resilient to higher applied voltages at higher concentrations due to the enhanced hydrophobic effect. In a typical 1 M salt buffer, the bilayer will tolerate up to approximately 120 mV of applied potential before it begins to display signs of ion leakage. When moving to a 3 M salt buffer, applied potentials approaching 200 mV will be tolerated. The

combination of the proportionally higher current and the capacity to apply a much higher voltage means that a greater signal-to-noise ratio can be achieved.

In a 2 M KCl buffer, CB[7] (10 µL of 10 mM stock) was added to the *cis* well. Much like with the 1 M KCl experiments, no immediate blockades were observed. However, intermittent long-lived events did occur after a period. Some of these blockages were tens of minutes long. An example of one of the blockages is shown in **Figure 2.10A**. Sub-levels could be observed within the new level, which provided promise that trapping was being observed. These trapped levels were characterised by recording the current as the applied potential was incrementally decreased. These data are shown in **Figure 2.10B** and showed a range of different I/V profiles.

These different I/V profiles indicated that they were not a single type of event. The possibility also remained that these were not genuine capture events and were instead attributed to voltage-driven gating of the channel. Other instances of longer-duration CB[7] capture events from the *cis*-side of the nanopore were also observed, and gave interesting data upon the addition of compound **1**, but the experiments were sadly not reproducible (**Chapter 5, Section 5.4, Figure 5.7** and **5.8**).

Despite some promise, reproducible capture of CB[7] from the *cis* side of the pore was not attained. This is not entirely unsurprising, as nanopore studies with other macrocycles have all focused on the addition to the *trans* well.[20] Nonetheless, successful capture of molecular adapters from the *cis* opening has been reported. In experiments with β-CD, no trapping events were observed with WT α-HL, even at extreme voltages and pH values.[14] However, when the 111, 113, and 147 were mutated to asparagine, binding events from the *cis* opening were observed that had similar dwell times to those observed upon *trans* addition. The authors therefore suggested that the removal of an internal barrier facilities *cis*-binding events with this mutant. While mutagenesis

has the potential to enhance the *cis* trapping of CB[7], the design principles are not obvious. Hence, the more pragmatic approach of examining the binding of CB[7] from the *trans* side of the pore was explored instead.

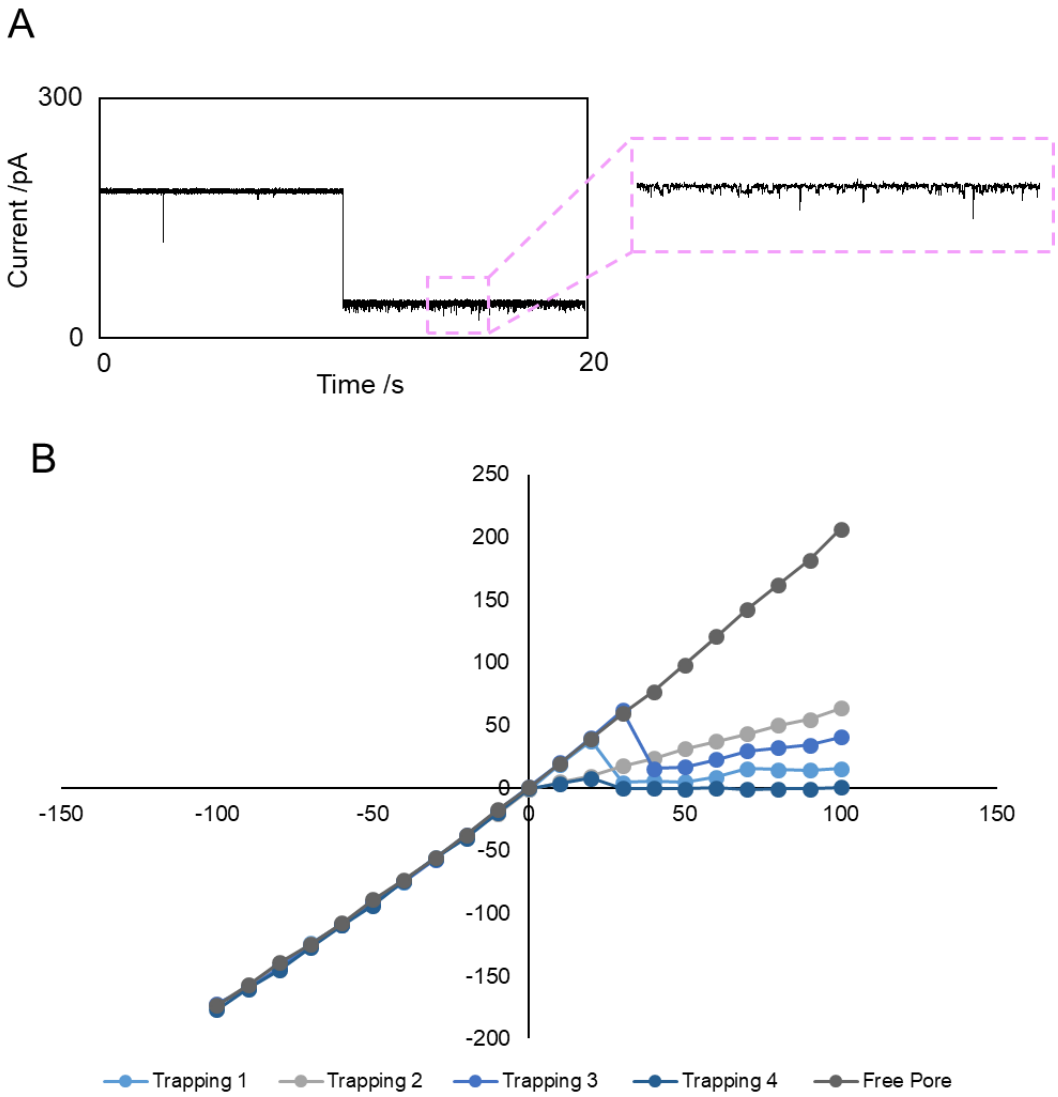

Figure 2.10: A) example of a potential capture event of CB[7]. Buffer 2 M KCl, 30 mM K_2HPO_4, pH 8. Voltage +100 mV. Lowpass Bessel filter 100 kHz and output gain x20. B) A waveform protocol was used in ClampEx 10.4 to apply a potential in decreasing 10 mV increments over 2 s durations and the output current was measured. The free pore trace shown in pale blue exhibits the characteristic asymmetric trace expected for an unobstructed channel.

Experimental examination of capture from the *trans* side

As indicated in the earlier section computational models suggested that capture of CB[7] may also be feasible from the *trans* opening (**Figure 2.7**). CB[7] was added to the *trans* side of an α-HL channel (**Figure 2.11A**). Almost immediately, reproducible binding events were observed (**Figure 2.11B**). An event is defined as a deviation from the free pore level (I_o) to a new, blocked level (I_b). To normalise data across experiments, the blockage is reported as the ratio I_b/I_o.

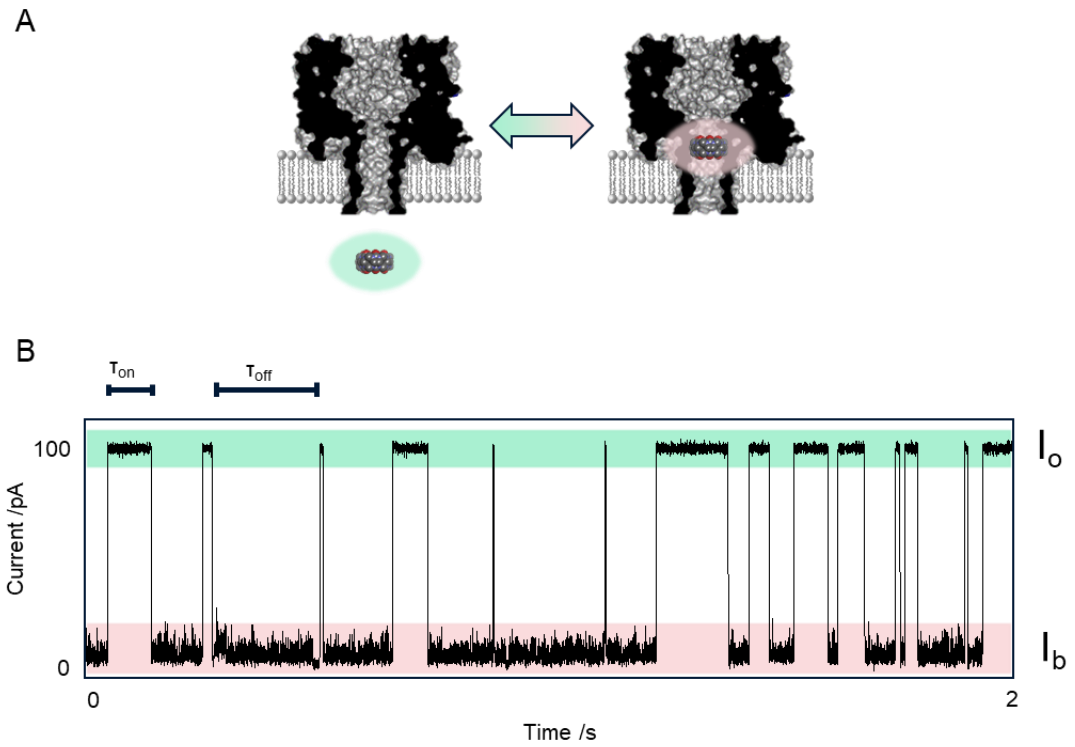

Figure 2.11: A) α-HL in a lipid bilayer showing the *trans* addition of CB[7]. B) Example nanopore trace for the addition of CB[7] (5 µL of 10 mM stock) to the *trans* well. The inter-event duration is defined as τ_{on} (teal) and the binding event duration is defined as τ_{off} (pink). Initial well volume 600 µL. Buffer 1 M KCl, 30 mM K_2HPO_4, pH 8. Voltage +100 mV. Lowpass Bessel filter 100 kHz and output gain x50. An occasional addition level at I_b/I_o of 0.55 and 0.34 was occasionally seen (not shown) that was attributed to minor CB[5] and CB[6] impurities (**Chapter 5, Section 5.4, Figures 5.9, 5.10** and **5.11).**

Binding of CB[7] from the *trans* side of the membrane therefore appeared to be better behaved than capture from the *cis* side. The CB[7] appears to enter

the channel in concordance with the direction of motion of cations, which may be due to association of CB[7] with cations,[15] and/or electro-osmotic forces. Hereafter, we explored approaches for enhancing the retention of single CB[7] molecules within the β-barrel to enable single-molecule monitoring of intramolecular Diels-Alder reactions. For the purposes of analysis, the time between events is referred to as τ_{on} and the time of the event is referred to as τ_{off}.

Optimisation of buffer composition

Encouraged by the reproducibility of capture from the *trans* side of the nanopore, optimisation of conditions for binding was undertaken. It was sought to develop a system whereby an intermediate dwell time could be achieved. If the dwell time was too short, then catalysis events may be missed. However, as the macrocycle has a high affinity for the product, as well as the reactant, then a long duration binding could result in the trapping of a poisoned catalyst.[37] It was decided to explore the effect of buffer concentration on the binding of CB[7]. It was also reasoned that increasing the salt concentration might affect the kinetics and thermodynamics of CB[7] binding within the nanopore (**Figure 2.12**). It was found that the concentration of the buffer salt had a notable effect on the dwell time of the macrocycle. The mean dwell time was found to be 54.2 ms in a 1M KCl buffer. A more intermediate dwell time was achieved in a 2 M KCl buffer, with a mean dwell time of 114.0 ms. However, the dwell time increased to 12644.9 ms (over x200 that observed in the 1 M KCl buffer) when the salt concentration was increased to 3M.

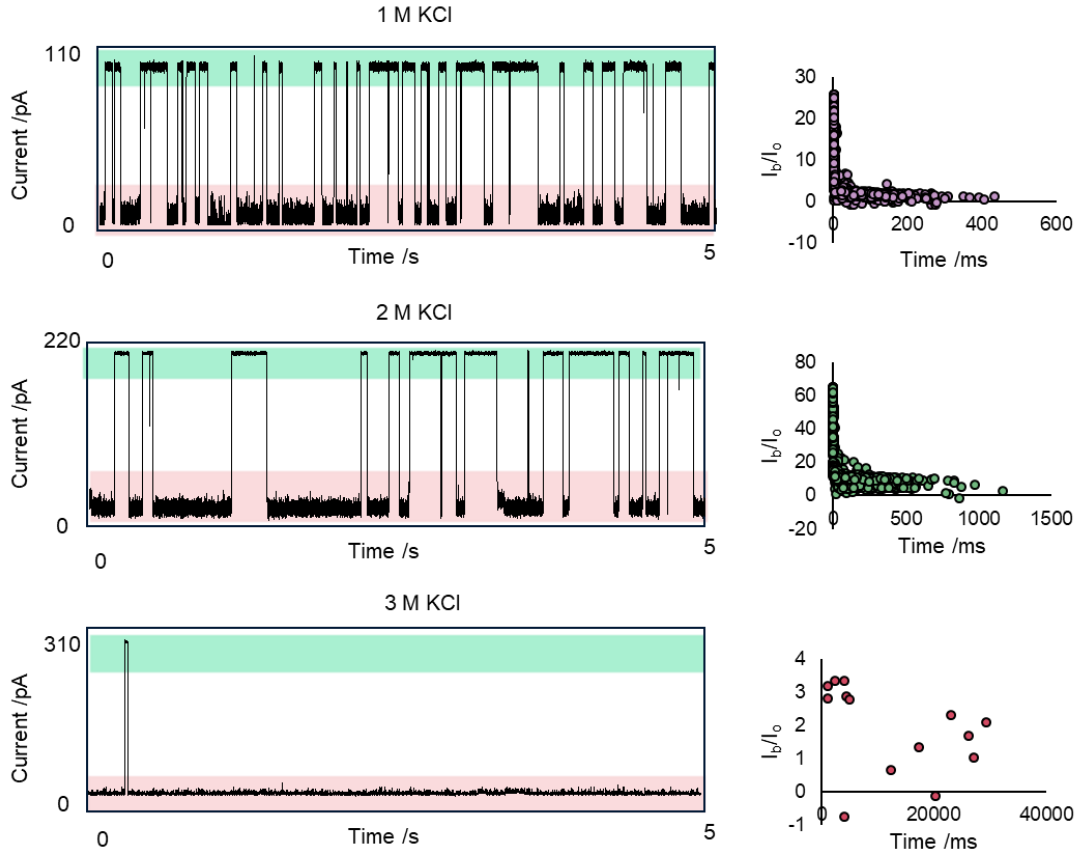

Figure 2.12: Example traces for binding events of CB[7] in 1 M, 2 M and 3 M KCl buffer (left) and accompanying scatter plots showing the I_b/I_o against time (right). CB[7] (10 µL of 10 mM stock) was added to the *trans* well. Mean dwell times for the binding events were 54.1 ms (1M KCl), 114.0 ms (2 M KCl), and 12644.9 ms (3 M KCl). 1, 2 or 3 M KCl, 30 mM K_2HPO_4, pH 8. Voltage +100 mV. Lowpass Bessel filter 100 kHz and output gain x50.

Voltage can also have a profound effect on binding kinetics and the position of equilibria in nanopore experiments.[42] Hence, the applied voltage was also systematically varied (**Figure 2.13**).

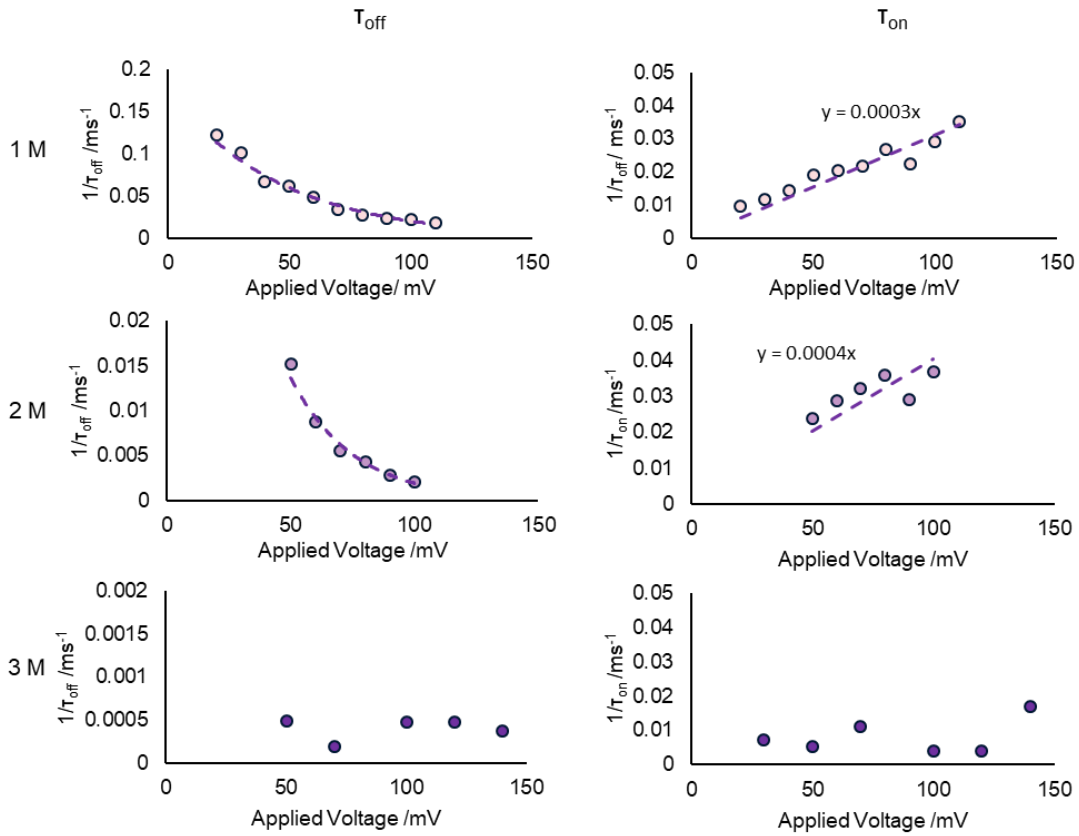

Figure 2.13: Comparison $1/\tau_{off}$ (Left) and $1/\tau_{on}$ (Right) for CB[7] (10 µL of 10 mM stock) binding events upon varying the voltage in different concentrations of KCl buffer. Plots fitted from current level histograms (**Appendix A, Figure A.1** (1M KCl), **A.2** (2 M KCl) and **A.3** (3M KCl).

The applied potential was decreased in 10 mV increments starting from an initial applied voltage of between +100 mV and +150 mV (depending on bilayer stability in each experiment). A linear relationship for $1/\tau_{on}$ against voltage was observed, but there was a nonlinear relationship for $1/\tau_{off}$. This suggests that at lower voltages the CB[7] enters and exits the β-barrel from the *trans* opening and does not pass through the constriction site. However, at higher voltages the macrocycle is forced through the constriction site and exits the channel *via* the *cis* opening.[19] Due to the extremely long duration of τ_{off} in the 3 M buffer, it was difficult to record a significant number of events at the higher applied potentials and subsequent analysis was performed only in 1 M and 2 M KCl buffer.

Following from this, the effect of the concentration of CB[7] was assessed in two different buffer concentrations: 1 M KCl and 2 M KCl (**Figure 2.14)**.

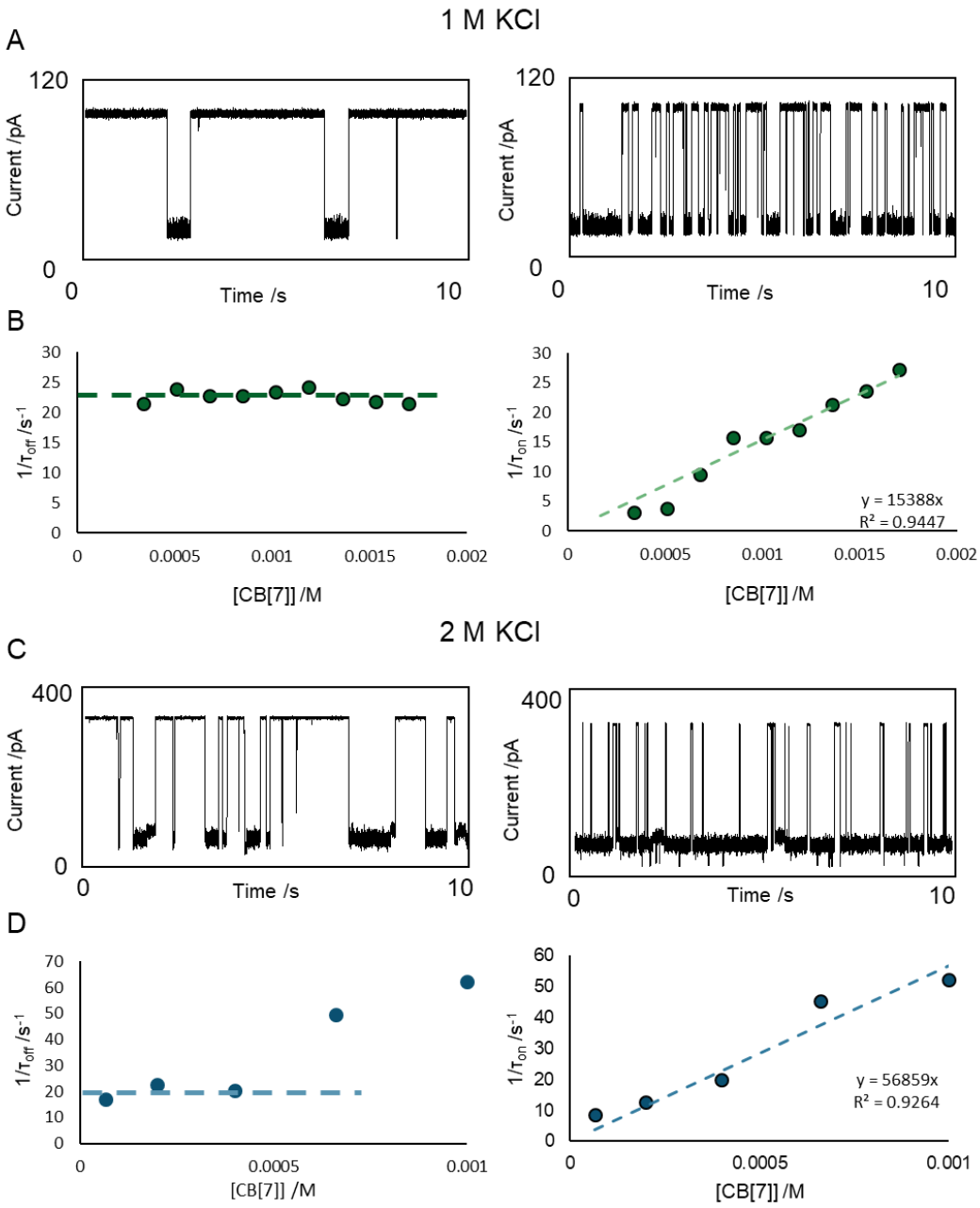

Figure 2.14: Concentration titrations were conducted for CB[7] in 1 M and 2 M KCl buffers. A) Example trace for binding events at a low CB[7] concentration (6.6 µM) (left) and high CB[7] concentration (100 µM) (right). 1 M KCl, 30 mM K_2HPO_4, pH 8. Voltage +150 mV. Lowpass Bessel filter 100 kHz and output gain x20. B) Plot of $1/\tau_{off}$ against [CB[7]] (left) and plot of $1/\tau_{on}$ against [CB[7]] (right) C) Example trace for binding events at a low CB[7] concentration (6.6 µM) (left) and high CB[7] concentration (100 µM) (right). 2 M KCl, 30 mM K_2HPO_4, pH 8.

Voltage +150 mV. Lowpass Bessel filter 100 kHz and output gain x20 D) Plot of $1/\tau_{off}$ against [CB[7]] (left) and plot of $1/\tau$on against [CB[7]] (right). The rate constant k_{on} was calculated as the gradient of the linear fit in the plot of $1/\tau_{on}$ against [CB[7]] and k_{off} was calculated as the y-intercept in the plot of $1/\tau_{off}$ against [CB[7]]

In the 1 M buffer, a linear increase can be seen for the time to the capture events (τ_{on}) as the concentration increases. The linear relationship suggests that the capture is a bimolecular process between the channel and the macrocycle. However, there appears to be no correlation between the dwell time of the event and the concentration (τ_{off}), meaning that the dwell time of the events is independent of the CB[7] concentration. In a 2 M KCl buffer a similar linear increase was observed for τ_{on} as the CB[7] concentration increased. The event duration (τ_{off}) appears to be independent of the concentration at lower [CB[7]] and the K_{on} is comparable to that observed in the 1 M KCl buffer (**Table 2.1**).

To determine k_{off} and k_{on}, the values of $1/\tau_{off}$ and $1/\tau_{on}$ were plotted against the concentration of CB[7] in the cell at 150 mV. Taking 100 s of data, a threshold event detection was applied in Clampfit 10.7 to detect each binding event. The subsequent event and inter-event durations were then plotted as a frequency count histogram and a single exponential decay function was plotted to calculate the values of τ_{off} and τ_{on} respectively (**Appendix A, Figure A.4 and A.5**). The voltage driven rate constant of CB[7] association with the pore (k_{on}) can be calculated as in **Equation 1**. Therefore the rate is dependent on the concentration of CB[7].

$$k_{on} = \frac{1}{\tau_{on}[CB[7]]} \qquad \textbf{Equation 1}$$

The voltage driven rate constant of CB[7] dissociation with the channel (k_{off}) can be calculated as in **Equation 2.** Therefore, it would be expected for k_{off} to be independent of the CB[7] concentration.

$$k_{off} = \frac{1}{\tau_{off}} \qquad \textbf{Equation 2}$$

From the plots in **Figure 2.13D**, k_{on} was determined from the slope of the plot of $1/\tau_{off}$ against [CB[7]] and k_{off} was from the y-intercept of $1/\tau_{on}$ against [CB[7]] (**Table 2.1**).The non-equilibrium association constant (K_a) can then be determined as the ratio of k_{on}/k_{off}.

Table 2.1: Kinetic data for the association of CB[7] with an α-HL nanopore under an applied potential of +150 mV. Buffers: 1 M KCl, 30 mM K_2HPO_4, pH 8 and 2 M KCl, 30 mM K_2HPO_4, pH 8.

	1 M KCl	**2 M KCl**
k_{on} /M^{-1} s^{-1}	1.54×10^4	5.89×10^4
k_{off} /s^{-1}	23	21
K_a / M^{-1}	669	2804

From the plots in **Figures 2.14 B and D**, k_{on} was found to be approximately four-fold greater in the 2 M salt conditions. At low CB[7] concentrations, k_{off} was found to be independent of both the buffer and CB[7] concentration. However, in the 2 M KCl buffer, a concentration dependence appears to emerge as [CB[7]] was increased. This suggests that at the higher concentrations, two CB[7] molecules may enter the pore. Therefore, all studies were conducted at [CB[7]] less than 0.5 mM. In turn, the non-equilibrium association constant was found to be four times greater in the 2 M salt buffer. Therefore, marginally tighter binding can be observed between the CB[7] and the nanopore in a higher salt concentration buffer.

From the calculated values of K_a and the dwell time analysis, it was decided to progress using a 2 M KCl buffer. This provided a good signal to noise, with binding events long enough to see potential binding/reactions on Diels-Alder substrates. However, the events were not so long that competitive binding from the product would be of concern.

Examination of Binding events

The voltage and concentration variation experiments also revealed one potential limitation of performing experiments in 2 M buffer. Two distinct states were occasionally observed within the CB[7] binding events (**Figure 2.15**). Such events became more apparent at higher voltages. As there was no guest present, the reason for this sub-level was unclear.

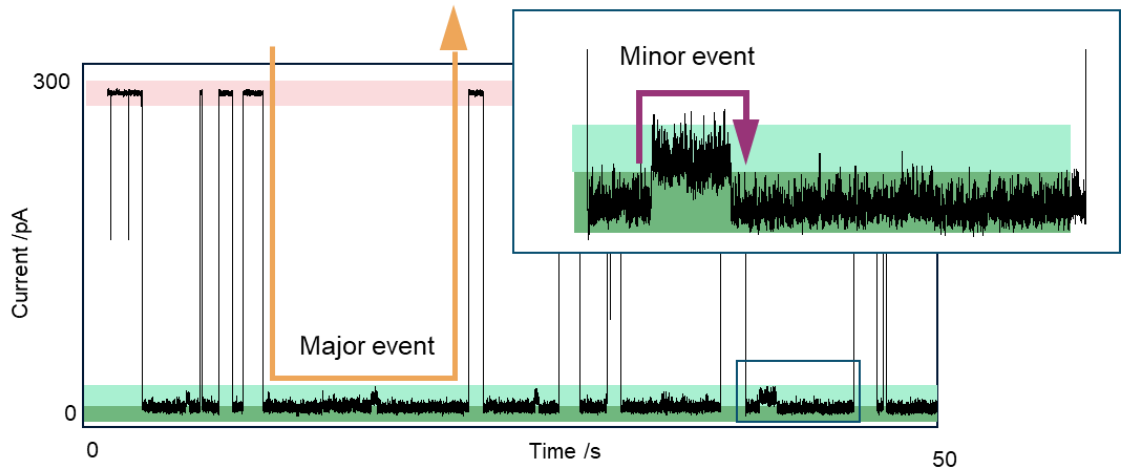

Figure 2.15: Example trace of CB[7] demonstrating upwards events within primary deep levels. The drop from the baseline is defined as the major event (orange), and the small upwards events within this level is defined as the minor event (purple). Well concentration of 163 µM CB[7]. 2 M KCl, 30 mM K_2HPO_4, pH 8. Voltage +150 mV. Lowpass Bessel filter 100 kHz and output gain x20.

To probe this further, the effect of concentration on the event sub-levels was analysed. Using single channel analysis, the average current of each sub-level in 100 s of recording was extracted. By histogram analysis, the number of

occurrences of each sub-level was plotted against the I_b/I_o for each concentration (**Figure 2.16A**).

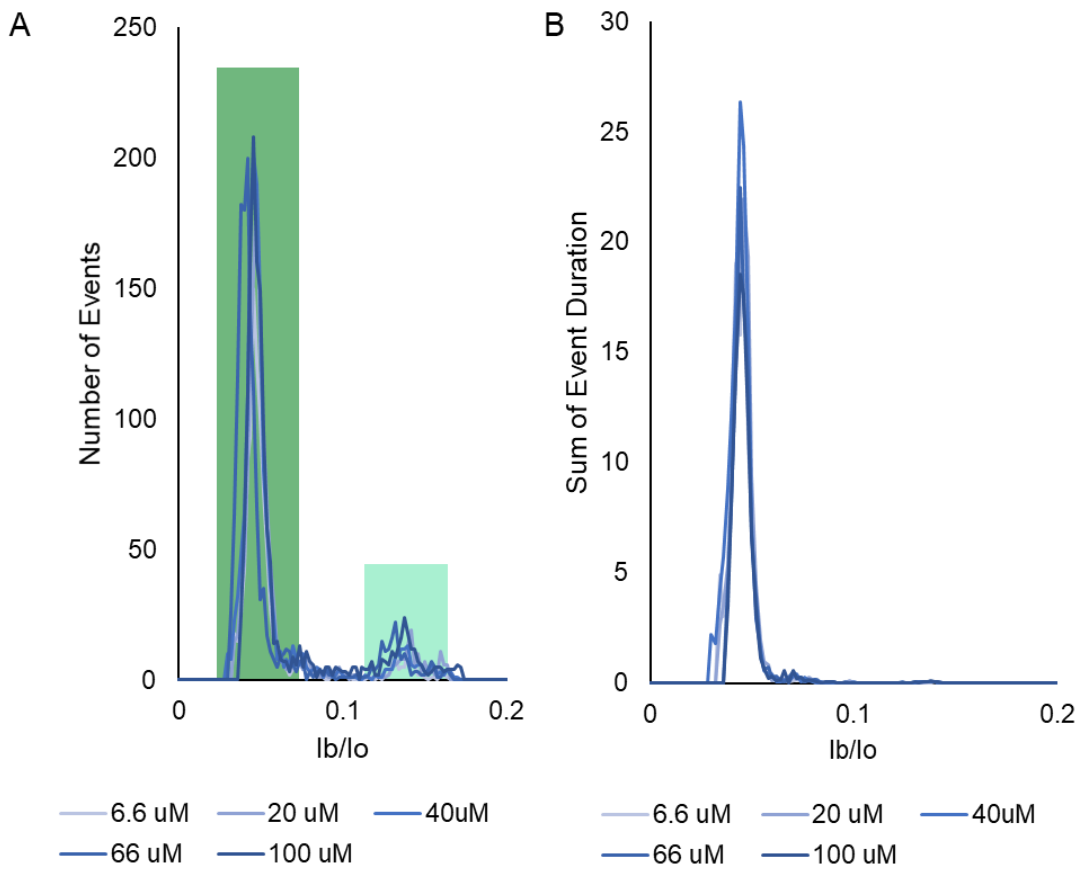

Figure 2.16: A) Binned histograms of the number of events at each sub-level in a 2 M KCl buffer. Across all voltages, distinct peaks can be seen at approx. 0.04 and 0.12. There is limited variation in the number of evets or the ratio of sub-levels as the [CB[7]] increases. B) Cumulative dwell time at each sub-level across increasing [CB[7]]. The minor peak at 0.12 has been lost in the signal noise due to the short-lived nature of this level.

Two distinct states were observed; a major level at approximately 0.05 and a minor at 0.14. No apparent variation was seen for the number of events at each level or in the ratio of major to minor events. Taking this further, the cumulative total of dwell time at each level was plotted against I_b/I_o. Here, the duration of the minor event was so short that it disappeared into the noise. However, the major peak remains prominent. Again, no correlation was

observed between the concentration of CB[7] and the accumulative dwell time of the events. Therefore, it can be concluded that the occurrence of sub-levels is independent of the concentration of CB[7] under these experimental conditions.

The occurrence of sub-levels may also be due to distortions of the macrocycle. Despite being relatively rigid, larger CB[n] variants have been shown to be prone to distortion, and may accompany the incorporation of a guest.[43] However, in the present system, variations to the baseline current occur in the absence of a guest – other that the cation of the buffer. Hence, the observed sub-levels may be due to the detection of different metal ion•CB[7] complexes as examined below.

Assessing the role cations in the buffer

Computational analysis of cation CB[7] interactions

Having established that entry of additional CB[7] molecules was not responsible for the observation of sub-levels during CB[7] binding events, we sought to examine whether discrete metal ion•CB[7] complexes might be responsible. Indeed, it is known that metal cations interact with CB[n].[34, 44] CB[7] is neutral molecule and in its native state it should not be electrophoretically driven into the nanopore. However, small macrocycles are known to be driven into the pore electrophoretically through association with a guest metal ion.[15] As it has been demonstrated that metal cations bind at the electron-rich carbonyl-lined portals of CB[n] (**Figure 2.17**), it was thought that this may drive the macrocycle into the pore.[45] However, such bound cations may act as a ‘lid’ to the macrocycle, which may interfere with guest binding.[44] For variants larger than CB[7], only partial ion capping has been suggested.[46] In some instances, metal ions may fully enter into the cavity of the

macrocycle.[47] However, it is known that metal ions such as K^+ will not enter smaller CB[n] homologues, such as CB[6].[48]

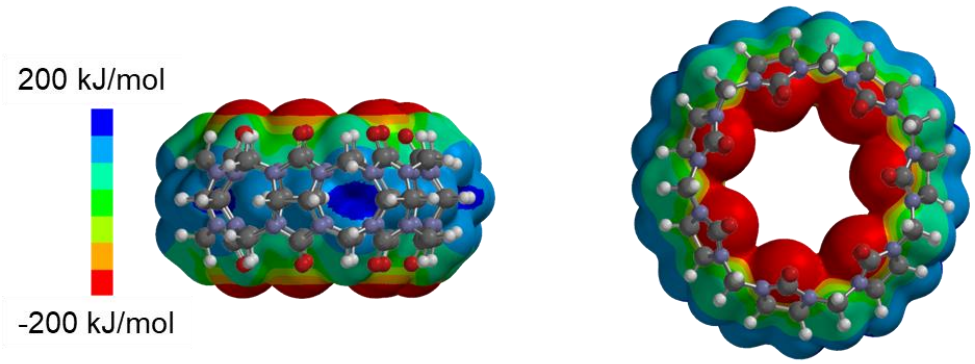

Figure 2.17: Electrostatic potential (ESP) map of free CB[6] scaled from +200 kJ mol^{-1} (blue) to -200 kJ mol^{-1} (red). The peripheral rings of oxygen atoms are electron rich (red) and are proposed to bind metal ions (blue). Equilibrium Geometry calculated using MM-MMF and electrostatic potential using B3LYP/6-31G* in Spartan '14.

It has also been suggested that the metal may join the host and guest to form a tertiary supramolecular complex that supports the binding of the guest.[49] Previous studies have shown that the association of a transition metal ion can facilitate chemoselective reactions in conjunction with CB[7].[50] On the other hand, recent work has demonstrated that cations may inhibit CB[7]-catalysed ester hydrolysis.[51]

Previous work by Piguet *et al.* showed that the dwell time of a β-CD molecule in an α-HL nanopore can be modulated by varying the cation.[52] This was suggested as being due to variations in the electroosmotic force with different anions and anion concentrations. β-CD had a greater selectivity for Li^+ than for K^+ and thus a greater EOF was observed in a LiCl buffer. Interestingly, captures were more frequent for β-CD in the KCl buffer, and at higher voltages, a greater dwell time was observed. In other words, the larger the cation the better the capture β-CD.

Based on the above work, and following on from the characterisation of KCl concentration on CB[7] binding described in the previous section, it was therefore decided to examine the influence of CsCl buffer due to the large size of Cs^+ cations relative to K^+. The computationally minimised structures of CB[7] complexed with K^+ and Cs^+ are shown in **Figure 2.18**, which highlights the relative sizes of the counter ions involved.

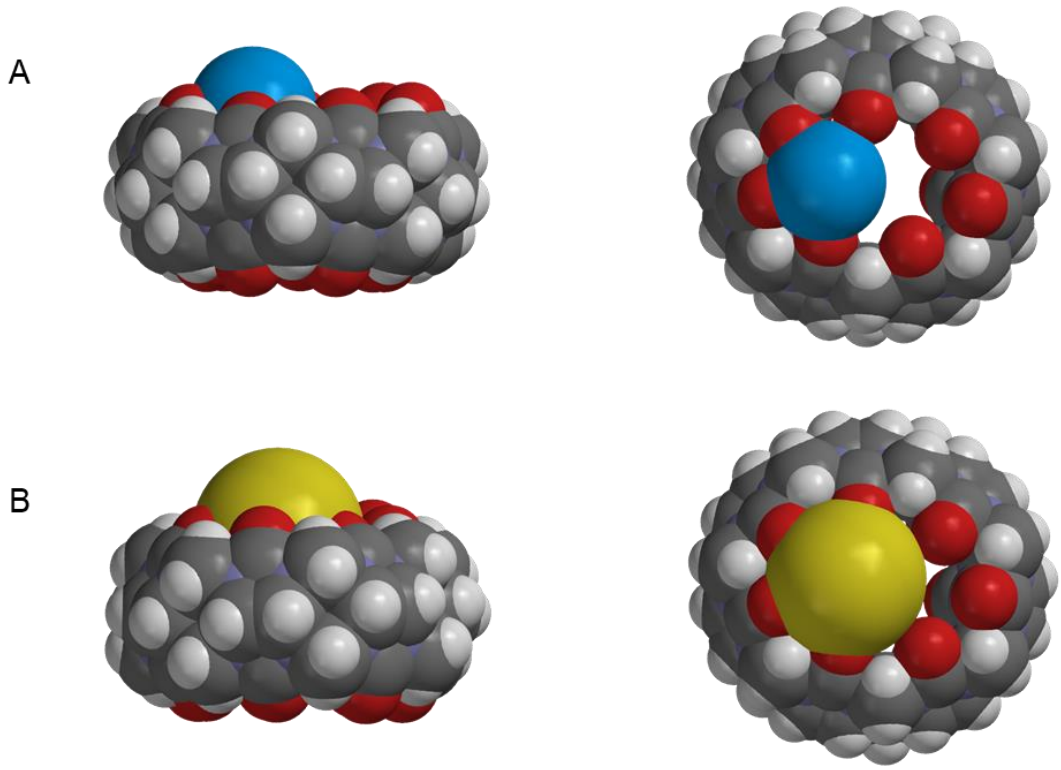

Figure 2.18: A) Space filling model of K^+ (blue) in complex with CB[7] with a side on (left) and top-down (right) view. Ionic radius is defined as 2.8 Å for Cs^+ based on the calculated 0.02 e-/a.u.^{3} isoelectron density surface. B) Corresponding complex but with Cs^+, also with a side on (left) and top-down (right) view. Ionic radius is defined as 3.6 Å for Cs^+ based on the calculated 0.02 e-/a.u.^{3} isoelectron density surface. Minimisations performed using ωB97X-D/LANL2DZ.

As the cations of the buffer will bind at the portal of the CB[7], there is a risk that the ions would compete with the host of interest. However, it has been established that the Diels-Alder reagents have a good affinity for CB[7] in other buffer systems. This likely occurs because the Diels-Alder reagents and host have a better size-complementary than the K^+ in isolation (**Figure 2.19**). It has

been established that host-guest complexes are most favoured when the guest has a volume 55 ± 9% of the host cavity.[53] Compound **1** has a calculated volume of 173 Å^3 (Spartan '14, CPK), compared to a cavity volume of 242 Å^3 for CB[7].[54] This gives a percentage volume occupancy of 71%, which puts Compound **1** slightly above the upper boundary for optimal binding. However, the binding of a single K^+ (11 Å^3),[55] would only occupy 5% of the cavity volume. Hence, compound **1** has a far more optimal size for binding within CB[7].

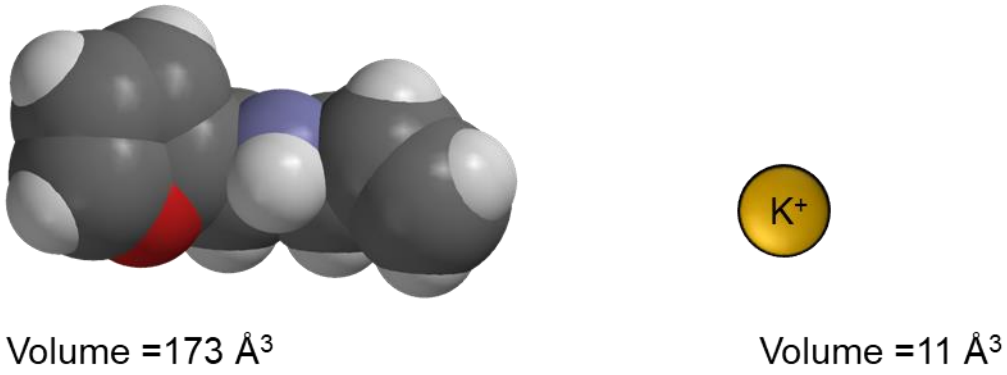

Figure 2.19: CPK structure of compound **1** (left) compared to a potassium cation (right).

Experimental assessment of CsCl buffer

To examine the whether the association between the metal salt and the CB[7] helps the macrocycle to be driven into the pore a comparison of CB[7] capture in 1 M KCl and 1 M CsCl was undertaken. The association of CB[7] with the different ions may govern the binding of CB[7] within the nanopore in two different ways. First, if the dominating driving force behind the binding events is the electrophoretic force, then a stronger association with the metal ion will result in longer dwell times. However, if it is the electroosmotic force that it the dominating factor, then the effect of the buffer on the surface charge of the protein will determine the binding duration.

Using either buffer 1 M KCl or 1 M CsCl buffer, CB[7] (5 µL of 10 mM stock) was added to the *trans* compartment, which led to the observation of regular

and reproducible events in both cases (**Figure 2.20**). Surprisingly, there was no major difference between the I_b/I_o for either salt buffer.

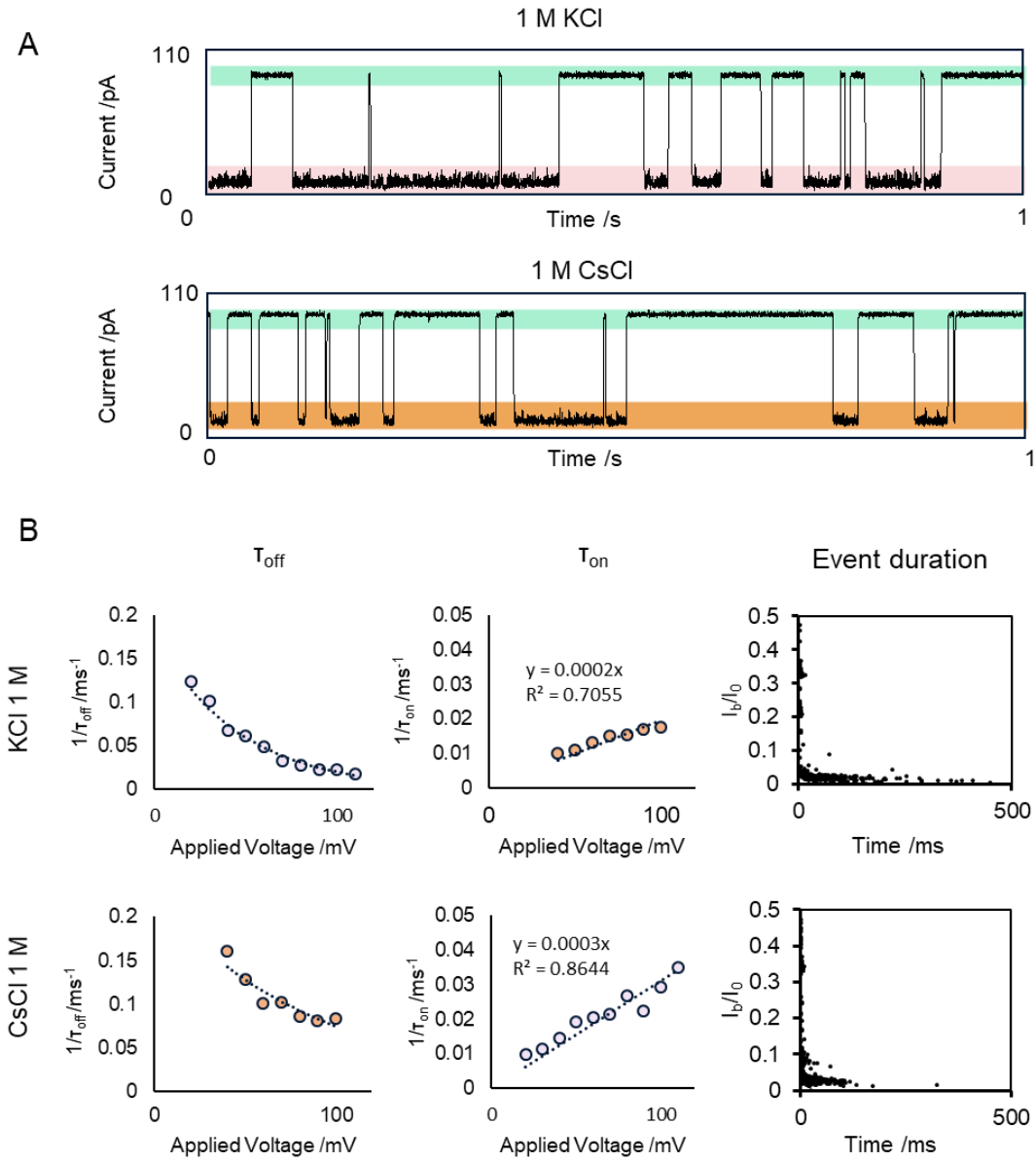

Figure 2.20: Comparison of CB[7] binding events with the pore in KCl and CsCl buffer. A) Example traces of binding events of CB[7] (5 µL of 10 mM stock) in KCl buffer (1 M KCl, 30 mM K_2HPO_4, pH 8) (mean Ib/Io = 0.06) and CsCl (1 M CsCl, 30 mM K_2HPO_4, pH 8) (mean Ib/Io = 0.09). Voltage +100 mV. Lowpass Bessel filter 100 kHz and output gain x50. B) Plots of $1/T_{off}$ (left) $1/T_{on}$ (middle) and event duration (right) as CB[7] concentration is varied in 1 M KCl and 1 M CsCl buffers. Plots fitted from current level histograms (**Appendix A, Figure A.6**).

The inter-event duration in the CsCl buffer was approximately twice as long as with KCl buffer (τ_{on}). In addition, the KCl system presented with the longer dwell time (τ_{off}). Although the CsCl buffer was not found to improve the retention of CB[7] within the nanopore, there was compelling evidence that Cs^+•CB[7] interactions could be detected. Most notably, greater numbers of sub-level currents were observed in the CsCl buffer compared to in KCl (**Figure 2.21**).

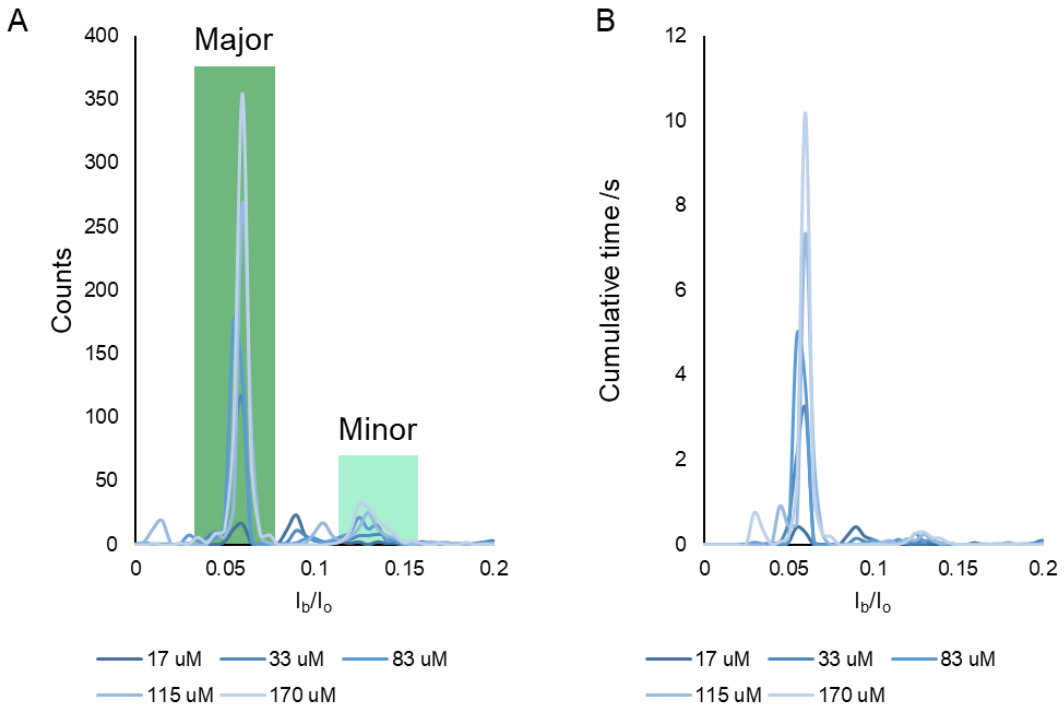

Figure 2.21: A) Plot of [CB[7]] against $1/T_{off}$ in a 1 M CsCl buffer. k_{off} can be extracted as the y-intercept. B) Plot of [CB[7]] against $1/T_{on}$ in a 1 M CsCl buffer. k_{on} can be extracted as the gradient of the slope. C) Binned histogram for the number of incidences of each sub-level, across a range of concentrations. D) Cumulative time at each sub-level, across a range of concentrations. 1 M CsCl, 30 mM K_2HPO_4, pH 8

Unlike with a 1 M KCl buffer, where no significant variation in sub-level events was observed on varying the CB[7] concentration, an increase in the number of events and the cumulative time of the sub-levels were observed in CsCl buffer. This suggested that the sub-levels stem from an association of the macrocycle with the cations of solution.

Voltage-variation experiments were performed to further examine the hypothesis that Cs^+•CB[7] association was the origin of the sub-levels (**Figure 2.22**).

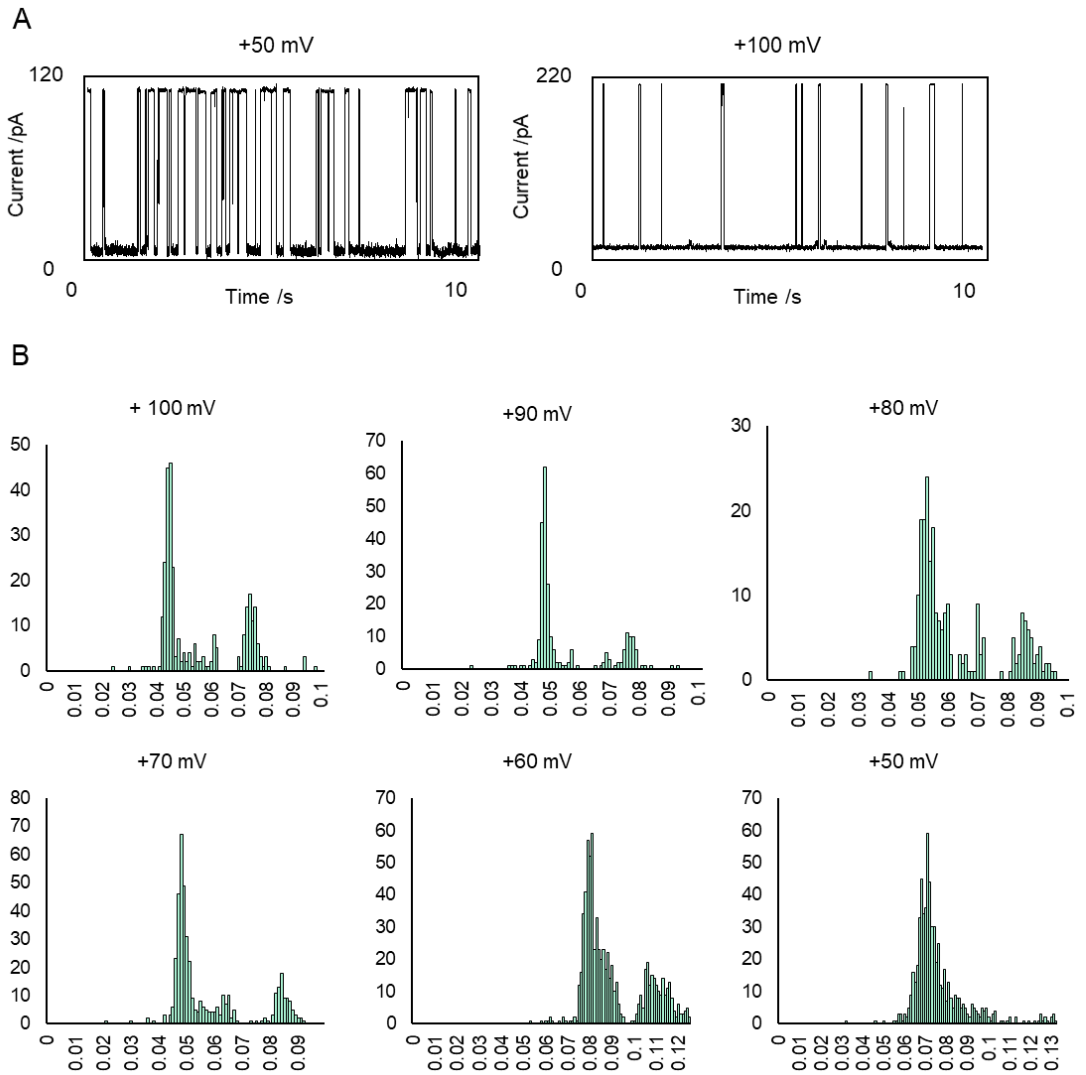

Figure 2.22: A) Example traces for +100 mV (left) and +50 mV (right) with a consistent [CB[7]]. It can be observed that the base line current decreases proportionally the applied potential, as is expected. In addition, the dwell time of the events decreases with the voltage. B) Single-channel analysis was conducted on sub-level events contained in 100 s of data. From +100 mV to +60 mV, two distinct peaks can be observed. However, at +50 mV, only one peak can be observed. 1 M CsCl, 30 mM K_2HPO_4, pH 8

It was reasoned that the capture and stability of the positively charged complex should be perturbed by changes in the applied electric field (*i.e.* voltage). Using

the single-channel search in Clampex 10.7, the individual sub-levels were characterised for 100 s of recording at six different applied voltages.

Interestingly, the dwell time for the major event (τ_{off}) increased as the voltage increased. This suggest that the voltage holds the macrocycle in place in the pore. Two distinct states can be observed at +100 mV, the main level and the sub-level. As the voltage decreases, the major sub-level ($I_b/I_o = 0.045$) remains largely static. However, the minor sub-level experiences a shift in I_b/I_o. Eventually, as the voltage decreases to +50 mV, only a single state is observed. The shift to higher I_b/I_o at higher voltages may suggest that the average orientation or shape of the complex responds to the voltage. This result supports the hypothesis that the sub-levels arise due to the association with a cation. Indeed, **Figure 2.18** shows the enormous size of the Cs^+ cation relative to the macrocycle adds plausibility to the suggestion that the Cs^+•CB[7]Cs^+ complex could be captured within the nanopore.

To further explore the effect of the cation on binding events of CB[7], a 5 µL aliquot of a CB[7] 10 mM stock solution made up in a 1 M CsCl buffer was added to the *trans* side of a single channel formed in a 3 M KCl buffer solution. Under an applied potential of +100 mV, events were immediately observed that had a very different characteristic to those observed in the KCl pure buffer (**Figure 2.23** *cf.* **Figure 2.12**). The event duration for binding was significantly shorter than expected for a 3 M KCl buffer. This is potentially due to the CsCl decreasing the hydrophobic effect, compared to pure KCl. In addition, the main blockage events and the sub-levels in the mixed salt experiment had higher I_b/I_o values than in pure 3 M KCl (**Figure 2.23A**). Future studies may look to CB[n] analogues as molecular adapters for the detection of cations. However, the increased prevalence of sub-levels meant that the CsCl buffer was not suitable for our primary objective of seeking to observe single-molecule catalysis within CB[7].

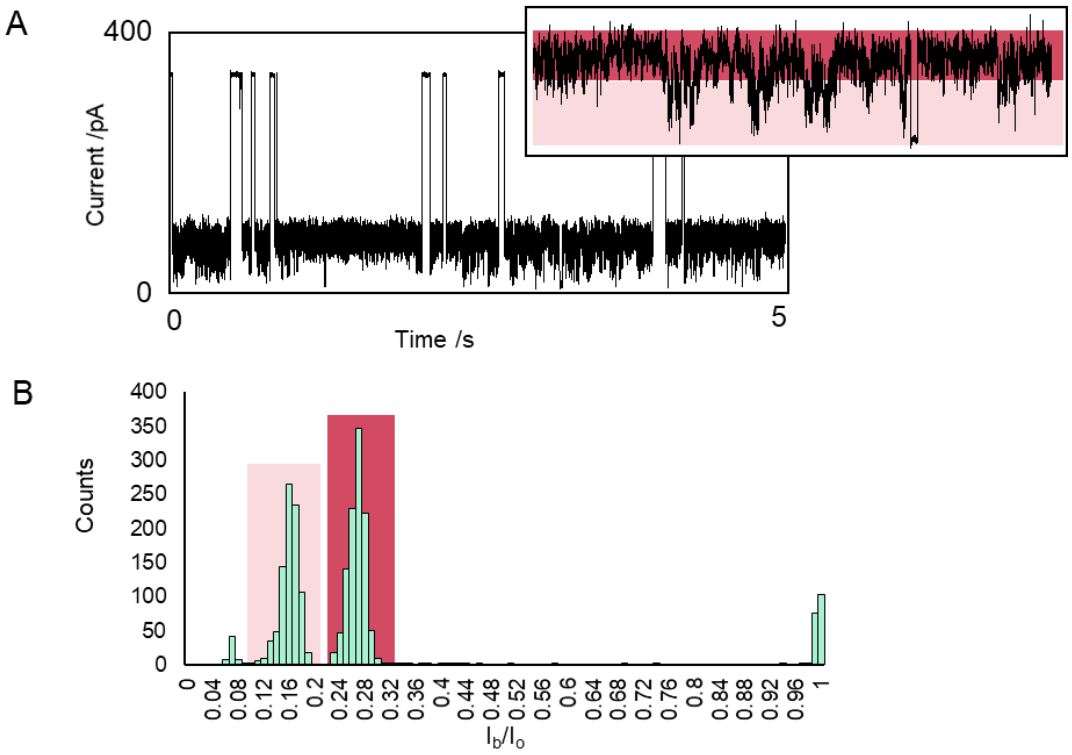

Figure 2.23: A) Example trace for the addition of CB[7] (5 µL of 10 mM stock) in a CsCl buffer added to a 1 M KCl buffered well. Ehanced section shown in upper right hand side. Buffer 3 M KCl, 30 mM K_2HPO_4, pH 8. Voltage +100 mV. Lowpass Bessel filter 100 kHz and output gain x50. B) Distribution of the dwell time against the average I_b/I_o. It should be noted that compared to the addition of CB[7] prepared in a KCl buffer to a KCl buffer well (**Figure 2.21**) there are significantly more events and the dwell time is much shorter.

Summary of buffer optimisations

Overall, these buffer experiments revealed that CB[7] capture can be achieved in a range of salt concentrations and two different salts. KCl buffer was found to give longer CB[7] captures, which increased with increasing KCl concentration. Indeed, when a 3 M buffer was used a near-constant block was observed. However, there were concerns that the high salt concentration could have implications on catalytic capacities of the macrocycle and the solubility of the reagent molecules. In addition, there would be no ability to monitor catalytic turn-over if capture of the reagent was not possible when CB[7] was trapped in the nanopore. Therefore, it was concluded that the 2 M KCl conditions would likely be the most conducive for observations of catalysis in the channel, since

this gives rise to CB[7] capture events with second-long duration, while still allowing some exchange with the bulk medium. From the assessment of the role of the buffer cation, it would appear that the appearance of sub-levels may be due to the association and dissociation with the metal ion. It was decided to progress with a KCl buffer as there were concerns that the large size of the Cs^+ ion would cap the CB[7] and prevent entry of reagents into the catalytic cavity. Nonetheless, the preliminary data indicates that the system may be useful for examining metal ion CB[7] binding in future work.

2.4 Examining the accessibility of CB[7] guests

Having examined the influence of the buffer composition on capture of CB[7] within the nanopore, the next stage was to examine the accessibility of guests to CB[7]. Ammonium ions are known to bind tightly within CB[7], while also possessing high water solubility.[56] A solution of CB[7] (5 µL of 10 mM stock) in buffer was added to the *trans* well. Shortly thereafter, reproducible blockages characteristic of CB[7] trapping were observed (**Figure 2.24A**). After a period, ammonia was added to the *trans* well (**Figure 2.24B**). Almost immediately, the dwell time of the CB[7] events was decreased (**Figure 2.24C and D**). These findings are consistent with the known chaotropes influence of the relatively large NH_4^+ and Cs^+ cations, which decreases the hydrophobic effect, which presumably plays a role in driving CB[7] association with the nanopore. Consistent with this hypothesis, K^+ on the other hand is a kosmotrope, which accounts for the higher stability of CB[7]•nanopore complexation at higher KCl concentrations reported above (**Figure 2.12**). The influence of NH_4^+ is reassuring as it is consistent with NH_4^+ binding to the CB[7]. However, the ion current traces did not reveal discrete NH_4^+ binding events, nor did it establish whether NH_4^+ could bind on, or off the CB[7] whilst captured within the nanopore.

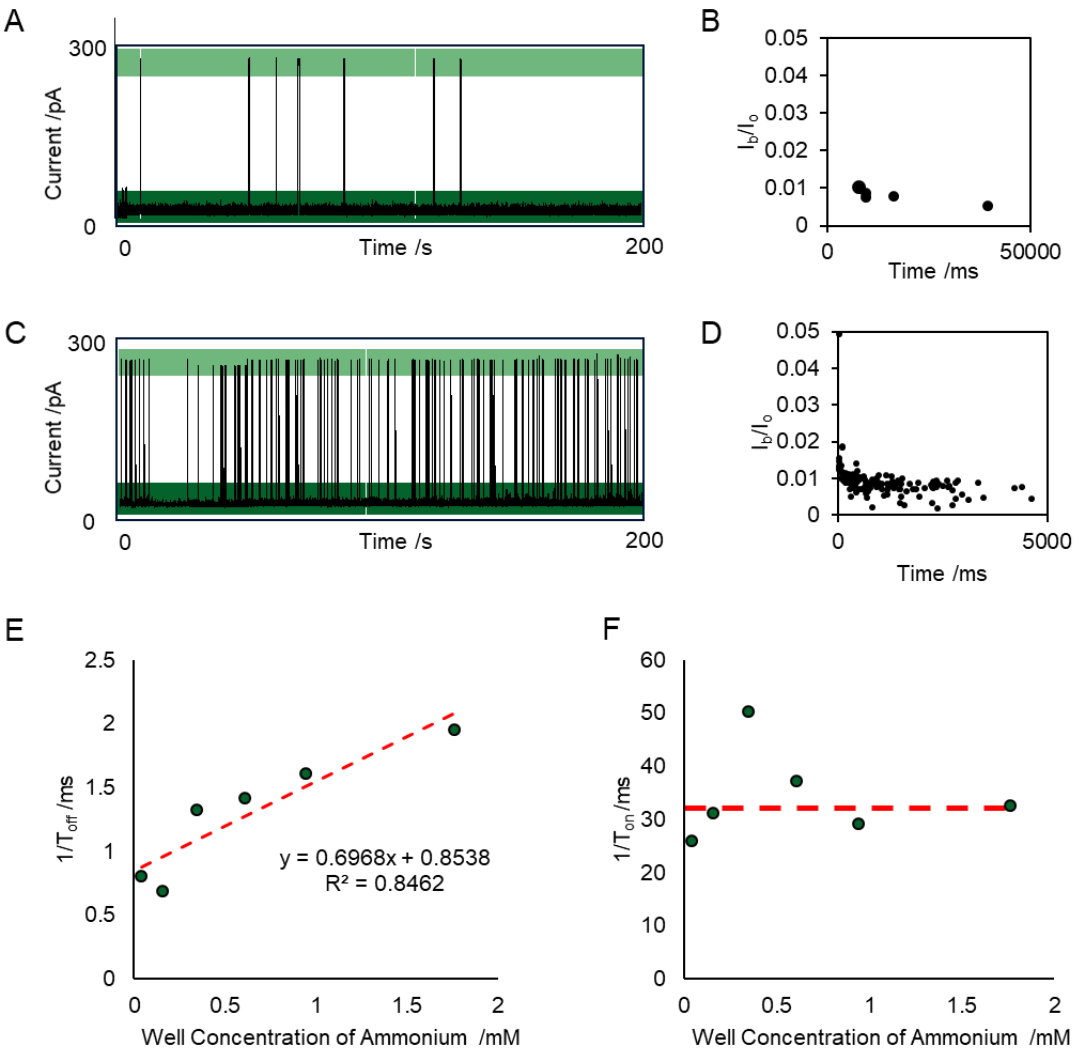

Figure 2.24: A) Example trace of a single channel with CB[7] (5 µL of 10 mM stock) added *trans.* 3 M KCl, 30 mM K_2HPO_4, pH 8. Voltage +100 mV. Lowpass Bessel filter 100 kHz and output gain x20. B) Plot of Ib/Io against time for the data shown in example trace A. C) Example trace of a single channel with CB[7] (5 µL of 10 mM stock) added *trans* and ammonia (1.76 mM). 3 M KCl, 30 mM K_2HPO_4, pH 8. Voltage +100 mV. Lowpass Bessel filter 100 kHz and output gain x20. D) Plot of Ib/Io against time for the data shown in example trace D. E) plot of $1/T_{on}$ against percentage volume of ammonia. F) Plot of $1/T_{off}$ against percentage volume of ammonia.

Hence it remained necessary to assess the accessibility of the CB[7] cavity, and it was hoped that the binding of a larger known CB[7] guest would give rise to detectable ion current changes. Accordingly, spermine was selected for this investigation (**Figure 2.25**).[57-58]

A control experiment was performed in which spermine was added to the *trans* side of the protein in the absence of CB[7], which produced no signals under a positive or negative applied potential. The same was observed when the polyamine was added to the *cis* side in the absence of CB[7]. Upon addition of CB[7] to the *trans* well, new levels were observed (**Figure 2.25C**).

Interestingly, these were at a higher current level that the blockade caused by CB[7] alone. Purely based on size, it would be expected that a host-guest complex would produce a greater blockage than the host alone. There are two proposed explanations for this observation; the encapsulation of the spermine may a) change the geometry or depth of penetration within the pore, and/or b) change the electronic properties of the CB[7], which in turn changes the flow of ions around the host-guest complex. While analyte geometry and size are generally accepted as having the dominating effect on current blockage, there is growing evidence in the literature that factors such as induced charge, electroosmotic flow and surface conductance can have drastic effects.[59] Regardless of the effect at play, this was a reassuring result, as it demonstrated that binding of a guest within CB[7] can be observed and that such events can occur on a time scale of several seconds.

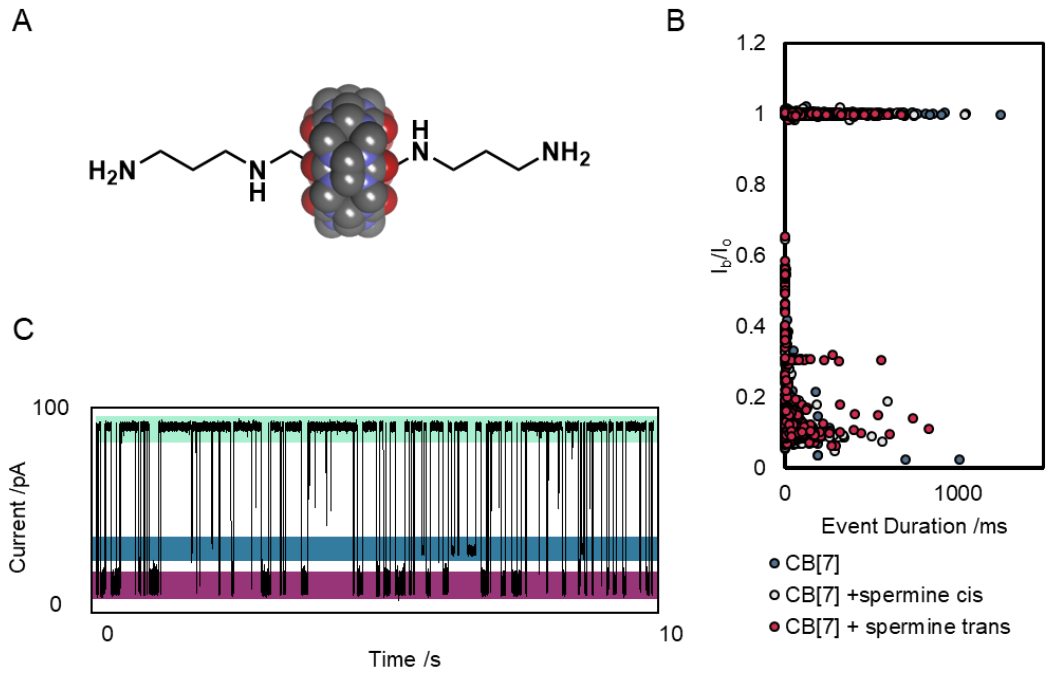

Figure: 2.25: A) Structure of spermine encapsulated by CB[7]. B) Plot of the I_b/I_o for the channel in the presence of CB[7] (blue), CB[7] with spermine added *cis* (white) and CB[7] with spermine added *trans* (red). A new cluster of points can be observed at I_b/I_o = 0.3 when spermine is added to the *trans* well in the presence of CB[7]. C) Example trace showing the major events attributed to CB[7] (purple) and the events attributed to spermine (blue).

To investigate this further, the pH of the experimental conditions were varied (**Figure 2.26**). Spermine is a polyamine, with two terminal primary amines and two internal secondary amines. While literature values vary slightly, the terminal amines have pK_a value of ~11 and ~10 and the internal amines have a pK_a ~8.[60-61] Therefore, at pH 8 it would be expected that around 50-75% of the amines would be protonated. By lowering the pH of the well to ~6, it would be expected that the spermine would be fully protonated. Moreover, it is know that encapsulation of amines within CB[7] can result in pH shifts of several log units, meaning that the extent of protonation in the bound state would be further enhanced.[62-63]

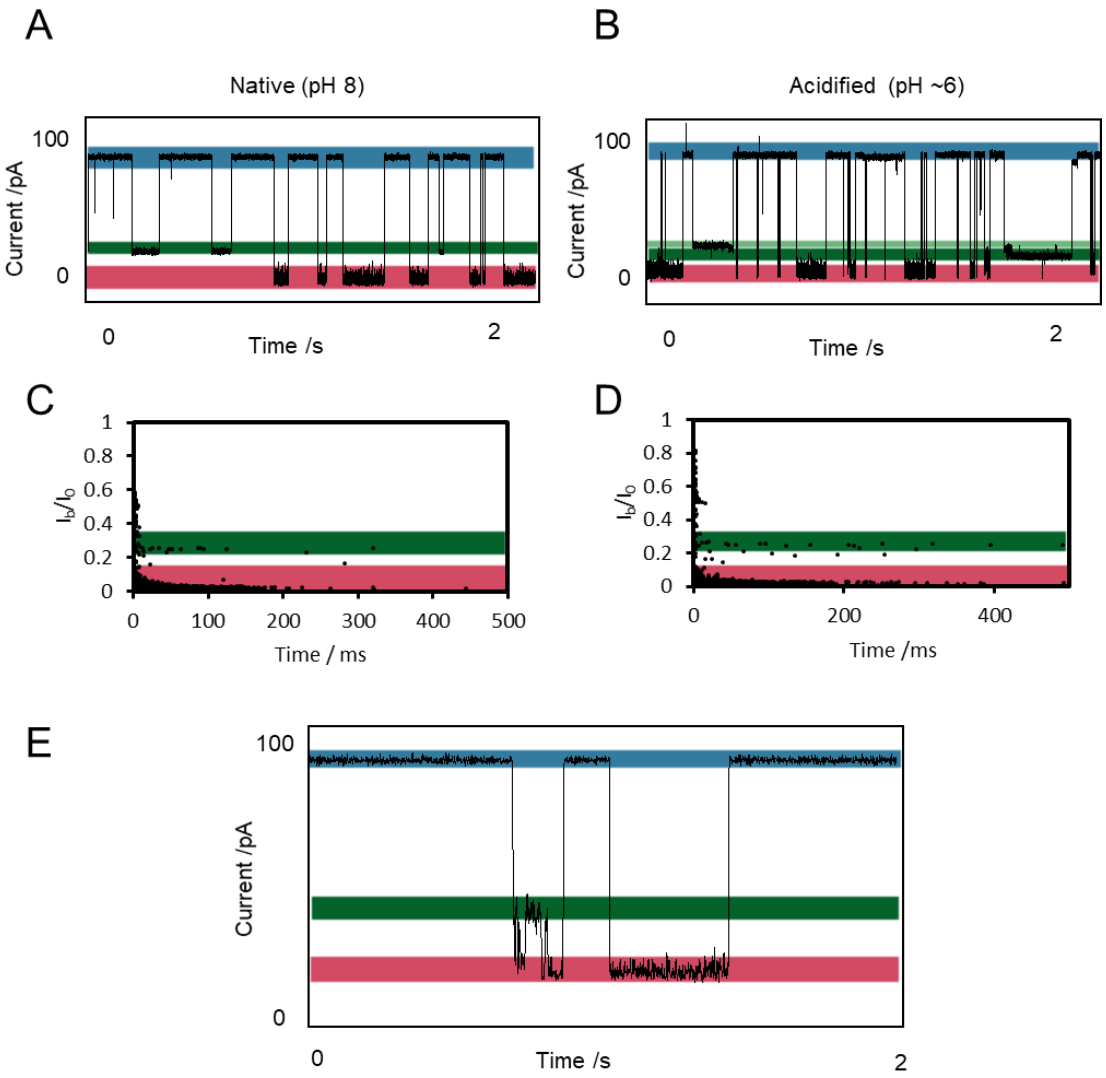

Figure 2.26: Binding events in the presence of spermine. A) CB[7] (10 µL of 10 mM stock) was added to the *trans* well and binding events were observed (pink). A new level (green) was observed when spermine (10 µL of 100 mM stock) was added to the *trans* side. B) The well was acidified to pH 6 by the addition of HCl (1 M). Events became longer and additional levels were observed. C) Plot showing the blockage against the dwell time for the binding events at pH 8 for CB[7] (pink) and the CB[7] + spermine level (green). D) Plot showing the blockage against the dwell time for the binding events at pH 6 for CB[7] (pink) and the CB[7] + spermine level (green). E) Example trace showing a rare occurrence of the event transitioning from CB[7] (pink) to CB[7] + spermine (green). 1 M CsCl, 30 mM K_2HPO_4, pH 8 or pH 6. Voltage +100 mV. Lowpass Bessel filter 100 kHz and output gain x50.

Interestingly, as the reaction buffer was acidified, there was a marked change to the observed events attributed to the host-guest complex (**Figure 2.26B**). While there was no marked change in the lower CB[7] level, the duration of the

host-guest events increased by several orders of magnitude. In addition, a new sub-level emerged (**Figure 2.26**, light green). This level was always reached from a previously established host + guest level, and never directly occupied from the free state (**Figure 2.26**, dark green). This would suggest that the new level is inherently connected with the original. It was proposed that the shift in level corresponds with a shuttling of the macrocycle between different amine stations of the spermine. Due to the breaking of symmetry upon capture within the nanopore, there are four potential amine•CB[7] binding stations.

A further analysis of the ordering of the current levels was performed to provide insight into the mechanism by which CB[7] enters the pore with a guest. Across several hundred events, only limited instances were observed where a transition was observed from the lower CB[7] level (**Figure 2.26,** pink) to the upper CB[7] + guest level (**Figure 2.26**, green). All transitions from the lower CB[7] occurred from the previously discussed minor event (**Figure 2.12**). This supports the hypothesis that the minor event arises from the dissociation of the bound cation within the pore. As such, the macrocycle is only capable of achieving capture of a guest during the minor event.

However, it would appear that capture of the guest is predominantly occurring in the bulk and not while the macrocycle is resident in the channel. When not inherently problematic, this does raise some concerns for consideration in future studies. It also suggests that while the cavity of CB[7] is (rarely) accessible when it is captured within the pore, it is significantly less accessible than in the bulk solution. Therefore, if a reactive guest is captured prior to entry to the pore, initial reaction steps may occur in the bulk and not be observed within the pore. Nonetheless, this study demonstrated that CB[7] can be captured in the lumen of an α-HL nanopore in a KCl buffered solution.

2.5 Single-molecule observation of cucurbituril-catalysed Diels-Alder reactions

The Scherman group have shown that CB[7] can catalyse the intramolecular Diels-Alder reaction of alkyne-terminated furan substrates, and the turn-over rates of differently substituted substrates was examined (**Figure 2.27**).

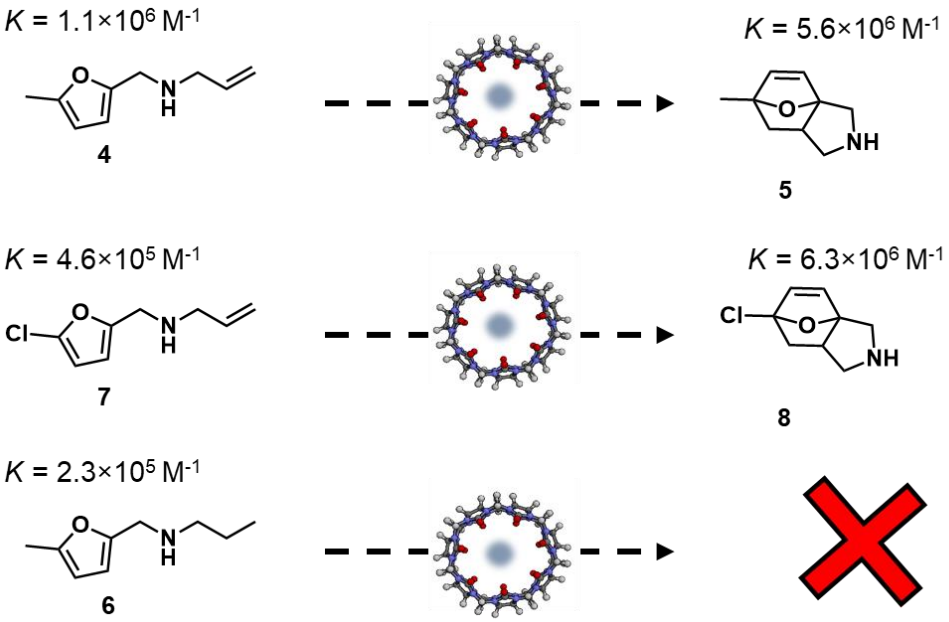

Figure 2.27: Compounds **4** and **7** were provided by the Scherman group. These compounds will undergo Diels-Alder reactions in the presence of CB[7]. The products **5** and **7** were also provided. The control compound **6** was also provided. It has a similar size and chemical properties, but lacks the alkene needed to undergo the cyclisation reaction. Binding constants (*K*) are shown above each compound.

From studies conducted by the Scherman group, 50% conversion of the methyl-substituted compound (compound **4**) occurred within 1.2 hours, while the chloro-substituted compound (compound **7**) saw 50% conversion in 0.3 hours at 37 ˚C in D_2O.[58] To better characterise the interactions within the pore, a sample of the non-reactive control (compound **6**) was initially obtained from the Scherman group and later synthesised in-house. Compound **6** is known to bind with CB[7] in a similar fashion to the reactive alkene-terminated variants.

However, as compound **6** contains a non-reactive terminal alkane it cannot undergo intramolecular Diels-Alder.

Additional experimental considerations must be made for our studies. Notably, the reaction conditions used in previous work could not be directly applied to nanopore experiments. Reaction temperatures were lowered from 37 ˚C to room temperature, due to a lack of heating capacity for the nanopore cells (see note on room temperature in **Chapter 5, Section 5.1**). Moreover, the original kinetic studies were conducted in D_2O, but this would be unsuitable for nanopore experiments since we require a substantial salt concentration for ion-current detection. Accordingly, it was necessary to first assess whether the reaction could progress in the conditions to be employed for nanopore studies.

Bulk observations of Diels-Alder catalysis

To determine whether the established nanopore conditions were suitable, the reaction progression was observed *via* ^{1}H NMR. Using a deuterated buffer to account for isotope effects (1 M KCl, 30 mM KPi, pD 7.2), a solution of CB[7] (20 mM) was made in 600 µL. To this, compound **1** was added to give a final concentration of 2.4 mM. A ^{1}H NMR spectrum was recorded immediately after this addition, and subsequent points were recorded at 0.5, 1, 2, 6, 12, and 24 hours (**Chapter 5. Section 5.4, Figure 5.12**).

Since the CB[7] concentration was constant through the experiment it could be used as an internal standard. Hence, the consumption of the starting material was monitored using the CB[7] peak at 4.42 ppm as an internal standard. Full encapsulation occurred almost immediately and no free compound **1** was observed in solution at the time of the first measurement. The peak at 4.21 ppm was used as the reference peak for the reagent. This corresponds to proton d of the encapsulated compound **1** (**Chapter 5. Section 5.4, Figure 5.12**). After 12 hours, 47% of the starting material had been consumed (**Chapter 5, Section 5.4, Figure 5.13**). This was compared to a 50%

conversion in 1.2 hours in D_2O at 37 °C.[37] The slower turnover rate was likely due to the lower reaction temperature. However, this was a very encouraging result as it demonstrated that the catalytic capabilities of CB[7] were not diminished by the presence of salt buffer. Control studies of the Diels-Alder reagents in the absence of CB[7] were not conducted, as this the turnover without a catalyst has previously been shown to be incredibly slow.[37]

While a single channel can persist for many hours, the inherent instability of the membrane can greatly reduce viable experimental time. In addition, long-duration experiments can lead to drift in the electrode potentials and buffer evaporation that can have detrimental effects on the reliability of observations. Therefore, reactions that occur on a shorter time scale are more suited to nanopore studies. Hence, we also examined turn-over of the more reactive chloro-substituted reagent (compound **7**) in the 2 M KCl buffer to ensure that the increased salt concentration did not impede the reaction.

Using deuterated buffer (2 M KCl, 30 mM KPi, pH 7.2) a solution of CB[7] (44 mM) was made in 600 µL. To this, compound **7** was added to give a final concentration of 44 mM (1:1 equivalents of CB[7] to reagent). A ^{1}H NMR spectrum was recorded immediately, and subsequent points were recorded at 0.5, 1, 2, 6, 12, and 24 hours (**Figure 2.28**).

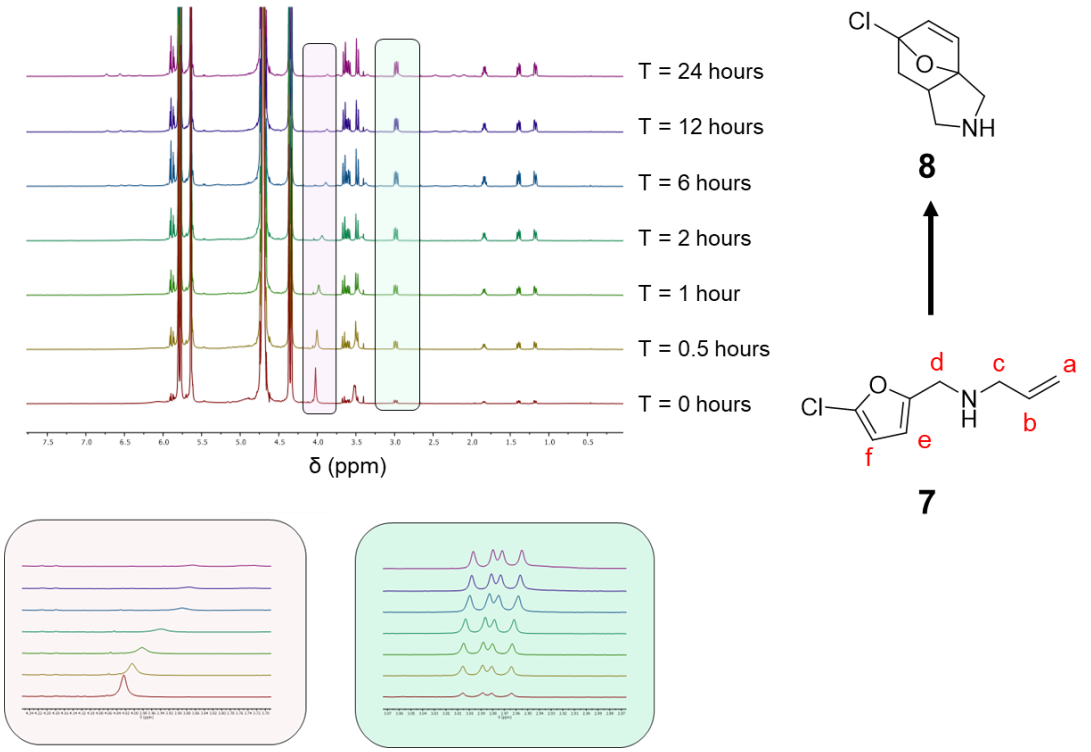

Figure 2.28: Turnover of compound **7** by CB[7], as observed by proton NMR in 2 M KCl buffer. Consumption of compound **7** was observed from the peak at 4.04 ppm (pink). Formation of compound 1 b was observed by the emergence of the peat at 2.99 ppm (green). As the concentration of CB[7] remained constant throughout, this was used as an internal standard. The peak at 4.42 ppm was selected as the standard peak. A solution of CB[7] (44 mM) was made in 600 µL. To this, compound **7** was added to give a final concentration of 44 mM. 2 M KCl, 30 mM KPi, pD 7.2

Since the CB[7] was constant throughout the experiment it could be used as an internal standard for quantification of concentrations (**Figure 2.29A**, grey). Clear signals could be observed for the encapsulated starting material (**Figure 2.29A**, purple) and the encapsulated product (**Figure 2.29A**, green). After ~4 hours, 50% of the starting material had been consumed (**Figure 2.29B**). This was pleasing in two respects: it demonstrated that the Diels-Alder reaction would turn over in a higher salt concentration buffer and that a faster turn over could be obtained under ambient conditions. See **Chapter 5, Section 5.4, Figure 5.14** for tabulated data.

It is known that CB[7] binds compound **8** with high affinity (K = 6.3×10^6), which means it may compete with the binding for the starting material compound **7**

(K = 6.3×10^6).[37] However, notable binding of compound **8** does not appear to occur until approximately 6 hours after incubation of CB[7] and compound **7** **(Figure 2.29B)**.

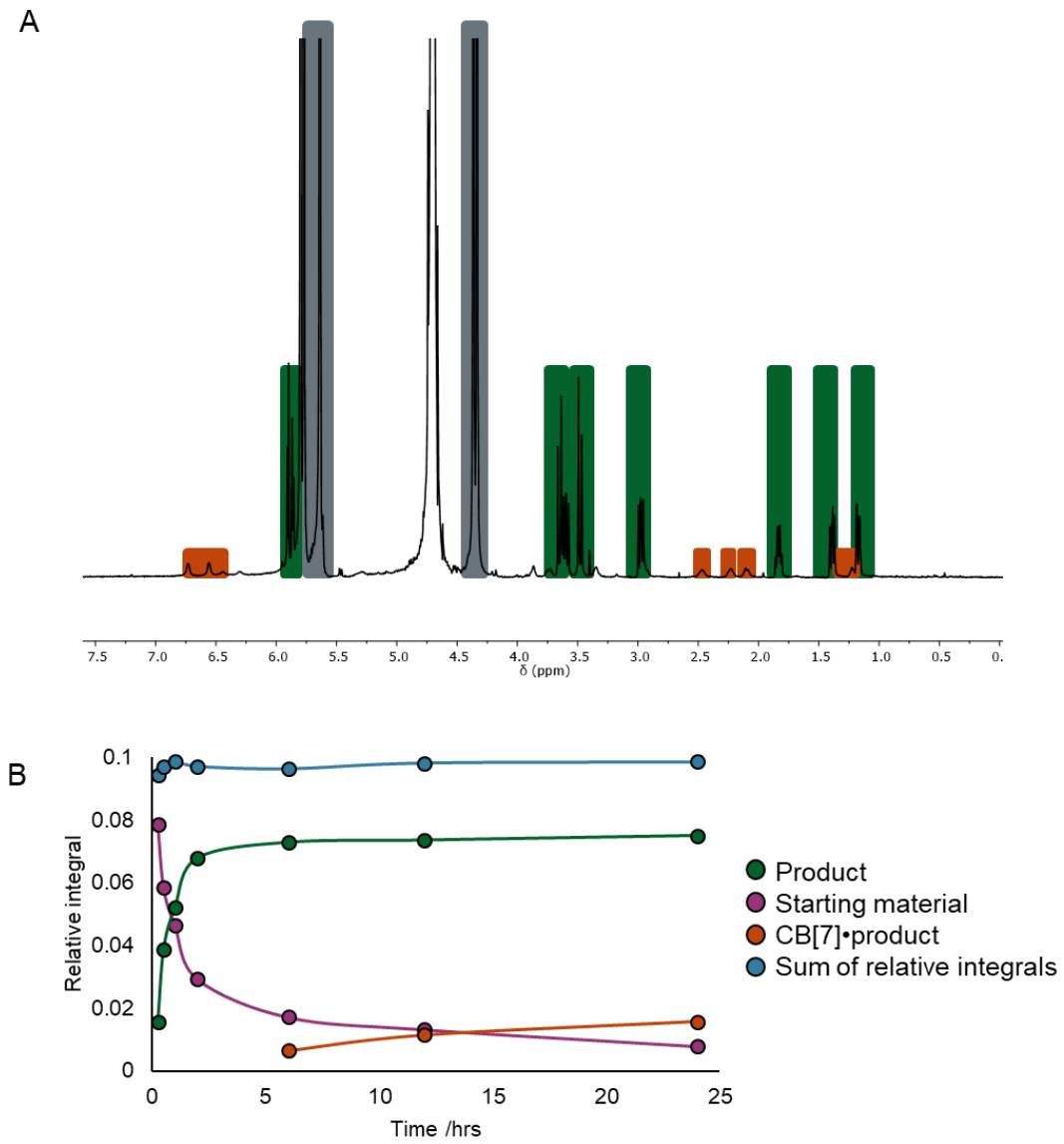

Figure 2.29: A) Proton spectrum of compound **7** after 24-hour incubation with CB[7]. CB[7] signals are shown in grey, compound **8** in green and CB[7]•compound **8** in orange. B) Plot of the time against the relative integral for compound **7** (purple) and the formed compound **8** (green) and CB[7]•compound **8** (orange). The sum of all three is plotted in blue. See **Chapter 5, Section 5.4, Figure 5.14** for tabulated data.

While it is reassuring that the reaction will turn over in conditions relevant for nanopore studies, some caution must still be taken. There is a stark difference between bulk kinetics and single-molecule turnover of a reaction. While a reaction may take hours to reach 50% conversion in the bulk, reactions occurring on the single-molecule level are stochastic and span vast orders of magnitude in the individual kinetics of different molecules. In addition, reactions occurring within the nanopore will be under an applied potential (*i.e.* electric field), which is known to have substantial kinetic effects (**see Section 3.5** in **Chapter 3**).[64] Nonetheless, the bulk studies form a firm foundation.

Single molecule observations of Diels-Alder catalysis

Control experiment: Diels-Alder reagent interactions with α-HL

To dissect the observed interactions of the host-guest complex with the nanopore, it was necessary to characterise the interaction of each component independently. The interaction of CB[7] with the channel has been discussed extensively in the previous sections. To investigate the interaction of the guest with α-HL a single channel was formed. No binding events were seen when a solution of compound **7** in water (10 mM, 10 µL) was introduced to the *trans* well of single channel under a constant applied potential of +100 mV (**Figure 2.30A**). The all points histogram (**Figure 2.30D**) of the binned current levels of the free pore (**Figure 2.30A**) and the channel in addition of compound **7** (**Figure 2.30B**) shows near-identical overlap. In addition, the histogram exhibits a non-Gaussian distribution and has prominent tailing in the lower potentials. This is characteristic of random signal noise, and is to be expected in all data. It was concluded that addition of compound **7** to the *trans* well of α-HL did not result in any measurable binding events. Therefore, any events observed that deviate from that expected from CB[7] when both the host and guest are present can be attributed to a host-guest complex and not compound **7** interacting with the pore.

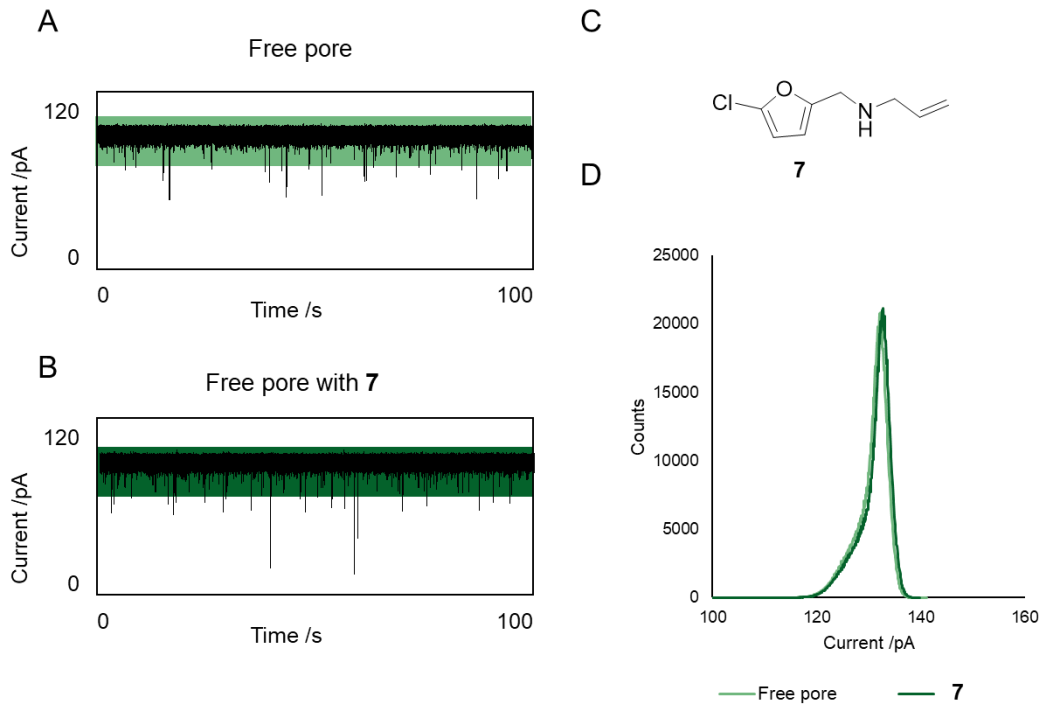

Figure 2.30: A) Nanopore trace for the free pore under a constant applied potential. 1 M KCl, 30 mM K_2HPO_4, pH 8. Voltage +100 mV. Lowpass Bessel filter 100 kHz and output gain x50. B) Nanopore trace for the channel in the presence of compound **7**. 1 M KCl, 30 mM K_2HPO_4, pH 8. Voltage +100 mV. Lowpass Bessel filter 100 kHz and output gain x50. C) Structure of compound **7**. D) All-points histogram for the nanopore traces shown in A) and B). Current bins set at 0.1 pA.

Binding of guest in a high salt buffer

As discussed in the previous sections, 2 M KCl buffer was identified as being most likely to be a suitable buffer for the observation of events. However, it was still decided to explore the interaction of the host and a guest in 3 M KCl buffer, due to the long channel dwell times of CB[7] at this higher concentration. A single channel was formed and prolonged binding events occurred following the addition of CB[7] to the *trans* well. These binding events had a single, defined level (**Figure 2.31A**), which is reflected as a normal distribution in the all-points frequency histogram (**Figure 2.31C**). As compound **1** was titrated into the well, a notable shift was observed in the current trace (**Figure 2.31B**).

From the all-points histogram, a very minor, but new level appeared at ~2 pA (**Figure 2.31C**).

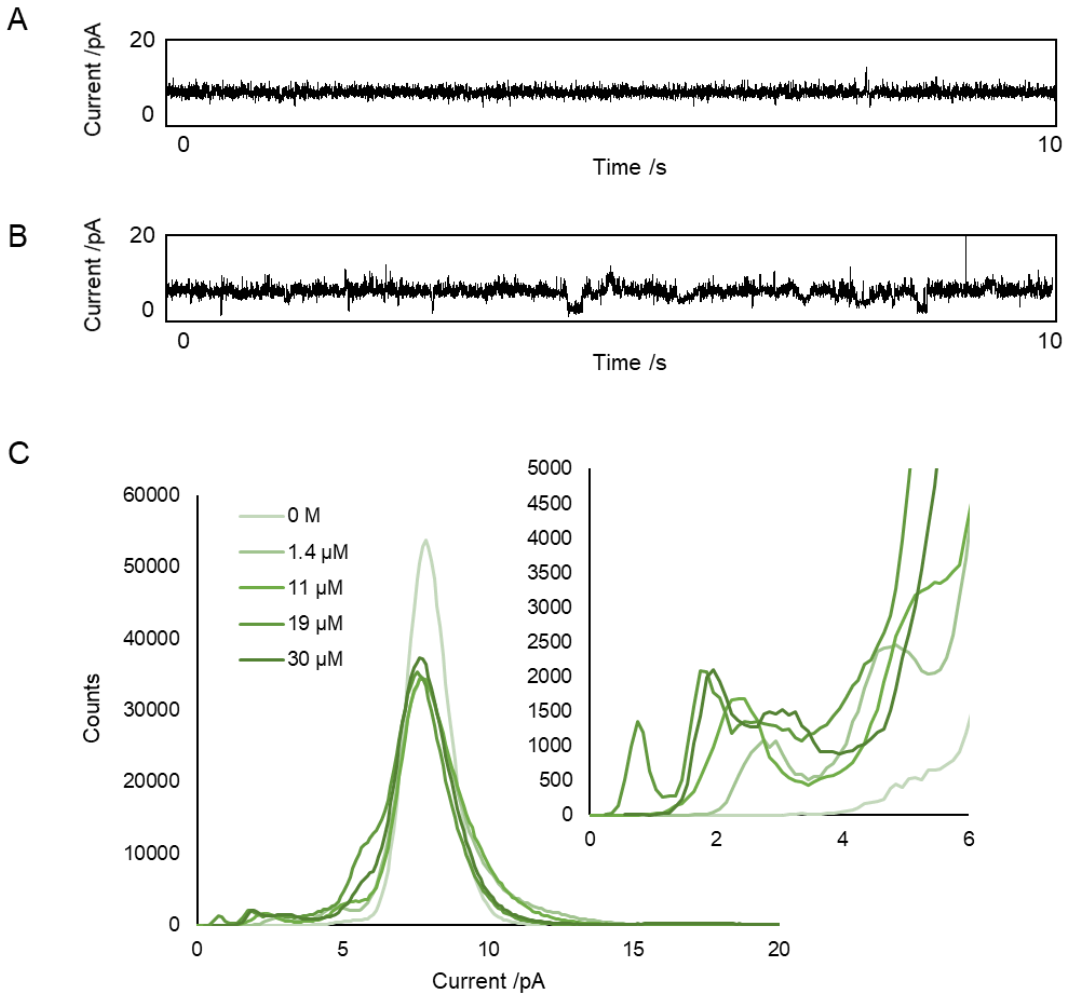

Figure 2.31: A) Current trace for the binding event of CB[7]. 3 M KCl, 30 mM K_2HPO_4, pH 8. Voltage +100 mV. Lowpass Bessel filter 100 kHz and output gain x20. B) Current trace for the binding events of CB[7] in the presence of compound **1** (30 µM). Deviations from the base line current can be observed. 3 M KCl, 30 mM K_2HPO_4, pH 8. Voltage +100 mV. Lowpass Bessel filter 100 kHz and output gain x20. C) All-points frequency histogram of the binding events as the concentration of compound **1** was increased.

Despite the low prevalence of this state, this is a promising observation as it suggests that the host-guest complex can be distinguished from the host alone. However, due to the poor resolution it was not possible to observe the turnover of the Diels-Alder reaction at the single-molecule level. Therefore, attention

was turned to the 2 M buffer system. As previously discussed two distinct levels could be seen: the major and minor event. It was though that the minor event may be due to the dissociation of the metal ion. If this were the case, it would make the macrocycle more accessible to a host. This was verified by the studies with spermine (**Section 2.4**). Therefore, attention was focused on the minor events.

Using to a 2 M buffer, a single channel was formed and CB[7] was added to the *trans* well. Under an applied voltage of +150 mV, deep major binding events were observed. As discussed previously, there were well defined minor events within these major binding events (**Figure 2.32A**). For this study, compound **7** was selected as the guest (**Figure 2.32B**). Upon addition of compound **7** to the *trans* well, new levels were observed within the upper level (**Figure 2.32B**).

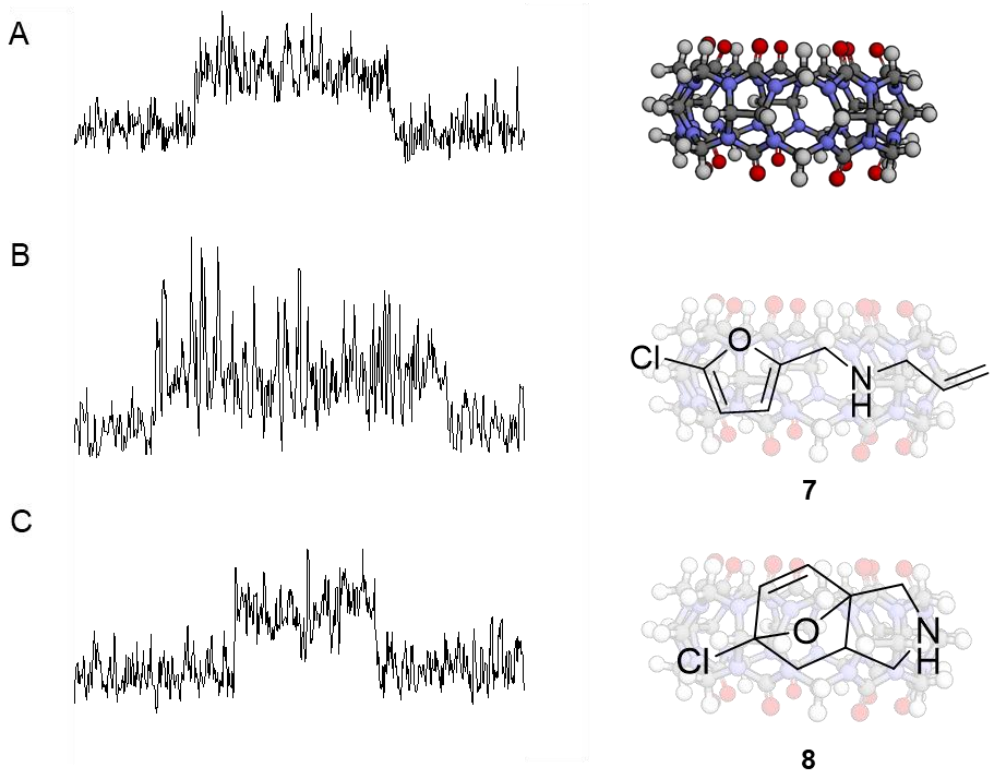

Figure 2.32: A) Characteristic current trace of the minor event within the binding events upon addition of CB[7] (10 µL of 10 mM stock) to the *trans* well. B) Characteristic current trace of the minor event within the binding events upon addition of CB[7] (10 µL of 10 mM stock) in the presence of compound **7** (10 µL of 10 mM stock). Further examples are shown in **Appendix A, Figure A.10** and **A.11**. C) Characteristic current trace of the minor event within the binding events upon addition of CB[7] (10 µL of 10 mM stock) in the presence of compound **8** (10 µL of 10 mM stock). 2 M KCl, 30 mM K2HPO4, pH 8. Voltage +150 mV. Lowpass Bessel filter 100 kHz and output gain x50

From visual inspection of the events it would appear a new level has emerged upon the addition of compound **7**. However, the interchange between the states is rapid and distinct levels cannot be resolved. In addition, no regular or repeating patterns were observed, which would be indicative of the iterative steps of reaction turn over. Attempts at single channel level detection of the sub-levels were unsuccessful due to the rapid level changes and poor signal to noise ratio. In order to quantify these levels, the experiment was repeated on an identical set up with compound **8** (**Figure 2.33C**) in place of compound

7. Both compound **8** and **7** are known to bind with CB[7],[37] therefore distinct signals would be expected for each. As compound **7** is turned over to **8** it would be expected that both signals would be present. For comparison, binding events in the presence of compound **9** were recorded under identical conditions. Compound **9** will bind with CB[7] but unlike compounds **7** and **8**, it will not enter into a hairpin conformation.[37] Therefore, a difference would be expected when comparing the signals.

As distinct levels could not be detected, the events within the minor event were analysis *via* all-points histogram. Due to the small magnitude of current changes within the minor level, the signals became lost in the noise when all-points analysis was conducted on both the major and minor event. Therefore, only the levels occurring within the minor event were analysed. In Clampfit 10.7, cursors were positioned at the first and last point of the upper level (**Appendix A, Figure A.12**). Upper-level events that coincided with the beginning or end of the major binding event (**Appendix A, Figure A.13**) were excluded. All-points between the cursors were extracted using the 'Transfer Trace' function and from this histogram analysis was conducted in Excel. This process was completed for the minor events in the presence of CB[7], CB[7]•compound **7**, CB[7]•compound **8** and CB[7]•compound **9.**

From the all points histogram, the minor event is observed as a single Gaussian distribution at I_b/I_o= 0.16 in the presence of CB[7] alone (**Figure 2.33**, black). Upon the addition of compound **7** (**Figure 2.33**, red), two additional peaks are seen to emerge at I_b/ I_o = 0.15 and I_b/ I_o = 0.12. Interestingly, a similar level is observed at $I_b/$= 0.12 when compared to the binding events when compound **8** (**Figure 2.33**, blue) was introduced. This would suggest that the level at I_b/I_o = 0.12 corresponds to the CB[7]•compound **8** complex and the peak I_b/I_o = 0.15 corresponds to the intermediate product. In contrast, when compound **9** was introduced, no peak was observed at I_b/I_o = 0.15 or 0.12. However, a prominent peak was observed at I_b/I_o = 0.05. This is consistent

with a CB[7]•compound **9** complex forming. As compound **9** will bind with the macrocycle but not enter into a hairpin conformation, a distinctly different signal would be expected. From this, it can be determined that the catalytic turnover of a Diels-Alder reaction can be observed at the single molecule level.

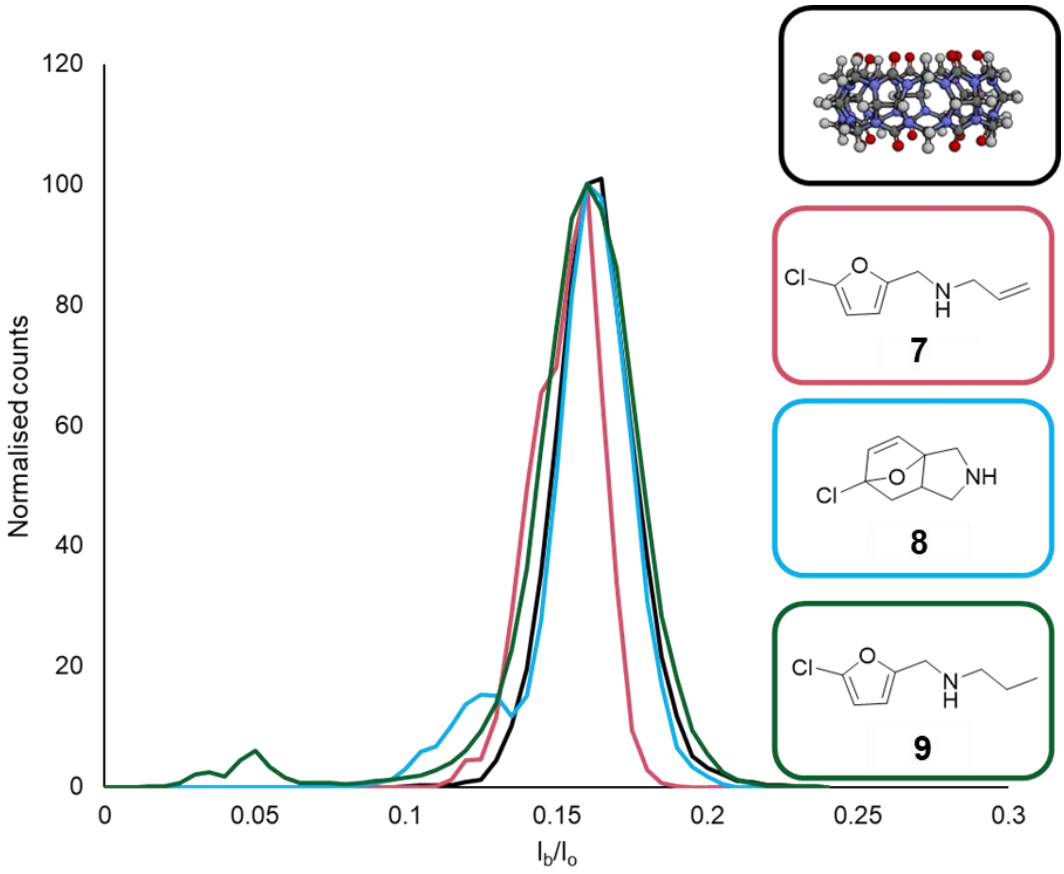

Figure 2.33: All points histograms for the I_b/I_o for the minor events for CB[7] (black), CB[7]•compound **7** (red), CB[7]•compound **8** (blue) and CB[7]•compound **9** (green). move the legend to the box. CB[7] (10 µL of 10 mM stock) was added to the *trans* well followed by compound **7** (10 µL of 10 mM stock), compound **8** (10 µL of 10 mM stock) or compound **9** (10 µL of 10 mM stock). The I_b/I_o was normalised to the level of CB[7] and the counts were given as a percentage of the total counts.

2.6 Conclusions

Here, we have determined that CB[7] can be applied as a molecular adapter for nanopore technology. The dwell time of the binding events can be controlled by modulation of the applied current or buffer salt concertation.

Through studies with K^+ and Cs^+, there is evidence to suggest that CB[7] may be used as a tool for the detection of metal cations. However, to fully consolidate this, further studies with other cations are required.

CB[n] present an exciting avenue of research for supramolecular chemistry. As a host, CB[n] presents a cavity with a similar polarisability as in the gas phase.[65] At present, many studies of supramolecular chemistry, particularly those of intermolecular forces, validate experimental data with computational studies.[66] However, the majority of these studies occur in the gas phase, and do not account for the interaction of solvents. More directly compatible data could be obtained by utilising CB[n] as a molecular adapter for such. Further coupling of established approaches to study non-covalent interactions with nanopore technology has vast potential to expand fundamental knowledge.

As a host, it has been shown that CB[7] can used to be detect an intramolecular Diels-Alder reaction at the single molecule level. However, this scope of this does appear to be limited. Detection could only occur in a short window, referred to as the minor effect. It is hypothesised that this is where the metal cation dissociates from the macrocycle and allows access to the inner cavity. Despite this, enticing early evidence shows that the starting material, intermediate, and product can each be detected. While the pore signal-to-noise ratio means that limited information about the mechanism can be elucidated, it provided an exciting proof of concept that catalyses can be observed in a nanopore. Future optimisation of the system may lead to an improved signal to noise ratio, which will allow further information to be gleaned.

2.7 References

1. Wisniak, J., Jöns Jacob Berzelius A Guide to the Perplexed Chemist. *The Chemical Educator* **2000,** *5* (6), 343-350.

2. Kirby, A. J., Enzyme Mechanisms, Models, and Mimics. *Angew. Chem. Int. Ed.* **1996,** *35* (7), 706-724.

3. Leeuwen, P. W. N. M. v.; Wiley, I.; Conference on Supramolecular Approaches to, C., *Supramolecular catalysis*. Weinheim : Wiley-VCH: Weinheim, 2008.

4. Lehn, J.-M., Supramolecular Chemistry. *Science* **1993,** *260* (5115), 1762-1763.

5. Lehn, J.-M., Supramolecular Chemistry—Scope and Perspectives Molecules, Supermolecules, and Molecular Devices (Nobel Lecture). *Angew. Chem. Int. Ed.* **1988,** *27* (1), 89-112.

6. Tabushi, I., Cyclodextrin catalysis as a model for enzyme action. *Acc. Chem. Res.* **1982,** *15* (3), 66-72.

7. Cram, D. J., Molecular container compounds. *Nature* **1992,** *356* (6364), 29-36.

8. Houk, K. N.; Nakamura, K.; Sheu, C.; Keating Amy, E., Gating as a Control Element in Constrictive Binding and Guest Release by Hemicarcerands. *Science* **1996,** *273* (5275), 627-629.

9. Ringe, D.; Petsko Gregory, A., How Enzymes Work. *Science* **2008,** *320* (5882), 1428-1429.

10. Meeuwissen, J.; Reek, J. N. H., Supramolecular catalysis beyond enzyme mimics. *Nat. Chem* **2010,** *2* (8), 615-621.

11. Petrosko, S. H.; Johnson, R.; White, H.; Mirkin, C. A., Nanoreactors: Small Spaces, Big Implications in Chemistry. *J. Am. Chem. Soc.* **2016,** *138* (24), 7443-7445.

12. Ying, Y.-L.; Gao, R.; Hu, Y.-X.; Long, Y.-T., Electrochemical Confinement Effects for Innovating New Nanopore Sensing Mechanisms. *Small Methods* **2018,** *2* (6), 1700390.

13. Van Meervelt, V.; Soskine, M.; Singh, S.; Schuurman-Wolters, G. K.; Wijma, H. J.; Poolman, B.; Maglia, G., Real-Time Conformational Changes and Controlled Orientation of Native Proteins Inside a Protein Nanoreactor. *J. Am. Chem. Soc.* **2017,** *139* (51), 18640-18646.

14. Gu, L.-Q.; Bayley, H., Interaction of the Noncovalent Molecular Adapter, β-Cyclodextrin, with the Staphylococcal α-Hemolysin Pore. *Biophys. J.* **2000,** *79* (4), 1967-1975.

15. Braha, O.; Webb, J.; Gu, L.-Q.; Kim, K.; Bayley, H., Carriers versus Adapters in Stochastic Sensing. *ChemPhysChem* **2005,** *6* (5), 889-892.

16. Wu, H.-C.; Astier, Y.; Maglia, G.; Mikhailova, E.; Bayley, H., Protein Nanopores with Covalently Attached Molecular Adapters. *J. Am. Chem. Soc.* **2007,** *129* (51), 16142-16148.

17. Villiers, A., Sur la transformation de la fécule en dextrine par le ferment butyrique. *Compt. Rend. Fr. Acad. Sci* **1891,** *112*, 435-438.

18. Clarke, J.; Wu, H.-C.; Jayasinghe, L.; Patel, A.; Reid, S.; Bayley, H., Continuous base identification for single-molecule nanopore DNA sequencing. *Nat. Nanotechnol* **2009,** *4* (4), 265-270.

19. Sanchez-Quesada, J.; Ghadiri, M. R.; Bayley, H.; Braha, O., Cyclic Peptides as Molecular Adapters for a Pore-Forming Protein. *J. Am. Chem. Soc.* **2000,** *122* (48), 11757-11766.

20. Gu, L.-Q.; Braha, O.; Conlan, S.; Cheley, S.; Bayley, H., Stochastic sensing of organic analytes by a pore-forming protein containing a molecular adapter. *Nature* **1999,** *398* (6729), 686-690.

21. Soskine, M.; Biesemans, A.; Maglia, G., Single-Molecule Analyte Recognition with ClyA Nanopores Equipped with Internal Protein Adaptors. *J. Am. Chem. Soc.* **2015,** *137* (17), 5793-5797.

22. Das, D.; Scherman, O. A., Cucurbituril: At the Interface of Small Molecule Host–Guest Chemistry and Dynamic Aggregates. *Isr. J. Chem.* **2011,** *51* (5-6), 537-550.

23. Masson, E.; Ling, X.; Joseph, R.; Kyeremeh-Mensah, L.; Lu, X., Cucurbituril chemistry: a tale of supramolecular success. *RSC Adv.* **2012,** *2* (4), 1213-1247.

24. Barrow, S. J.; Kasera, S.; Rowland, M. J.; del Barrio, J.; Scherman, O. A., Cucurbituril-Based Molecular Recognition. *Chem. Rev.* **2015,** *115* (22), 12320-12406.

25. Behrend, R.; Meyer, E.; Rusche, F., I. Ueber Condensationsproducte aus Glycoluril und Formaldehyd. *Justus Liebigs Annalen der Chemie* **1905,** *339* (1), 1-37.

26. Freeman, W. A.; Mock, W. L.; Shih, N. Y., Cucurbituril. *J. Am. Chem. Soc.* **1981,** *103* (24), 7367-7368.

27. Tang, B.; Zhao, J.; Xu, J.-F.; Zhang, X., Cucurbit[n]urils for Supramolecular Catalysis. *Chem. Eur. J.* **2020,** *26* (67), 15446-15460.

28. Kim, J.; Jung, I.-S.; Kim, S.-Y.; Lee, E.; Kang, J.-K.; Sakamoto, S.; Yamaguchi, K.; Kim, K., New Cucurbituril Homologues: Syntheses, Isolation, Characterization, and X-ray Crystal Structures of Cucurbit[n]uril (n = 5, 7, and 8). *J. Am. Chem. Soc.* **2000,** *122* (3), 540-541.

29. Cheng, X.-J.; Liang, L.-L.; Chen, K.; Ji, N.-N.; Xiao, X.; Zhang, J.-X.; Zhang, Y.-Q.; Xue, S.-F.; Zhu, Q.-J.; Ni, X.-L.; Tao, Z., Twisted Cucurbit[14]uril. *Angew. Chem. Int. Ed.* **2013,** *52* (28), 7252-7255.

30. Peerannawar, S. R.; Gobre, V. V.; Gejji, S. P., Molecular electrostatic potentials in Cucurbit[n]uril (n=13–16) hosts. *Comput. Theor. Chem.* **2011,** *966* (1), 154-158.

31. Li, Q.; Qiu, S.-C.; Zhang, J.; Chen, K.; Huang, Y.; Xiao, X.; Zhang, Y.; Li, F.; Zhang, Y.-Q.; Xue, S.-F.; Zhu, Q.-J.; Tao, Z.; Lindoy, L. F.; Wei, G., Twisted Cucurbit[n]urils. *Org. Lett.* **2016,** *18* (16), 4020-4023.

32. Cao, L.; Šekutor, M.; Zavalij, P. Y.; Mlinarić-Majerski, K.; Glaser, R.; Isaacs, L., Cucurbit[7]uril·Guest Pair with an Attomolar Dissociation Constant. *Angew. Chem. Int. Ed.* **2014,** *53* (4), 988-993.

33. Rekharsky Mikhail, V.; Mori, T.; Yang, C.; Ko Young, H.; Selvapalam, N.; Kim, H.; Sobransingh, D.; Kaifer Angel, E.; Liu, S.; Isaacs, L.; Chen, W.; Moghaddam, S.; Gilson Michael, K.; Kim, K.; Inoue, Y., A synthetic host-guest system achieves avidin-biotin affinity by overcoming enthalpy–entropy compensation. *PNAS* **2007,** *104* (52), 20737-20742.

34. Assaf, K. I.; Nau, W. M., Cucurbiturils: from synthesis to high-affinity binding and catalysis. *Chem. Soc. Rev.* **2015,** *44* (2), 394-418.

35. Zheng, L.; Sonzini, S.; Ambarwati, M.; Rosta, E.; Scherman, O. A.; Herrmann, A., Turning Cucurbit[8]uril into a Supramolecular Nanoreactor for Asymmetric Catalysis. *Angew. Chem. Int. Ed.* **2015,** *54* (44), 13007-13011.

36. Mock, W. L.; Irra, T. A.; Wepsiec, J. P.; Manimaran, T. L., Cycloaddition induced by cucurbituril. A case of Pauling principle catalysis. *J. Org. Chem.* **1983,** *48* (20), 3619-3620.

37. Palma, A.; Artelsmair, M.; Wu, G.; Lu, X.; Barrow, S. J.; Uddin, N.; Rosta, E.; Masson, E.; Scherman, O. A., Cucurbit[7]uril as a Supramolecular Artificial Enzyme for Diels–Alder Reactions. *Angew. Chem.* **2017,** *129* (49), 15894-15898.

38. Li, T.; Liu, L.; Li, Y.; Xie, J.; Wu, H.-C., A Universal Strategy for Aptamer-Based Nanopore Sensing through Host-Guest Interactions inside α-Hemolysin. *Angew. Chem. Int. Ed.* **2015,** *54* (26), 7568-7571.

39. Aksimentiev, A.; Schulten, K., Imaging α-Hemolysin with Molecular Dynamics: Ionic Conductance, Osmotic Permeability, and the Electrostatic Potential Map. *Biophys. J.* **2005,** *88* (6), 3745-3761.

40. Song, L.; Hobaugh, M. R.; Shustak, C.; Cheley, S.; Bayley, H.; Gouaux, J. E., Structure of Staphylococcal α-Hemolysin, a Heptameric Transmembrane Pore. *Science* **1996,** *274* (5294), 1859-1865.

41. Gu, L.-Q.; Cheley, S.; Bayley, H., Electroosmotic enhancement of the binding of a neutral molecule to a transmembrane pore. *PNAS* **2003,** *100* (26), 15498.

42. Borsley, S.; Haugland, M. M.; Oldknow, S.; Cooper, J. A.; Burke, M. J.; Scott, A.; Grantham, W.; Vallejo, J.; Brechin, E. K.; Lusby, P. J.; Cockroft, S. L., Electrostatic Forces in Field-Perturbed Equilibria: Nanopore Analysis of Cage Complexes. *Chem* **2019,** *5* (5), 1275-1292.

43. Samsonenko, D. G.; Virovets, A. V.; Lipkowski, J.; Geras'ko, O. A.; Fedin, V. P., Distortion of the Cucurbituril Molecule by an Included 4-Methylpyridinum Cation. *J. Struct. Chem.* **2002,** *43* (4), 664-668.

44. Jeon, Y.-M.; Kim, J.; Whang, D.; Kim, K., Molecular Container Assembly Capable of Controlling Binding and Release of Its Guest Molecules: Reversible Encapsulation of Organic Molecules in Sodium Ion Complexed Cucurbituril. *J. Am. Chem. Soc.* **1996,** *118* (40), 9790-9791.

45. Buschmann, H. J.; Jansen, K.; Schollmeyer, E., Cucurbituril as host molecule for the complexation of aliphatic alcohols, acids and nitriles in aqueous solution. *Thermochim. Acta* **2000,** *346* (1), 33-36.

46. Lü, J.; Lin, J.-X.; Cao, M.-N.; Cao, R., Cucurbituril: A promising organic building block for the design of coordination compounds and beyond. *Coord. Chem. Rev.* **2013,** *257* (7), 1334-1356.

47. Gerasko, O. A.; Fedin, V. P., Inclusion compounds of cucurbit[n]urils with metal complexes. *Russ. J. Inorg, Chem.* **2011,** *56* (13), 2025-2046.

48. Tarmyshov, K. B.; Müller-Plathe, F., Ion Binding to Cucurbit[6]uril: Structure and Dynamics. *J. Phys. Chem. B.* **2006,** *110* (29), 14463-14468.

49. Márquez, C.; Hudgins, R. R.; Nau, W. M., Mechanism of Host−Guest Complexation by Cucurbituril. *J. Am. Chem. Soc.* **2004,** *126* (18), 5806-5816.

50. Koner, A. L.; Márquez, C.; Dickman, M. H.; Nau, W. M., Transition-Metal-Promoted Chemoselective Photoreactions at the Cucurbituril Rim. *Angew. Chem. Int. Ed.* **2011,** *50* (2), 545-548.

51. Rad, N.; Sashuk, V., Effect of Na+ and K+ on the cucurbituril-mediated hydrolysis of a phenyl acetate. *Chem. Commun.* **2022,** *58* (34), 5249-5252.

52. Piguet, F.; Discala, F.; Breton, M.-F.; Pelta, J.; Bacri, L.; Oukhaled, A., Electroosmosis through α-Hemolysin That Depends on Alkali Cation Type. *J. Phys. Chem, Lett.* **2014,** *5* (24), 4362-4367.

53. Mecozzi, S.; Rebek, J. J., The 55 % Solution: A Formula for Molecular Recognition in the Liquid State. *Chem. Eur. J.* **1998,** *4* (6), 1016-1022.

54. Nau, W. M.; Florea, M.; Assaf, K. I., Deep Inside Cucurbiturils: Physical Properties and Volumes of their Inner Cavity Determine the Hydrophobic Driving Force for Host–Guest Complexation. *Isr. J. Chem.* **2011,** *51* (5-6), 559-577.

55. Marcus, Y.; Donald Brooke Jenkins, H.; Glasser, L., Ion volumes: a comparison. *J. Chem. Soc., Dalton Trans.* **2002,** (20), 3795-3798.

56. Hoffmann, R.; Knoche, W.; Fenn, C.; Buschmann, H.-J., Host–guest complexes of cucurbituril with the 4-methylbenzylammonium Ion, alkali-metal cations and NH4+. *J. Chem. Soc., Faraday Trans.* **1994,** *90* (11), 1507-1511.

57. Chen, Y.; Huang, Z.; Zhao, H.; Xu, J.-F.; Sun, Z.; Zhang, X., Supramolecular Chemotherapy: Cooperative Enhancement of Antitumor Activity by Combining Controlled

Release of Oxaliplatin and Consuming of Spermine by Cucurbit[7]uril. *ACS Appl. Mater. Interfaces* **2017,** *9* (10), 8602-8608.

58. Chen, Y.; Sun, Z., Supramolecular Chemotherapy Based on the Host–Guest Complex of Lobaplatin–Cucurbit[7]uril. *ACS Appl. Bio Mater.* **2020,** *3* (4), 2449-2454.

59. Wen, C.; Zhang, S.-L., On current blockade upon analyte translocation in nanopores. *J. Appl. Phys.* **2021,** *129* (6), 064702.

60. Casero, R. A.; Woster, P. M., Recent Advances in the Development of Polyamine Analogues as Antitumor Agents. *J. Med. Chem.* **2009,** *52* (15), 4551-4573.

61. Blagbrough, I. S.; Metwally, A. A.; Geall, A. J., Measurement of Polyamine pKa Values. In *Polyamines: Methods and Protocols*, Pegg, A. E.; Casero, J. R. A., Eds. Humana Press: Totowa, NJ, 2011; pp 493-503.

62. Wu, J.; Isaacs, L., Cucurbit[7]uril Complexation Drives Thermal trans–cis-Azobenzene Isomerization and Enables Colorimetric Amine Detection. *Chem. Eur. J.* **2009,** *15* (43), 11675-11680.

63. Pischel, U.; Uzunova, V. D.; Remón, P.; Nau, W. M., Supramolecular logic with macrocyclic input and competitive reset. *Chem. Commun.* **2010,** *46* (15), 2635-2637.

64. Haugland, M. M.; Borsley, S.; Cairns-Gibson, D. F.; Elmi, A.; Cockroft, S. L., Synthetically Diversified Protein Nanopores: Resolving Click Reaction Mechanisms. *ACS Nano* **2019**.

65. Marquez, C.; Nau, W. M., Polarizabilities Inside Molecular Containers. *Angew. Chem. Int. Ed.* **2001,** *40* (23), 4387-4390.

66. Elmi, A.; Cockroft, S. L., Quantifying Interactions and Solvent Effects Using Molecular Balances and Model Complexes. *Acc. Chem. Res.* **2021,** *54* (1), 92-103.

Chapter 3

Chemical Modification of Protein Nanopores

Abstract

Protein nanopores have been extensively exploited for their ability to form reproducible and atomically precise transmembrane channels. Seminal studies primarily utilised native protein channels for sensing applications. As outlined in **Chapter 1**, subsequent studies employed modified channels to achieved enhanced resolution and functionality. The majority of these modifications have relied on mutagenesis to incorporate new functionality or reactive groups. Herein, we explore methods to achieve *in situ* chemical modification of an α-hemolysin nanopore. Three resides within the channel were selected as prospective targets. Successful modification was achieved at lysine residues using an activated ester derived from a carboxylic acid. In a more selective approach, attachment was possible at the single methionine site of the protein by reaction with an oxaziridine derivative. Finally, modification of tyrosine residues was attempted within the pore. However, this did not yield an irreversible modification.

Contributions: Early work on irreversible lysine bioconjugation was carried out by Dr Stefan Borsley. Work on methionine modification was completed in collaboration with Dr Marius Haugland. This has been highlighted accordingly within the text. Unless otherwise started, all other work has been conducted by DCG.

Publications: Section **3.5** was published as **Synthetically Diversified Protein Nanopores: Resolving Click Reaction Mechanisms**. M. M. Haugland, S. Borsley, D. F. Cairns-Gibson, A. Elmi, and S. L. Cockroft*. *ACS Nano*, **2019**, 13 (4), 4101-4110.

3.1 Introduction

In the early days of nanopore sensing, Deamer and Branton hypothesised that the technique would eventually be employed to sequence single strands of DNA (**Figure 3.1**).[1] At the time, this was not possible as the transit of the negatively charged DNA strand through the pore was much too rapid to resolve the individual bases. However, by using the same α-HL framework that Kasinowicz introduced some 30 years earlier, it is now possible to resolve single bases in a ssDNA sequence.[2]

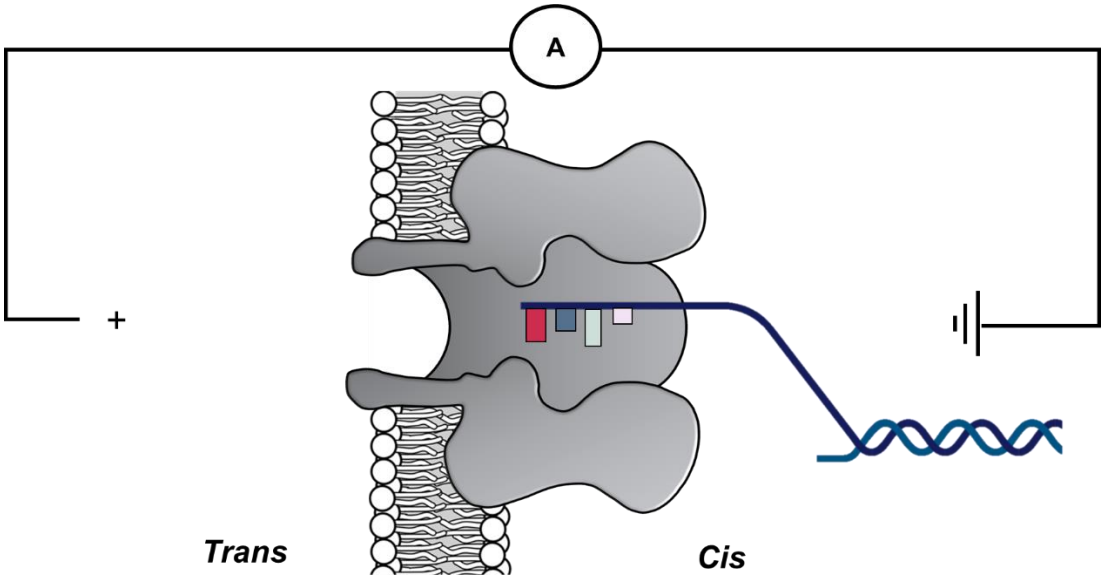

Figure 3.1: Cartoon representation of DNA capture in an α-HL nanopore.

In several cases, this has been achieved through the modification of the protein channel. Such features have been applied to slow the ingress of negatively charged DNA through the channel,[3-4] or to enhance the trapping characteristics.[5] Indeed, it is even possible to modulate the selectivity and sensitivity of a biological nanopore by using mutagenesis.[6] These modifications are often achieved through changes to the protein primary structure.[7] Aside from the technical difficulties involved in mutagenesis, changes to the amino acid sequence can have far-reaching implications on the

ability of the protein subunits to correctly fold, assemble, and insert into a lipid bilayer.[8-9] Therefore, while the application of mutagenesis for the functionalisation of biological nanopores has undoubtedly been highly successful, *in situ* chemical modification remains an enticing goal. The reasoning for this is two-fold: It circumvents potential issues of protein instability and observations of the *in situ* modification can be made in real time.

Seminal work in the 1990s demonstrated the capacity to selectively ligate protein fragments at their termini.[10] More recently, approaches have been developed to selectively modify the N-terminal of proteins.[11] While such methodologies are invaluable for the incorporation of protein labels, they are incompatible with the functionalisation of nanopores as the N-terminus is unlikely to be within the lumen of the channel. Therefore, it is imperative that we look to other approaches to develop methods of selective modification.

Bioconjugation is a chemical method to covalently modify a biomolecule, such as a protein.[12] Historically, cysteine and lysine have been frequent targets for *in situ* chemical modification. As ionisable residues, they can act as reactive nucleophiles in bioconjugation reactions.[13] While lysine is often solvent exposed, it is one of the more promiscuous and prolific amino acids. Therefore, it is not well suited for targeted modification of single residues. Cysteine, on the other hand, is naturally found in lower abundance and may offer greater control over site selectivity. Unfortunately, α-HL contains no natural cysteine residues, so it must be artificially incorporated. Care must be taken when introducing cysteine to a protein due to its ability to form disulfide bonds. Despite this caveat, the Bayley group have extensively incorporated a cysteine residues into the lumen of α-HL in a variety of methods (**Figure 3.2**). As the WT-αHL contains no cysteine residues, this is an extremely attractive approach – by designing the exact location of the cysteine residue, it affords absolute control over the location of the reactive site. Using this method, the

Bayley group have gone onto attach molecular adaptors,[14] observe reaction kinetics,[15] and even design a molecular walker.[16]

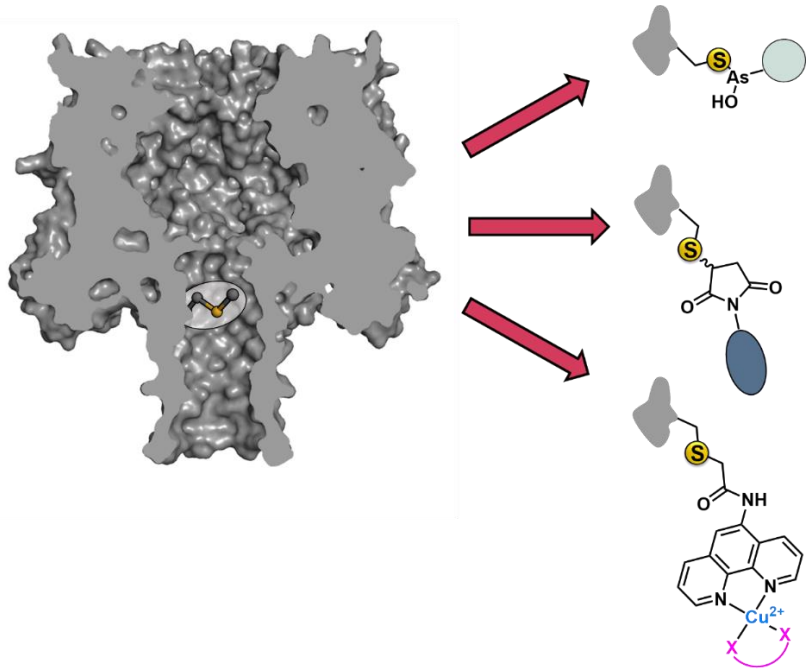

Figure 3.2: Location of cysteine modification at residue 117 in α-HL (left). Select highlight of synthetic modifications appended to the cysteine reside (right).

The toolkit of potentially nanopore-compatible bioconjugation reactions has grown immensely in recent years.[17] Herein, we will discuss approaches to the development of single molecule methods for the *in situ* modification of biological nanopores. Aside from cysteine, residues such as lysine, methionine, and tyrosine have been explored as alternative bioconjugation sites and are explored in the context of nanopore modification in this thesis.

3.2 Project Aim

In this project, we looked to develop a toolkit of chemical methods for modification of wild type (WT) α-hemolysin nanopore embedded in an artificial lipid bilayer. Such *in situ* modification circumvents the need for more arduous approaches such as site-directed mutagenesis and provides a more facile methodology for creating a bespoke single channel. Primary focus has been given to three amino acid resides within α-HL: lysine, methionine and tyrosine. However, this is not an exhaustive list of the solvent-exposed residues within the lumen of the pore.

3.3 Protein selection and identification of viable modification sites

α-HL was the seminal protein used in the 1990s for the development of nanopore sensing.[18] In recent years, a growing number of alternative protein pores and synthetic channels have been explored.[19-21] However, for this work, α-HL was used as a platform for the development of *in situ* chemical modifications to a protein nanopore. α-HL remains one of the most well-established, characterised, robust and commercially available transmembrane channels. The protein consists of a *cis* opening, which widens into the inner lumen of the cap domain before narrowing at the constriction site that leads onto the transmembrane β-barrel with a roughly consistent diameter (**Figure 3.3**).[22] The confinement of the inner cavity can facilitate the attachment of a reactive substrate to the protein. This is of particular significance if the substrate in question is small enough to pass through the *cis* opening, but large enough that passage through the constriction site is not possible.

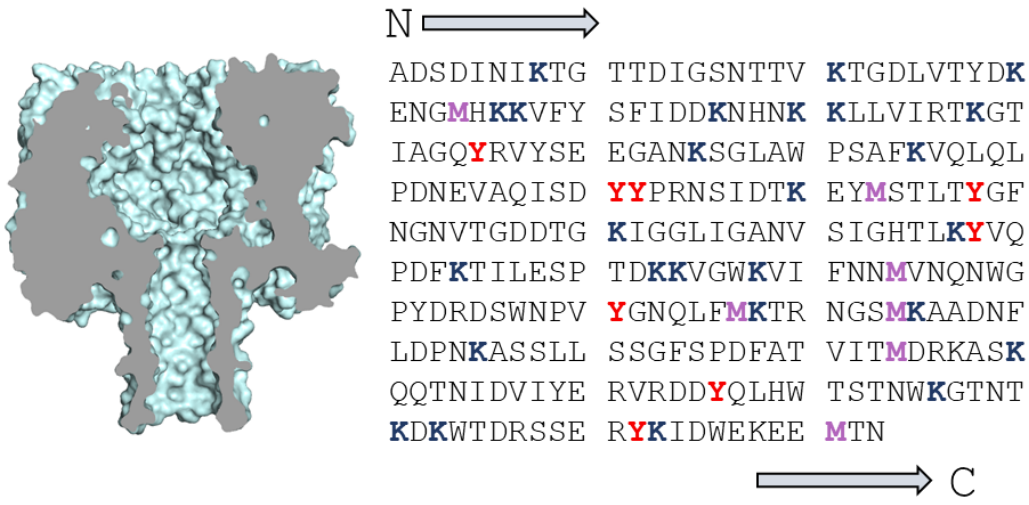

Figure 3.3: Cross-section structure of an assembled hexametric α-HL channel (left). Amino acid sequence of α-HL. Lysine (blue), methionine (purple), and tyrosine (red) are highlighted (right).

Lysine has a prolific abundance in nature, and the reactivity of its primary amine side chain make it a prime target for post-translational modifications (PTM).[23] These properties can be exploited for *in situ* chemical modification of a protein nanopore. α-HL presents with a multitude of lysine residues throughout (**Figure 3.4A**). However, only those that are solvent exposed within the lumen of the pore are practical targets for modification, as these modifications may be oserved. Previous work within the Cockroft group has identified three distinct rings of lysine within α-HL that are accessible for modification.[24] Conveniently, these are located at the *cis* and *trans* openings and at the constriction site (**Figure 3.4B-D** and **Figure 1.14** in **Chapter 1**). It was intended to expand upon on this work, and demonstrate a method to attach a broad scope of substrates to the channel.

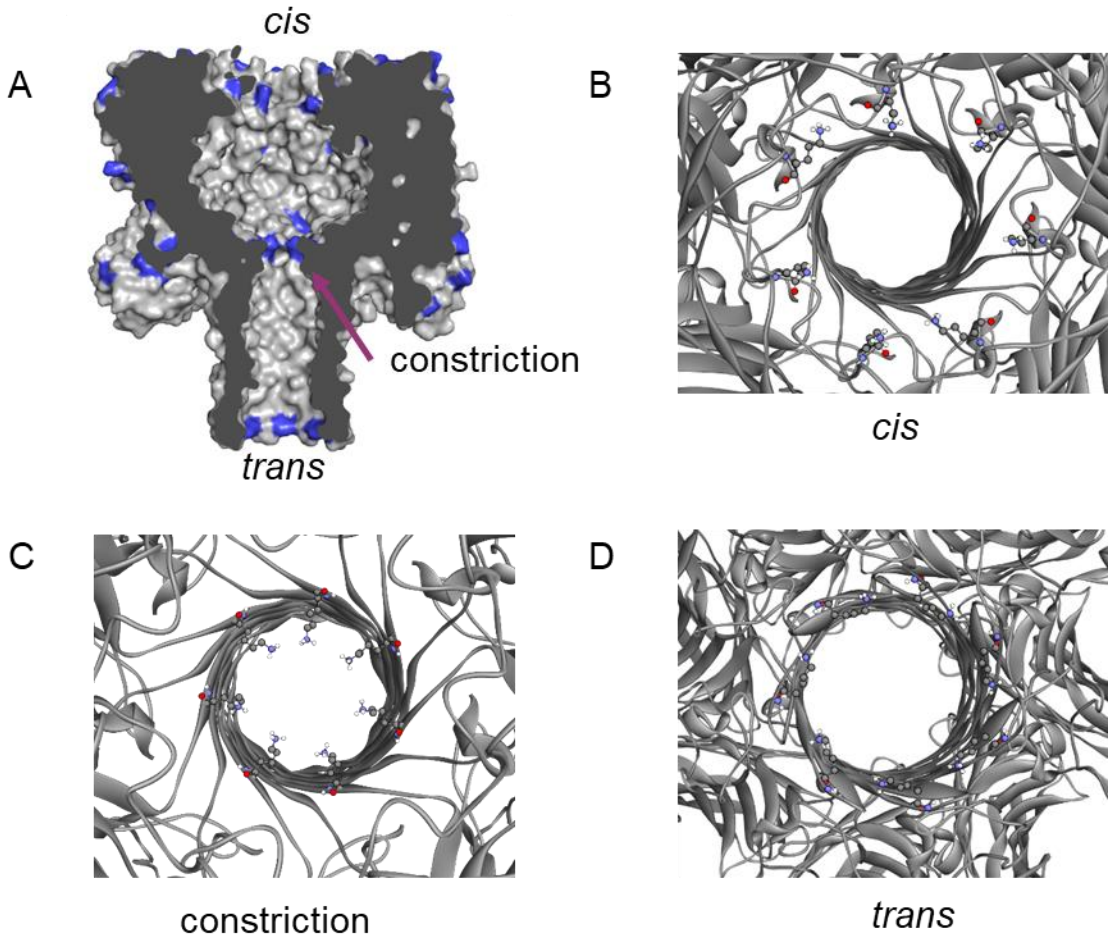

Figure 3.4: A) Location of lysine sites at the *cis, trans* and constriction-site within α-HL nanopore. B) Model showing the location of the *cis* lysine ring. C) Model showing the location of the constriction site lysine ring. D) Model showing the location of the *trans* lysine ring.

Methionine is, perhaps, a less obvious target for modification. Unlike lysine, it is one of the least common canonical amino acids and its hydrophobic nature means that it is rarely solvent exposed. However, α-HL presents a single ring of solvent-exposed methionine residues within its channel, making it a prime target for site-selective modification (**Figure 3.5**). Conveniently, the solvent-exposed methionine residues sit at the constriction site. Such positioning would likely facilitate successful bioconjugation due to the confinement at that site.

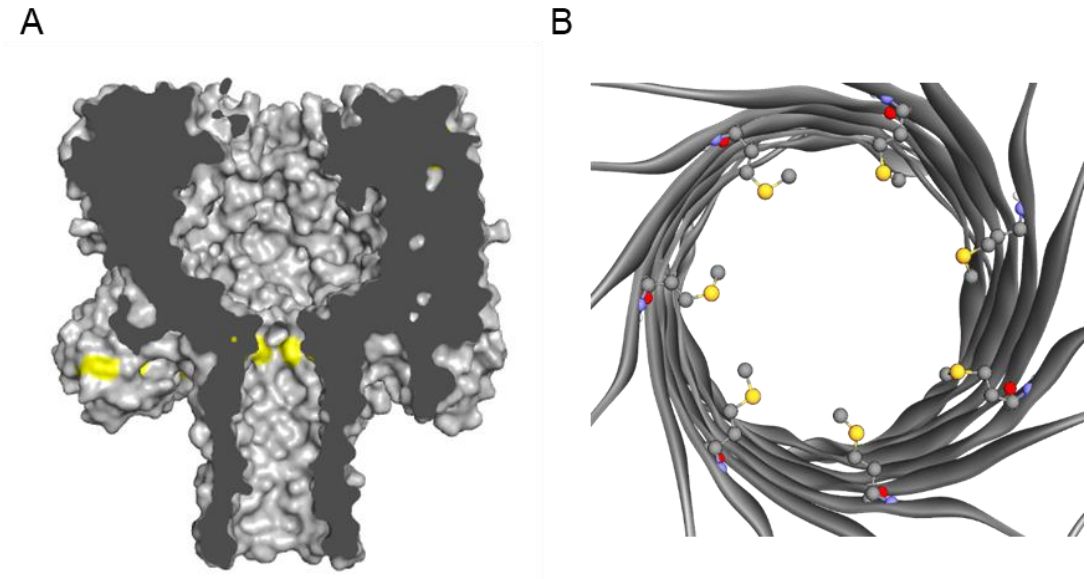

Figure 3.5: A) Cross section of α-HL showing location of methionine residues within the channel. While there are several methionine locations within the protein, only Met113 is solvent exposed within the lumen of the pore. B) Enlarged view of the constriction site of α-HL showing a single Met113 residue protruding into the inner cavity of the pore.

The third and final residue targeted was tyrosine. In previous work, it has been demonstrated that in a basic environment, or with optimal surrounding residues, selective tyrosine modification can be achieved at physiological conditions.[25-26] It was demonstrated that when tyrosine is adjacent to an arginine residue in the protein, site-selective modification of the tyrosine moiety could be achieved.[26] Using protein visualisation software, it was found that the α-HL contained a solvent exposed tyrosine, with an adjacent arginine (**Figure 3.6**). It was then hypothesised that site selective modification could be achieved at the tyrosine site of α-HL.

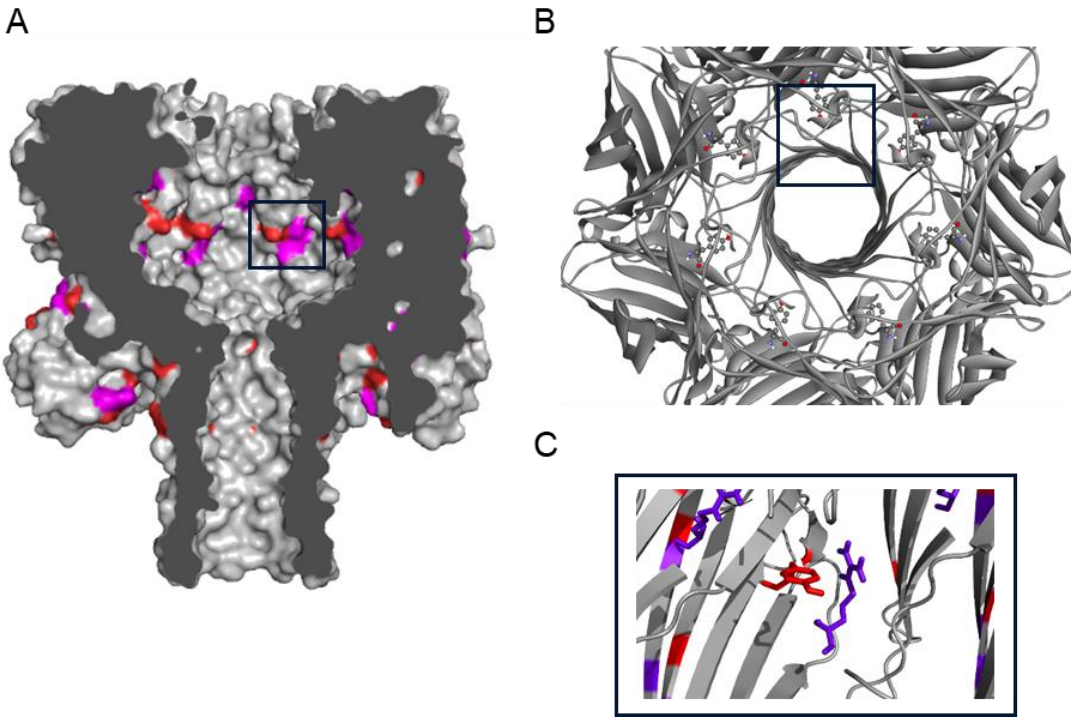

Figure 3.6: Cross-section of α-HL, with tyrosine (red) and arginine (purple) shown. Highlighted section shows the structures of the amino acids and their proximity to one another.

Of course, this is not an exhaustive list of available residues available for bioconjugation in α-HL. Neither is α-HL the only nanopore protein suitable for bioconjugation reactions. However, α-HL does have distinct solvent-exposed residues. MspA, another commonly used transmembrane nanopore protein, exhibits no solvent-exposed lysine, methionine, or tyrosine residues (**Figure 3.7A**) and would therefore require mutagenesis to undergo bioconjugation at any such residues. Looking to other transmembrane proteins, the picture is a bit more optimistic. The ClyA nanopore (**Figure 3.7B**) exhibits solvent exposed lysine and tyrosine residues. However, too many reactive residues could result in uncontrollable modification. Aerolysin (**Figure 3.7C**) on the other hand is similar to α-HL, as it presents a heptameric structure with three solvent-exposed lysine rings. Therefore, future work may see lysine bioconjugation reactions employed with aerolysin. Even solid-state nanopores have exploited bioconjugation reactions for nanopore studies.[27]

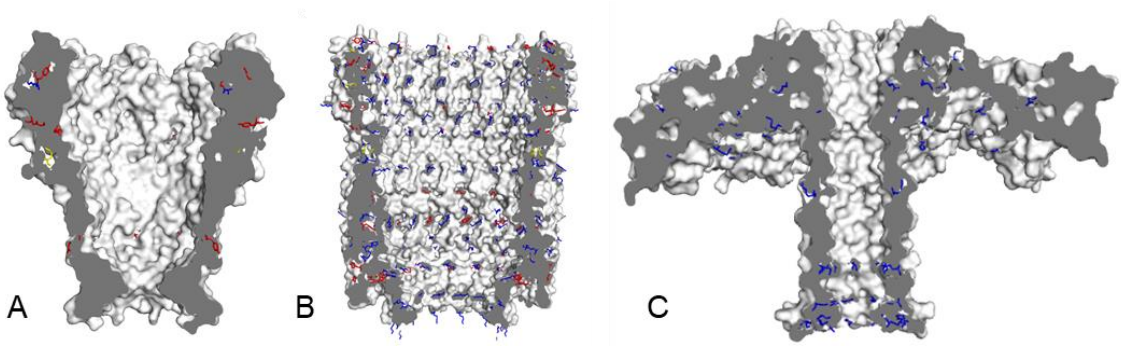

Figure 3.7: Cross section of MspA (A), ClyA (B) and aerolysin (C). Lysine (blue), tyrosine (red) and methionine (yellow) residues are shown.

Herein, we explore various methods for *in situ* bioconjugation of a protein nanopore.

3.4 Attachment of an activated acid at a lysine residue

Previous work within the Cockroft group has established that an α-HL channel can be modified both reversibly and irreversibly at the constriction site lysine ring and the peripheral *cis* and *trans* lysine rings (**Figure 3.8A**).[24] Using iminoboronate chemistry (**Figure 3.8B, upper**), multiple reversible modifications could be achieved. Such systems are of use to study the reaction kinetics between the reactive residue of the pore and the introduced molecule. However, permanent attachment is required for true bioconjugation. To achieve irreversible modification, the lysine reside was modified with an *N*−hydroxysuccinimide (NHS) ester, 3-sulfo-*N*-succinimidyl benzoate sodium salt (**Figure 3.8B, lower**). This gave four stepwise reductions in the current over a prolonged period, suggesting that not all seven of the available lysine residues had been modified. This was most likely due to the steric hindrance exerted in the remaining unmodified lysine residues by the attached benzyl group. A single irreversible modification (**Figure 3.8C**) was achieved by quenching the reaction with excess 3-amino-1-propanesulfonic acid sodium salt, which scavenged excess reagent.

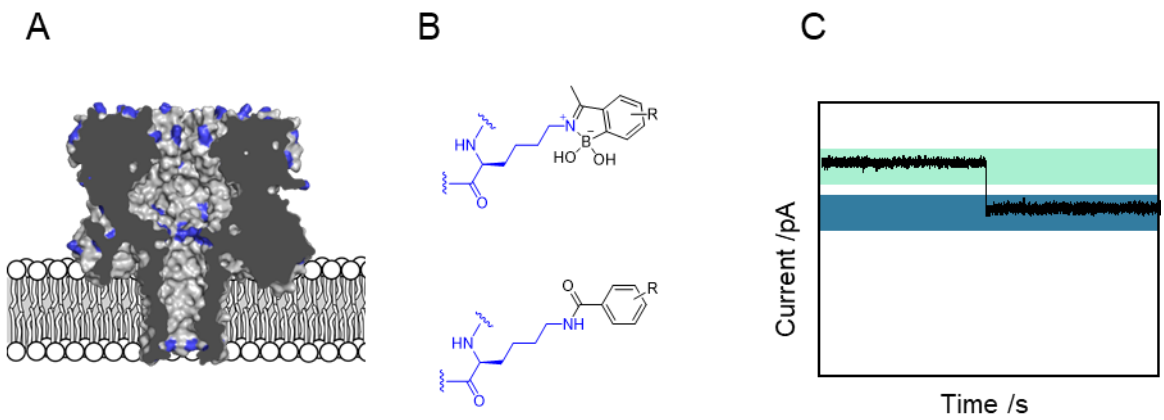

Figure 3.8: A) structure of α-HL, showing the location of lysine residues (blue). B) Structure of lysine, showing the attachment of the reversible iminoboronate (top) and the irreversible amide (bottom). C) Example trace showing the change in current upon an irreversible modification.[24]

The prior work attained modification by adding the acid to the nanopore experiment, which was followed by the addition of the NHS activation reagent. An alternative method for *in situ* activation of the acid moiety for amide coupling was explored as part of this thesis. For this, 1-ethyl-3-(3-dimethylaminopropyl)carbodiimide (EDC) coupling was used (**Figure 3.9**).

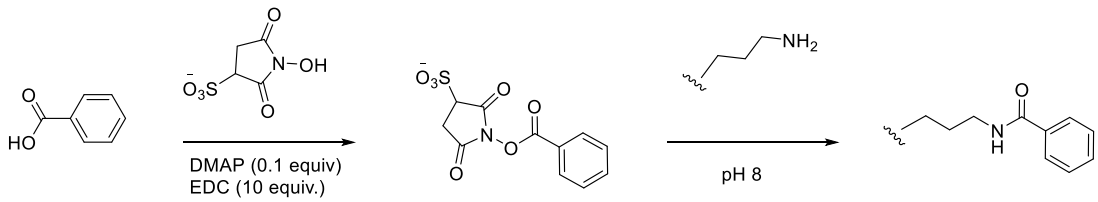

Figure 3.9: Scheme for the attachment of benzoic acid to lysine residue of α-HL.

EDC is well-established reagent for the amide coupling of carboxylic acids and amines.[28] However, the EDC-coupled intermediate exhibits poor water stability as it will undergo competitive nucleophilic attack from water.[29] A work-around for this in the introduction of sulfo-NHS, which reacts with the reactive intermediate to form a more stable intermediate.[30] The sulfo-analogue is used over NHS due to its enhanced water solubility. While the coupling will progress in water, DMAP can be added to increase the efficiency.[31]

To probe whether this alternative coupling method could achieve *in situ* modification of a protein nanopore, a channel was formed under standard procedures. The reaction mixture containing benzoic acid (15 mM), EDC (150 mM), sulfo-NHS (150 mM) and DMAP (0.15 mM) was incubated at room temperature for a minimum of 20 minutes. To avoid the risk of hydrolysis of the activated product, the reaction mix was left for no longer than 2 hours. Under an applied potential of +100 mV, the reaction mixture (10 µL of 15 mM stock) was added to the *cis* well. Assuming all of the benzoic acid was activated, this would yield a maximum well concentration of 240 µM. Pleasingly, modification was observed using this pre-mixing approach, which was signified by a sudden irreversible drop in current (**Figure 3.10A**). The successful modification was characterised by applying an incremental voltage in 10 mV steps between +100 and -100 mV (**Figure 3.10B**). An I_b/I_o = 0.92 was observed, which is consistent with what had been observed using the commercially available activated acid.[24] From this, it can be said with a high degree of confidence that a coupling reaction was occurring between the activated benzoic acid and lysine residues of the protein.

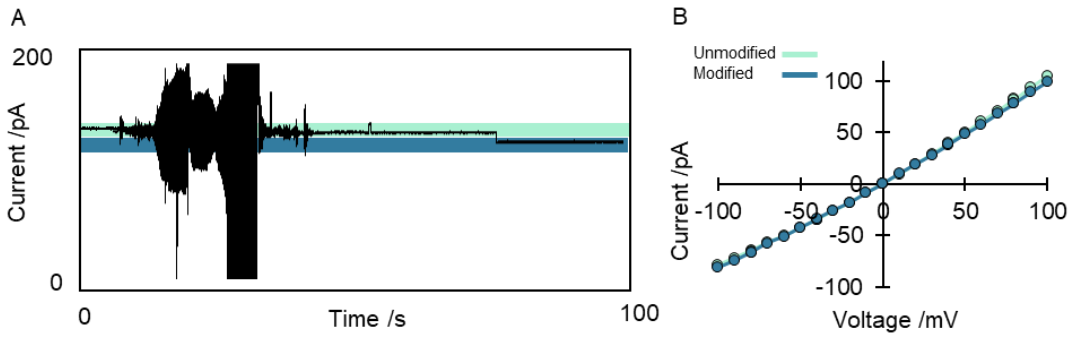

Figure 3.10: Addition of benzoic acid in 1M KCl buffer. A) A solution of benzoic acid (10 mM, water) was prepared. A separate solution of EDC (300 mM), sulfo-NHS (300mM) and DMAP (30 mM) was prepared in water. The two solutions were mixed 1:1 to give a stock acid concentration of 5 mM. The solution was incubated at room temperature for 20 minutes before being added to the *cis* well in 10 µL increments. Buffer 1 M KCl, 30 mM K_2HPO_4, pH 8. Voltage +100 mV. Lowpass Bessel filter 100 kHz and output gain x50. B) I/V trace showing the difference between the unmodified (teal) and modified (blue) pore.

To ensure that the modification observed was due to the formation of an activated acid complex, and not a reaction of the sulfo-NHS or EDC with the pore, control studies were conducted. A solution of EDC (100 mM), sufo-NHS (100 mM) and DMAP (0.1 mM) was mixed in water and reacted for 20 minutes before being added to the *cis* well (**Chapter 5, Section 5.5, Figure 5.16**). While some transient and gating events were observed, there was no irreversible modification. This confirms that the modification could be attributed to the activated acid.

To further explore the scope of the attachment chemistry, the capability of the chemistry was tested in a higher salt concentration buffer. Using the same protocol as before, the activated acid mix was introduced to the *cis* well of a nanopore cell constructed with a 3 M KCl buffer. While a modification occurred, it was characteristically different to the modification in the 1 M buffer (**Figure 3.11**). A small irreversible change in the ion current of 2.3 pA was observed, which equated to $I_b/I_o = 0.99$. This small change in current is consistent with the modification of one of the *cis*-ring lysine residues, and confirm that the protein can undergo bioconjugation at high salt concentrations. The observation of a smaller proportional current change than that observed for similar modifications in the 1 M salt buffer is commensurate with other studies that have examined nanopore modification in different concentrations of buffer.[32]

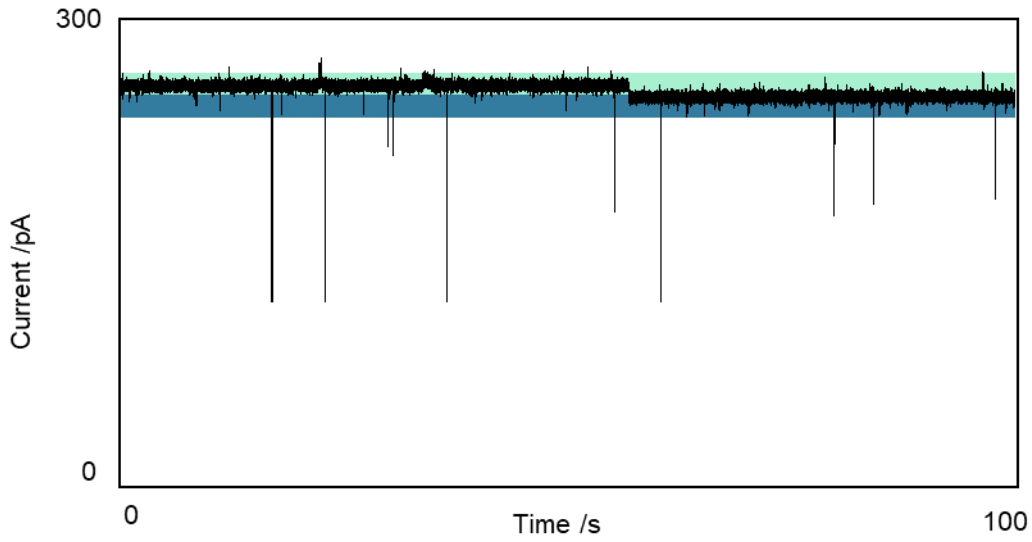

Figure 3.11: Attachment of benzoic acid in 3M KCl buffer. A solution of benzoic acid (30 mM, water) was prepared. A separate solution of EDC (300 mM), sulfo-NHS (30 mM) and DMAP (0.3 mM) was prepared in water. The two solutions were mixed 1:1 to give a stock acid concentration of 15 mM. The solution was incubated at room temperature for 20 minutes before being added to the *cis* well in 10 µL increments. Buffer 3 M KCl, 30 mM K_2HPO_4, pH 8. Voltage +100 mV. Lowpass Bessel filter 100 kHz and output gain x20. For characterisation, see **Chapter 5, Section 5.5, Figure 5.17**.

The covalent modification of nanopores presents an exciting avenue for the development of transmembrane molecular machines. Indeed, molecular machines functionalised with carboxylic acids might be attached to a protein channel (**Chapter 4**). However, such systems are considerably larger than the benzoic acid employed in the proof-of-concept work above. Therefore, it was proposed to attach a simple molecular switch using the same approach. A sulfo-hydrazone switch (compound **10**), previously synthesised within the Cockroft group, was selected. A solution of compound **10** (3 mM) shown in **Figure 3.12B** was prepared and mixed in a 1:1 (v/v) ratio with a solution of EDC (30 mM), sulfo-NHS (30 mM) and DMAP (0.03 mM) and reacted at room temperature for 20 minutes. The reaction mixture (10 µL) was then added to the *cis* well of the channel and the well was mixed. After approximately 200 s, a sharp drop in current was observed in a single step (**Figure 3.12A**). This new level was resistant to inversion of the potential, which suggested that it was a

genuine irreversible modification. This level had an I_b/I_o = 0.74, which is a notably larger blockage than that caused by benzoic acid. To ensure that no subsequent modifications occurred, 3-amino-1-propane (5 µL, 1 M) was added as a quenching reagent. The modified channel was characterised by applying incremental potential difference between +100 and -100 mV (**Figure 3.12C**). A far greater variation from the free pore characterisation trace was observed in the positive than in the negative, which is consistent with ion current rectification.[33]

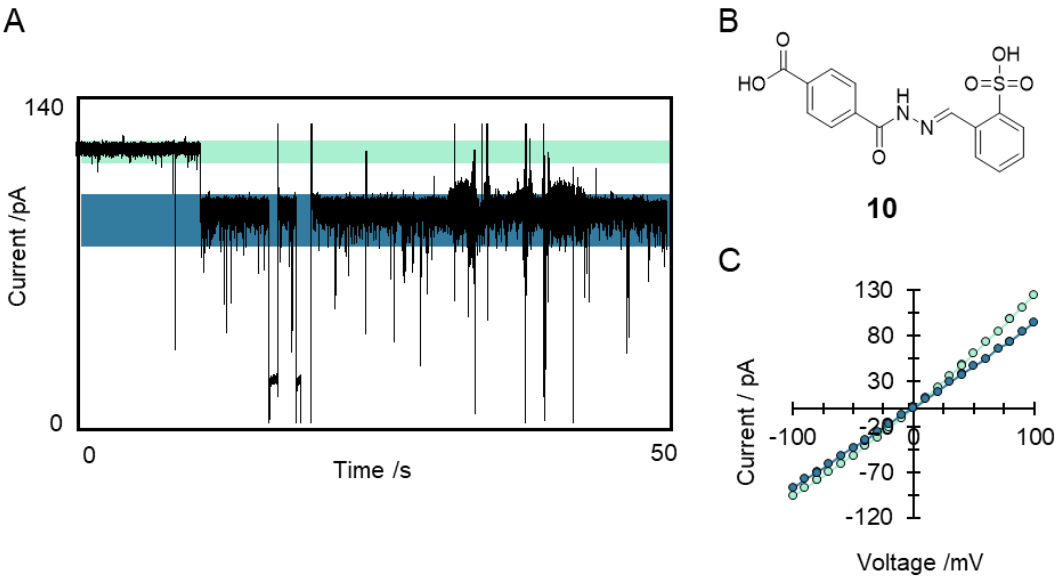

Figure 3.12: A) Example trace of the modification with compound **10**. Under a constant applied potential of +100 mV, a sudden drop in current signifies that a modification has occurred. Inversion of the applied potential confirms that a genuine modification has occurred. A quenching reagent was then added to ensure that no further modifications occurred. The lower panel denotes the applied potential corresponding to the above trace. Buffer 1 M KCl, 30 mM K_2HPO_4, pH 8. Voltage +100 mV. Lowpass Bessel filter 100 kHz and output gain x50. B) Structure of the sulfo-hydrazone switch C) Characterisation trace, showing the free pore current distribution (green) and the modified channel (purple). The deviation from the free pore current flow is greatest in the positive due to ion current rectification.

This proved that molecules that are larger and more functionally complicated than benzoic acid can be attached toa a nanopore, which paves the way for the attachment of more sophisticated molecular machines (**Chapter 4**). Hence,

we have demonstrated a robust method for the amide attachment of water-soluble carboxylic acid derivatives to an α-HL channel.

3.5 Oxaziridine functionalisation of methionine

As previously discussed, cysteine is a frequent candidate for *in situ* chemical modification. As the only amino acid with a thiol group, it has a high and often selective, reactivity. Methionine on the other hand, while also sulfur-containing, is less reactive due to the methyl cap and weaker nucleophilicity. Despite this, methionine it is an attractive target for bioconjugation as the low reactivity will negate unwanted side reactions. Until relatively recently, the scope for bioconjugation at methionine sites was limited, and many of the options available were not viable under the conditions required for nanopore studies (**Table 3.1**).[34]

Table 3.1: Comparison of methods for methionine modification. Adapted from Zang *et al.*[34]

Mechanism	Acid-base Reaction			Redox-reaction
Reagent	Alkyl halides  X = Br, I, OTf	Epoxide 	Hypervalent iodine 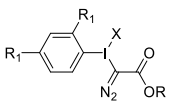 R_1 = H, F; X = OTf, BF_4	Oxaziridine 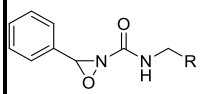
Conditions	Aqueous/organic solution pH <3 24-72 hours	Aqueous/organic solution pH <3 24-48 hours	Aqueous/organic solution pH ~3 Minutes	Aqueous solution pH ~7 Minutes
Reagent Stoichiometry	1.1-3 equiv.	1.5-3 equiv.	>500 equiv.	1.1-10 equiv.

Product	Sulfonium 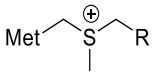	Sulfonium 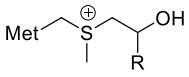	Sulfonium 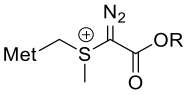	Sulfimine 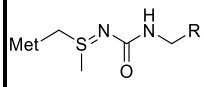
Product stability	Dealkylation reagents treatment (e.g. thiourea)	Dealkylation reagents treatment (e.g. APDC)	TCEP. Adjacent nucleophilic amino acid.	High temperature treatment. Strong thiol reducing agents treatment.
Suitable for biological nanopore studies	No	No	No	Yes

Toste and Chang have developed of a methionine-selective bioconjugation reaction that can occur under physiological conditions similar to those employed in protein nanopore experiments.[35] As there are a myriad of canonical amino acids that have a greater nucleophilicity than methionine, acid-base bioconjugation was an unlikely candidate for the development of selective modification. Toste and Chang therefore looked to exploit the redox reactivity of the amino acid to achieve chemoselective bioconjugation.

Previously, it had been established that imidation at a sulfur centre could be achieved using an oxaziridine moiety, resulting in an O-transfer product (OTP, sulfoxide) or a N-transfer product (NTP, sulfimide) (**Figure 3.13**).[36] By careful tuning of the oxaziridine substituents and the reaction conditions, Toste and Chang were not only able to achieve chemoselectivity for methionine, but also demonstrate the selectivity for the desired NTP product.[35]

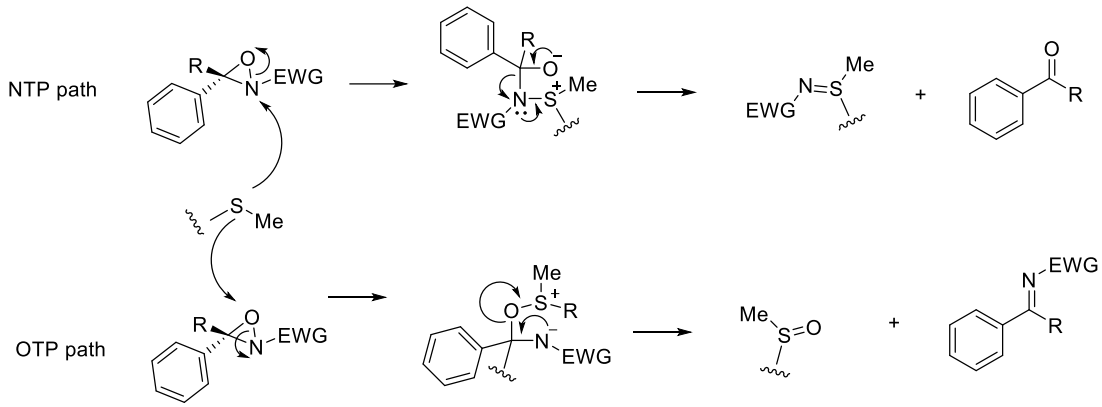

Figure 3.13: Scheme for the formation of the NTP or the OTP.

The authors went on to demonstrate that this oxaziridine chemistry could achieve selective modification of proteins. As noted in **section 3.3**, α-HL contains a single, solvent-exposed ring of methionine residues within the lumen. This is highly advantageous as unlike lysine, which has three solvent exposed rings within the lumen, the exact location of the methionine modification within the pore would be known.

Within the Cockroft group, Dr Haugland developed a method for the methionine-selective modification of α-HL nanopores with alkyne functionalities using this oxaziridine chemistry.[37] Using this approach, the modification of a methionine residue using an alkyne-functionalised oxaziridine could be reproduced (**Figure 3.14**).

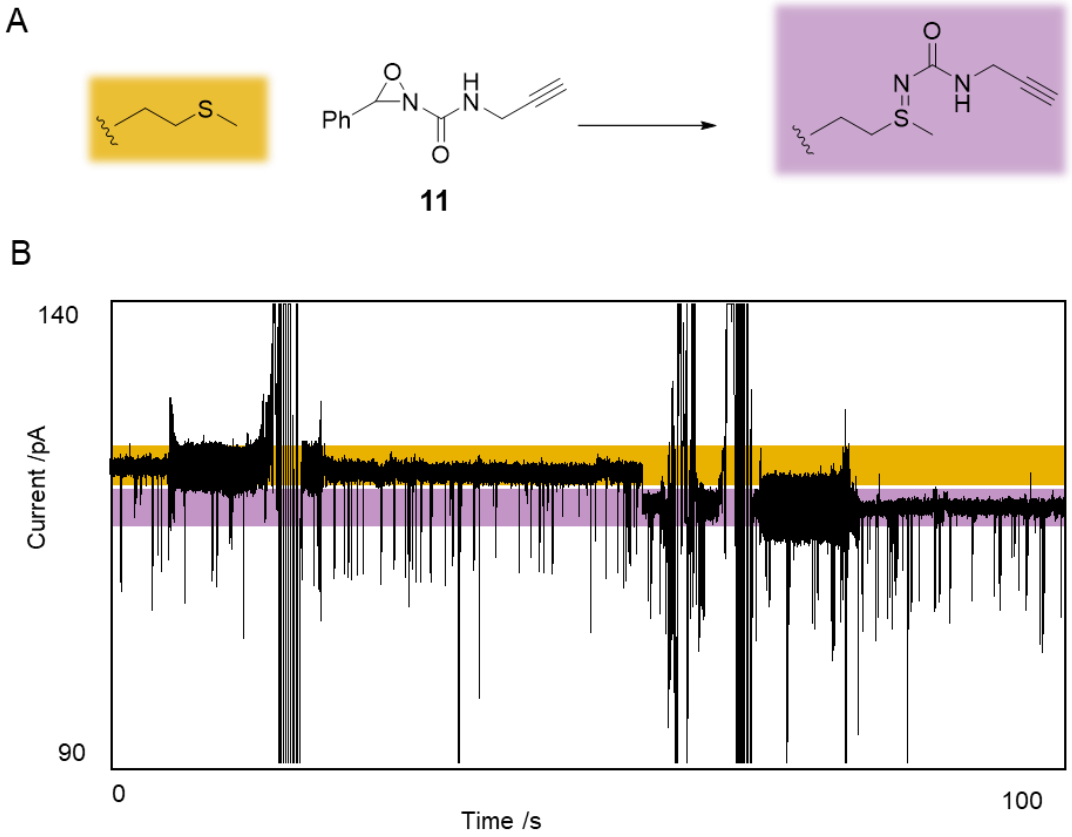

Figure 3.14: 3-Phenyl-*N*-(prop-2-yn-1-yl)-1,2-oxaziridine-2-carboxamide (compound **11**) (1 µL of 100 mM stock) was added to the *cis* well of the pore. Within 30 s, an irreversible modification was observed (I_b/I_o 0.97). Immediately, methionine (8 µL, 250 mM) was added to the *cis* well with mixing. Regions of enhanced noise are attributed to the opening of the Faraday cage. Buffer 1 M KCl, 30 mM K_2HPO_4, pH 8. Voltage +100 mV. Lowpass Bessel filter 100 kHz and output gain x50.

Under a constant applied potential of +100 mV, compound **11** was added to the *cis* well of the system. In reproducing these experiments, it was found that increasing the excess of the quenching methionine to 20 eq. was more effective for ensuring that the modification of single methionine was attained. A further five modifications were seen to occur if no methionine was added. After 200 s no further modifications were observed, which ensured that all of the reagent had been quenched. The modified pore was characterised by applying incremental voltages between +100 and -100 mV and found to be in accord with previous work (**Chapter 5, Section 5.5, Figure 5.18**).

Hence, the attachment of a single alkyne moiety within the lumen of the α-HL provides a handle for further functionalisation of the channel. Indeed, during the course of these studies it was discovered that these alkyne-modified channels provided an ideal opportunity for examining Cu(I)-catalysed azide-alkyne [3+2] cycloaddition (CuAAC) reactions at the single-molecule level.

The term ‘click chemistry’ was coined in the early 2000s by Barry Sharpless.[38] It describes not just one chemical reaction, and is an overarching term for a class of reactions, many of which are exploited in bioconjugation and bioorthogonal chemistry. CuAAC is one such example of a bioorthogonal click reaction but, despite its extensive use, the mechanism and identity of the reactive intermediates has been subject to debate. In the exploration of reaction mechanism, single-molecule observations could be of vast benefit. Indeed, previous precedent has been set by the Bayley group that protein nanopores can be used to explore click chemistry at the single-molecule level.[39-40]

There is a general consensus that the reaction begins as shown below (**Figure 3.15, blue**), with a Cu-alkyne π-complex converting to a Cu-acetylide. However, whether the reaction then follows the mono-Cu or bis-Cu pathway is disputed.

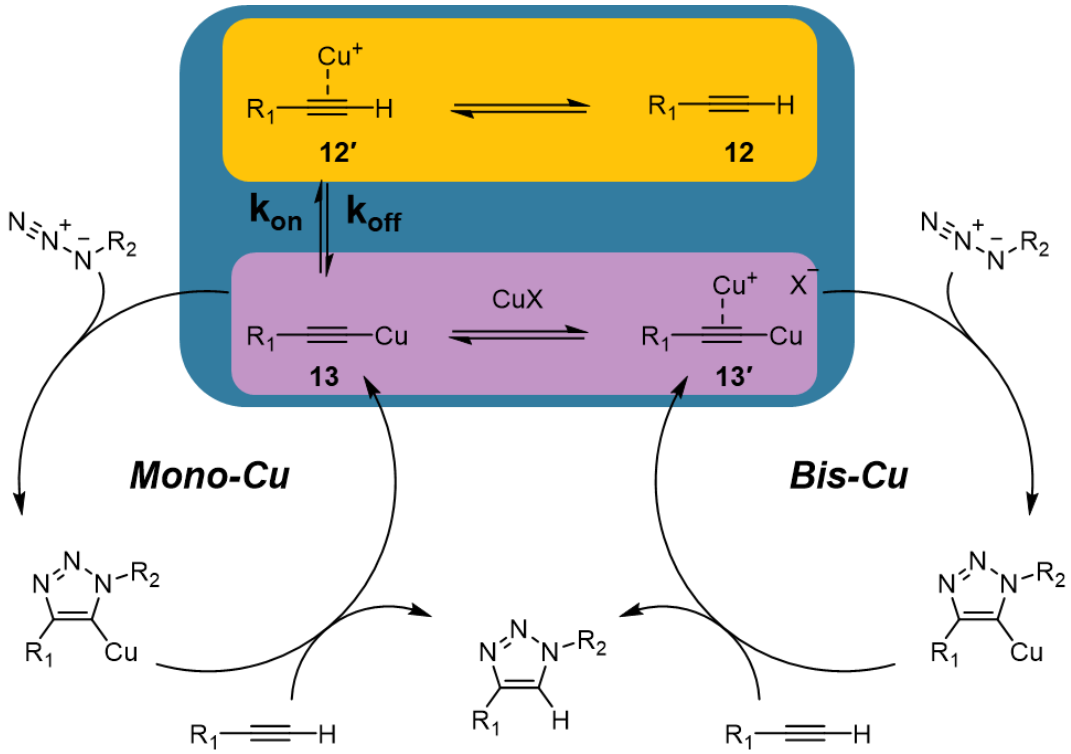

Figure 3.15: Proposed catalytic cycles for the mono- and bis-Cu catalysed click reaction. Cu^+ will associate with the alkyne (blue) before forming a Cu-acetylide (yellow).

Dr Haugland showed that there was a marked increase in the signal noise upon increasing the concentration of Cu^+ when using an alkyne modified pore. In addition, as the concentration of Cu^+ was increased, a well resolved secondary level emerged. As no such events were observed when Cu^+ was added to a WT α-HL channel, it was concluded that these events arose from the association between Cu^+ and the terminal alkyne. The upper level was assigned to the pore bound alkyne (compound **12**) and the lower level to the copper-terminated alkyne (compound **14**). The increased noise was attributed to the rapidly exchange between the copper-bound state of **12 – 12'** and **13 – 13'**.

One of the limitations of nanopore technology is that no chemical information is revealed from the magnitude of the current, making assignment of states an indirect process. Furthermore, to measure the current through the pore, a voltage must be applied, which shifts the population of states, especially for

charged intermediates. Hence, varying the applied voltage and observing the resulting shift in states provides a means of identifying the charge states of the species causing the levels.

To probe this, the voltage was varied while the concentration of Cu^{+} remained constant (**Figure 3.16**). When the voltage was varied from +60 mV to +30 mV, a voltage dependency in the population of states was observed (**Figure 3.16**). The binding events become more prolonged as the current was lowered. Indeed, as the voltage was reduced, the rate of exchange from the yellow to the purple level, k_{on}, was seen to decrease proportionally with the voltage, whereas the reverse process, k_{off} was seen to increase proportionally. This was attributed to the applied potential destabilising the like-charged cationic Cu-π complexes of compounds **12' and 13'**. The positive range data was collected by Dr Haugland.

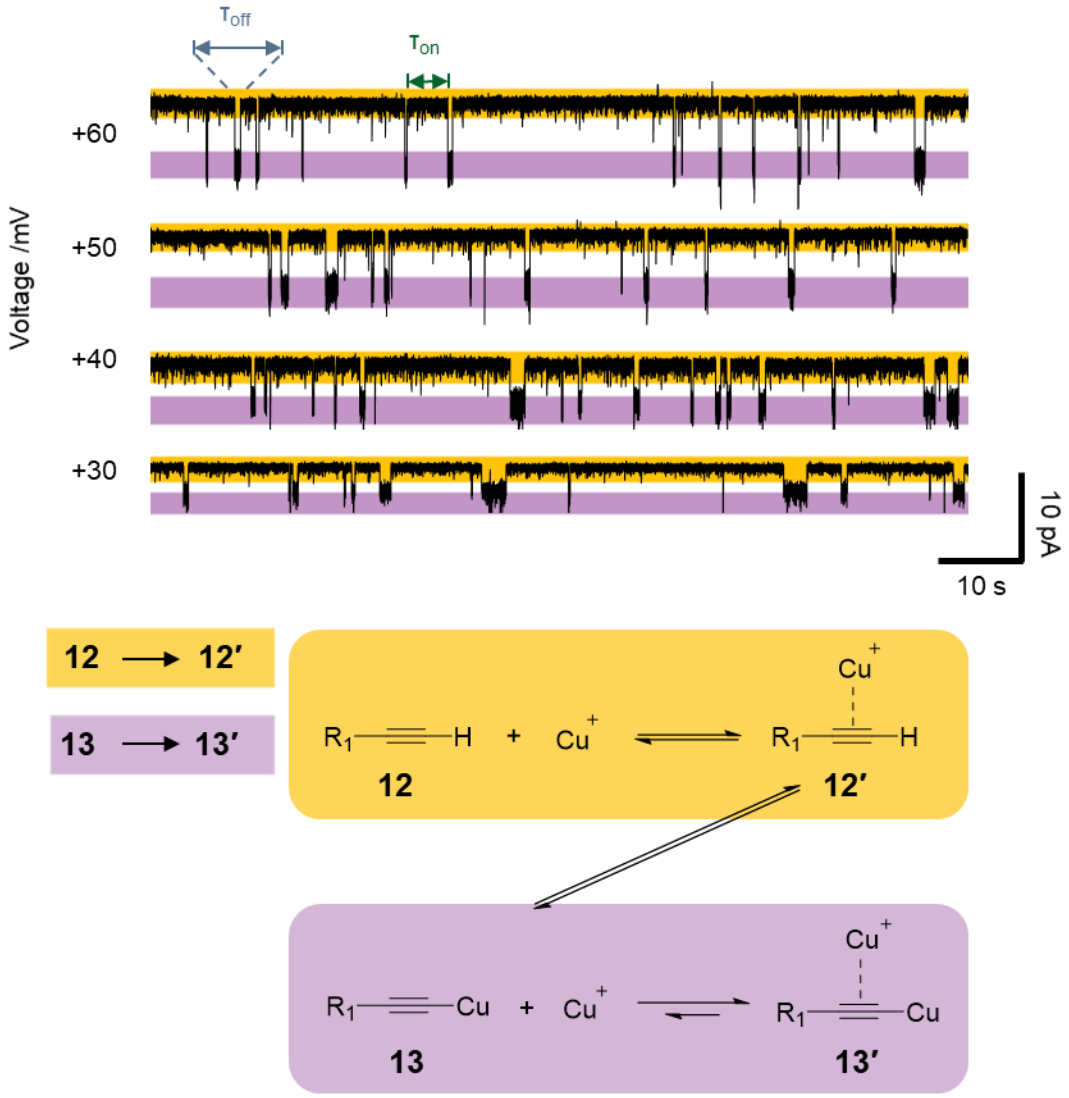

Figure 3.16: Binding events of copper to the functionalised alkyne group under a positive applied potential. This data was recorded by Dr Marius Haugland. The yellow level shows the transformation between compounds **12 and 12'** and the purple level the transformation between compounds **13 and 13'**.

With the observation that the purple level events became more prolonged at lower voltages, it was hypothesised that this effect would be extended into the negative applied potential. Indeed, the observation of a voltage-trapped state at a high negative potential would corroborate the observed shift in the equilibrium at an applied positive potential.

Data collected by the author of this thesis and shown in **Figure 3.17** supports the assignment of the bound Cu-acetylide states as the binding events become more prolonged as the voltage became more negative. Note that the reversal of the potential, means that the sign of the currents is also reversed, so the assignment of states is vertically flipped in **Figure 3.17** compared to **Figure 3.16**.

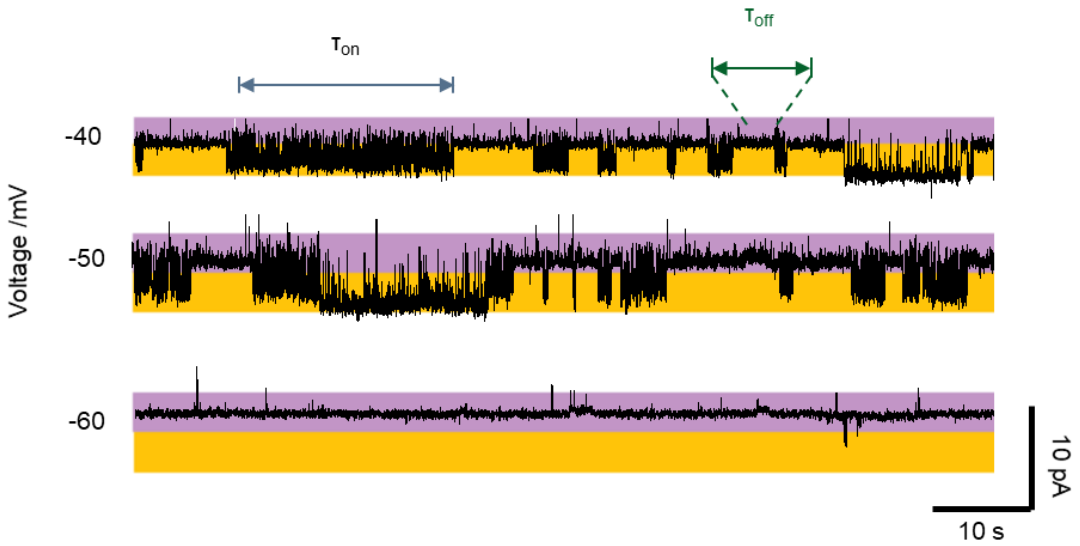

Figure 3.17: A single α-HL protein channel was inserted into a membrane under an applied voltage of +100 mV. Compound **11** (0.1 µmol) was added to the well under the applied voltage. After the first modification, free methionine (20 equiv.) was added to the well to quench the excess oxaziridine. Once a single modification was achieved, $CuSO_4$ (1 µL, 1 M) and sodium ascorbate (4 µL, 1 M) were added to the well and a negative potential was then applied. This was varied through a range of negative potentials. Binding of the Cu to the alkyne functionality at negative potentials. The yellow level shows the rapidly exchanging states corresponding compounds **12 and 12'**, and the purple level similarly to compounds **13 and 13'**. Buffer 1 M KCl, 30 mM K_2HPO_4, pH 8. Voltage variable. Lowpass Bessel filter 100 kHz and output gain x50. Data obtained DCG.

It can be seen there is a clear decrease in noise at the more negative potentials. The noise within the levels is reflective of the binding/unbinding of Cu^+ to the alkyne between compounds **13** and **12'** and compounds **13** and **13'**, respectively. Therefore, this reduction in signal noise at -60 mV indicated that a permanently bound state was been reached, which was assigned as corresponding to compound **12'**. Hence, this experiment enabled a more

confident assignment for the other states. In turn, this provided supporting evidence to the hypothesis that CuAAC reactions progress *via* a *bis*-Cu mechanism (**Figure 3.15, right**).

Reaction at a methionine residue provides an excellent means of modifying protein nanopores. A range of reactive handles, such as alkenes, alkanes and azides, [37] can be introduced to a single site within the channel and insight into the chemical mechanisms of these moieties can be gained through current trace analysis. In addition, the incorporation of an azide or alkyne provides a means of attaching a range of functionalised molecules to the channel through click chemistry. However, the synthesis of the oxaziridine moiety is not trivial, and the reactivity has implications on the stability of reagents and the synthetic cross-compatibility. Similarly, if several distinct pathways exist to modify multiple residues, then this would enable orthogonal bioconjugation with more than one modifying group. Hence, it is desirable to develop alternative means of nanopore bioconjugation.

3.6 Exploring *in situ* modification at tyrosine

As noted in **section 3.3** above, α-HL possesses tyrosine residues as potential sites for chemical modification (**Figure 3.6**). The sulfur(VI) fluoride exchange (SuFEx) reaction developed by Sharpless presents one option for bioconjugation.[41-42] The use of SuFEx chemistry has grown dramatically in just a few years, and the full scope is documented in several excellent reviews.[43-45] In the context of protein modification, it has been demonstrated that tyrosine will undergo selective modification with a SuFEx reagent in the presence of adjacent arginine residues.[26]

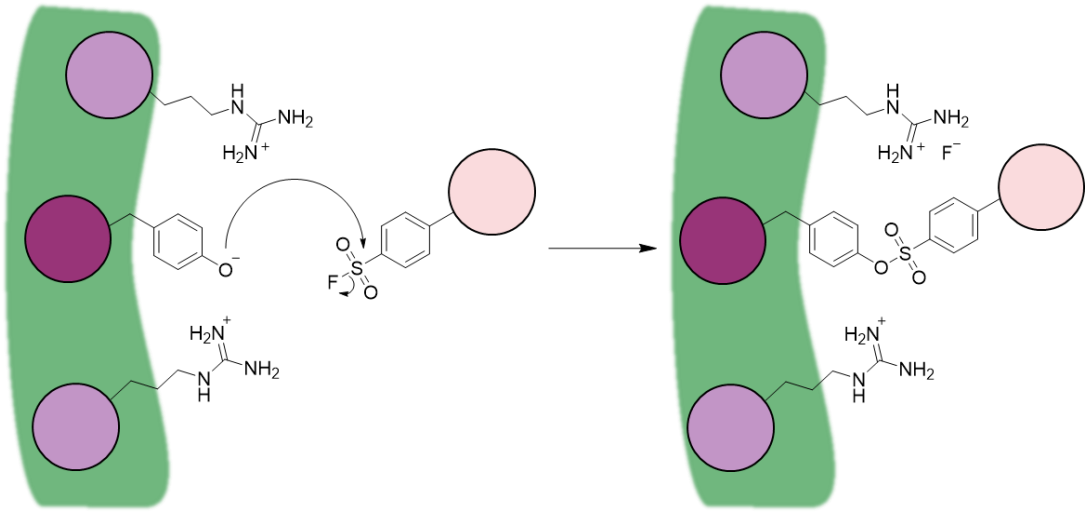

Figure 3.18: General scheme showing a SuFex reaction. It has been observed that reaction will occur at a tyrosine reside when adjacent arginine residues are present. It is proposed that this is due to the stabilising effect of the arginine residues on the hydroxide group and the departing F^- anion.[26]

A simple biaryl SuFeX derivative was designed (compound **14, Figure 3.19**) to explore the availably of the tyrosine residue within the lumen of α-HL. It was designed such that it would be small enough to enter into the channel, but large enough that it would bring about a significant change in the ion current.

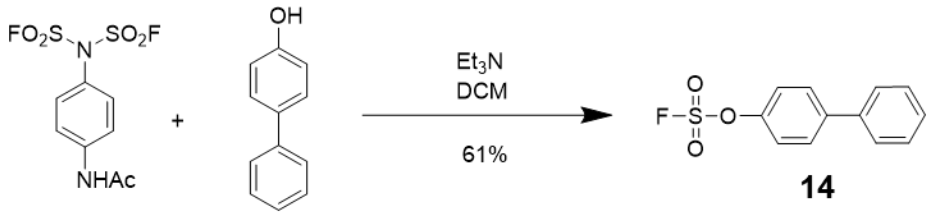

Figure 3.19: Synthetic route to compound **14**.

Compound **14** was synthesised following the procedure outlined in **Chapter 5.** A single channel was formed in 1 M KCl buffer at pH 8. A solution of compound **14** (500 mM) was made in acetonitrile. Under an applied potential of +100 mV, the solution (10 µL) was added to the *cis* well. Shortly thereafter, a deep block of $I_b/I_o = 0.42$ was observed, which then spontaneously shifted to $I_b/I_o = 0.49$. This new level was persistent, and resisted inversion of the potential, suggesting that modification had occurred (**Figure 3.20**). In a subsequent

experiment (**Chapter 5, Figure 5.19**), the same two-step modification was observed.

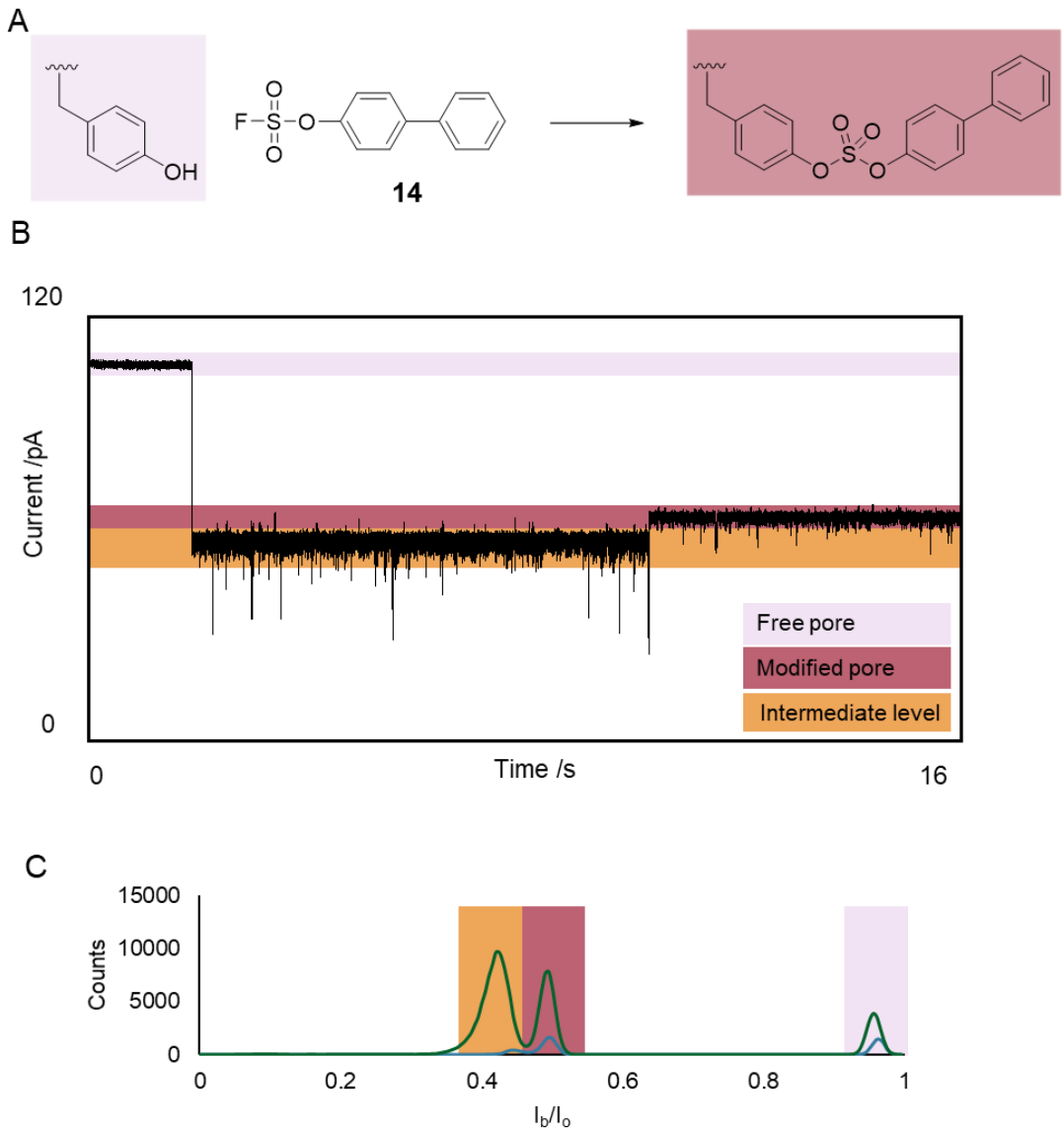

Figure 3.20: Possible attachment of SuFex in 1 M buffer. A) Scheme for the attachment of compound **14** to the tyrosine residue of the pore. B) Trace for the attachment of compound **14** to the channel. The attachment passes through a lower amplitude state (orange) before settling to an irreversibly bound level (red). C) All points histogram of I_b/I_o for two successful modifications of the channel with compound **14**. While the I_b/I_o of each modification maps identically, there is a notable difference for the counts at the lower (orange) level. 1 M KCl, 30 mM K_2HPO_4, pH 8. Voltage +100 mV. Lowpass Bessel filter 100 kHz and output gain x50.

However, despite this promising early success, subsequent attempts saw no modification. Approximately ten further modifications were attempted, using the same stock of reagent, but no other modifications were observed. This raised questions of the validity of the early modifications, and what, if anything, was genuinely being observed. It was hypothesised that the arginine residues were, in fact, not in a close enough proximity to promote the reaction (**Figure 3.18**). Therefore, an additional base was added to help drive the reaction in a subsequent attempt. A solution of compound **14** (500 mM) was added to the *cis* well. After 200 s, no modification had observed. A solution of 1,8-diazabicyclo[5.4.0]undec-7-ene (DBU) (1 mM, 1 µL) was added to the *cis* well. Almost immediately, new levels were observed (**Figure 3.21**). These had an amplitude of $I_b/I_o = 0.91$ and $I_b/I_o = 0.80$. The upper level ($I_b/I_o = 0.91$) was more frequently observed and the lower level ($I_b/I_o = 0.80$) was only accessed from the upper level. This would suggest that multiple reversible modifications were occurring. While this is promising, as it does suggest that the tyrosine residues may be accessible, it is disparaging for several reasons. While modifications are occurring, the events are short lived and reversible. In addition, the magnitude of the blocked current is distinct to that observed with compound **14**. This may suggest that the addition of DBU was promoting the reaction of compound **14** at an alternative residue. Indeed, the appearance of both large and small reversible current steps is highly reminiscent of the reversible reactions of iminoboronate with lysine residues in different sites within α-HL channels previously observed by Borsley and co-workers.[24]

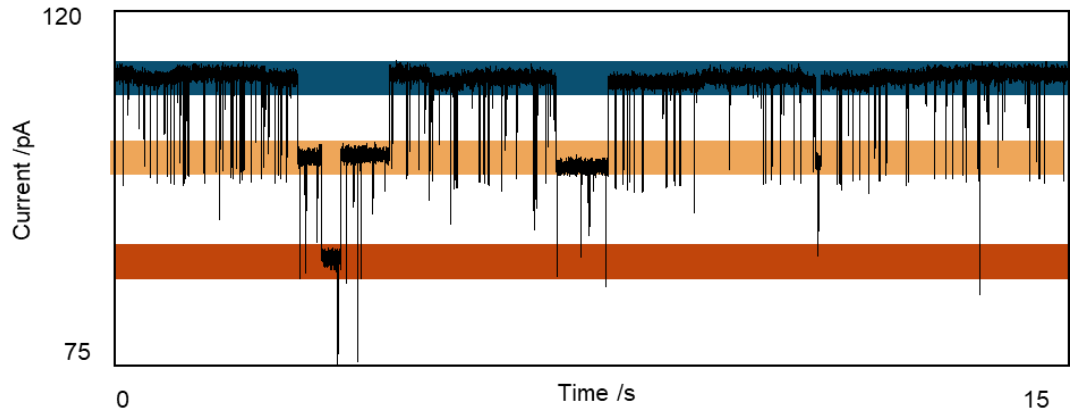

Figure 3.21: Addition of compound **14** (500 mM) to a channel in the presence of 1,8-diazabicyclo[5.4.0]undec-7-ene (1 mM). Major level changes are seen to the upper (yellow) and lower (orange) levels. The lower level was only ever accessed *via* the upper level, suggesting sequential reaction at different, but identical sites. Minor changes in the (blue) level may correspond to reversible reactions occurring away from the constriction site. 1 M KCl, 30 mM K_2HPO_4, pH 8. Voltage +100 mV. Lowpass Bessel filter 100 kHz and output gain x50.

Therefore, it was still perplexing as to why the modification with compound **14** could not be achieved consistently. One hypothesis was that the reagent could be decomposing or reacting with itself to form a more reactive intermediate such as a sulfonic anhydride. To evaluate this, *p*-toluenesulfonic anhydride was added under the same conditions that the proposed SuFex modification occurred (**Figure 3.22**). A high concentration solution of *p*-toluenesulfonic anhydride (73 mM) was added alternately to the *cis* and *trans* side of the channel in 10 µL increments, to give a final well concentration of 3.5 mM. Approximately 200 s was allowed between additions and the well was mixed after each addition.

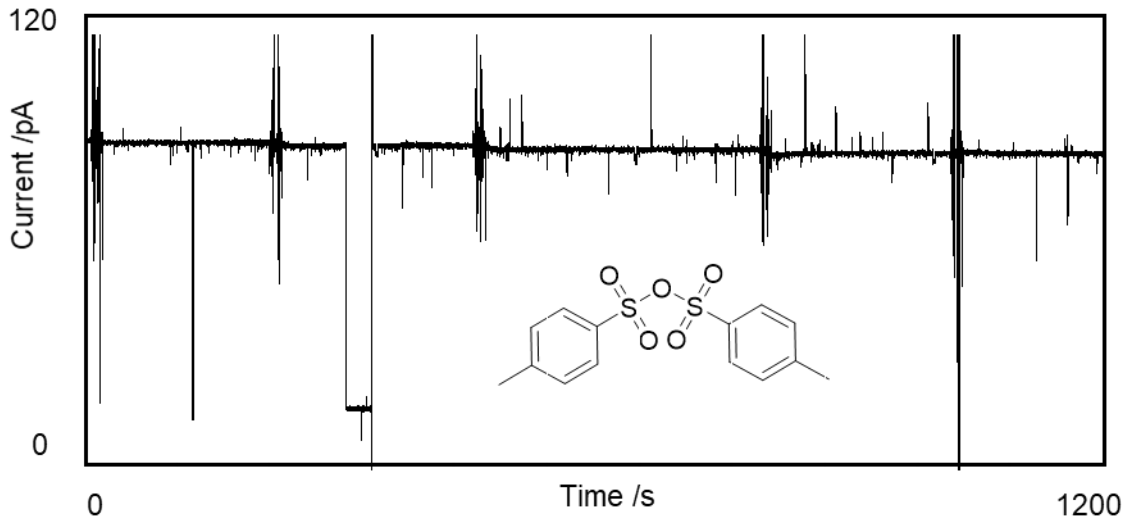

Figure 3.22: Addition of p-toluenesulfonylanhydride (73 mM, added in 10 µL increments to 600 µL well) *cis* and *trans*. Final concentration of 3.5 mM in each well. Additions are marked by the noise spikes. A small current drift can be observed after each addition due to dilution. 1 M KCl, 30 mM K_2HPO_4, pH 8. Voltage +100 mV. Lowpass Bessel filter 100 kHz and output gain x50. Post-acquisition low pass Bessel filter 200 Hz applied in Clampfit 10.7

After >1000 s, no modification was observed. It was therefore concluded that it was unlikely that the SuFex reagent was forming the sulfonic anhydride and subsequently reacting with the pore. Therefore, other established methods of tyrosine bioconjugation were attempted to explore the accessibility of the tyrosine residue in α-HL.

Mannich-like reactions have previously been used for the selective modification of tyrosine residues.[46] The three-component reaction brings together an aldehyde and an electron-rich aniline to react at a tyrosine residue (**Figure 3.23**).

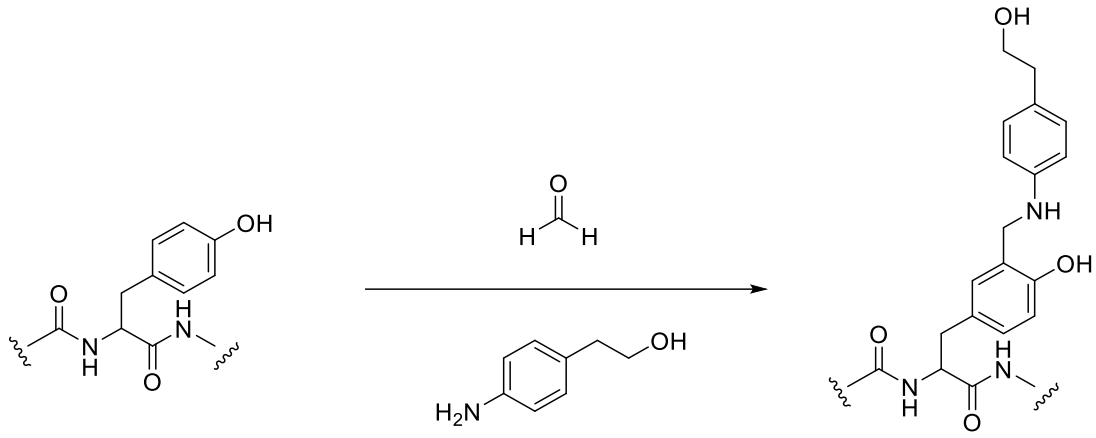

Figure 3.23: Mannich-like approach to tyrosine modification.

A solution of formaldehyde (10 mM) and 2-(4'-aminophenyl)ethyl alcohol (10 mM) was prepared in acetonitrile. The solution (10 µL) was added to the *cis* well of a single channel under an applied potential of +100 mV. When no modification was observed the applied potential was varied between +120 and -100 mV. It was likely that one or more of the reagents lacked suitable solubility to achieve successful modification. It was therefore decided to repeat the experiment with more suitable reagents. Propanal (10 mM) and 4-aminophenethyl alcohol (10 mM). Again, under an applied potential of +100 mV, the reagents were added to the *cis* well of the protein. Again, no modification was observed.

In previous work by the Barbas group, it was demonstrated that 4-phenyl-3*H*-1,2,4-triazole-3,5(4*H*)-dione (PTAD) would react with the tyrosine residue of a protein in mild conditions (**Figure 3.24**).[47] While the cyclic diazodicarboxamide would react with lysine in isolation, it demonstrated a selectivity for tyrosine when both residues were present. In control studies with the analogous *p*-cresol it was show that the formed C-N bond was stable to extreme temperatures and pH ranges. Therefore, this makes the system an excellent candidate for a selective means of selective bioconjugation of α-HL.

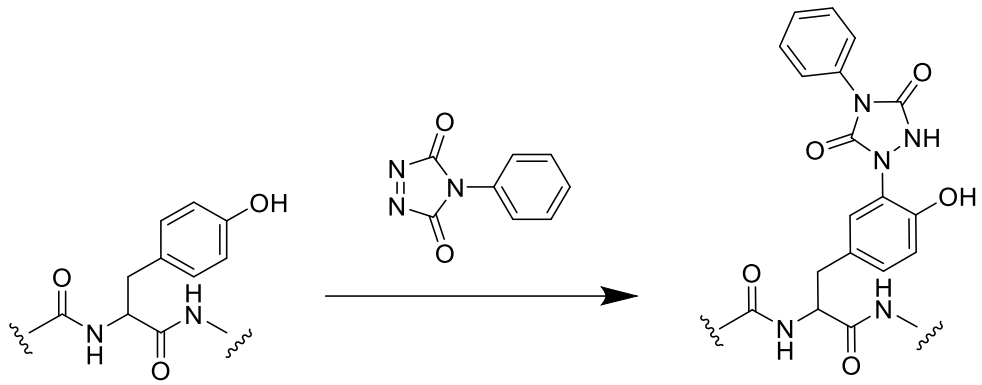

Figure 3.24: Alternative tyrosine modification approach.[47]

For the initial study, a single channel was formed in a 1 M KCl buffer at pH 8. A solution of PTAD (57 mM) was prepared in acetonitrile and the solution (5 µL) was added to both the *cis* and *trans* well to give a concentration of 0.48 mM on both sides of the membrane. However, no modification was seen even when the voltage was varied between -100 mV and +140 mV.

While the initial study did not report a major effect of the buffer condition on the viability of the reaction in the bulk, it was thought that this may not be the case in the confinement of a nanopore. To probe the effect of pH, two different buffer systems were examined; 1 M KCl at pH 6.8 and 1 M KCl at pH 9.8. In both instances, a single channel was formed and PTAD was added to both sides of the membrane to give a well concentration of 0.47 mM. No modification was observed in either pH buffer. Finally, it was decided to explore whether the cation could have any effect on the success of the modification. A channel was formed in a 1 M CsCl buffer at pH 8. A solution of PTAD (1.41 mM) in acetonitrile was added to the *cis* side of the well. Within 100 s a deep block with an $I_b/I_o = 0.02$ occurred. This then increased to a level that exhibited four distinct states (**Figure 3.25**). Initially, this new level appeared to be resistant to inversion of potential, suggesting that it was a genuine multi-state modification. However, upon attempting to perform an I/V sweep characterisation the system did not resist the incremental changes in applied potential.

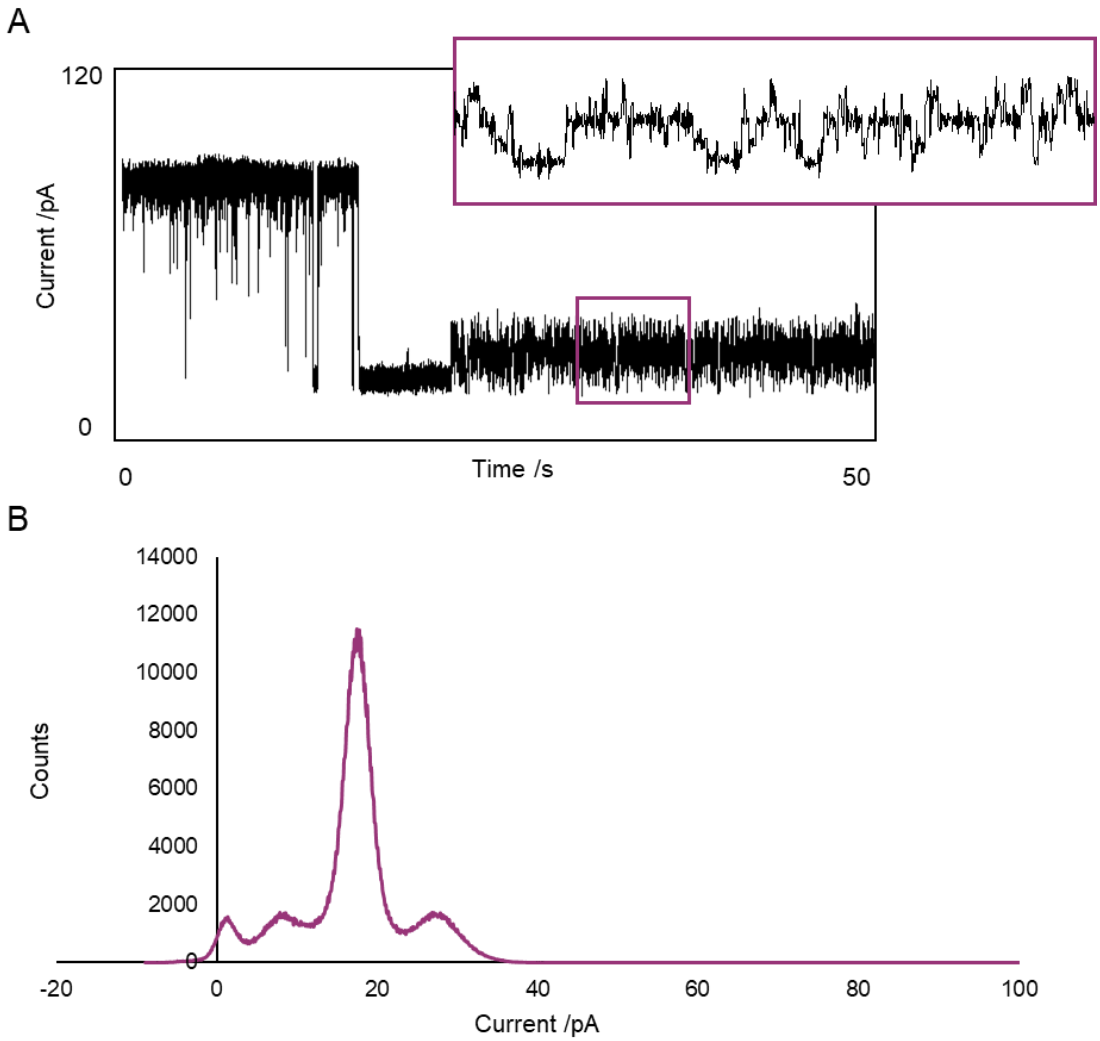

Figure 3.25: A) Example trace showing the potential modification of the channel with PTAD. The current progressed through a lower state, which then increased to a multistate level. 1 M CsCl, 30 mM K_2HPO_4, pH 8. Voltage +100 mV. Lowpass Bessel filter 100 Hz and output gain x50. B) Histogram of current /pA for the blocked level. This clearly shows four distinct states, with a major state observed at 18 pA.

This suggests that either channel gating, or a reversible modification may have occurred. This was not explored further as a reversible reaction would not be conducive to the development of a modified channel. In addition, it is desirable to develop a system where the modified state has a single, consistent level. Indeed, the observed change in current may not even be due to the desired bioconjugation at tyrosine. It is know that PTAD can decompose in aqueous

environments to form isocyanates.[48] This process may even be facilitated by the inherent electric field of nanopore experiments. Future work to achieve bioconjugation at a tyrosine residue in a nanopore may look to use an isocyanate scavenging buffer such as 2-amino-2-hydroxymethylpropane-1,3-diol (Tris) to mitigate this.

Therefore, it was concluded that the tyrosine residues within the lumen of α-HL are not sufficiently solvent exposed to achieve *in situ* modification. Unfortunately, early apparent success was found to be irreproducible. It is possible that these rare occurrences were due to a misfolded protein that exposed the otherwise inaccessible residue. Based on the literature, tyrosine presents as a potential reactive handle for bioorthogonal bioconjugation. However, this would require mutagenesis to incorporate a fully exposed tyrosine into the channel.

3.7 Conclusions

It has been demonstrated that α-HL can be selectively modified, *in situ*, at both lysine and methionine residues. While the protein presents a solvent-exposed tyrosine residue, attempts to reproducibility modify this site were unsuccessful.

Lysine bioconjugation could be achieved through the *in situ* activation of a carboxylic acid *via* EDC coupling. This was demonstrated to work at a range of salt concentrations. This approach presents an adaptable method for the attachment of a range of carboxylic acid functionalised molecules to an α-HL channel. Indeed, in this work we demonstrated that attachment of an acylhydrazone photoswitch to the channel. Future work will hopefully see higher-order molecular machinery being attached to form transmembrane molecular machines.

Methionine modification could be accessed *via* a redox-activated reaction with oxaziridine derivatives. This presents a method for the functionalisation of the

channel with a broad range of reactive handles. It was demonstrated that methionine modification could be used to probe the mechanism of the CuAAC reaction at the single-molecule level. The applied potential could be used to trap charged reaction intermediates and thereby help to assign ion current states to proposed intermediates. The data provided evidence in support of the CuAAC reaction proceeding through the bis-Cu pathway.

Unfortunately, tyrosine modification did not prove to be as assessable. While some evidence to support modification at tyrosine was presented, the reaction was not reproducible. Modification only occurred occasionally, suggesting that modification may only be possible in a malformed protein.

The bioconjugation reactions explored here are far from exhaustive. Indeed, there are several excellent reviews that explore the scope of bioconjugation at various amino acids, which could be explored in future work.[17] While not addressed in this work, there is a growing interest in the modification of unnatural amino acids. Their induction would allow for absolute control over the attachment site and negate any unwanted side reaction occurring.

3.8 References

1. Deamer, D. W.; Branton, D., Characterization of Nucleic Acids by Nanopore Analysis. *Acc. Chem. Res.* **2002,** *35* (10), 817-825.

2. Bayley, H., Nanopore Sequencing: From Imagination to Reality. *Clin. Chem.* **2015,** *61* (1), 25-31.

3. Rincon-Restrepo, M.; Mikhailova, E.; Bayley, H.; Maglia, G., Controlled Translocation of Individual DNA Molecules through Protein Nanopores with Engineered Molecular Brakes. *Nano Lett.* **2011,** *11* (2), 746-750.

4. Clarke, J.; Wu, H.-C.; Jayasinghe, L.; Patel, A.; Reid, S.; Bayley, H., Continuous base identification for single-molecule nanopore DNA sequencing. *Nat. Nanotechnol* **2009,** *4* (4), 265-270.

5. Wloka, C.; Van Meervelt, V.; Van Gelder, D.; Danda, N.; Jager, N.; Williams, C. P.; Maglia, G., Label-Free and Real-Time Detection of Protein Ubiquitination with a Biological Nanopore. *ACS Nano* **2017,** *11* (5), 4387-4394.

6. Wang, Y.-Q.; Cao, C.; Ying, Y.-L.; Li, S.; Wang, M.-B.; Huang, J.; Long, Y.-T., Rationally Designed Sensing Selectivity and Sensitivity of an Aerolysin Nanopore via Site-Directed Mutagenesis. *ACS Sens.* **2018,** *3* (4), 779-783.

7. Maglia, G.; Restrepo, M. R.; Mikhailova, E.; Bayley, H., Enhanced translocation of single DNA molecules through α-hemolysin nanopores by manipulation of internal charge. *PNAS* **2008,** *105* (50), 19720-19725.

8. Nisthal, A.; Wang Connie, Y.; Ary Marie, L.; Mayo Stephen, L., Protein stability engineering insights revealed by domain-wide comprehensive mutagenesis. *PNAS* **2019,** *116* (33), 16367-16377.

9. Spector, S.; Wang, M.; Carp, S. A.; Robblee, J.; Hendsch, Z. S.; Fairman, R.; Tidor, B.; Raleigh, D. P., Rational Modification of Protein Stability by the Mutation of Charged Surface Residues. *Biochem.* **2000,** *39* (5), 872-879.

10. Schnölzer, M.; Kent Stephen, B. H., Constructing Proteins by Dovetailing Unprotected Synthetic Peptides: Backbone-Engineered HIV Protease. *Science* **1992,** *256* (5054), 221-225.

11. Gilmore, J. M.; Scheck, R. A.; Esser-Kahn, A. P.; Joshi, N. S.; Francis, M. B., N-Terminal Protein Modification through a Biomimetic Transamination Reaction. *Angew. Chem. Int. Ed.* **2006,** *45* (32), 5307-5311.

12. Stephanopoulos, N.; Francis, M. B., Choosing an effective protein bioconjugation strategy. *Nat. Chem. Biol.* **2011,** *7* (12), 876-884.

13. Hermanson, G. T., *Bioconjugate Techniques*. Elsevier Science & Technology: Burlington, 2008.

14. Wu, H.-C.; Astier, Y.; Maglia, G.; Mikhailova, E.; Bayley, H., Protein Nanopores with Covalently Attached Molecular Adapters. *J. Am. Chem. Soc.* **2007,** *129* (51), 16142-16148.

15. Luchian, T.; Shin, S.-H.; Bayley, H., Kinetics of a Three-Step Reaction Observed at the Single-Molecule Level. *Angew. Chem. Int. Ed.* **2003,** *42* (17), 1926-1929.

16. Qing, Y.; Ionescu, S. A.; Pulcu, G. S.; Bayley, H., Directional control of a processive molecular hopper. *Science* **2018,** *361* (6405), 908.

17. Spicer, C. D.; Davis, B. G., Selective chemical protein modification. *Nat. Commun* **2014,** *5* (1), 4740.

18. Kasianowicz, J. J.; Brandin, E.; Branton, D.; Deamer, D. W., Characterization of individual polynucleotide molecules using a membrane channel. *PNAS* **1996,** *93* (24), 13770-13773.

19. Cao, C.; Ying, Y.-L.; Hu, Z.-L.; Liao, D.-F.; Tian, H.; Long, Y.-T., Discrimination of oligonucleotides of different lengths with a wild-type aerolysin nanopore. *Nat. Nanotechnol* **2016,** *11*, 713.

20. Zhang, J.; Cao, J.; Jia, W.; Zhang, S.; Yan, S.; Wang, Y.; Zhang, P.; Chen, H.-Y.; Li, W.; Huang, S., Mapping Potential Engineering Sites of Mycobacterium smegmatis porin A (MspA) to Form a Nanoreactor. *ACS Sens.* **2021**.

21. Soskine, M.; Biesemans, A.; Maglia, G., Single-Molecule Analyte Recognition with ClyA Nanopores Equipped with Internal Protein Adaptors. *J. Am. Chem. Soc.* **2015,** *137* (17), 5793-5797.

22. Tanaka, Y.; Hirano, N.; Kaneko, J.; Kamio, Y.; Yao, M.; Tanaka, I., 2-Methyl-2,4-pentanediol induces spontaneous assembly of staphylococcal α-hemolysin into heptameric pore structure. *Protein Sci.* **2011,** *20* (2), 448-456.

23. Azevedo, C.; Saiardi, A., Why always lysine? The ongoing tale of one of the most modified amino acids. *Adv. Biol. Regul.* **2016,** *60*, 144-150.

24. Borsley, S.; Cockroft, S. L., In Situ Synthetic Functionalization of a Transmembrane Protein Nanopore. *ACS Nano* **2018,** *12* (1), 786-794.

25. Choi, E. J.; Jung, D.; Kim, J.-S.; Lee, Y.; Kim, B. M., Chemoselective Tyrosine Bioconjugation through Sulfate Click Reaction. *Chem. Eur. J.* **2018,** *24* (43), 10948-10952.

26. Chen, W.; Dong, J.; Plate, L.; Mortenson, D. E.; Brighty, G. J.; Li, S.; Liu, Y.; Galmozzi, A.; Lee, P. S.; Hulce, J. J.; Cravatt, B. F.; Saez, E.; Powers, E. T.; Wilson, I. A.; Sharpless, K. B.; Kelly, J. W., Arylfluorosulfates Inactivate Intracellular Lipid Binding Protein(s) through Chemoselective SuFEx Reaction with a Binding Site Tyr Residue. *J. Am. Chem. Soc.* **2016,** *138* (23), 7353-7364.

27. Ali, M.; Yameen, B.; Neumann, R.; Ensinger, W.; Knoll, W.; Azzaroni, O., Biosensing and Supramolecular Bioconjugation in Single Conical Polymer Nanochannels. Facile Incorporation of Biorecognition Elements into Nanoconfined Geometries. *J. Am. Chem. Soc.* **2008,** *130* (48), 16351-16357.

28. Carraway, K. L.; Koshland, D. E., [56] Carbodiimide modification of proteins. In *Methods Enzymol.*, Academic Press: 1972; Vol. 25, pp 616-623.

29. Keleştemur, S.; Altunbek, M.; Culha, M., Influence of EDC/NHS coupling chemistry on stability and cytotoxicity of ZnO nanoparticles modified with proteins. *Appl. Surf. Sci.* **2017,** *403*, 455-463.

30. Bartczak, D.; Kanaras, A. G., Preparation of Peptide-Functionalized Gold Nanoparticles Using One Pot EDC/Sulfo-NHS Coupling. *Langmuir* **2011,** *27* (16), 10119-10123.

31. Boden, E. P.; Keck, G. E., Proton-transfer steps in Steglich esterification: a very practical new method for macrolactonization. *J. Org.Chem.* **1985,** *50* (13), 2394-2395.

32. Howorka, S.; Bayley, H., Probing Distance and Electrical Potential within a Protein Pore with Tethered DNA. *Biophys. J.* **2002,** *83* (6), 3202-3210.

33. Misakian, M.; Kasianowicz, J. J., Electrostatic Influence on Ion Transport through the αHL Channel. *Mol. Membr. Biol.* **2003,** *195* (3), 137-146.

34. Zang, J.; Chen, Y.; Zhu, W.; Lin, S., Chemoselective Methionine Bioconjugation on a Polypeptide, Protein, and Proteome. *Biochem.* **2020,** *59* (2), 132-138.

35. Lin, S.; Yang, X.; Jia, S.; Weeks, A. M.; Hornsby, M.; Lee, P. S.; Nichiporuk, R. V.; Iavarone, A. T.; Wells, J. A.; Toste, F. D.; Chang, C. J., Redox-based reagents for chemoselective methionine bioconjugation. *Science* **2017,** *355* (6325), 597.

36. Bizet, V.; Hendriks, C. M. M.; Bolm, C., Sulfur imidations: access to sulfimides and sulfoximines. *Chem. Soc. Rev.* **2015,** *44* (11), 3378-3390.

37. Haugland, M. M.; Borsley, S.; Cairns-Gibson, D. F.; Elmi, A.; Cockroft, S. L., Synthetically Diversified Protein Nanopores: Resolving Click Reaction Mechanisms. *ACS Nano* **2019**.

38. Kolb, H. C.; Finn, M. G.; Sharpless, K. B., Click Chemistry: Diverse Chemical Function from a Few Good Reactions. *Angew. Chem. Int. Ed.* **2001,** *40* (11), 2004-2021.

39. Qing, Y.; Liu, M. D.; Hartmann, D.; Zhou, L.; Ramsay, W. J.; Bayley, H., Single-Molecule Observation of Intermediates in Bioorthogonal 2-Cyanobenzothiazole Chemistry. *Angew. Chem. Int. Ed.* **2020,** *59* (36), 15711-15716.

40. Qing, Y.; Pulcu, G. S.; Bell, N. A. W.; Bayley, H., Bioorthogonal Cycloadditions with Sub-Millisecond Intermediates. *Angew. Chem. Int. Ed.* **2018,** *57* (5), 1218-1221.

41. Dong, J.; Krasnova, L.; Finn, M. G.; Sharpless, K. B., Sulfur(VI) Fluoride Exchange (SuFEx): Another Good Reaction for Click Chemistry. *Angew. Chem. Int. Ed.* **2014,** *53* (36), 9430-9448.

42. Dong, J.; Sharpless, K. B.; Kwisnek, L.; Oakdale, J. S.; Fokin, V. V., SuFEx-Based Synthesis of Polysulfates. *Angew. Chem.* **2014,** *126* (36), 9620-9624.

43. Barrow, A. S.; Smedley, C. J.; Zheng, Q.; Li, S.; Dong, J.; Moses, J. E., The growing applications of SuFEx click chemistry. *Chem. Soc. Rev.* **2019,** *48* (17), 4731-4758.

44. Szijj, P. A.; Kostadinova, K. A.; Spears, R. J.; Chudasama, V., Tyrosine bioconjugation – an emergent alternative. *Org. Biomol. Chem.* **2020,** *18* (44), 9018-9028.

45. Dondoni, A.; Marra, A., SuFEx: a metal-free click ligation for multivalent biomolecules. *Org. Biomol. Chem.* **2017,** *15* (7), 1549-1553.

46. Joshi, N. S.; Whitaker, L. R.; Francis, M. B., A Three-Component Mannich-Type Reaction for Selective Tyrosine Bioconjugation. *J. Am. Chem. Soc.* **2004,** *126* (49), 15942-15943.

47. Ban, H.; Gavrilyuk, J.; Barbas, C. F., Tyrosine Bioconjugation through Aqueous Ene-Type Reactions: A Click-Like Reaction for Tyrosine. *J. Am. Chem. Soc.* **2010,** *132* (5), 1523-1525.

48. Hu, Q.-Y.; Allan, M.; Adamo, R.; Quinn, D.; Zhai, H.; Wu, G.; Clark, K.; Zhou, J.; Ortiz, S.; Wang, B.; Danieli, E.; Crotti, S.; Tontini, M.; Brogioni, G.; Berti, F., Synthesis of a well-defined glycoconjugate vaccine by a tyrosine-selective conjugation strategy. *Chem. Sci.* **2013,** *4* (10), 3827-3832.

Chapter 4

α-Hemolysin as a Framework for Transmembrane Molecular Machines

Abstract

Biological molecular machines are vital to life. While huge advances have been made in recent years in the development of artificial molecular machines, the elegance and application of their biological counterparts has yet to be matched. A broad range of machine and machine-like systems have been developed that act in the bulk. However, to strive towards systems analogous to those of nature, it is necessary to develop membrane-bound machines. Herein, we explore methods for the amalgamation of molecules with established machine-like characteristics with a transmembrane protein nanopore. Through application of the lysine bioconjugation chemistry discussed in **Chapter 3**, several photoswitches were attached to a single protein channel. However, the systems did not yield the stability required for application as a molecular machine. Similarly, several Feringa style rotary motors were attached to the lysine resided of the pore but resulted in membrane instability. Greater success was made towards the development of a transmembrane molecular pump. A functionalised carboxylic acid was attached at a lysine residue. A notable change in the channel current was observed upon the addition of a photoisomerisable axle to the system, which is indicative of pumping at the single molecule level. Unfortunately, due to limited supply of reagents, further studies could not be conducted.

Contributions: work in this chapter has been completed in collaboration with Prof. Alberto Credi, University of Bologna and Prof. Nicolas Giuseppone, University of Strasbourg and Prof Ivan Aprahamian, Dartmouth College. Reagents were supplied for each collaborator as specified in the text. Unless otherwise stated, all experimental work discussed was completed by Dominic Cairns-Gibson.

4.1 Introduction

A molecular machine is a molecular construct that converts energy into useful work.[1] In 2016 Sir Fraser Stoddart, Ben Feringa and Jean-Pierre Sauvage were awarded the Nobel Prize in Chemistry for their pioneering work on molecular machines.[2] Further advances have sought to achieve the transformation of stimuli-driven nano-mechanical motion into the transport of macroscopic objects.[3-5] Often, the ultimate goal of these systems it to achieve the efficiency and functionality of biological molecular machines.

A major challenge in the field of supramolecular chemistry is how to harness the work produced by a molecular machine. When such machines act in the bulk, the produced work is typically dissipated into solution.[6] Therefore, anchoring a machine to a scaffold has been proposed as a initial step in harnessing their work. For example, it has been shown that interlocked [2]catenanes can be incorporated to a Langmuir monolayer (**Figure 4.1A**).[7] The monolayer was not presented as a means of coordinating the actions of molecular machinery. However, there is potential in similar systems to extract work. Herein, it is proposed that a biological nanopore could act as a scaffold for molecular machines. It is hoped that the amalgamation of known machine-like systems and protein nanopores could provide gateways to artificial membrane-bound molecular machines that could match the functionality of biological systems in the near future.

While countless examples of sophisticated molecular machines exist, few have been fused with nanopore technology. As discussed in **Chapter 1**, the Cockroft group have previously demonstrated a membrane-bound molecular machine that acted as an autonomously reciprocating nanoactuator (**Figure 1.28 and 4.1B**).[8] This was achieved by passing an axle through the channel and stoppering it to form a trapped pseudorotaxane.

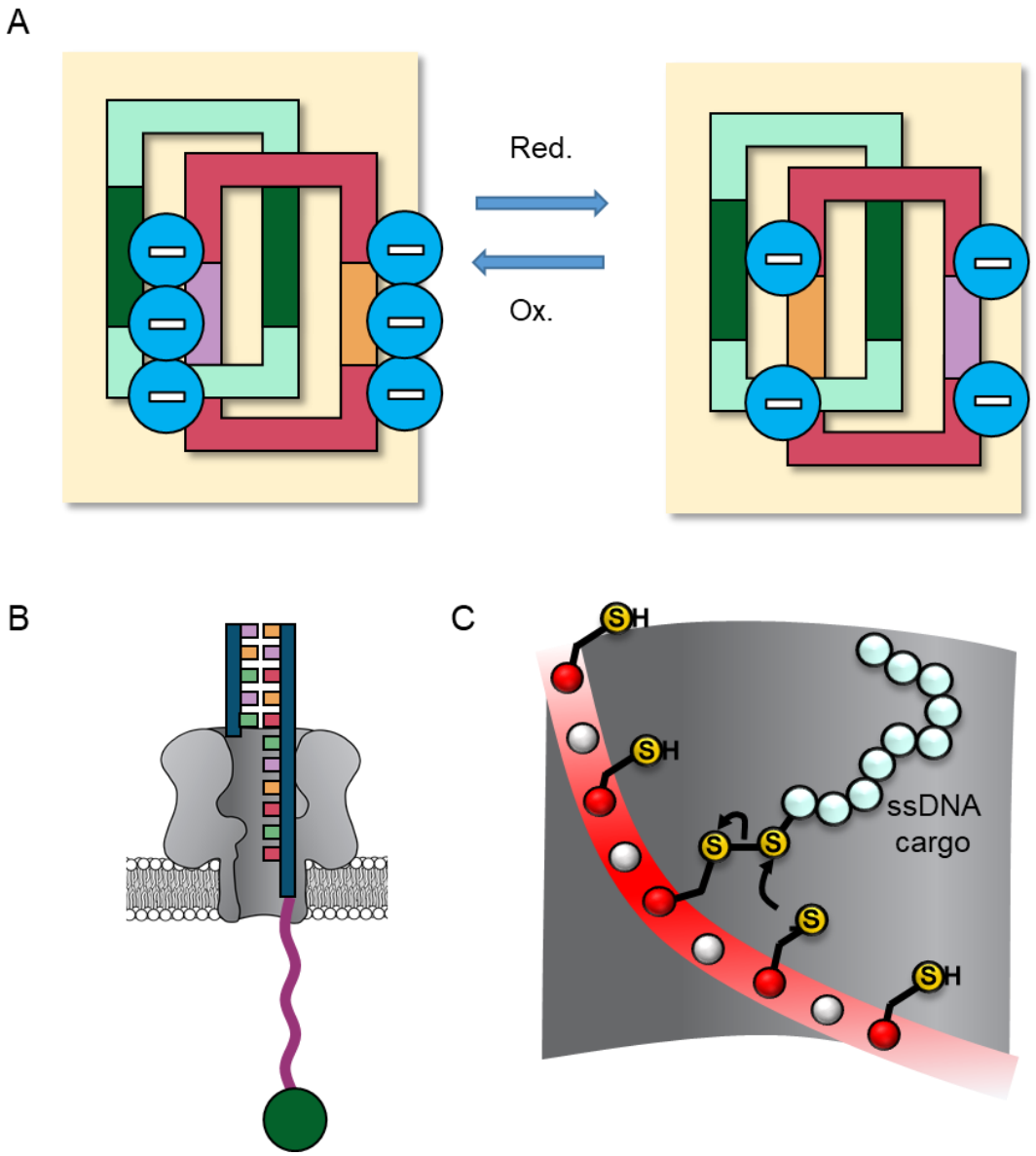

Figure 4.1: A) representation of a [2]catenane deposited onto a Langmuir film (yellow). The redox state of the [2]catenane can be modulated while bound to the Langmuir film on both mica and gold surfaces. In turn, the surface morphology and voltage characteristics can be modulated by control of the redox states.[7] B) Representation of a autonomously reciprocating transmembrane nanoactuator. A cycle of DNA strand displacement and subsequent enzyme mediated primer degradation repeatedly pulls the thread against the applied potential (see **Figure 1.28**)[8] C) Representation of a molecular walker, which is capable of carrying a DNA cargo along a cysteine track. The sequential formation of disulfide bonds in the direction of the applied potential moves the walker in a unidirectional fashion (see **Figure 1.13**).[9]

A range of successful artificial molecular machines have been developed, and an elegant extension of this work is the covalent attachment of these systems

to a protein scaffold. As previously discussed, success has been achieved attaching a molecular walker to a mutated protein channel (**Figure 4.1C**).[10] This is an impressive system whereby α-HL is used as a platform for a machine-like construct. It is hoped that by attaching systems with a more established function to a protein nanopore, it will eventually be possible to harness this work.

Several systems were proposed for the creation of membrane-bound molecular machines, such as switches, motors, and pumps (**Figure 4.2**). As previously noted, molecular switches (**Figure 4.2B**) will move between fixed states and are not autonomous nor unidirectional. On the other hand, Conversely, molecular rotors (**Figure 4.2A**) and pumps (**Figure 4.3C**) exhibit true machine like properties. While vastly different in their construct and function, all shared a commonality in that they may derive their energy source from photons of light. Light-driven systems are highly advantageous; light can penetrate into reaction media, it is easy to control, and is generally non-destructive.[11] Unlike chemically driven systems, there is no need to add, scavenge or recycle fuel to achieve continuous operation. This is perhaps where artificial molecular machines deviate from their biological counterparts. Biological machinery such as ATPsynthases rely on an electrochemical gradient to generate ATP, while the generated ATP is consumed by other biological molecular machines.[12]

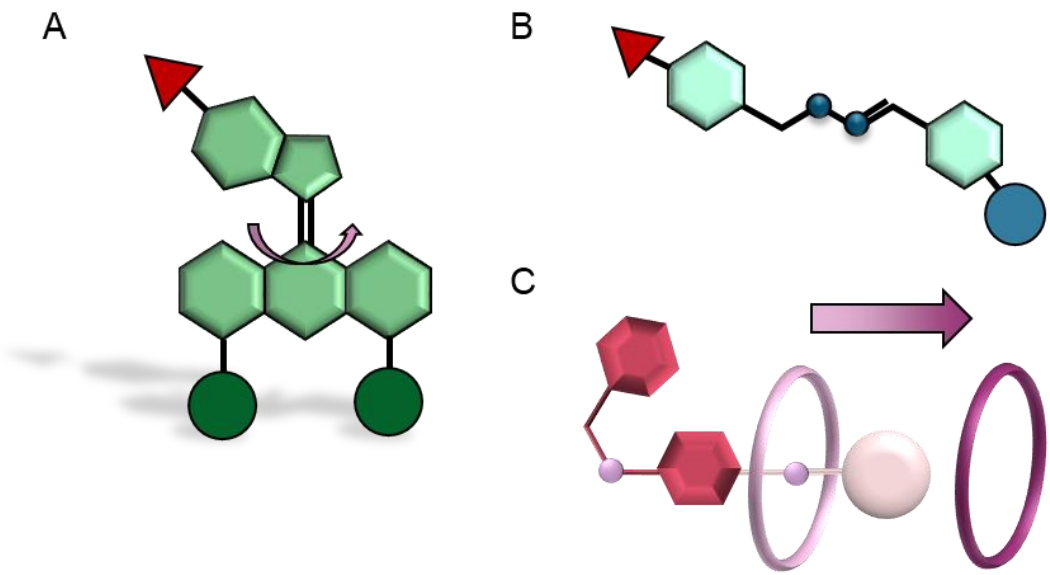

Figure 4.2: A) Cartoon representation of a molecular rotor. B) Cartoon representation of a molecules switch. C) Cartoon representation of a molecular pump.

Molecular switches are perhaps the most simplistic molecular systems that can be considered as having machine-like properties. However, molecular switches are not strictly molecular machines; they exist in two or more states yet are not unidirectional or autonomous.[13] However, molecular photo-switches may be used as components of a machine-like system. The functionalisation of a protein nanopore with a molecular switch is not a novel concept. Indeed, simple azobenzene moieties have previously been attached to a mutated α-HL channel[14] and photo-controlled valves have been embedded in a bilayer.[15] An α-HL channel was constructed with a single cysteine mutant at position 117 (T117C) and an azobenzene derivative was attached (**Figure 4.3**).

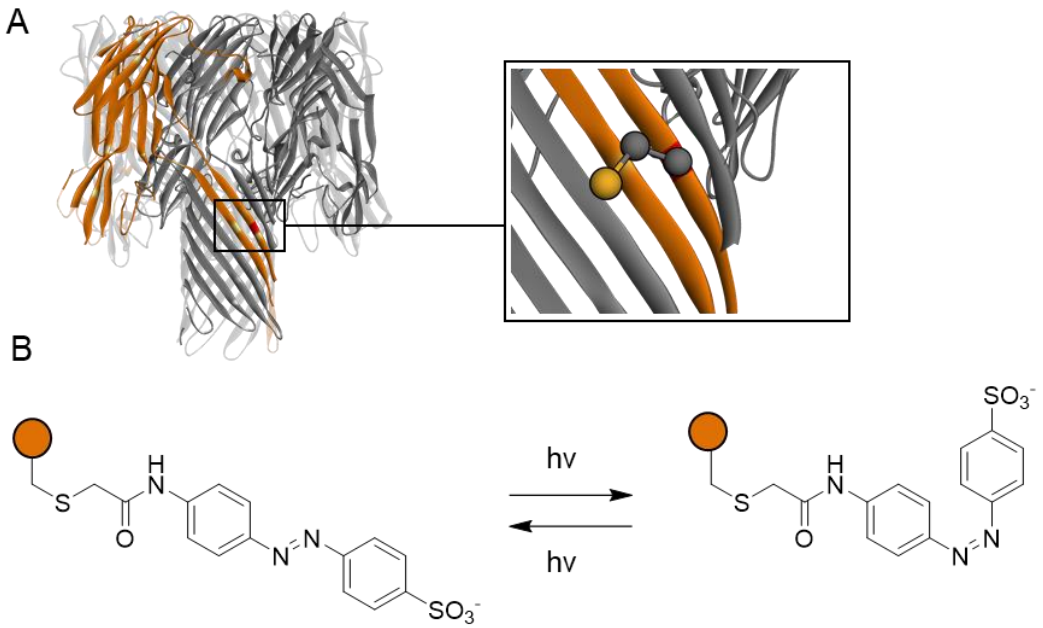

Figure 4.3: A) A mutant α-HL pore was produced. In a single strand (orange) a cysteine was introduced at position 117 (red). As this is the only cysteine in the protein, it gives absolute control over where the modification occurs. B) Structure of the azobenzene bound to the pore. The switch will isomerise between the *trans* (left) and *cis* (right) isomer upon irradiation with UV light (λ = 330 nm).[14]

Upon irradiation with 330 nm light, both *cis* and *trans* isomerisation were achieved, which could be observed by variation in the output current. While this system presents an intriguing insight into the kinetics of light driven isomerisation, the authors do not present it as having machine-like characteristics. A notable caveat of this system is the rapid *cis/trans* isomerisation at a singular wavelength. Future switch-based transmembrane molecular machines would require molecules with discreet and distinct photostationary points for the *cis* and *trans* isomerisation. An enticing alternative to azobenzenes as switching moieties in a transmembrane molecular machine is the application of hydrazones. These tend to distinct photostationary points and are more resistant to thermal relaxation, and hence provide more finesse in their control.[16]

Moving on from simple switching systems, more complex machines have been developed. Examples range from the nanocar,[17] to molecular elevators,[18] and a full discussion of the field would fill several volumes. However, detailed discussion can be found in excellent reviews.[13, 19-20] For the purpose of this work, focus has been given to molecular pumps and motors. Like their biological counterparts, motors and pumps can be applied to move ions across a membrane. As nanopore technology inherently relies on the measurement of a flow of ions, they present excellent platforms to study these machines.

4.2 Project Aims

This project aims to explore the development of covalently modified membrane-bound transmembrane molecular machines. Much of the work was completed in collaboration with Prof. Alberto Credi and Prof. Nicolas Giuseppone, who previously developed systems that demonstrated machine-like properties in the bulk. Herein, we explore the approaches to attach the molecular machines to a protein nanopore and observe their actions at the single-molecule level. Ultimately, the aim is to harness the work done by such machines by creating/maintaining a concentration or potential gradient across a membrane.

4.3 Molecular Switches

Photoisomerisable switches are well established: from early azobenzenes[21] to more robust acyl hydrazones.[22] As discussed, photoswitches have previously been attached to a protein nanopore to observe the switching of the molecule.[14] Here, we hypothesise that photoswitches could be attached to α-HL to achieve machine-like functionality. For example, attachment of photoswitches to the transmembrane α-HL protein channel could be used to make light-controlled transmembrane valves. While a simple system could be developed with a single switch, the attachment of two orthogonal switches presents the truly exciting prospect of the construction of a transmembrane valve. As discussed in **Chapter 3**, it has been demonstrated that activated carboxylic acids can be used to modify lysine residues within the α-HL channel. Two different acylhydrazone systems were explored. The first generation switches (**Figure 4.4 and 4.5**) were previously synthesised in the Cockroft group by DCG during undergraduate research. The second-generation switches (**Figure 4.6**) were provided by Prof Ivan Aprahamian.

Modification was initially achieved with the first generation switches (**Figure 3.12 and 4.4A**) at the constriction-site (**Figure 4.4B**) and *cis*-lysine (**Figure 4.4D**). The modification at the constriction-site with compound **10** gave significant signal noise when irradiated with UV light from an LED (λ = 355 nm, **Figure 4.4**). This increase in signal noise was an exciting result, as it signified movement at the molecular level. However, it did not yield the quantised states and stable photostationary point required for a transmembrane switch. On the other hand, the *cis* modification yielded a more consistent level (**Figure 4.4D).**

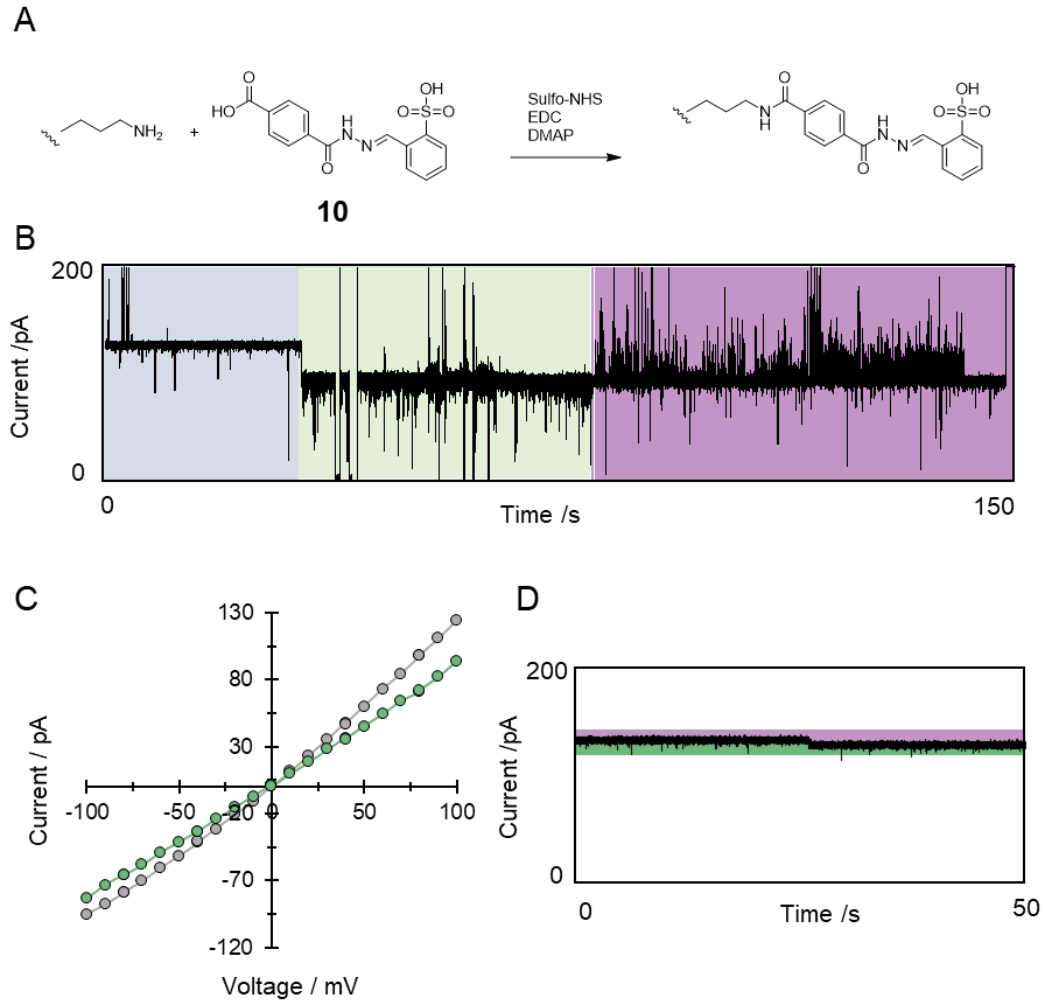

Figure 4.4: Attachment of the compound **10** to an α-HL channel. A) Reaction scheme for the attachment of compound **10** to a lysine residue. B) Current trace for the attachment of compound **10**. Compound **10** (10 mM stock) was activated and added to the *cis* well (See: General attachment protocol, **Chapter 5, Section 5.5**). Initially, a free pore current of 130 pA (blue) was observed. A sharp drop to 85 pA (green) was observed upon modification. When the system was irradiated with UV light (λ = 365 nm, purple) a large increase in signal noise was observed. C) I/V trace for the free pore current (grey) and the modified pore (green). D) Current trace for a *cis* lysine modification. Here a much smaller change in current (130 pA to 124 pA) was observed.

Subsequently, modification of the pore with compound **15** (**Figure 4.5A)** was achieved. An activated solution of compound **15** was added to the *cis* well and an irreversible modification was observed ~50 minutes after the first addition (**Figure 4.5B**). A reproducible I/V sweep was obtained, suggesting that the modification was genuine (**Figure 4.5C**). However, unlike previous

modifications with simple molecules, discrete single current levels were not observed. Instead, the trace presented significant signal noise and multiple states.

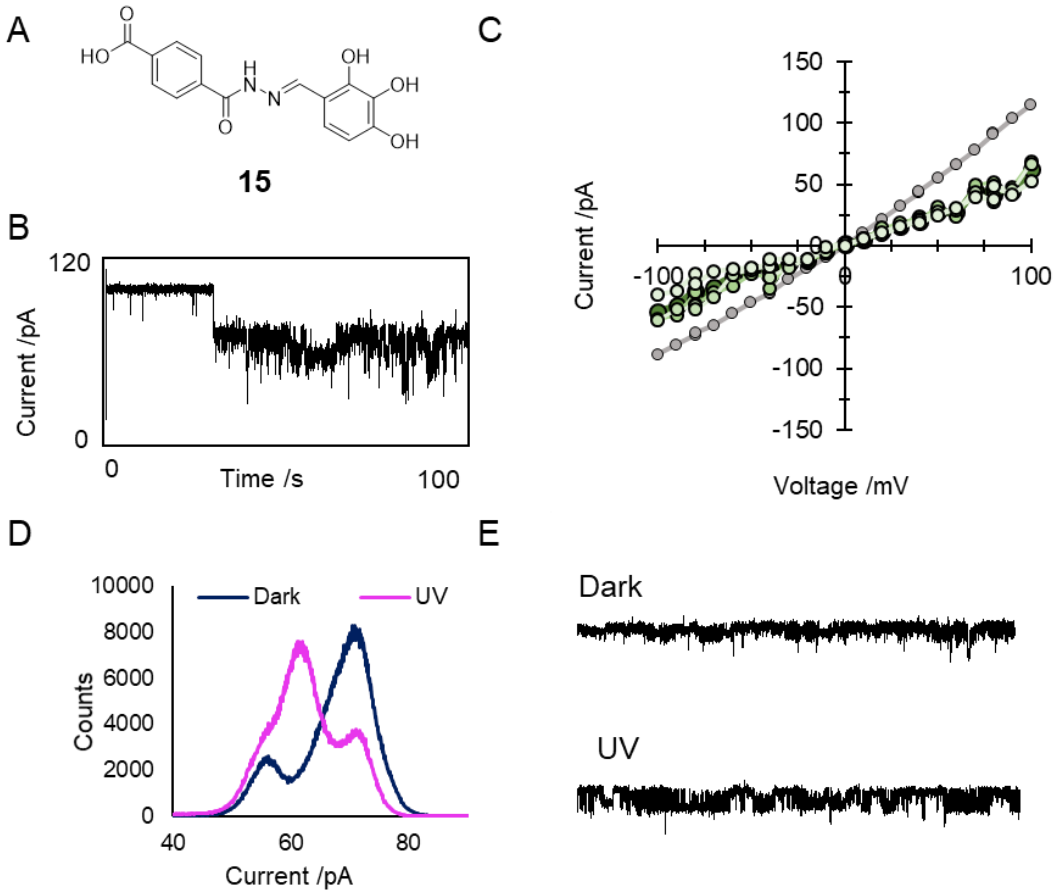

Figure 4.5: A) Structure of compound **15**. B) Example current trace for the modfication with compound **15**. Compound **15** (10 mM stock) was activated and added to the *cis* well (See: General attachment protocol, **Chapter 5, Section 5.5**). Five subsequent additions of 10 µL were made. After 50 minutes, single step down was observed and the new level exhibited multiple states. Applied voltage +100 mV. Buffer 1 M KCl, 30 mM K_2HPO_4, pH 8. Lowpass Bessel filter 300 kHz applied. C) Characterisaton trace for the modified pore. Free pore is shown in (grey). Modified channel is shown in green. Reproducible sweeps were observed for the modiciation. D) All-points histogram for the modified channel in the dark (blue) and upon irradiation with UV light (λ =365 nm) (purple). E) Example current trace for the modified level in the dark (top) and under UV (bottom). Two defined levels can be observed.

An all-point histogram analysis (**Figure 4.5D**) revealed that at least three states could be observed in both the non-irradiated and irradiated states. Nonetheless, LED irradiation of the well (λ = 355 nm) gave a distinct shift in

the major and minor peaks. In addition, the current traces had different characteristics in the presence and absence of light (**Figure 4.5E**).

The observation of different states in both conditions provides evidence that the photoswitching is occurring. While it does seem possible to induce switching by application of UV light, the fine control required for a transmembrane valve was not achieved. Indeed, this may intrinsic to the nature of the single-molecule approach. In the bulk, the population may lie towards the *cis* or *trans* isomer under different conditions, but at the single-molecule level all fluctuations into and out of these states are observed. Similarly, it might be possible that the applied potential might also provide a stimulus for isomerisation to occur. While not explored here, future work may look to examine the effect of an applied potential on photoswitching properties.

Since no satisfying explanation could be given for the three states observed in **Figure 4.5D**, it was decided to examine the behaviour of a different photoswitch. The second-generation hydrazone switches (**Figure 4.6**) were selected in the hope that they would have distinct photostationary points so that orthogonal switching could be achieved. These were provided by Prof. Ivan Aprahamian (Dartmouth College, USA) and were carboxylic acid derivatives of previously established photoswitches.[23] These switches possess a carbonyl group that allows an intramolecular hydrogen bond to form with the hydrazone in the Z isomer (**Figure 4.6A**). *Ortho, meta,* and *para* carboxylic acid variants were provided (**Figure 4.6B**).

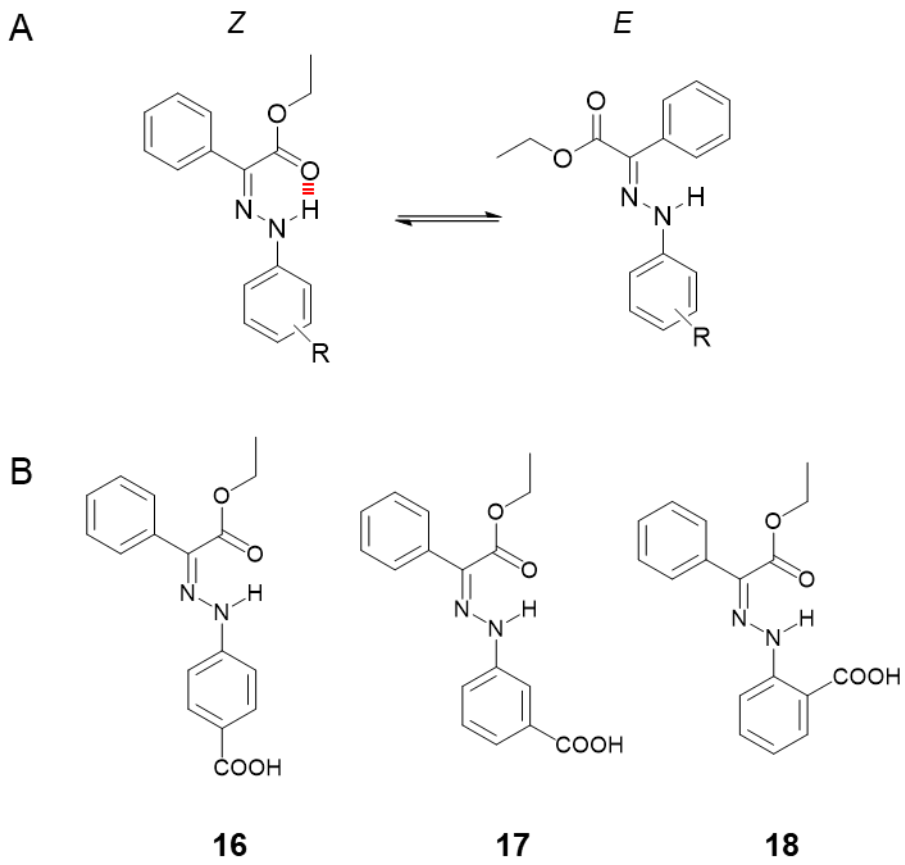

Figure 4.6: A) Generic structure of second-generation switches. In the *Z* conformation, a stabilising H-bond can form. B) Structure of the *para*, *meta*, and *ortho* switches (left to right). Synthesised and provided by the Aprahamian group (Dartmouth College, USA).

Unfortunately, unlike the first-generation switches, nine attempts to attach compound **17** and compound **18** to individual α-HL pores failed. Addition of these switches to the buffer wells resulted in the formation of a precipitate that induced membrane leakage and ultimately membrane rupture before attachment could occur.

Successful attachment of compound **16** was achieved on one occasion (**Figure 4.7**, attachment protocol in detailed in **Chapter 5, Section 5.5**). However, the current trace became immediately distressed upon the addition of the switch solution (**Figure 4.7**). The current trace then showed a blockage, as demonstrated by the large drop in current, followed by a large current (greater than the free pore current). As this increase was far too small to be

the insertion of a second pore, therefore it is reasonable to conclude that compound **16** also induced membrane stress. The current was then seen to drop, before rising to a new consistent current level, which is lower than that of the free pore current. This current level is highly distressed, with a great deal of signal noise being observed. The enhanced section of **Figure 4.7** shows subsequent modifications occurring. This suggests that the modifications are occurring on the *cis*-lysine ring of the protein, as modification at the smaller constriction-site lysine ring would result in a larger drop in current. The more hindered nature of the internal constriction site also makes multiple modifications unlikely.

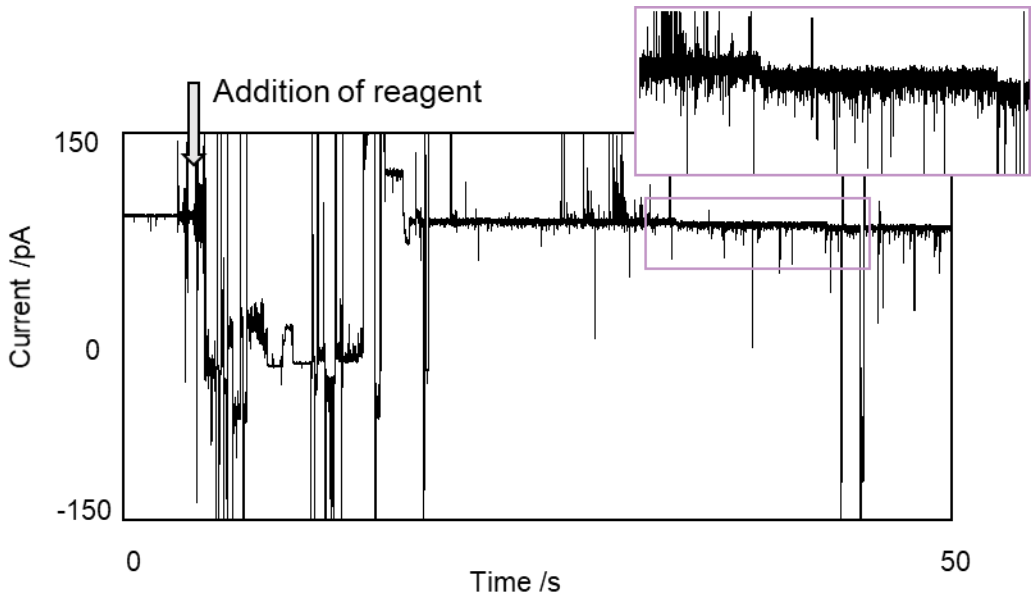

Figure 4.7: Attachment of the para second-generation switch to the protein channel. A solution of compound **16** (17 mM stock) was activated and added to the *cis* well (see: General attachment protocol **Chapter 5, Section 5.5**). Immediately, a deep blockage occurred that was resistant to inversion of the potential. The current then returned to its original level, through a high current intermediate. Large upwards spikes in current suggest that the membrane is unstable. Two steps down were then observed in quick succession (enlarged section, top left). Applied voltage +100 mV. Buffer 1 M KCl, 30 mM K_2HPO_4, pH 8. Lowpass Bessel filter 300 kHz applied.

The development of a successful transmembrane valve would be benefited by modification at the outer lysine rings, therefore this switch is a viable candidate. However, the instability of the membrane negated the use of these switches in

further work. Future work would rely on the development of water-soluble photoswitches that have distinct photostationary state and do not disrupt the membrane. While the development of a light-mediated transmembrane valve is enticing, the applications are somewhat limited. Passage of analytes could be mediated by the valve, but the movement of molecules would still be reliant on factors such as concentration gradients or an applied potential. In the context of biological application, UV light has poor penetration properties, meaning that these systems would have limited scope in potential therapeutics. Despite limited success with the development of transmembrane switches, it was decided to invest efforts in the attachment of molecular rotors.

4.4 Molecular rotors

As previously discussed, molecular switches do not constitute true molecular machines.[13] However, their attachment and responsiveness to UV light provides proof-of-concept that the operation of UV-controlled molecular machines attached to protein nanopores is possible. Prof. Ben Feringa shared the 2016 Nobel Prize for Chemistry for his contributions to molecular machines and is most well-known for his work on light-driven molecular motors (**Figure 4.8**).[24]

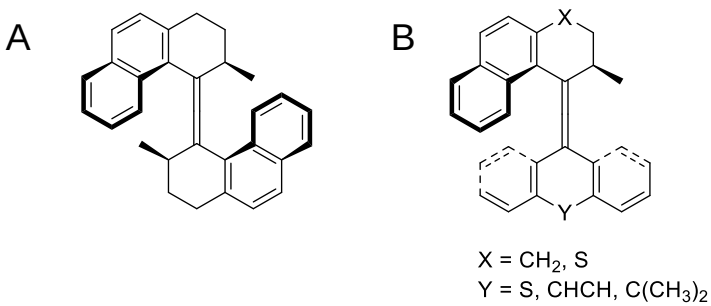

Figure 4.8: A) First-generation rotary motor from the Feringa group. The motor turns around the double bond. B) Second-generation rotary motor.[25]

These motors, first developed in the late 90s, share some characteristics with the rotary systems seen in biology, such as ATP synthase.[26] However, the

synthetic rotary motors are much simpler and function *via* a *cis/trans* photoisomerisation step followed by a thermal conversion about the double bond.[25] The helical nature of the molecules results in irreversible thermal isomerisation, which *via* thermal relaxation down the least hindered (chiral pathway) results in unidirectional motion of the molecule. Further development led to the second-generation motors, which, upon varying the substituents, can have tuned rotation speed. These rotors can have a huge range of rotation speeds, with the rate varying from 10^{-11} to 10^{8} Hz.[27] Many systems containing Feringa motors have been developed, such as those by the Giuseppone group. For example, the Giuseppone group have synthesised light-controlled polymer gels functionalised with motor molecules.[28] By working in collaboration with the Giuseppone group (University of Strasbourg) it was hoped that nanopore technology would provide new opportunities for the development of transmembrane molecular machines.

The first such system that was investigated was the so-called “nanoswimmer” (compound **19**, **Figure 4.9A**). These compounds shared structural similarities to those used previously in the polymer gel. It was hypothesised that under ambient conditions, the compound **19** would interact with the channel stochastically. However, upon UV-irradiation of the cell, the compound **19** would rotate directionally, which would then influence its movement through the chiral pore.

A solution of the compound **19** was added to the *cis* well under an applied positive potential. Post-addition, minor transient events were observed (**Figure 4.9B**). Upon irradiation with UV light (λ = 365 nm) no visible change in the current trace was observed (**Figure 4.9B**). To confirm this, an all points histogram of the I_b/I_o was plotted (**Figure 4.9C**). From this, it can be observed that there is no difference between the levels observed with and without the application of UV light. There was concern that the applied potential may be interfering with the capability of the motor to rotate. To test this, the applied

potential was varied between +120 mV and -120 mV. However, no notable change in the event profile was observed.

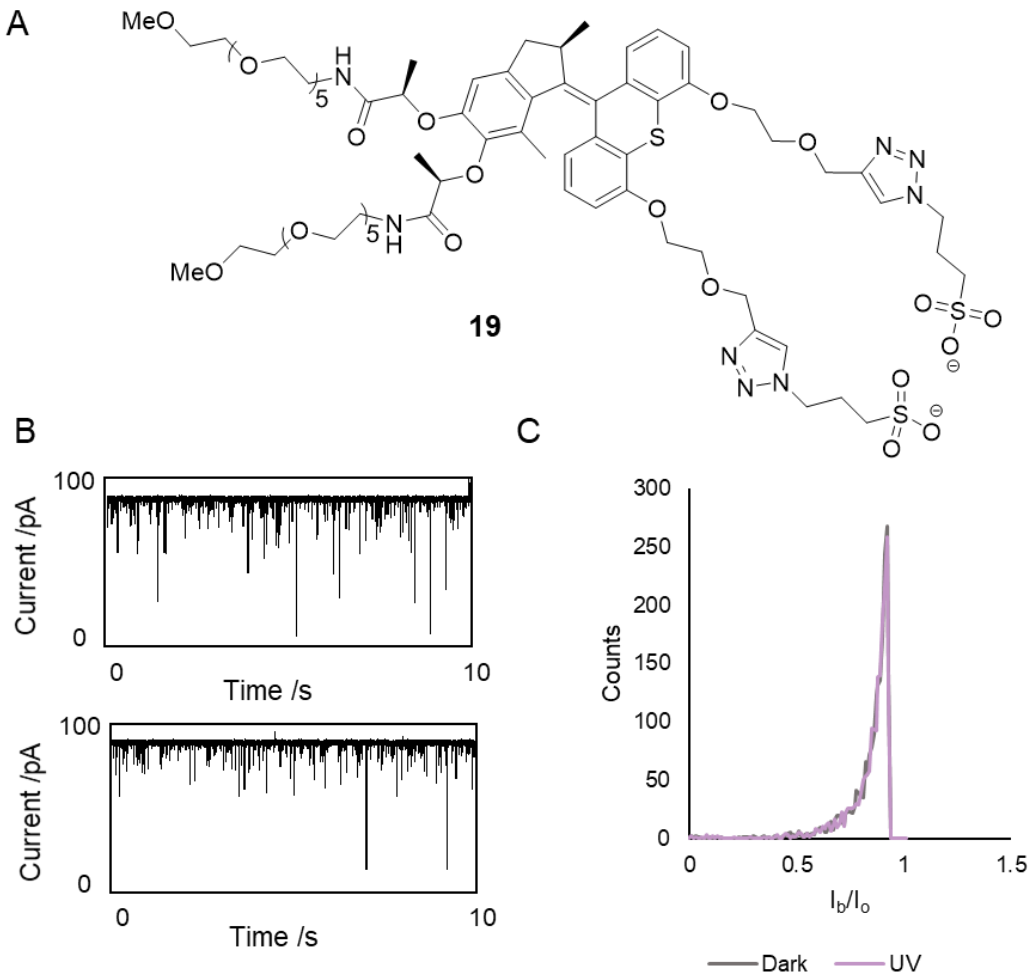

Figure 4.9: A) Structure of the molecular swimmer (compound **19**). B) A solution of compound **19** (20 mM, DMSO) was prepared and added to the *cis* well under an applied positive potential. Current traces after the addition of the compound **19** in the absence of light (upper) and with UV light applied (lower, λ = 365 nm). Buffer 1 M KCl, 30 mM K_2HPO_4, pH 8. Voltage +100 mV. Lowpass Bessel filter 300 kHz applied. C) All points histogram of the event levels observed from the trace in darkness (grey) and when UV light (λ = 365 m). No variation was observed between the two conditions.

Therefore, attention was turned to attaching a molecular motor with the appropriate functional groups to the nanopore. The reasons for this would be two-fold; to allow observation of the motor turning in real time, and to work towards achieving a transmembrane molecular motor. Biology has developed

many rotary systems that work away from equilibrium, and it is hoped that protein channel might be a step towards developing artificial transmembrane molecular pumps.

A series of bidentate molecular motors were provided by the Giuseppone group, which all shared a consistent core structure (**Figure 4.10**). This system uses a Feringa-like rotary bond that undergoes isomerisation upon irradiation with UV light. Moreover, the two carboxylic acid groups might provide a means of anchoring it to two lysine residues within the pore.

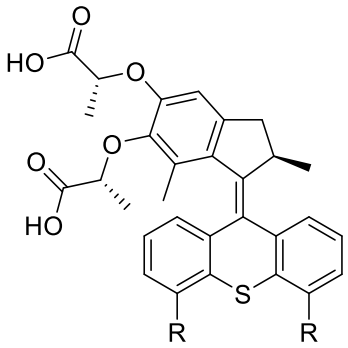

Figure 4.10: General structure of the carboxylic acid functionalised Feringa-style motor used for motor attachment experiments.

As a very small quantity of the bidentate motor was provided by the collaborator, it was decided to explore analogous systems to improve the likelihood of achieving successful attachment. One of the more pressing issues was whether mono or bidentate attachment would be achieved – previous systems explored have only utilised molecules with a single carboxylic acid. Here, the bidentate attachment is required to create a non-rotatable anchor to the pore. To explore whether attachment could occur, the two analogues shown in (**Figure 4.11**) were selected. Attachment was achieved following the protocol outlined in **Chapter 5, Section 5.6**.

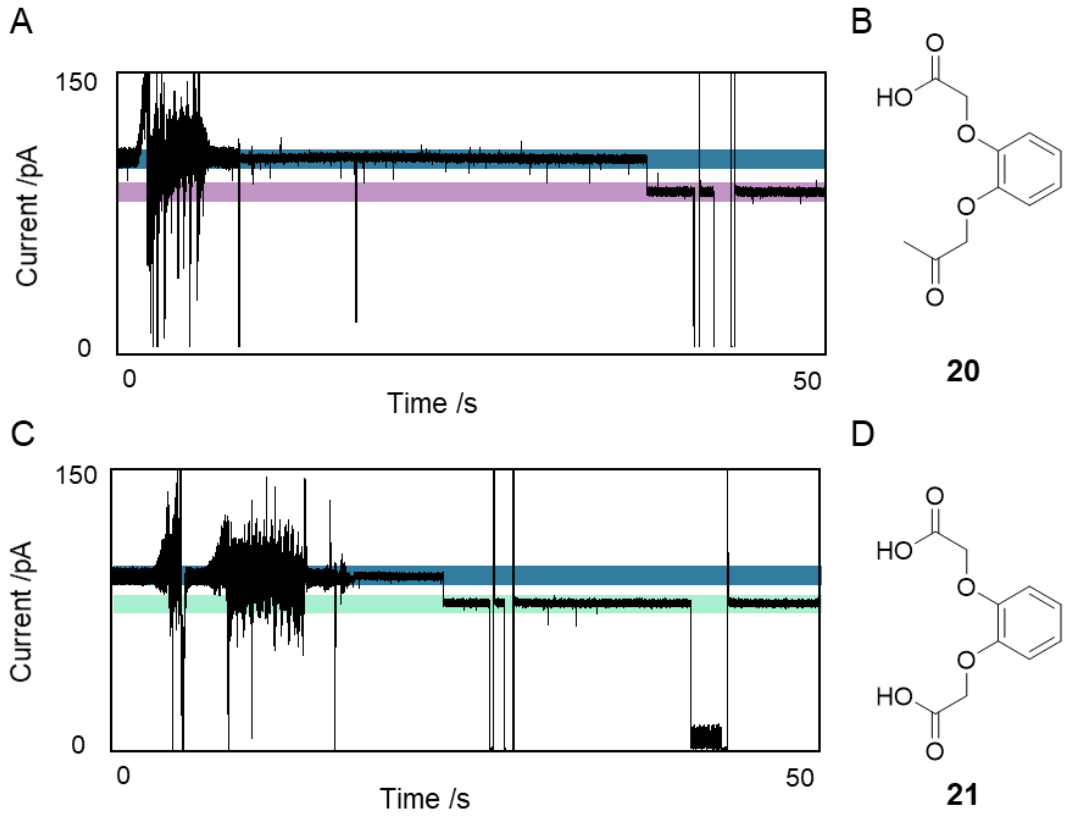

Figure 4.11: A) Modification of the channel with compound **20**. Modification was seen as a single step with I_b/I_o = 0.81. B) Structure of the compound **20**. C) Modification trace with the compound **21**. The reaction progressed *via* a single-step process with I_b/I_o =0.84. D) structure of the compound **21**. Volume 600 µL. Buffer 1 M KCl, 30 mM K_2HPO_4, pH 8. Voltage +100 mV. Lowpass Bessel filter 100 kHz and output gain x50.

Attachment with a compound **20** analogue was achieved using the previously established EDC coupling protocol (See: General attachment protocol, **Chapter 5, Section 5.5**). The attachment appeared to go through a single step before a consistent current was observed. This was then compared to the attachment of a compound **21** (**Figure 4.11C and D**). Here, a single step was also observed. If bidentate attachment was occurring, it would be expected that two steps would be observed unless the two modifications were to occur simultaneously. However, the more probable explanation is that only a single modification is occurring. This may be attributed to steric effects that prevent the secondary modification from occurring. Alternatively, the second activated carboxylic ester may have hydrolysed in this experiment back to the unreactive

carboxylic acid group. While bidentate attachment would provide added stability to the attachment of the machine, it was not deemed necessary for its success. However, future designs may look to optimise the geometry of the machine to achieve bidentate attachment.

Initial studies were conducted with compound **22** (**Figure 4.12A**), as it was hoped that its larger size would result in well-resolved perturbations of the ion current. Several attempts were made to attach the motor to the *cis* side of the channel, but these either did not yield modification or resulted in membrane instability. However, a successful modification under an applied negative potential was attained from the *trans* well (**Figure 4.12B**). The current was seen to pass through a transition state, before regular and recurring events occurred. At least three distinct and well resolved levels were resolved. Sublevels were present within these states. Unfortunately, the membrane holding the modified pore appeared unstable, and within 100 s the membrane burst. Subsequent attempts to modify the pore on the *trans* side all resulted in membrane instability and did not yield a permanently modified pore.

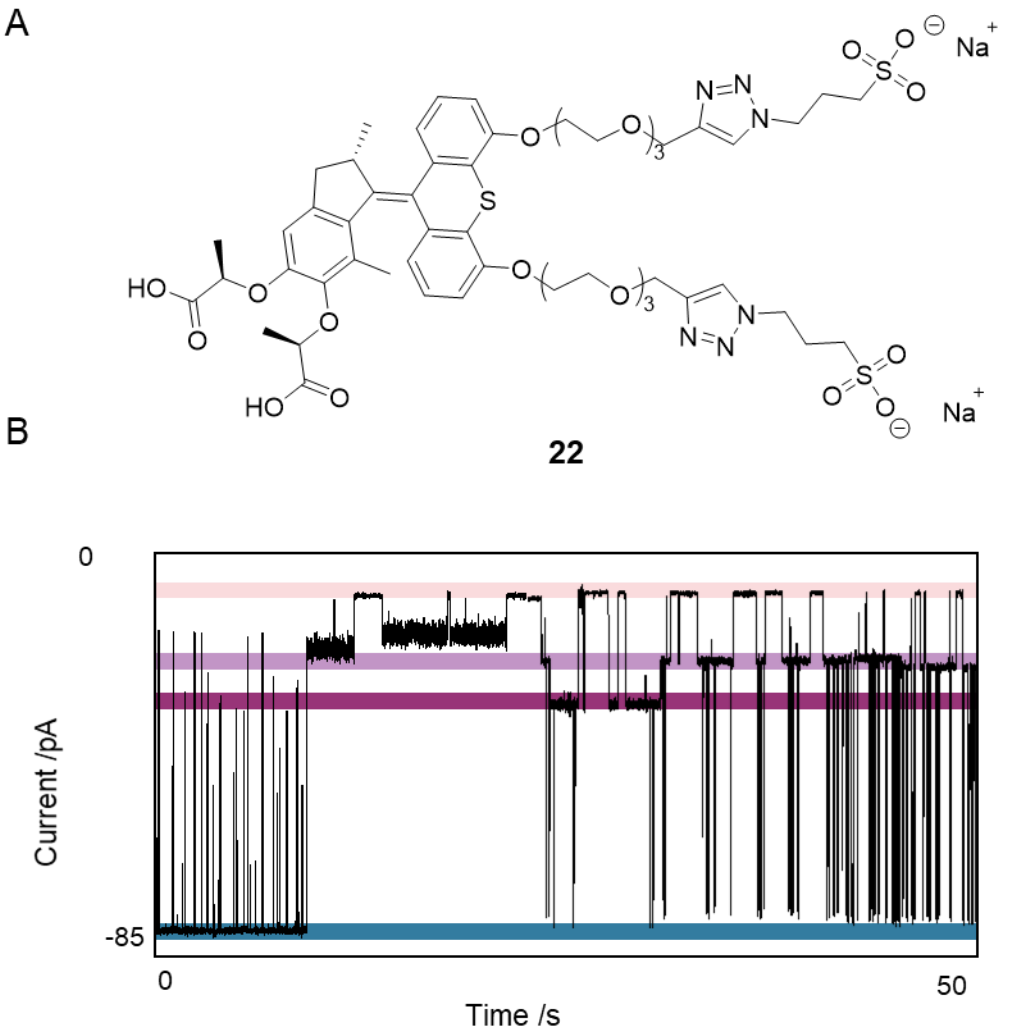

Figure 4.12: A) Structure of compound **22** B) Current trace for the attachment of compound **22**. A solution of compound **22** (10 mM) prepared following the general attachment protocol (**Chapter 5, Section 5.5**). From the free pore current (blue), deep but short-lived binding events are observed. A more prolonged blockage then occurs, which passes through several states, before entering into a multi-state system. At least 4 distinct current levels can be resolved. Applied potential -100mV. Volume 600 µL. Buffer 1 M KCl, 30 mM K_2HPO_4, pH 8. Lowpass Bessel filter 100 kHz and output gain x50.

It was therefore hypothesised that the molecule may be disrupting the membrane. Indeed, the molecule shares structural similarities with sodium lauryl sulfate (SLS), which is known to have membrane disrupting properties.[29] To verify this, a solution of compound **22** was added against a bilayer in the absence of a protein channel. Within 70 s of addition, membrane disruption

was observed (**Figure 4.13**). This lasted for less than 1 s before total membrane degradation occurred. The same effect was observed across several bilayers, confirming that the membrane was not stable to compound **22.**

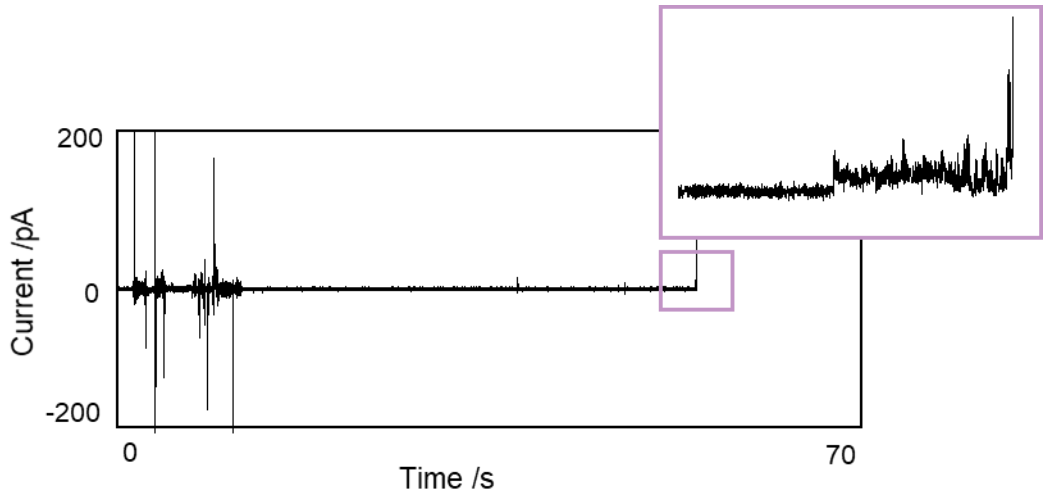

Figure 4.13: Membrane disruption study with bis-sulfo motor. A solution of compound **22** (20 mM of 10 µL stock) was added to the *cis* side of the membrane with mixing. Membrane disruption was observed within 70 seconds (enlarged panel, top right). Applied potential +100 mV. Volume 600 µL. Buffer 1 M KCl, 30 mM K_2HPO_4, pH 8.. Lowpass Bessel filter 100 kHz and output gain x50.

To combat this instability, the uncharged analogue depicted in **Figure 4.14A** (compound **23**) was trialled. The alkyne derivative was similar in size to the previously used compound **23**. A solution of the activated compound **23** was added to the *cis* side of an α-HL channel. Shortly after, a drop in current was observed to I_b/I_o = 0.95 (**Figure 4.14B, dark blue to purple**). This level exhibited large, millisecond variations in the ion-current blockage. However, the states were poorly resolved when plotted as an all-points histogram (**Figure 4.14C**). This state persisted for 145 s, at which point a second downwards step was observed to a new level (I_b/I_o = 0.93) (**Figure 4.14B, purple to green**). This second drop in current was similar in magnitude to the first, suggesting that a bidentate attachment had occurred. Here, there was a pronounced difference in the observed events. To compare the events, the

magnitude of the blockage was plotted against the event duration (**Appendix B, Figure B.1**), but this did show any significant difference. However, a notable difference was observed in the all-points histograms of the two states (**Figure 4.14C**). For the singly attached motor, the levels are poorly resolved. Conversely, when the second attachment occurred approximately 8 individual states could be resolved. This suggests that once a bidentate attachment has occurred, that the states of a rotating molecular motor can be resolved.

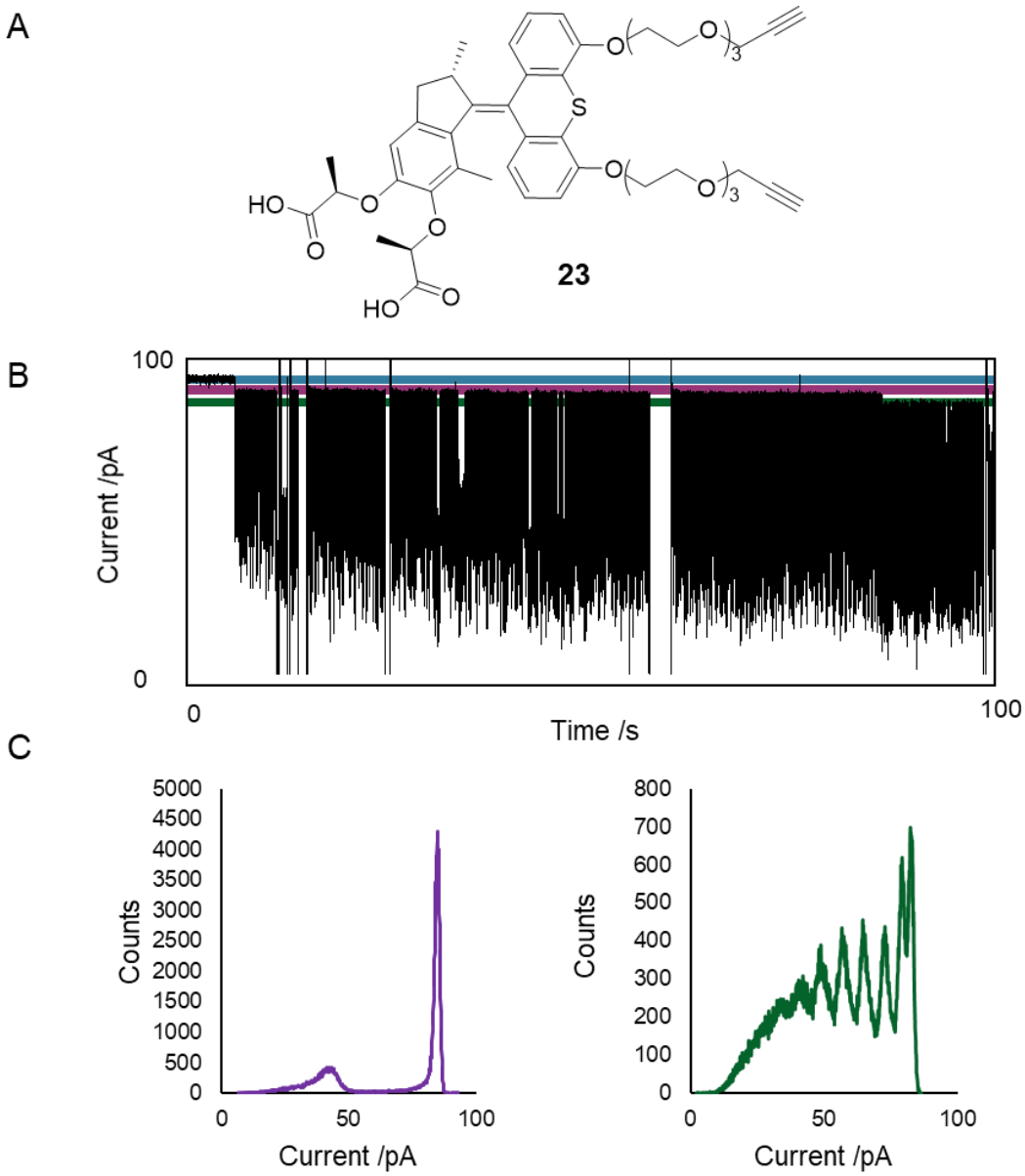

Figure 4.14: A) Structure of the compound **23**. B) Current trace for the attachment of the compound **23**. A solution of compound **23** (10 mM) prepared and added following the general attachment protocol (**Chapter 5, Section 5.5**). A consistent free-pore current was observed (dark blue). Modification was indicated by a sudden sharp drop to a new noisy level (dark blue to purple, I_b/I_o = 0.95). A second modification then followed (purple to green, I_b/I_o = 0.93). C) All-points histogram of the levels observed after the first attachment (left) and the second attachment (right). Volume 600 µL. Buffer 1 M KCl, 30 mM K_2HPO_4, pH 8. Voltage +100 mV. Lowpass Bessel filter 100 kHz and output gain x50.

Despite the initial promising result of achieving a bidentate attachment to the pore, this success was short-lived. The bidentate attached state lasted for

approximately 30 s before a near total blockage occurred. Further attempts to modify subsequent pores with compound **23** all resulted in a system with a near total blockage. One hypothesis is that the large dynamic molecule eventually works itself into a position that blocks the channel. An alternative scenario is that the attachment of the motor and subsequent rotations may be destabilising the pore in the bilayer.

As higher salt concentrations are known to stabilise the bilayer, it was decided to attempt the attachment at a higher concentration. Attachment was achieved in a 3 M KCl buffer (**Figure 4.15A**). Interestingly, the profile of the attachment was very different to that observed in 1 M KCl. In the low salt concentration system, a shallow block to a high noise state was observed. However, in the higher salt system a large drop in current (I_b/I_o = 0.24) occurred through two intermediate steps. This new level appeared irreversible and gave a reproducible characterisation trace (**Appendix B, Figure B.2**). This new level was persistent for several 100s of seconds, and showed no variation in the current level. Upon irradiation with UV light (λ = 355 nm), there was no immediate change in the profile. After 100 s it was noted that intermittent upwards events were occurring (**Figure 4.15C**). When plotted as an all-points frequency histogram, these levels are well resolved from the baseline. However, these events appeared random in their temporal distribution and after a short period, ceased to occur.

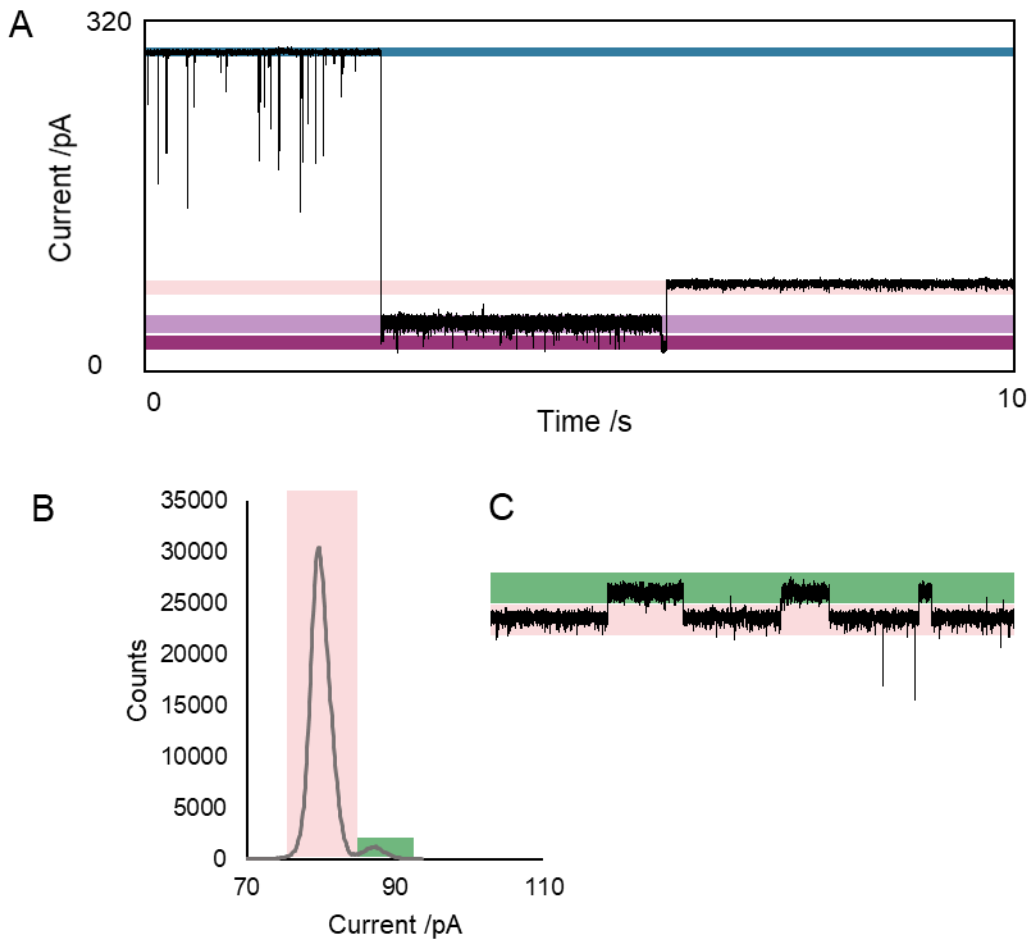

Figure 4.15: A) Attachment of compound **23**. From the free pore current (blue) a drop is observed to a low current level through an intermediate step (light purple to dark purple). This then progressed to the final level (pink), which represents the irreversible modification. Volume 600 µL. Buffer 3 M KCl, 30 mM K_2HPO_4, pH 8. Voltage +100 mV. Lowpass Bessel filter 100 kHz and output gain x50. B) All-points histogram for the levels upon irradiation with UV light (λ = 355 nm). The original state (pink) is the predominate level, but there is a well-defined upper level (green). C) Example trace for the upwards events observed. Lowpass Bessel filter (400 Hz) applied post acquisition.

As limited success was achieved with attaching the larger motor species, it was decided to attach a motor analogue with no bulky tail groups to the channel. Compound **24** (**Figure 4.16**) was provided by the Guiseppone group.

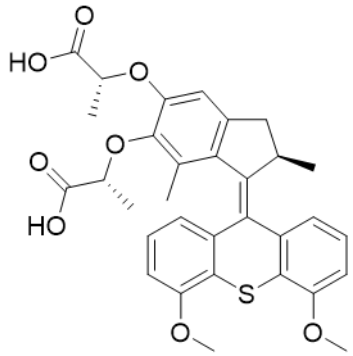

24

Figure 4.16: Structure of compound **24** provided by Nicolas Giuseppone.

Based on evidence of membrane perturbation caused by compounds **22** and **23**, there was a concern that compound **24** would also disrupt the membrane. To test this membrane stability studies were conducted. A solution compound **24** was added to the *cis* side of the bilayer in the absence of any nanopores under an applied potential of +100 mV. Initially, the system was placed in darkness (**Figure 4.17, orange**) and no initial membrane distress was observed. Upon irradiation with UV light (**Figure 4.17, purple**), there was no notable change in the output current. The UV light was then removed, and some membrane distress was observed which presented as short, sharp spikes. The membrane remained stable until it was manually destroyed by the application of a 2 V zap. This was done to ensure that the membrane was indeed genuine, as a membrane multilayer would not be destroyed by such a zap.

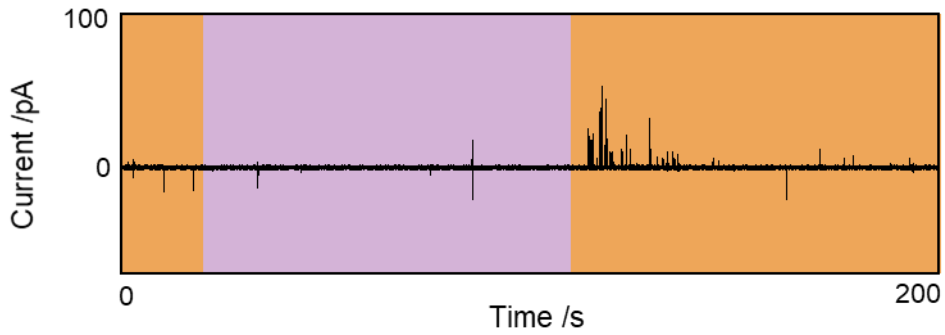

Figure 4.17: Membrane stability study with the compound **24** Solution of compound **24** (10 mM, 10 µL) in DMSO was added to the *cis* well. The system was either in the dark (orange) or irradiated (λ = 355 nm, purple). Some short-lived perturbations in current were observed, but the membrane appeared to be stable to the motor under both light conditions. Volume 600 µL. Buffer 1 M KCl, 30 mM K_2HPO_4, pH 8. Voltage +100 mV. Lowpass Bessel filter 100 kHz and output gain x50.

Once it was confirmed that the membrane was stable to the compound **24**, it could then be attached to the channel. A solution of activated compound **24** was added to the *cis* well under a positive applied potential. Numerous short-lived binding events were observed, but these were poorly resolved and seemingly random in distribution. Under an applied negative potential, far fewer events were observed, suggesting that the applied positive potential was drawing the molecule into the channel. However, despite these interactions with the channel, no modification was observed.

Unfortunately, no reproducible evidence of light mediated transmembrane molecular rotors was achieved. While there was success in attaching compounds **22** and **23** to a protein nanopore, these structures appeared to case significant membrane instability. Compound **24** appeared not to disrupt the membrane, but it was not possible to attach this to the pore. Future work may look to optimise the nanopore conditions in order to achieve a system with adequate membrane stability. However, due to the complex multistep synthesis and limited availability of compounds **22, 23** and **24**, this was not possible at present.

4.5 Molecular Pumps

Here, we seek to develop a transmembrane molecular pump based on Alberto Credi's (University of Bologna) pseudo-rotaxane system (**Figure 4.18**).[30] This system has been demonstrated to be capable of pumping an azobenzene axle (compound **25**) unidirectionally through a 2,3-dinaphtho[24]crown-8 ether macrocycle (**Figure 4.18**). At one end of the axle there is a simple toluene moiety, over which the macrocycle will thread most rapidly when the azobenzene axle is in the *E* conformation (**Figure 4.18A**). The macrocycle will then dock at the central ammonium recognition site. Finally, the axle ends in a methylcyclopentyl unit, which acts as a pseudo-stopper. While the axle is in the *E* conformation it is disfavoured for the macrocycle to pass over the pseudo-stopper. However, upon light-induced isomerisation of the axle to the *Z* conformation (**Figure 4.18B**), the supramolecular complex becomes destabilised, and it becomes kinetically favoured for the macrocycle to pass over the stopper (**Figure 4.18C**). Photochemical or thermal relaxation then returns the axle to the *E* conformation, allowing the cycle to repeat.

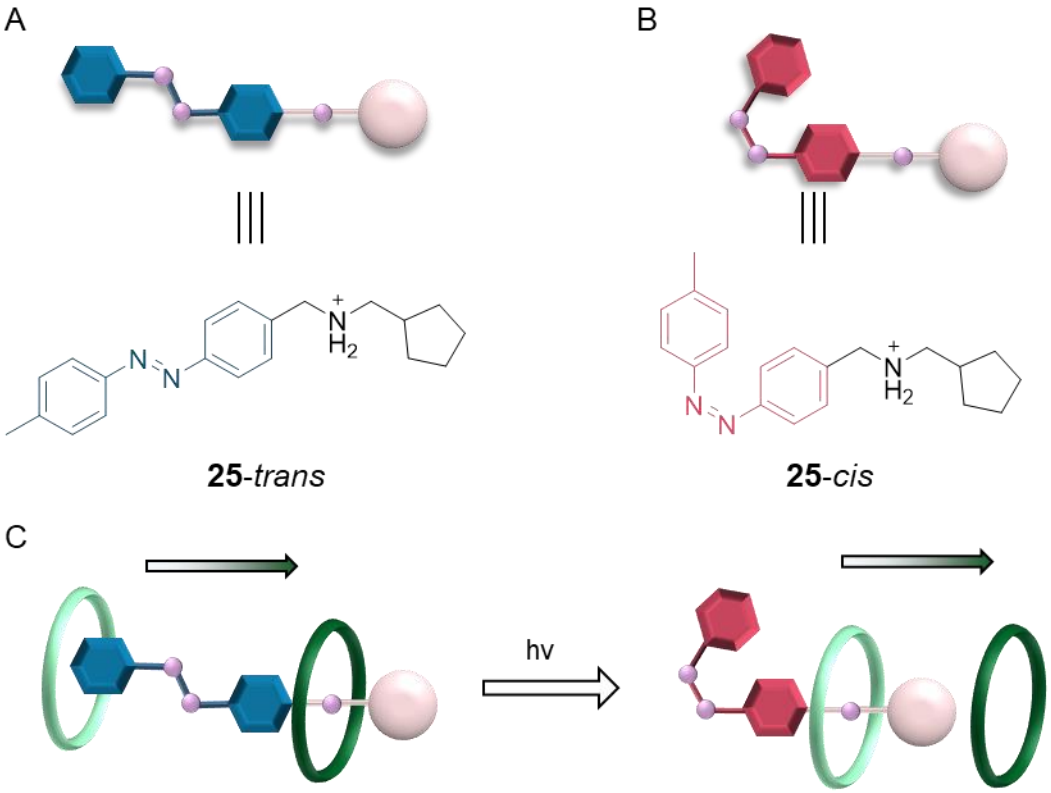

Figure 4.18: Structure of the molecular ratchet pump (compound **25**) by the Credi group. The macrocycle will thread onto the molecular axle most rapidly when it is in the *trans* conformation. Upon irradiation with light the axle undergoes *trans*/*cis* isomerisation and this conformational change makes passage of the macrocycle over the pseudo-rotaxane stopper most favoured, and hence drives unidirectional motion.

To date, this process has been demonstrated to occur free in solution, which presents a common problem with many machine-like systems as it is challenging to harness work from an untethered system at the molecular level. We endeavour to develop a system whereby the molecular ratchet could be associated with the α-HL protein channel and act as a transmembrane pump (**Figure 4.19**). In the bulk, this machine would give perpetual unidirectional motion provided there is a constant source of light. However, this work done is immediately lost as there is no partitioning of the pumped and non-pumped molecules. In the nanopore-based system, the partition of the membrane enables a concentration to be established. The machine would work against equilibrium and move analyte from one side of the membrane to another. Due

to the unidirectional motion, eventually all axle molecules would congregate on one side of the bilayer. The system might also be able to work against the applied potential.

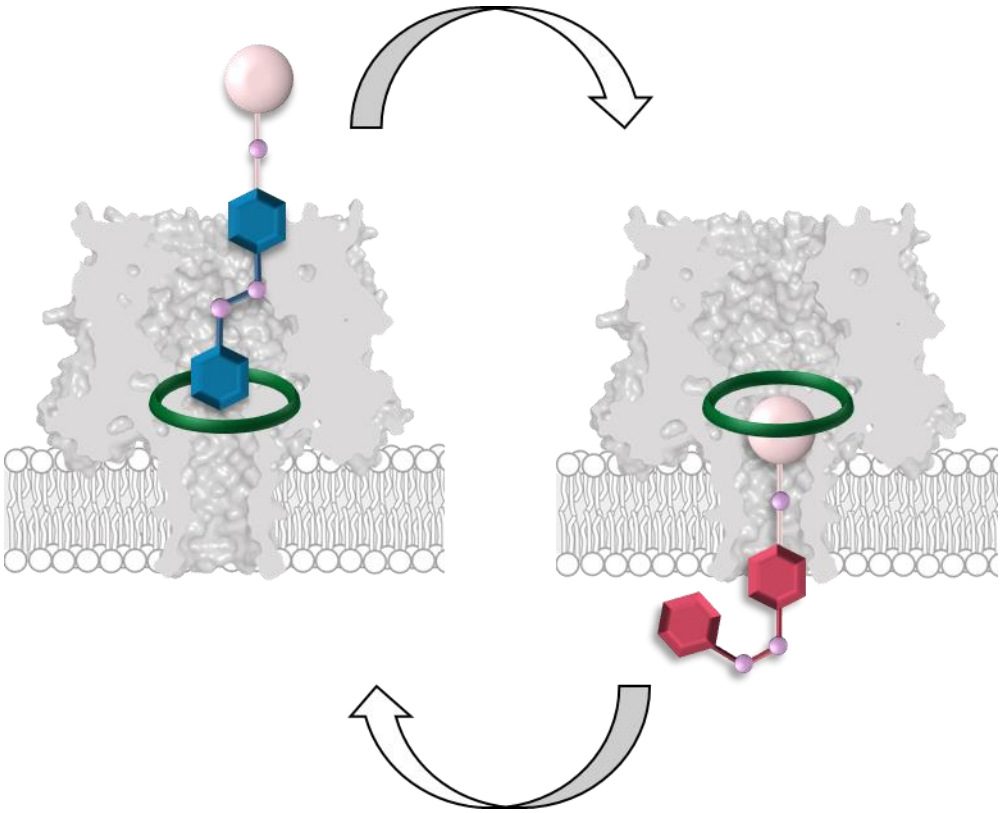

Figure 4.19: Cartoon representation of the molecular ratchet threading through the pore. While in a linear conformation, the ratchet will easily thread through the macrocycle, but the pseudo-rotaxane stopped inhibits it from passing all the way through. Upon irradiation, a conformational change of the axle drags the ratchet through the pore. This process can occur perpetually and in a unidirectional fashion to create a pump.

It has previously been shown that macrocycles such as crown ethers can stack in the membrane and perturb it.[31-32] Indeed, using a Feringa-style rotary motor in conjunction with a crown either, a transmembrane ion transporter has been developed.[33] Hence, prior to attempting nanopore experiments, a controls experiment was performed to check that the pump macrocycle, dibenzo-24-crown-8 would not perturb the membrane. Reassuringly, no channel forming events were observed when macrocycle was added against a membrane in the absence of a protein channel (**Figure 4.20A**).

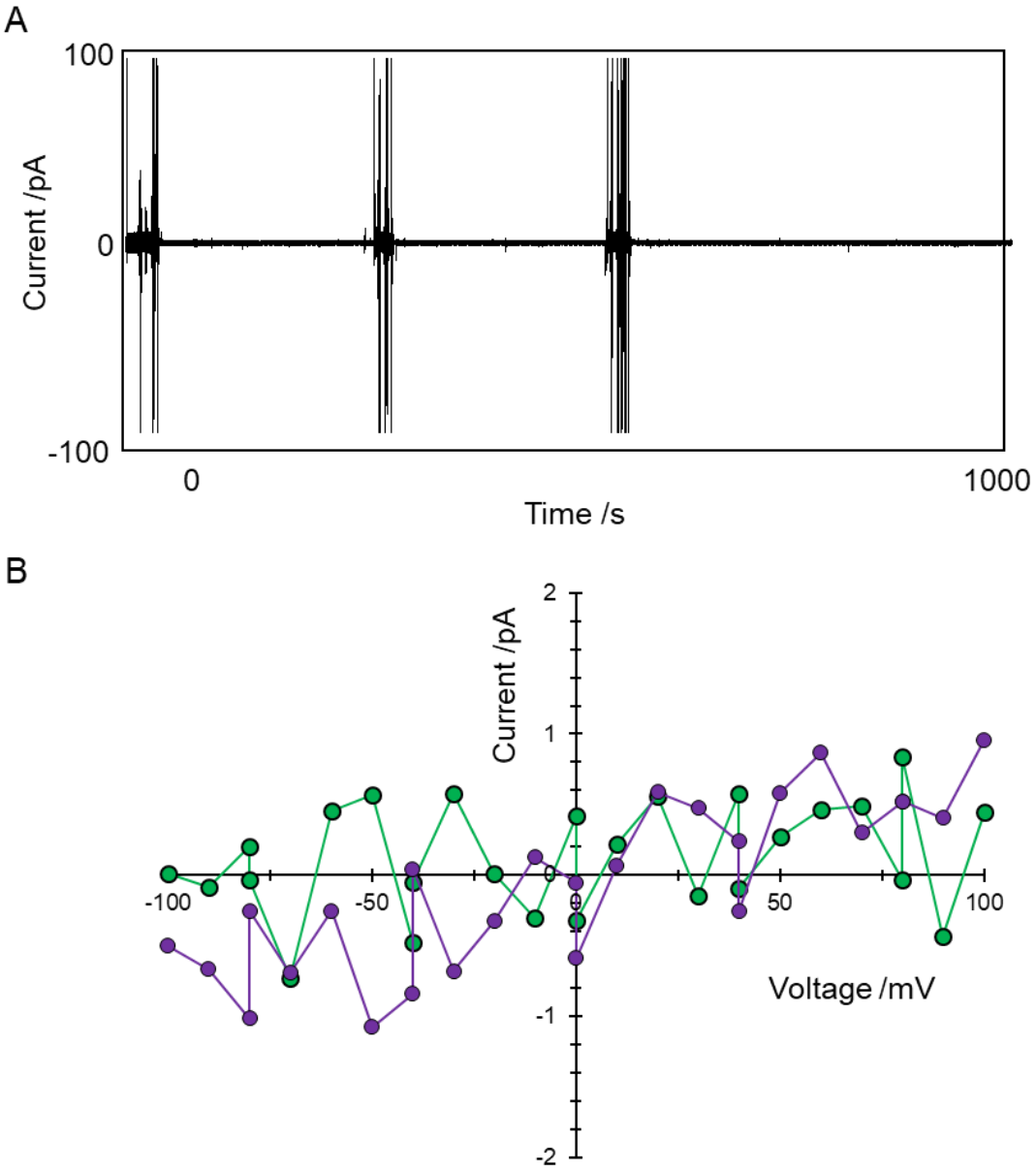

Figure 4.20: A) Dibenzo-24-crown-8 solution (10 mM, acetonitrile) was added to the *cis* well without a pore present. Three aliquots (10 µL of the 10 mM stock) were added over the course of 10 minutes. No channel forming properties were observed. Volume 600 µL. Buffer 1 M KCl, 30 mM K_2HPO_4, pH 8. Voltage +100 mV. Lowpass Bessel filter 100 kHz and output gain x50. B) The membrane was characterised by the application of incremental 10 mV steps between +100 and -100 mV. Characterisation trace for the membrane prior to addition (green) and post addition of the macrocycle (purple) show limited variation.

Studies of the interaction of the macrocycle with an α-HL channel were then commenced. Dibenzo-24-crown-8 was introduced into the pore under an applied potential of +100 mV without mixing (**Figure 4.21B**). Initially, no events were observed (**Chapter 5, Section 5.6, Figure 5.23**), but frequent short-lived and shallow events were observed after the addition of a second aliquot (10 µL, 10 mM, DMSO) with mixing (**Figure 4.21A**). These events were analysed using threshold detection and plotted as a level frequency histogram of the I_b/I_o, which revealed that the events did not follow a normal distribution (**Figure 4.21C**). Large numbers of these short-lived events were observed under a positive applied potential (**Figure 4.21A, teal**), but none were seen at negative potentials (**Figure 4.21A, pink**). Similarly, when the macrocycle was applied to the opposite (*trans*) well and a positive potential was applied, no events were observed (**Chapter 5, Section 5.6, Figure 5.24**).

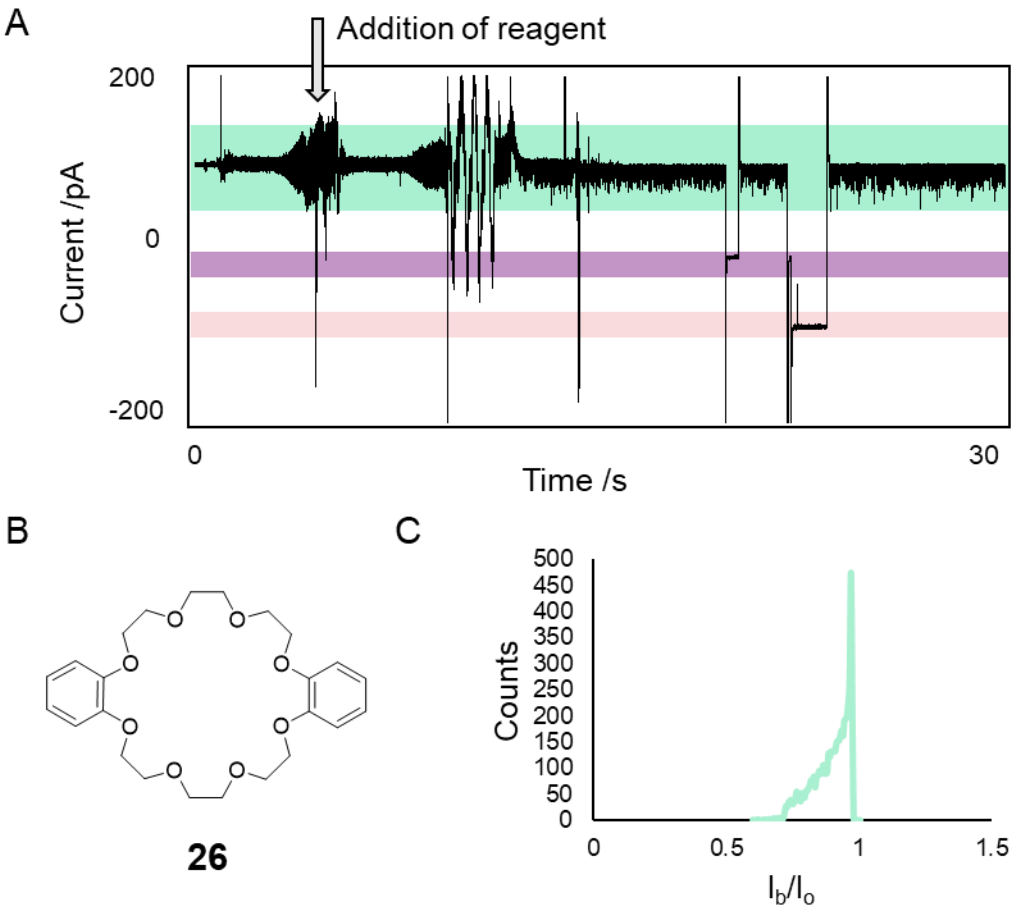

26

Figure 4.21: A) Example trace for the addition of dibenzo-24-crown-8 (compound **26**) (20 µL, 10 mM, DMSO) to the *cis* well of an α-HL nanopore with mixing. Immediately, a large number of short-lived events were observed under a positive applied potential (green). No membrane noise was observed when 0 V was applied (purple). No events were observed when -100 mV was applied (pink). Buffer 1 M KCl, 30 mM K_2HPO_4, pH 8. Voltage +100 mV. Lowpass Bessel filter 300 kHz applied. B) Structure of dibenzo-24crown-8. C) All points histogram for the levels observed under an applied positive potential. No discrete levels are observed, suggesting that the binding events are random.

The data in **Figure 4.21** indicate that the macrocycle events were short lived and likely involved transit through the pore. Hence, to assess whether the macrocycle could be threaded with an axle in the pore, and potentially captured, a biotin/streptavidin stoppered DNA thread was selected. It is well established that ssDNA is narrow enough to pass through the pore, whereas the biotin/streptavidin stopper is much too large to even enter the pore. In addition, the negatively charged DNA will be driven electrophoretically into the pore. Indeed, similar models have been used within the Cockroft group in the design of a molecular ratchet. Dibenzo-24-crown-8 (10 µL of 10 mM stock, DMSO) was added to the *cis* well. A biotinylated PEG-DNA strand (10 µL of 10 mM stock) (**Figure 4.22A**) was incubated with excess streptavidin at 37 °C for 30 minutes. This was then added to the *trans* well of the channel. A voltage of +100 mV was applied and shortly thereafter, a blockage event occurred that was consistent with the capture of the streptavidin-capped DNA strand within the pore. This event progressed through a short-lived ms-scale intermediate level (**Figure 4.21B, pink**, I_b/I_o = 0.08) before setting to a stable final level (**Figure 4.21B, purple**, I_b/I_o = 0.41). Upon the inversion of the potential, the current returned to the free pore current, which was consistent with the electrophoretic ejection of DNA from the pore (**Figure 4.21B,** teal).

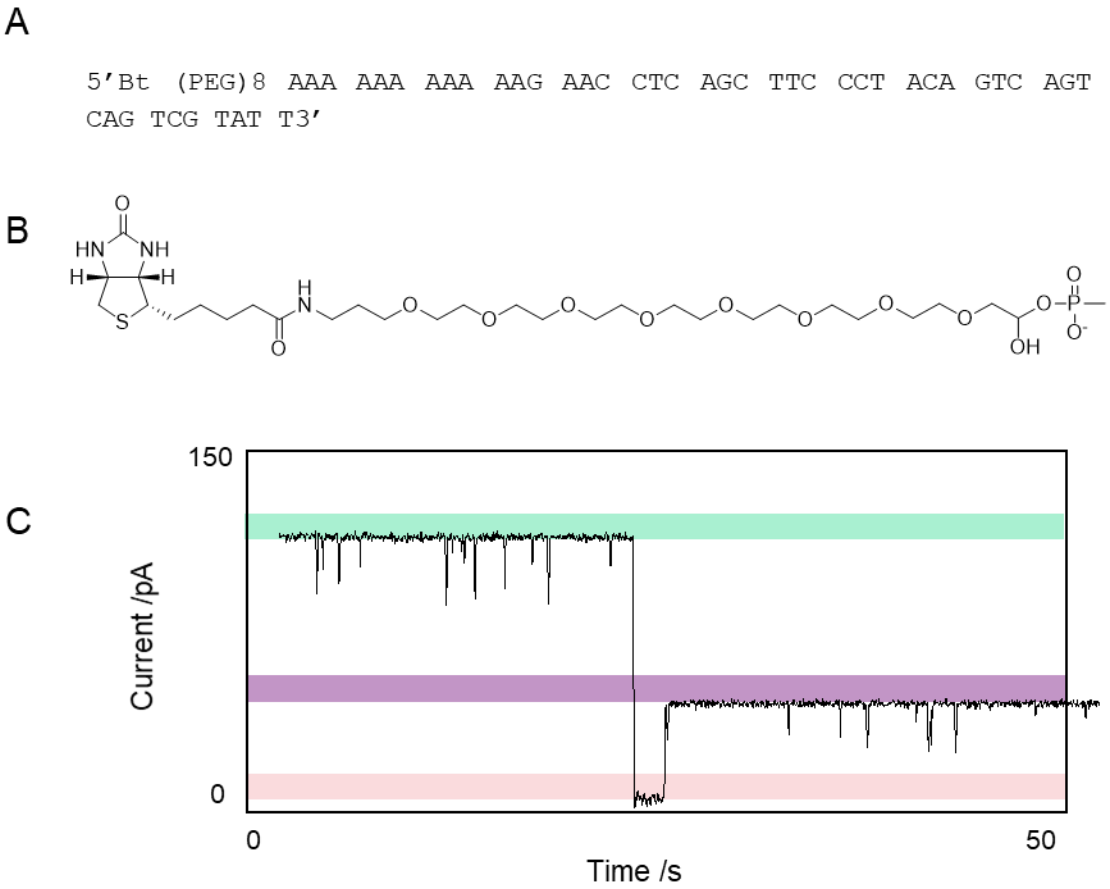

Figure 4.22: A) DNA sequence for the thread. Structure of the biotin head group (Bt) and the PEG linker are shown in the upper panel. The biotin will complex with added streptavidin to form a large stopper that enables capture, but prevents the thread from passing through the pore. B) Example current trace for a threading event. From the free pore current (green), the current passes through a near total blockage state (pink) before settling to a trapper state. The system was under an applied potential of +100 mV. No modification was observed. Buffer 1 M KCl, 30 mM K_2HPO_4, pH 8. Lowpass Bessel filter 300 kHz applied.

However, a further control experiment in which the biotinylated PEG-DNA was captured in the pore in the absence of dibenzo-24-crown-8 gave identical current levels to the prior experiment (**Chapter 5, Section 5.6, Figure 5.25**). This indicated that the PEG-DNA was entering the pore, but it was not threading through the macrocycle. The experiments shown in **Figures 4.21** and **4.22** suggest that the macrocycle was too flexible to become captured in the pore. Therefore, it was decided to covalently bind the macrocycle to the pore.

A carboxylic acid functionalised macrocycle (compound **33**) was designed to enable attachment to the α-HL nanopore via lysine functionalisation (**Figure 4.23** and **Chapter 3**). While a doubly functionalised version may provide better attachment, it would have required careful optimisation of the size of the macrocycle to ensure sufficient reach between the two anchoring lysine residues.

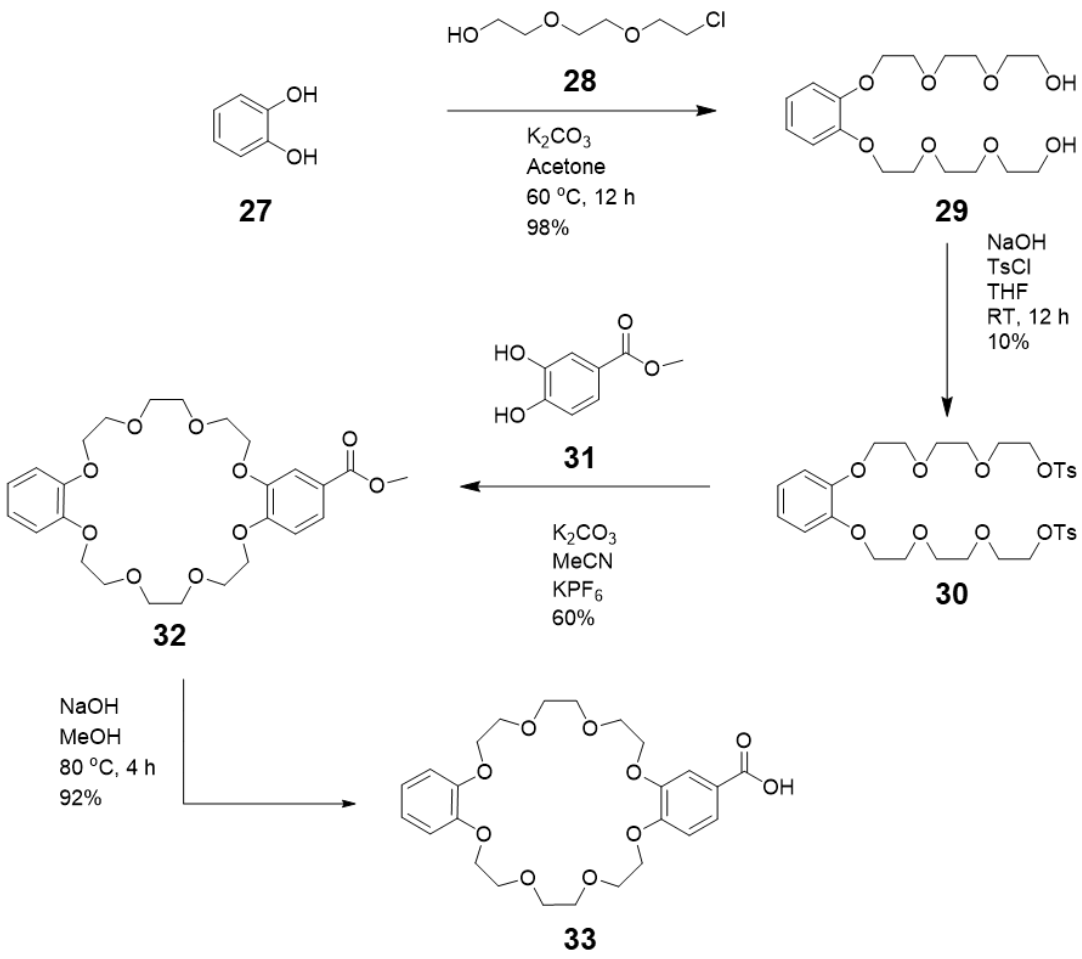

Figure 4.23: Overall synthetic scheme for the synthesis of the tethered macrocycle (compound **33**).

Catechol was PEGylated in high yield, before activating tosyl groups were attached. Using potassium as template, the macrocycle was closed with the protected methyl ester before hydrolysing to give the desired carboxylic acid functionalised crown ether (full details in **Chapter 5**).

Using the previously established EDC-coupling protocol, compound **33** was attached to the pore (**Figure 4.24A**). Modification was seen to process through a two-step process (**Figure 4.24B**). The modified channel was characterised by applying an incremental voltage (**Figure 4.24C**). Here, a rather interesting effect was observed. At the more positive and less negative applied potentials, there was a blockage in the current. However, at the less positive and more negative potentials, the channel does not display any blockage characteristics. This suggests that a strongly positively or weakly negative applied potential are required to hold compound **33** in place. Most likely, this is due to the monodentate nature of the attachment in combination with the size of the molecule. Coupled, this necessitates the applied potential to hold the macrocycle in place.

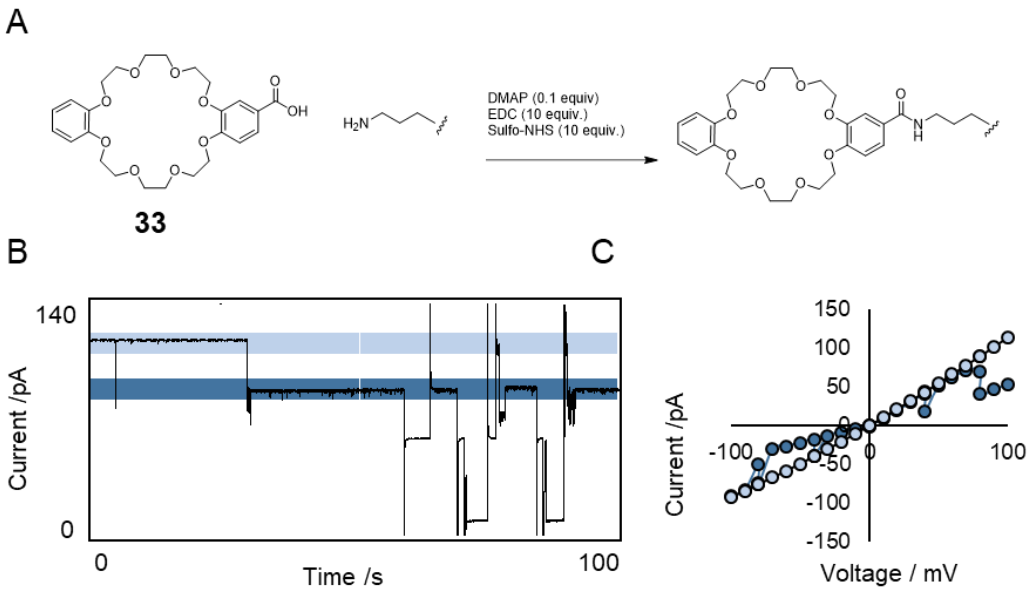

Figure 4.24: A) Scheme of the attachment of compound **33** to the lysine residue of the pore. B) Example trace for the attachment of compound **33** to α-HL. A solution of compound **33** (10 mM) was prepared and mixed with a solution of EDC (100 mM), DMAP (0.1 mM) and sulfo-NHS (100 mM) 1:1 v/v. This was reacted at room temperature for 20 minutes prior to addition. The activated acid (10 µL) was added to the cis well. The attachment passed through a brief intermediate stage before settling at a permanently modified level. No modification was observed. Buffer 1 M KCl, 30 mM K_2HPO_4, pH 8. Voltage +100 mV. Lowpass Bessel filter 300 kHz applied. C) Characterisation trace for the DBC modified channel.

Once modification was achieved, the molecular axle (**Figure 4.25A**) was introduced. Prior to the addition, a consistent current was observed for the modified pore (**Figure 4.25B, purple**). The solution was added to the *cis* well with mixing under an applied positive potential. Immediately, a shift in the current was observed (**Figure 4.25, dark green**). Upon irradiation at 355 nm a small but notable drop in current occurred (**Figure 4.25, orange**). When the source of irradiation was removed, the current then returned towards the original level (**Figure 4.25, teal**). This can be visualised as an all points histogram of the current levels (**Figure 4.25C**). Unfortunately, multiple additional pores inserted into the bilayer before further cycles could be completed, rending the system unusable. The data suggests that the axle is binding and unbinding from the macrocycle (in both the *E* and the *Z* forms) on a sub-millisecond timescale. The ability to resolve the differences in the dynamics in the absence and presence of 355 nm light is remarkable and very promising.

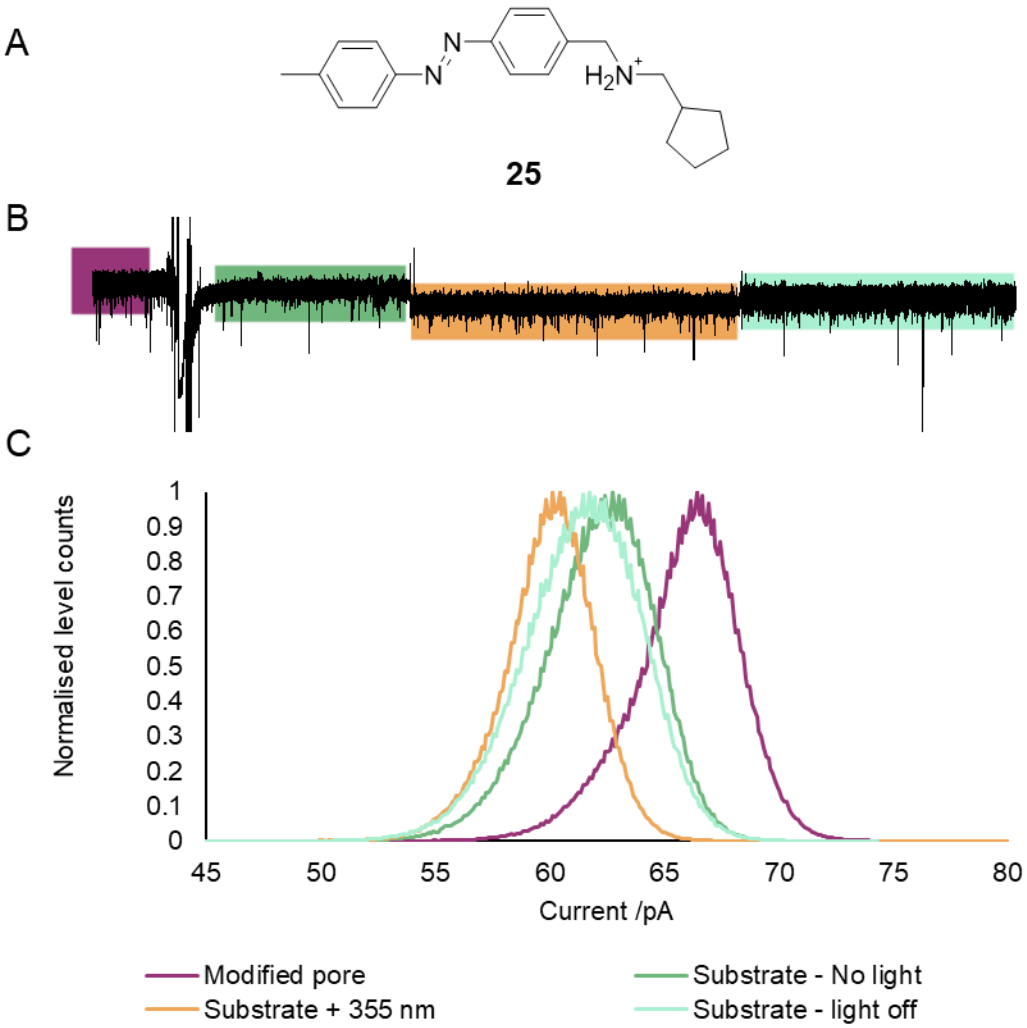

Figure 4.25: A structure of the molecular axle. B) Example trace showing the change in current level upon the addition of the axle to a channel modified with compound **33**. The modified current (purple) dropped to a new level upon the addition of the molecular axel (dark green). Upon irradiation with light (λ = 355 nm, orange) and removal of light (teal) a shift in current was also noted. C) All-points histogram showing the normalised counts and current level for each condition.

Unfortunately, at this stage in the project, the stock of carboxylic acid modified macrocycle ran out. Meanwhile research focus at this time was directed towards completion of the CB[7]-catalysis project (**Chapter 2**). Nonetheless, the work lays promising groundwork for the future development of a transmembrane pump.

4.6 Conclusions and future work

Biological molecular machines are sophisticated systems upon which all life relies. Huge advances have been made in the field of artificial molecular machines, yet the elegance of biology has yet to be emulated. A major goal in the field of artificial molecular machines is the ability to harness the work produced. Here, we have explored preliminary approaches to assemble membrane-bound molecular machines using a transmembrane protein nanopore as a scaffold.

Initial attempts explored the application of a nanopore as a scaffold for a transmembrane valve. Using simple acyl hydrazones available within the Cockroft group, attachment was achieved. However, these systems did not yield the robust trapped states that were hoped for. Instead, behaviour more akin to that seen previously for azobenzenes was observed, with the switch seemingly moving independently between two quantised states. When moving to a more stabilised acyl hydrazone, these switches appeared to perturb the bilayer and bring about rapid membrane degradation. Unfortunately, no finite evidence was found of a fully photo-controlled transmembrane switch. However, it has been demonstrated that photo-switchable moieties can be covalently bound to a protein nanopore. Future work may look to the development of more stable systems where photoswitching could be achieved at the single-molecule level.

Significant early work was conducted on the construction of a transmembrane motor. These motors were based on a Feringa-style rotary motor. It was shown that motor analogue could be successfully bound to a protein nanopore using EDC-coupling chemistry. However, attempts to attach larger motor species to the channel were unsuccessful due to the induced membrane instability. Successful modification was achieved using a functionalised motor molecule, but no photo-isomerisation was observed.

Progress has been made towards the development of a transmembrane pump. Using a system adapted from Prof. Alberto Credi, a dibenzo-24-crown-8 derivative was synthesised with a tethering carboxylic acid side group. This was successfully attached to the interior of an α-HL channel. Upon addition of a molecular axle and irradiation with UV light, a clear shift in the current was observed. This presents the exciting potential for the future development of a transmembrane pump. Future work would look to introduce other axles to the system to fully characterise the behaviour of the pump.

4.7 References

1. Stoddart, J. F., Molecular Machines. *Acc. Chem. Res.* **2001,** *34* (6), 410-411.

2. Leigh, D. A., Genesis of the Nanomachines: The 2016 Nobel Prize in Chemistry. *Angew. Chem. Int. Ed.* **2016,** *55* (47), 14506-14508.

3. Krause, S.; Feringa, B. L., Towards artificial molecular factories from framework-embedded molecular machines. *Nat. Rev. Chem.* **2020,** *4* (10), 550-562.

4. Goswami, A.; Saha, S.; Biswas, P. K.; Schmittel, M., (Nano)mechanical Motion Triggered by Metal Coordination: from Functional Devices to Networked Multicomponent Catalytic Machinery. *Chem. Rev.* **2020,** *120* (1), 125-199.

5. Berná, J.; Leigh, D. A.; Lubomska, M.; Mendoza, S. M.; Pérez, E. M.; Rudolf, P.; Teobaldi, G.; Zerbetto, F., Macroscopic transport by synthetic molecular machines. *Nat. Mater* **2005,** *4* (9), 704-710.

6. Moulin, E.; Faour, L.; Carmona-Vargas, C. C.; Giuseppone, N., From Molecular Machines to Stimuli-Responsive Materials. *Adv. Mater.* **2020,** *32* (20), 1906036.

7. Asakawa, M.; Higuchi, M.; Mattersteig, G.; Nakamura, T.; Pease, A. R.; Raymo, F. M.; Shimizu, T.; Stoddart, J. F., Current/Voltage Characteristics of Monolayers of Redox-Switchable [2]Catenanes on Gold. *Adv. Mater.* **2000,** *12* (15), 1099-1102.

8. Watson, M. A.; Cockroft, S. L., An Autonomously Reciprocating Transmembrane Nanoactuator. *Angew. Chem. Int. Ed.* **2016,** *55* (4), 1345-1349.

9. Chen, S.; Wang, Y.; Nie, T.; Bao, C.; Wang, C.; Xu, T.; Lin, Q.; Qu, D.-H.; Gong, X.; Yang, Y.; Zhu, L.; Tian, H., An Artificial Molecular Shuttle Operates in Lipid Bilayers for Ion Transport. *J. Am. Chem. Soc.* **2018,** *140* (51), 17992-17998.

10. Pulcu, G. S.; Mikhailova, E.; Choi, L.-S.; Bayley, H., Continuous observation of the stochastic motion of an individual small-molecule walker. *Nat. Nanotechnol* **2015,** *10* (1), 76-83.

11. Balzani, V.; Credi, A.; Venturi, M., Light powered molecular machines. *Chem. Soc. Rev.* **2009,** *38* (6), 1542-1550.

12. Boyer, P. D., The ATP synthase--a splendid molecular machine. *Annu Rev Biochem* **1997,** *66*, 717-49.

13. Watson, M. A.; Cockroft, S. L., Man-made molecular machines: membrane bound. *Chem. Soc. Rev.* **2016,** *45* (22), 6118-6129.

14. Loudwig, S.; Bayley, H., Photoisomerization of an Individual Azobenzene Molecule in Water: An On−Off Switch Triggered by Light at a Fixed Wavelength. *J. Am. Chem. Soc.* **2006,** *128* (38), 12404-12405.

15. Koçer, A.; Walko, M.; Meijberg, W.; Feringa, B. L., A Light-Actuated Nanovalve Derived from a Channel Protein. *Science* **2005,** *309* (5735), 755-758.

16. Aprahamian, I., Hydrazone switches and things in between. *Chem. Commun.* **2017,** *53* (50), 6674-6684.

17. Rapenne, G.; Joachim, C., The first nanocar race. *Nat. Rev. Mater.* **2017,** *2*, 17040.

18. Badjić, J. D.; Balzani, V.; Credi, A.; Silvi, S.; Stoddart, J. F., A Molecular Elevator. *Science* **2004,** *303* (5665), 1845.

19. Balzani, V.; Credi, A.; Raymo, F. M.; Stoddart, J. F., Artificial Molecular Machines. *Angew. Chem. Int. Ed.* **2000,** *39* (19), 3348-3391.

20. Erbas-Cakmak, S.; Leigh, D. A.; McTernan, C. T.; Nussbaumer, A. L., Artificial Molecular Machines. *Chem. Rev.* **2015,** *115* (18), 10081-10206.

21. Bandara, H. M. D.; Burdette, S. C., Photoisomerization in different classes of azobenzene. *Chem. Soc. Rev.* **2012,** *41* (5), 1809-1825.

22. van Dijken, D. J.; Kovaříček, P.; Ihrig, S. P.; Hecht, S., Acylhydrazones as Widely Tunable Photoswitches. *J. Am. Chem. Soc.* **2015,** *137* (47), 14982-14991.

23. Tatum, L. A.; Su, X.; Aprahamian, I., Simple Hydrazone Building Blocks for Complicated Functional Materials. *Acc. Chem. Res.* **2014,** *47* (7), 2141-2149.

24. Kassem, S.; van Leeuwen, T.; Lubbe, A. S.; Wilson, M. R.; Feringa, B. L.; Leigh, D. A., Artificial molecular motors. *Chem. Soc. Rev.* **2017,** *46* (9), 2592-2621.

25. Koumura, N.; Geertsema, E. M.; van Gelder, M. B.; Meetsma, A.; Feringa, B. L., Second Generation Light-Driven Molecular Motors. Unidirectional Rotation Controlled by a Single Stereogenic Center with Near-Perfect Photoequilibria and Acceleration of the Speed of Rotation by Structural Modification. *J. Am. Chem. Soc.* **2002,** *124* (18), 5037-5051.

26. Feringa, B. L., The Art of Building Small: From Molecular Switches to Molecular Motors. *J. Org. Chem.* **2007,** *72* (18), 6635-6652.

27. Corbet, B. P.; Lubbe, A. S.; Crespi, S.; Feringa, B. L., Chiroptical Molecular Switches and Motors. *Molecular Photoswitches: Chemistry, Properties and Applications*, 2022; pp 213-251.

28. Foy, J. T.; Li, Q.; Goujon, A.; Colard-Itté, J.-R.; Fuks, G.; Moulin, E.; Schiffmann, O.; Dattler, D.; Funeriu, D. P.; Giuseppone, N., Dual-light control of nanomachines that integrate motor and modulator subunits. *Nat. Nanotechnol* **2017,** *12* (6), 540-545.

29. Piret, J.; Lamontagne, J.; Bestman-Smith, J.; Roy, S.; Gourde, P.; Désormeaux, A.; Omar, R. F.; Juhász, J.; Bergeron, M. G., In vitro and in vivo evaluations of sodium lauryl sulfate and dextran sulfate as microbicides against herpes simplex and human immunodeficiency viruses. *J. Clin. Microbiol.* **2000,** *38* (1), 110-9.

30. Ragazzon, G.; Baroncini, M.; Silvi, S.; Venturi, M.; Credi, A., Light-powered, artificial molecular pumps: a minimalistic approach. *Beilstein J. Nanotechnol.* **2015,** *6*, 2096-2104.

31. Sun, Z.; Barboiu, M.; Legrand, Y.-M.; Petit, E.; Rotaru, A., Highly Selective Artificial Cholesteryl Crown Ether K+-Channels. *Angew. Chem. Int. Ed.* **2015,** *54* (48), 14473-14477.

32. Liu, Z.; Zhang, H.; Han, J., Crown ether–pillararene hybrid macrocyclic systems. *Org. Biomol. Chem.* **2021,** *19* (15), 3287-3302.

33. Yang, H.; Yi, J.; Pang, S.; Ye, K.; Ye, Z.; Duan, Q.; Yan, Z.; Lian, C.; Yang, Y.; Zhu, L.; Qu, D.-H.; Bao, C., A Light-Driven Molecular Machine Controls K+ Channel Transport and Induces Cancer Cell Apoptosis. *Angew. Chem. Int. Ed.* **2022,** *61* (26), e202204605.

Chapter 5

Experimental

5.1 General Nanopore Set-Up

All nanopore experiments were carried out at room temperature and pressure. Due to unpredictable Scottish weather and ageing building infrastructure, temperatures ranged from 14 °C to 32 °C. Experiments were not conducted at temperatures below 16 °C due to reagents freezing or above 29 °C due to risk of apparatus overheating. Experiments were conducted in buffered solution, as specified in the experimental. Molecular biology grade water (Fisher) was used for all buffer.

Measurements were taken using an Axopatch 200B patch clamp, digitised on a Digidata 1322. The high sensitivity of the equipment made measurements liable to vibrational and electrical interference. Electrical interference was minimised by isolating experiments inside a Faraday cage (Studiospare/Halcyonics) and grounding any additional electrical sources. Vibrational noise reduction was achieved using an anti-vibration platform (Halcyonics) or precision application of a pressure-sensitive adhesive (Blu Tack). Unless otherwise stated, all single-channel nanopore current traces were recorded with a sampling frequency of 10 kHz and using a 2 kHz lowpass Bessel filter. Unless otherwise stated, all measurements were made at a 50 kHz continuous recording protocol. Measurement and analysis was conducted using ClampFit 10.4, ClampEx 10.4, and Microsoft Excel.

Ag/AgCl Electordes for Nanopore Electrophysiology

Ag/AgCl pellet electrodes (pellet: 1.0 × 2.5 mm; wire: 0.25 × 75 mm) were purchased from Warner. The wire was bent to the appropriate length and soldered in place to a gold-plated plug or receptacle connector pin (Farnell). To prolong electrode lifespan and reduce experimental noise, the AgCl surface was replenished after approximately 50 hours of use. This was achieved by electrolysis in a 3 M KCl solution. A potential difference of 10 V was applied for approximately 1 minute using a gel electrophoresis power supply. The electrode being replenished acted as the positive electrode and a platinum wire was used in place of the negative electrode. Electrodes were replaced when they broke, or the residual noise made them unusable. It should be noted that electrodes used in higher salt concentration buffers require more frequent recoating and are more inclined to break.

Formation of Aperture

A single aperture was formed into a Teflon sheet (25 µm, Goodfellow). Teflon was purchased as a 10 × 10 cm sheet, which was cut into 2.5 × 2.5 cm squares. A spark generator (Ealing Spark Source) was arranged such that there was a 2 mm gap between the two electrodes. This was isolated inside a faraday cage and grounded to a nearby pipe. The operator removed any accessories (rings, watches, etc.) to which the spark may jump. A single cut square of Teflon was placed onto the platform of the spark generator, so that it was equidistant between the two electrodes. Between 15 and 25 discharges were performed at a potential difference of 35 kV at 0.5 Hz, until a single aperture was formed. Care must be taken to observe that the spark is passing through the newly formed aperture and not passing around the Teflon sheet. An audible difference could be heard in the spark when the aperture had formed. The size, shape, and location of the aperture was assessed using microscope analysis.

Any sheets with multiple aperture or a single damaged aperture were discarded.

Cell Design and Construct

A custom cell was crafted for conducting nanopore experiments (**Figure 5.1**). The cell consists of two mirror image Teflon blocks. Each block has a well bored into it, with a perpendicular channel connecting the two wells. Each well has two mitred channels at a 45° to allow for ease of access to the buffered well during experimentation.

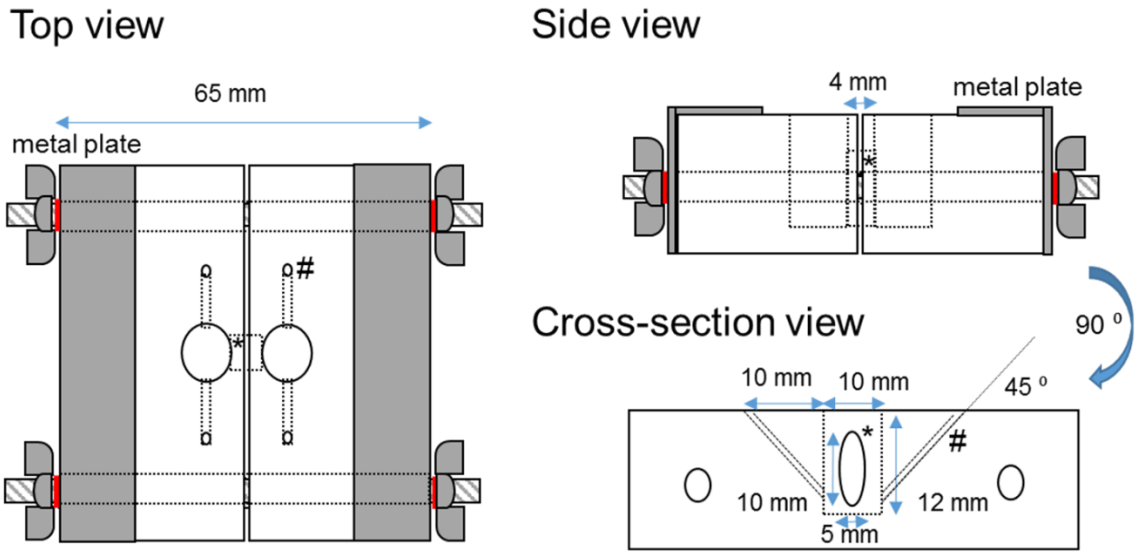

Figure 5.1: Diagram of custom cell of nanopore experiments. The cell was formed from a solid block of Teflon and holes were bored as specified in the cross-section view. The blocks were held together using metal brackets. A tight seal was ensured by using silicon glue.

A thin sheet of Teflon, with a single aperture, was used to separate the two wells of the Teflon block. The Teflon sheet was affixed between the two blocks using a silicone glue (3140 RTV coating, Dow Corning) such that the aperture was positioned at the bottom centre of the partition between the two wells. The two blocks were then firmly secured using two parallel bolts. The cells were left for 12 hours to allow the glue to fully dry before conducting any experiments.

Preparation of Hexadecane

Hexadecane (Sigma-Aldrich) was stored at room temperature. For use in single molecule studies, 50 µL of hexadecane was dissolved in n-pentane (450 µL) to give a 10% solution. Solution was made fresh at the beginning of each week. During the warmer months, when the lab temperature exceeded 25 °C, the solution was made daily. During the winter months, when lab temperatures were below 16 °C, hexadecane was thawed and held at a useable temperature in a tepid water bath.

Preparation of α-HL

α-Hemolysin (α-HL) was purchased from Sigma Aldrich UK as a lyophilized powder with approx. 60% protein content. The protein powder was stored at 8 ^{o}C until it was reconstituted. Care must be taken when opening the vial as the powder is very fine and will aerosolise if the vial is opened too quickly.

The α-HL (0.5 mg) was reconstituted in molecular biology grade water (1.6 mL) to give an approx. concentration of 0.02% w/v. This was divided into 5 µL aliquots; a small batch of these aliquots were stored at −20 °C for day-to-day use and the rest was stored at −80 °C until required. For use in experiments, one 5 µL pellet (0.02%) was diluted with molecular biology grade water (45 µL). This was split into 10 x 5 µL aliquots (0.002%), which are frozen as ice pellets at -20 ^{o}C. Immediately prior to an experiment, one pellets is again diluted in molecular biology grade water (45 µL) to give a final concentration of 0.0002% w/v. This sample could then be used for pore formation. Any excess of the 0.0002% sample was discarded at the end of the experiment.

Preparation of Lipid

Lipid (1,2-diphytanoyl-sn-glycero-3-phosphocholine) was purchased from Avanti Polar Lipids. Lipid was stored at -20 ^{o}C in 5-10 mg solid aliquots. At the

beginning of each week, or as required, one pellet of lipid was reconstituted in n-pentane to a concentration of 10 µg μL^{-1}. This solution was divided into 50 µL aliquots, and the pentane evaporated at room temperature. Each aliquot was again stored at -20 ^{o}C until required for used.

5.2 Formation of a Single Channel

Lipid Bilayer Formation

To form the lipid bilayer in the aperture, a single hanging drop of hexadecane (4 µL, 10% v/v in *n*-pentane) was added to either side of the Teflon sheet. The cell was left for approx. 1 minute to allow the pentane to evaporate. The hexadecane acted as a support for the lipid and facilitated the formation of the bilayer (**Figure 5.2**).

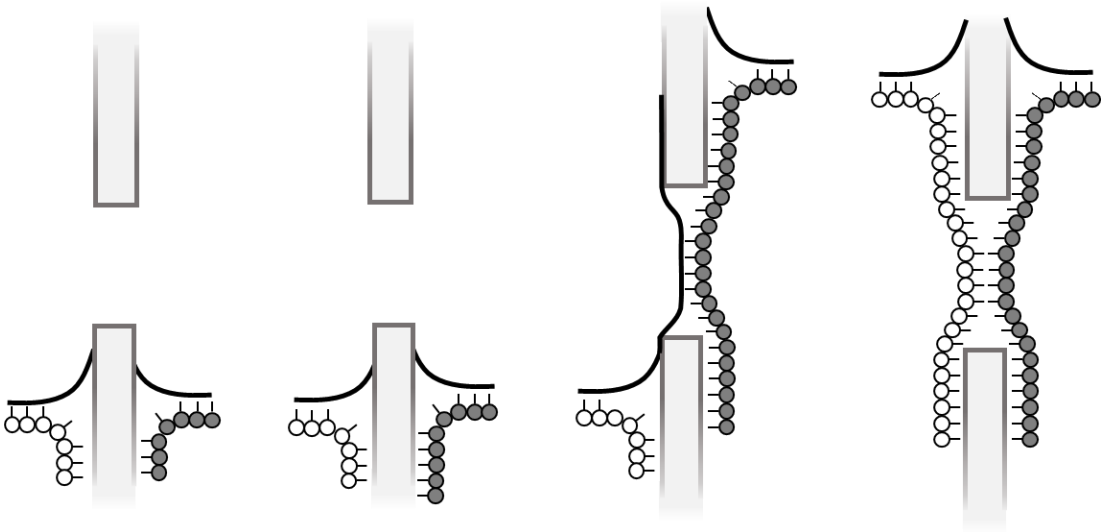

Figure 5.2: Representation of the formation of a lipid bilayer across an aperture. Hexadecane is applied to both sides of the Teflon sheet and acts as a scaffold for the bilayer to form. A thin layer of will persist in the hydrophobic region of the bilayer. If excess hexadecane is applied, then this layer will inhibit the capacitance characteristics of the bilayer.

A buffered solution (600 µL) was added to both wells. Unless otherwise stated, a standard buffer of 1 M KCl, 30 mM KPi, pH 8 was used. Various buffered

solutions were using for different experiments; however, the same buffer was always added to each well. Attempts to use asymmetric buffers saw highly unstable membranes. To both wells, approximately 8 µL of 10 µg/µL solution of 1,2-diphytanoyl-*sn*-glycero-3-phosphocholine in *n*-pentane was added as a hanging drop to the surface of the buffer. Again, approx. 1 minute was allowed for the pentane to evaporate. The cell was placed into a Faraday cage in order to reduced electrical noise. (**Figure 5.3**)

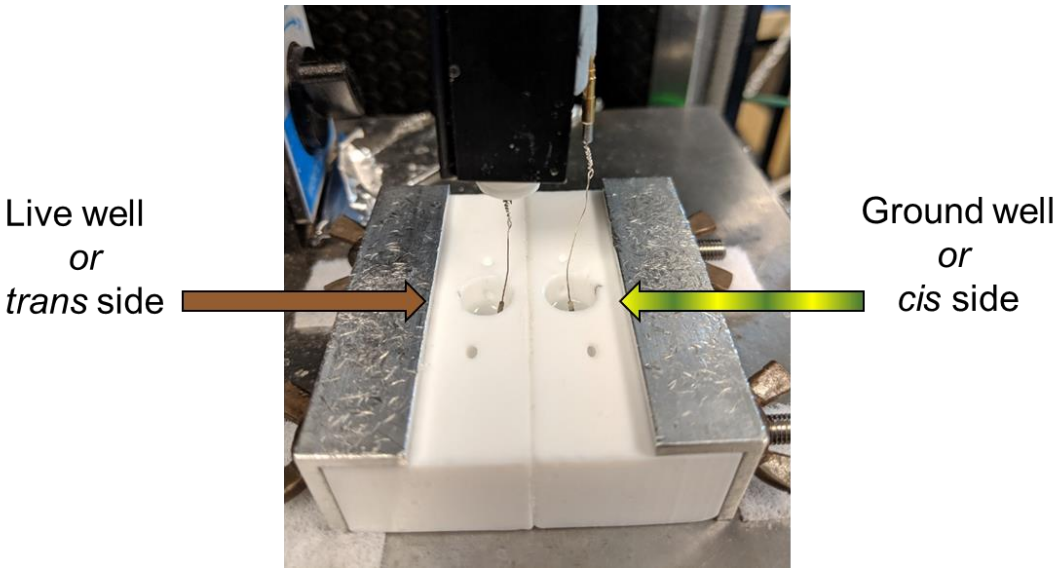

Figure 5.3: Teflon cell used for nanopore studies. The cell is symmetrical and can be used in either orientation. Each well is filled with 600 µL of a buffer. The electrodes are submerged below the surface of the buffer, ensuring that the do not make contact with the Teflon. The right hand well houses the ground electrode and the left hand well the live electrode. Protein is always added to the ground well, but reagents can be added to either well. The cell is isolated in a faraday cage.

The operator was grounded to the Faraday cage in an attempt to reduce static interference and subsequent electric shocks. Ag/AgCl electrodes (Warner) were placed into each well of the cell. These were connected to a patch clamp amplifier (Axopatch 200B, Molecular Devices). Using a Hamilton micro syringe the live well was first aspirated by drawing the buffer out of the will and then returning it in one single smooth action. This was then repeated with the ground well in order to paint the lipid across the aperture and form the membrane. Additional lipid was added in 2 µL increments if a stable membrane

could not initially be formed. A ±1 mV pulse applied at 1333 Hz to determine when a bilayer was obtained (capacitance >40 pF, resistance 1.6 GΩ). Once a stable membrane was formed, a single protein channel could then be inserted into the membrane.

The formed lipid bilayer was characterised by measuring the output current under an applied voltage across the membrane from +100 mV to -100 mV in 10 mV steps. In the instance of a single bilayer being formed, there should be near total electrical isolation of the two electrodes, with no more than a 1 pA drift in current (**Figure 5.4**).

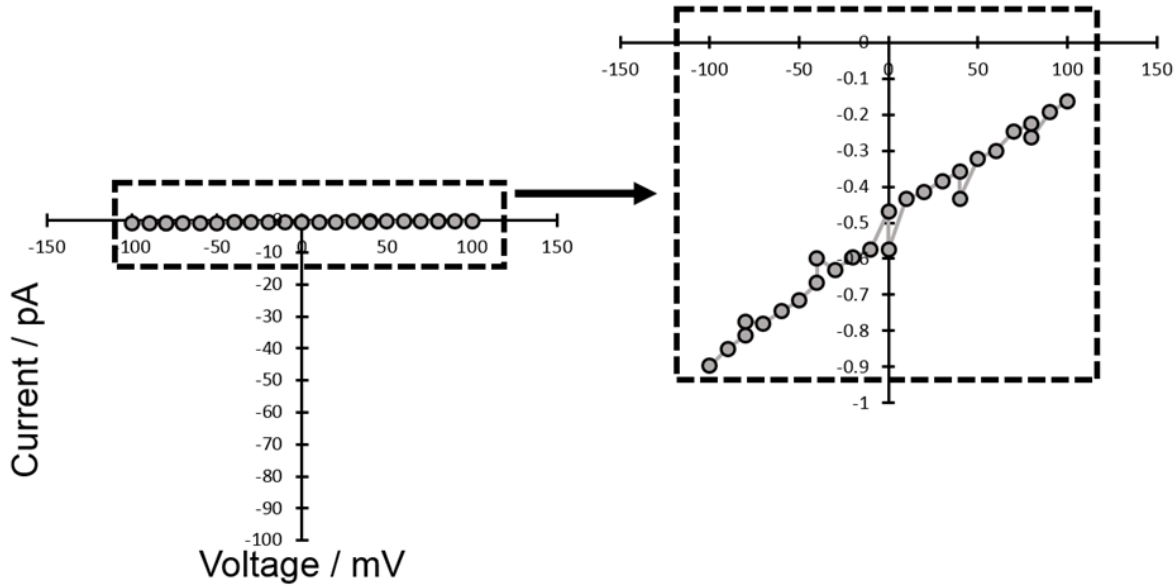

Figure 5.4: characterisation trace for a membrane. A 10 mV incremental voltage was applied between +100 and -100 mV. In the presence of a membrane suitable for nanopore studies, a current variance of no more than 1 pA should be observed. As the membrane is not a perfect insulator, a small increase in the current should be expected as the voltage increases.

Formation of a Multilayer

If a capacitance of less than 40 pA was observed, this was indicative that a multilayer had formed. This phenomenon is where the lipid layer has malformed and is predominantly comprised of hexadecane. Such a membrane

is unusable for nanopore studies, as a protein pore is unable to form. Unlike a lipid bilayer, the insulation properties of a multilayer mean that it cannot be dissipated by a short duration application of a high potential difference – a 'zap'. Instead, firm application of mechanical force to the metal bracket of the cell will disrupt the multilayer and unblock the aperture. A wrench works well, although other blunt instruments may be used.

Insertion of α-HL

α-HL will spontaneously self-assemble into a membrane spanning heptameric channel. At low concentrations, the probably of channel formation are low and rely on the stochastic coming together of the monomers at the surface of the membrane.[1] At a high bulk concentration, pore formation is far more likely and therefore multiple channels will form. This is, however, undesirable for nanopore studies as multiple channels vastly complicates the data to the point that it is often incomprehensible. In order to achieve a single channel, a high local concentration of the protein is formed at the surface of the membrane. Using a mechanical pipette equipped with a gel-loading tip, approximately 1 µL of α-HL (~250 µM in water) was drawn up. With an applied voltage of +100 mV, the tip was submerged into the buffer and directed at the approximate position of the aperture and the α-HL as injected into the solution. Between 1 to 5 minutes was allowed for an insertion of a pore into the membrane. If this did not happen on this timescale then the process was repeated until a single protein channel was formed. When a sharp single step up to approximately +100 pA was observed, this was indicative that a single protein channel with the correct heptameric configuration had been achieved.

The α-HL will insert the β-barrel into the membrane with the *cis* side of the protein at the ground well of the cell and the *trans* at the live well. In the standard buffer, a current trace proportional to the applied voltage was seen in the positive (*i.e.* an applied voltage of +100 mV will give an output current of

+100 pA). However, the channel gives a highly characteristic asymmetry in current in the negative; a current of approximately -75 pA will be seen for an applied voltage of -100 mV. This arises from the shape of the protein channel and the distribution of charges throughout.

Once a single protein channel has been formed, the system was left for approximately 5 minutes to ensure that a second pore did not insert. The insertion of protein channels is, unfortunately, stochastic and there are limited ways to prevent the subsequent insertion of pores. Once it appeared that the channel was relatively stable, the channel was characterised by applying a +100 mV to -100 mV potential in 10 mV increments across the pore. This gave a highly a highly reproducible I/V trace which was used to confirm the formation of a single protein channel (**Figure 5.5**).

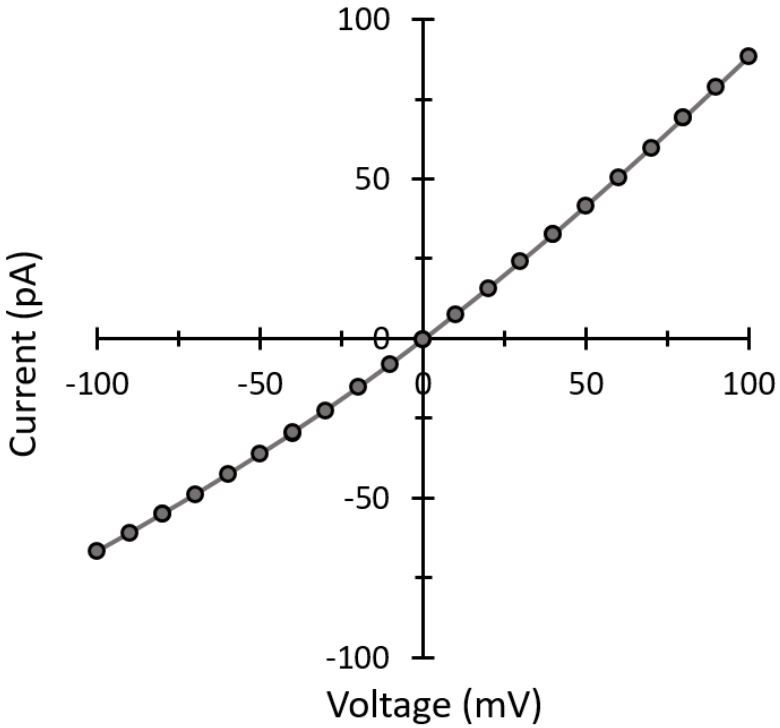

Figure 5.5: I/V trace for an unmodified wild type α-hemolysin protein channel. The voltage was varied in 10 mV increments between +100 and -100 mV. Buffer 1 M KCl, 30 mM K_2HPO_4, pH 8. Lowpass Bessel filter 100 Hz and output gain x50.

Once a stable pore had been characterised, experimentation on the channel could commence.

Post-Experiment

Waste from the wells was disposed of in the appropriate waste stream, or retained for recovery of materials. The cell was washed in three cycles with water and ethanol. If the water/ethanol wash was not sufficient (e.g. contamination in subsequent experiments, residual residue on cell) concentrated H_2SO_4 was applied to each well for approximately 5 minutes, before quenching and a second cycle of water/ethanol washes. All ethanol must evaporate before the cell is used for experiments. Hamilton syringes were washed by drawing and expelling water (3 × 50 µL) and ethanol (3 × 50 µL) three times. Electrodes were washed by thoroughly rinsing with water and ethanol or by electrolysis (see “Ag/AgCl Electordes for Nanopore Electrophysiology”).

5.3 Design of an irradiation circuit

To irradiate the buffered well during nanopore recordings, an LED circuit was designed. LEDs and LED drivers were purchased from Roithner LaserTechnik. A single AA battery (1.6 V) was used as a power source and a switch was installed. The circuit was soldered together as per the diagram in **Figure 5.6.** The circuit was grounded from the driver to the faraday cage to minimise electrical interference.

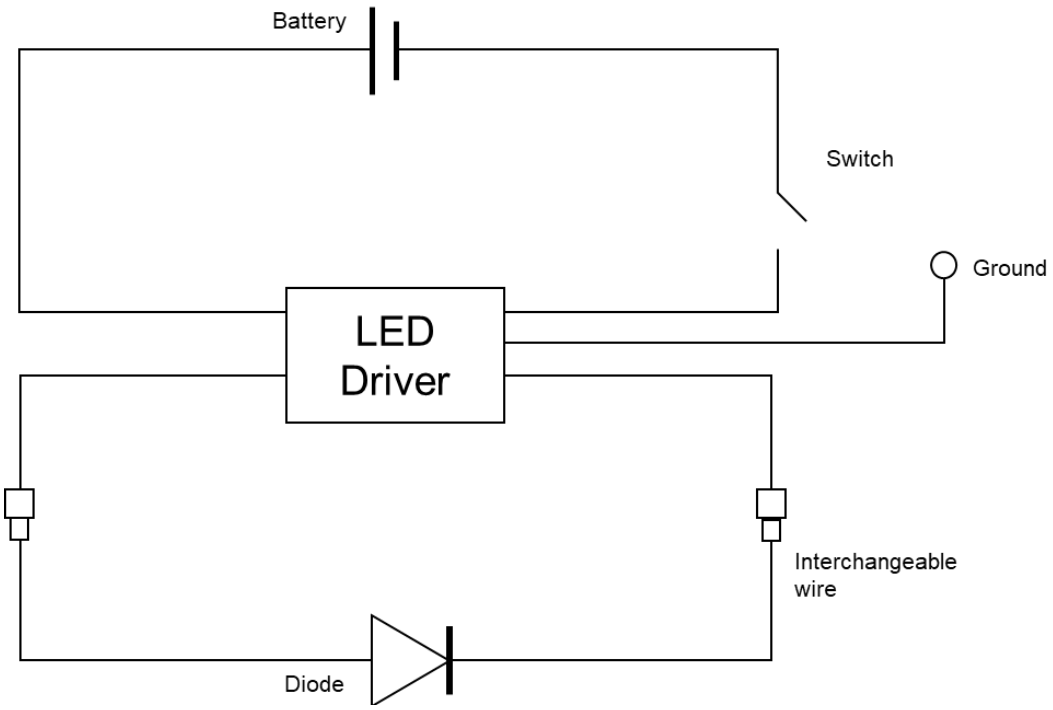

Figure 5.6: Circuit diagram for the irradiation of nanopore experiments The diode was connected on an interchangeable wire so that different wavelengths could be used with the same set up. The circuit was grounded to reduce electrical noise.

5.4 Cucurbituril catalysis at the single molecule level

General experimental

All CB[n] homologues were provide by the Scherman Group, University of Oxford. Solutions of CB[n] were prepared in a 1 M salt buffer. Unless otherwise stated, the same buffer was used to solubilise CB[n] as was used in the nanopore cell.

Nanopore experiments were conducted in a custom Teflon cell (**Figure 5.3**). All experiments were conducted with 600 µL of buffer in each well. Various buffer systems were used, as specified in each experimental. CB[n] was added either to the *cis* or *trans* well, as specified. The well was mixed by aspiration (50 µL x 5) post addition of CB[n].

All experiments were conducted at atmospheric pressure and room temperature.

Longer blockages and addition of compound 1

Following the experimental procedure outlined above, CB[7] (10 µL of 10 mM stock) added to the *cis* well (**Figure 5.7A**)

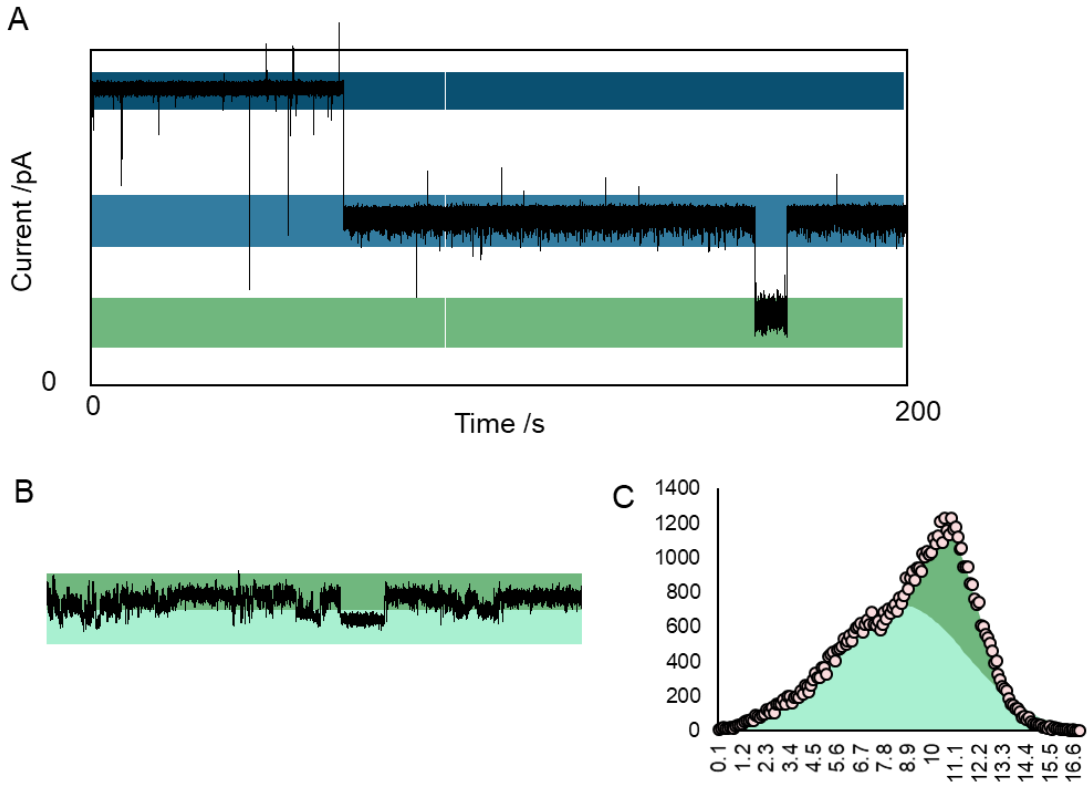

Figure 5.7: A) Example trace for the addition of CB[7] (10 µL of 10 mM stock) added to the *cis* well. Initial trapped level of I_b/I_o = 0.48 was observed (pale blue), which gave way to a second trapped state of I_b/I_o = 0.08 (green). B) Magnification of the second trapped state, which appears to be comprised of at least two distinct states. C) All points histogram of the lower trapped state (green), demonstrating two poorly resolved levels. Buffer 1 M KCl, 30 mM K_2HPO_4, pH 8. Voltage +100 mV. Lowpass Bessel filter 100 Hz and output gain x50.

In a 3 M KCl buffer, CB[7] (10 µL of 10 mM stock) was added to the *cis* side (**Figure 5.8A**).

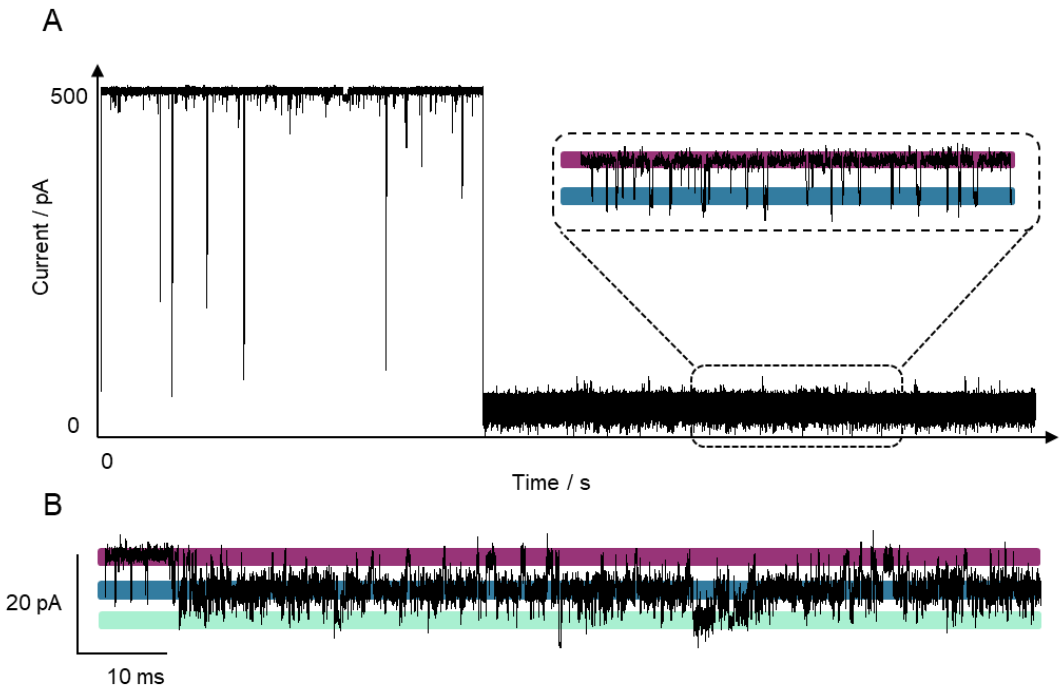

Figure 5.8: A) Current trace showing potential trapping of CB[7] (10 µL of 10 mM stock) in the pore. The free pore current sits at approximately 500 pA, with frequent deep drops in the current that are most likely due to the CB[7] transiently interacting with the pore but not becoming trapped. There is then a large current drop to approximately 50 pA. Within this new level, two distinct sub-states can be seen. B) Upon addition of compound **1** a further drop in current was observed. Three distinct sub levels could then be seen; the original two, shown in purple and pale blue, and a new lower level in dark blue. Buffer 3 M KCl, 30 mM Tris, pH 8. Applied voltage 160 mV. Lowpass Bessel filter 100 Hz and output gain x20.

High fidelity detection of homologues

Studies with in both a KCl and CsCl buffer have shown that transient trapping of CB[7] can be achieved with an α-HL nanopore. Due to the varying size, a discrete level would be expected for each of the CB[n] homologues. In a control experiment, CB[7] (5 µL, of 10 mM stock) was added to the trans well and events were observed (**Figure 5.9**).

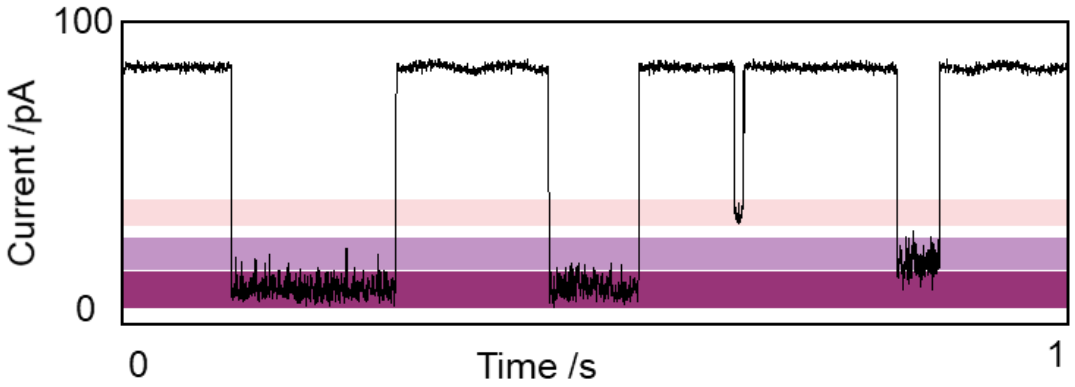

Figure 5.9: Levels and sub-levels when CB[7] sample is added to the pore. In a control experiment, CB[7] (5 µL, of 10 mM stock) was added to the trans well and events were observed. The lower level (magenta) was the most frequently observed and attributed to CB[7]. The two upper levels (lavender and pink) were hypothesised to result from CB[6] and CB[5] respectively. 1 M KCl, 30 mM K_2HPO_4, pH 8. Voltage +100 mV. Lowpass Bessel filter 100 Hz and output gain x50.

To probe the hypothesis that other homologues were present, samples of CB[5] and CB[6] were obtained. These were seen to be pure isolated products by NMR. CB[5] (5 µL, of 10 mM stock) and CB[6] (5 µL, of 10 mM stock) were added to a channel and the events recorded (**Figure 5.10A**). The major level attributed to each homologue (**Figure 5.10C**) was then compared to the unassigned levels in the CB[7] sample (**Figure 5.10B**).

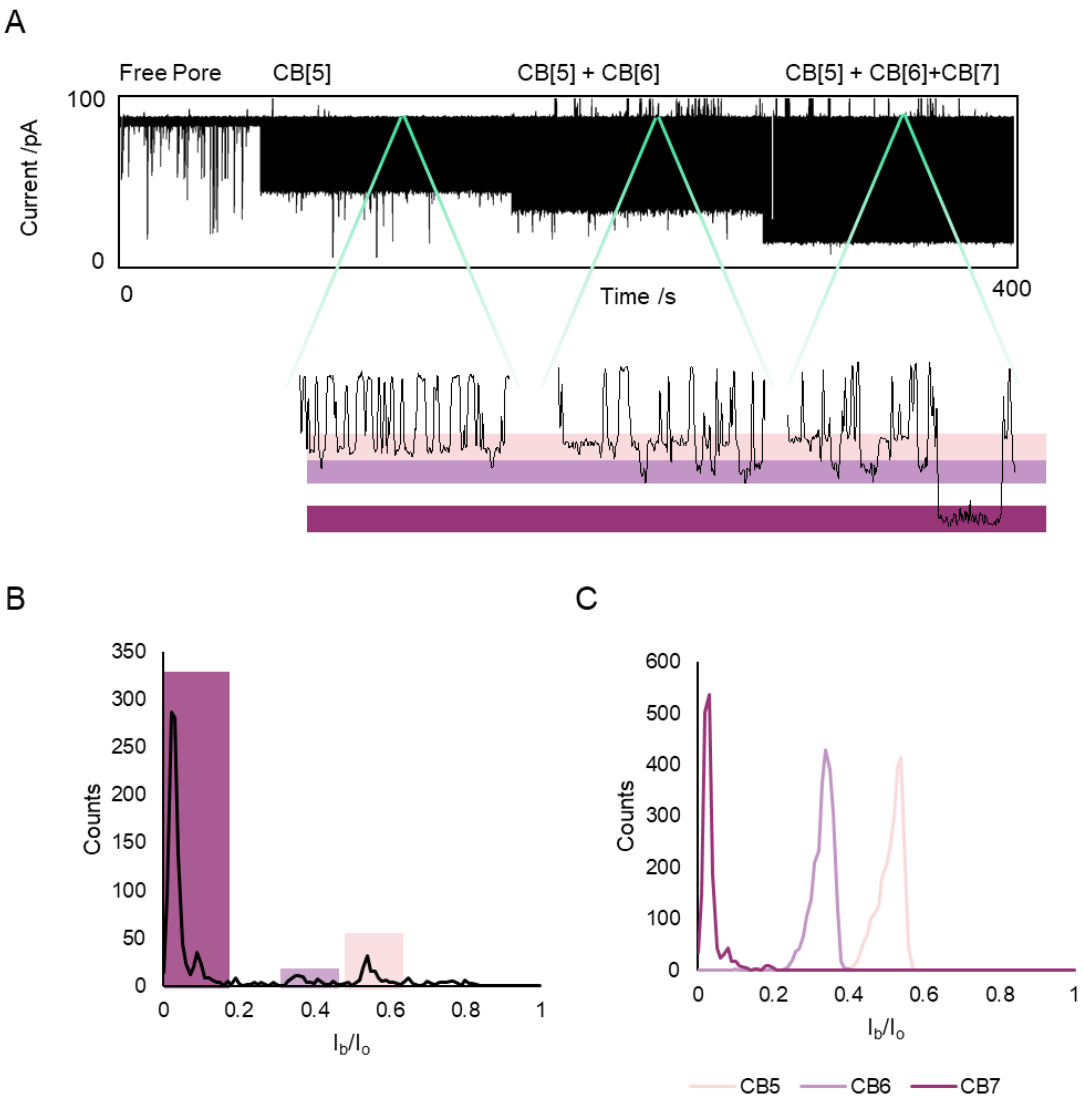

Figure 5.10: A) Example trace showing the free pore current, followed by successive addition of CB[5] (5 µL, of 10 mM stock), CB[6] (5 µL, of 10 mM stock), and CB[7] (5 µL, of 10 mM stock). The rapid nature of the events means that they initially appear as a single black box; however, upon magnification (lower panel) quantised levels can be seen. With the addition of each macrocycle, a new level can be observed. 1 M CsCl, 30 mM K_2HPO_4, pH 8. Voltage +100 mV. Lowpass Bessel filter 100 Hz and output gain x50 B) All points histogram for CB[7] for 100 s of recording. The major event corresponding to CB[7] is observed at $I_b/I_o = 0.03$. Two additional levels are observed at $I_b/I_o = 0.38$ and $I_b/I_o = 0.55$. C) Using threshold search, the individual events for CB[7], CB[6] and CB[5] were extracted and the incidence of each assessed by histogram analysis. A maximum of 100 s or 2,500 events were recorded. The events attributed to CB[5] (pink) and CB[6] (violet) directly correspond to the minor events observed in the pure CB[7] sample at $I_b/I_o = 0.38$ and $I_b/I_o = 0.55$ respectively.

For present studies, it is of interest to note that other homologues appear to be present in the sample. Indeed, there does appear to be binding between CB[6] and compound **7**. When CB[6] and CB[5] were introduced to a single channel, signals were seen at $I_b/I_o = 0.59$ and $I_b/I_o = 0.72$ respectively (**Figure 5.11**).

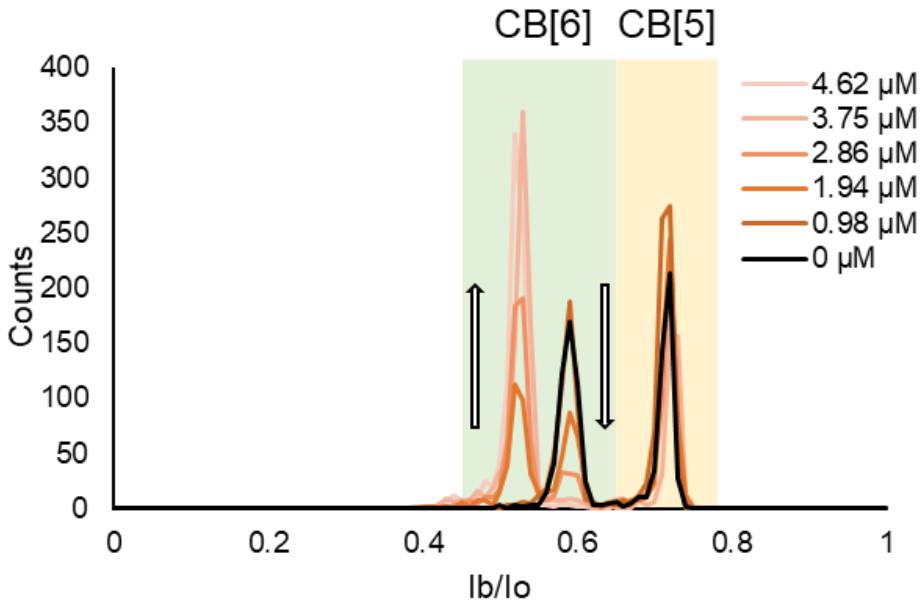

Figure 5.11: Frequency histogram for the binding events under a consistent concentration of CB[5] (66.2 µM) and CB[6] (66.2 µM) as the concentration of compound **7** was increased. The peak corresponding to CB[5] (yellow) stays consistent, whereas the peak corresponding to CB[6] diminishes and a new peak emerges. 1 M KCl, 30 mM K_2HPO_4, pH 8. Voltage +100 mV.

Bulk observations of CB[7]

It was previously established that CB[7] would catalyse the Diels-Alder reaction of compounds **1, 4,** and **7** in D_2O at 37 °C.[2] An NMR study was conducted to ensure that the same reactions would turn over under the conditions required for nanopore experiments. CB[7] was used as the internal standard as its concentration was consistent throughout. The reaction was monitored over 24 hours (**Figure 5.12**)

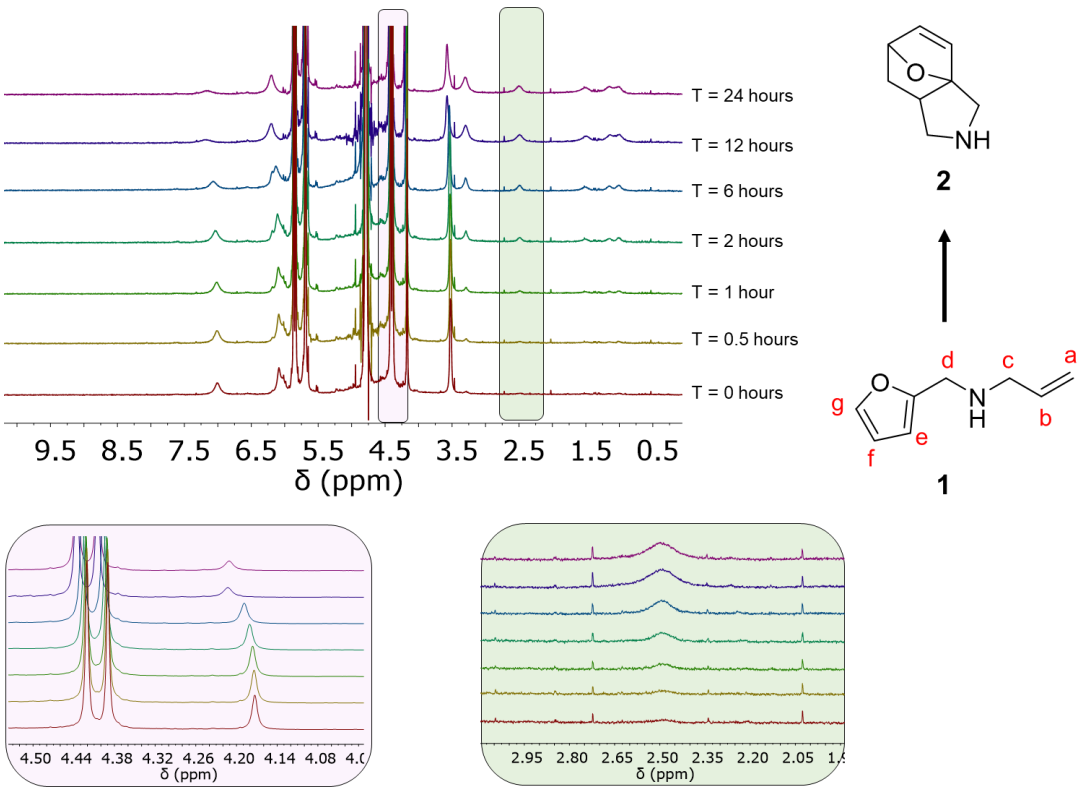

Figure 5.12 Turnover of compound **1** by CB[7], as observed by proton NMR. Consumption of compound **1** was observed from the peak at 4.17 ppm (pink). Formation of compound **2** was observed by the emergence of the peat at 2.47 ppm (green). As the concentration of CB[7] remained constant throughout, this was used as an internal standard. The peak at 4.42 ppm was selected as the standard peak. A solution of CB[7] (20 mM) was made in 600 µL. To this, compound **1** was added to give a final concentration of 2.4 mM. 1 M KCl, 30 mM KPi, pD 7.2

Using the CB[7] signal at 4.40 ppm as the reference, the relative integral of the starting material (compound **1**) signal at 4.17 ppm was monitored over time (**Figure 5.13**).

A

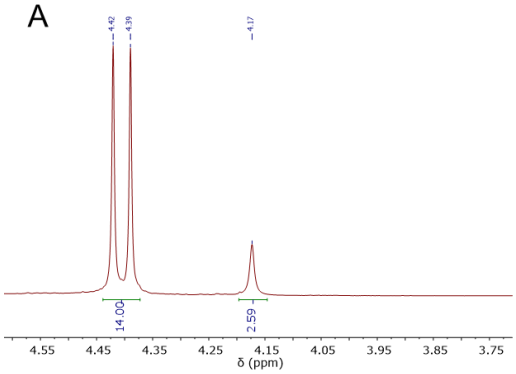

B

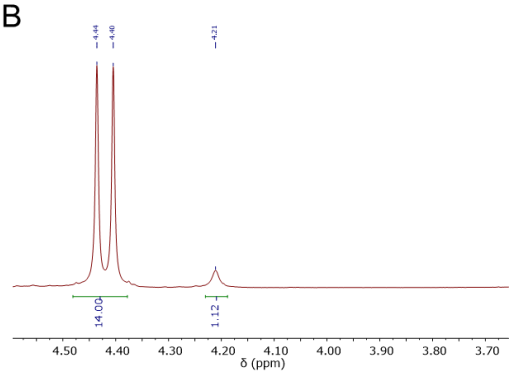

C

Time	Integral CB[7]	Integral Compound **1**	Relative integral
0	14	2.53	1
0.5	14	2.46	0.972
1	14	2.26	0.893
2	14	2.12	0.837
6	14	1.98	0.782
12	14	1.17	0.463
24	14	1.12	0.447

D

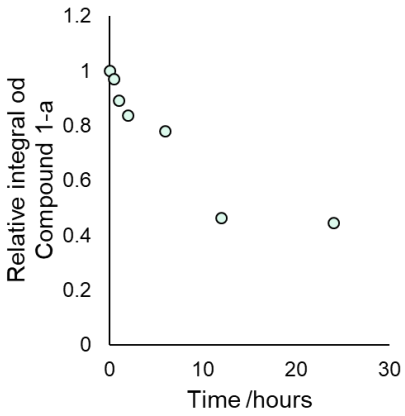

Figure 5.13: Turnover of compound **1** in 1 M KCl buffer. Ratio of 0.1:1 FUC:CB[7]. A) Ratio of the peaks for CB[7] (4.41 ppm) and compound **1** (4.17 ppm) at (t=0). B) Ratio of the peaks for CB[7] (4.41 ppm) and compound **1** (4.17 ppm) at (t=24).C) Table showing the integral values for CB[7] and compound **1** over time. D) Plot showing the relative integral against time from the data given in (C). A solution of CB[7] (20 mM) was made in 600 µL. To this, compound **1** was added to give a final concentration of 2.4 mM. 1 M KCl, 30 mM KPi, pD 7.2

The same process was repeated for the observation of the turnover of compound **7** (**Figure 5.14**).

A

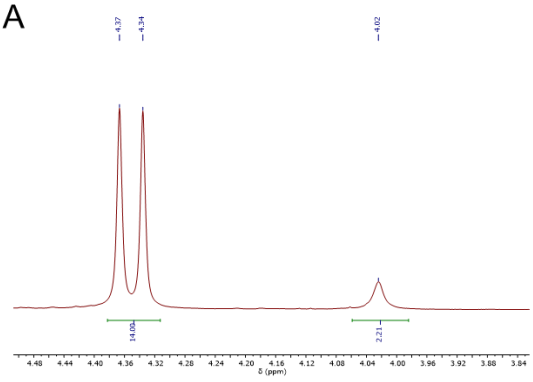

B

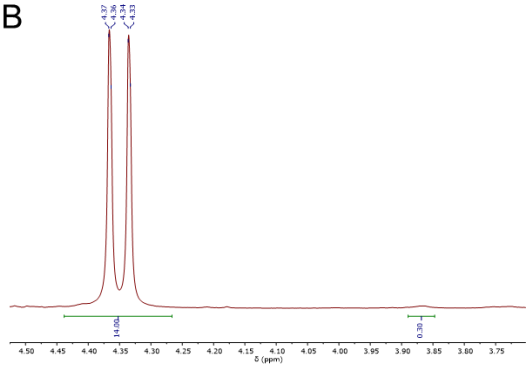

C

Time /h	Integral CB[7]	Compound **7**	Relative integral
0.25	14	2.2	1
0.5	14	1.64	0.745
1	14	1.3	0.591
2	14	0.82	0.373
6	14	0.48	0.218
12	14	0.37	0.168
24	14	0.30	0.1

D

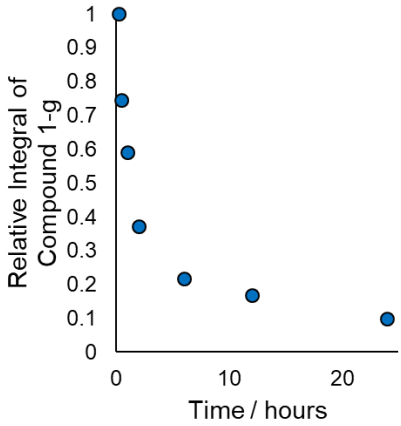

Figure 5.14: Turnover of compound **7** in 1 M KCl buffer. Ratio of 0.1:1 FUC:CB[7]. A) Ratio of the peaks for CB[7] (4.41 ppm) and compound **7** (4.02 ppm) at (t=0). B) Ratio of the peaks for CB[7] (4.41 ppm) and compound **7** (4.03 ppm) at (t=24).C) Table showing the integral values for CB[7] and compound **7** over time. D) Plot showing the relative integral against time from the data given in (C). A solution of CB[7] (44 mM) was made in 600 µL. To this, compound **7** was added to give a final concentration of 44 mM. 1 M KCl, 30 mM KPi, pD 7.2

5.5 Modifications of a protein nanopore

General lysine modification protocol

A carboxylic acid functionalised reagent (10 mM) was prepared in a solution of DMSO. Separately, an activation mixture of EDC (100 mM), sulfo-NHS (100 mM) and DMAP (1 mM) was prepared in water (**Figure 5.15**). The two solutions were mixed 1:1 v/v to give an acid concentration of 5 mM. The mixture was reacted at room temperature for 20 minutes. To the *cis* chamber (600 µL) of a buffered cell containing a single α-HL channel, the activated acid solution (10 µL) was added with mixing. A potential difference of +100 mV was applied.

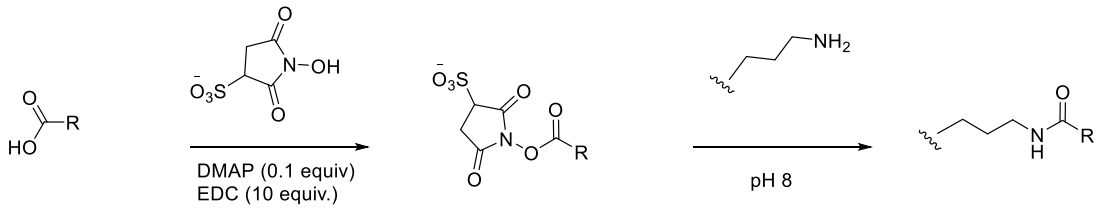

Figure 5.15: General scheme for the attachment of a water-soluble carboxylic acid to the lysine residue of an α-HL nanopore.

A solution of EDC (100 mM), sulfo-NHS (100 mM) and DMAP (0.01 mM) was prepared and added to the *cis* side under an applied potential. No irreversible modification had occurred after an excess of 3000 s (**Figure 5.16**).

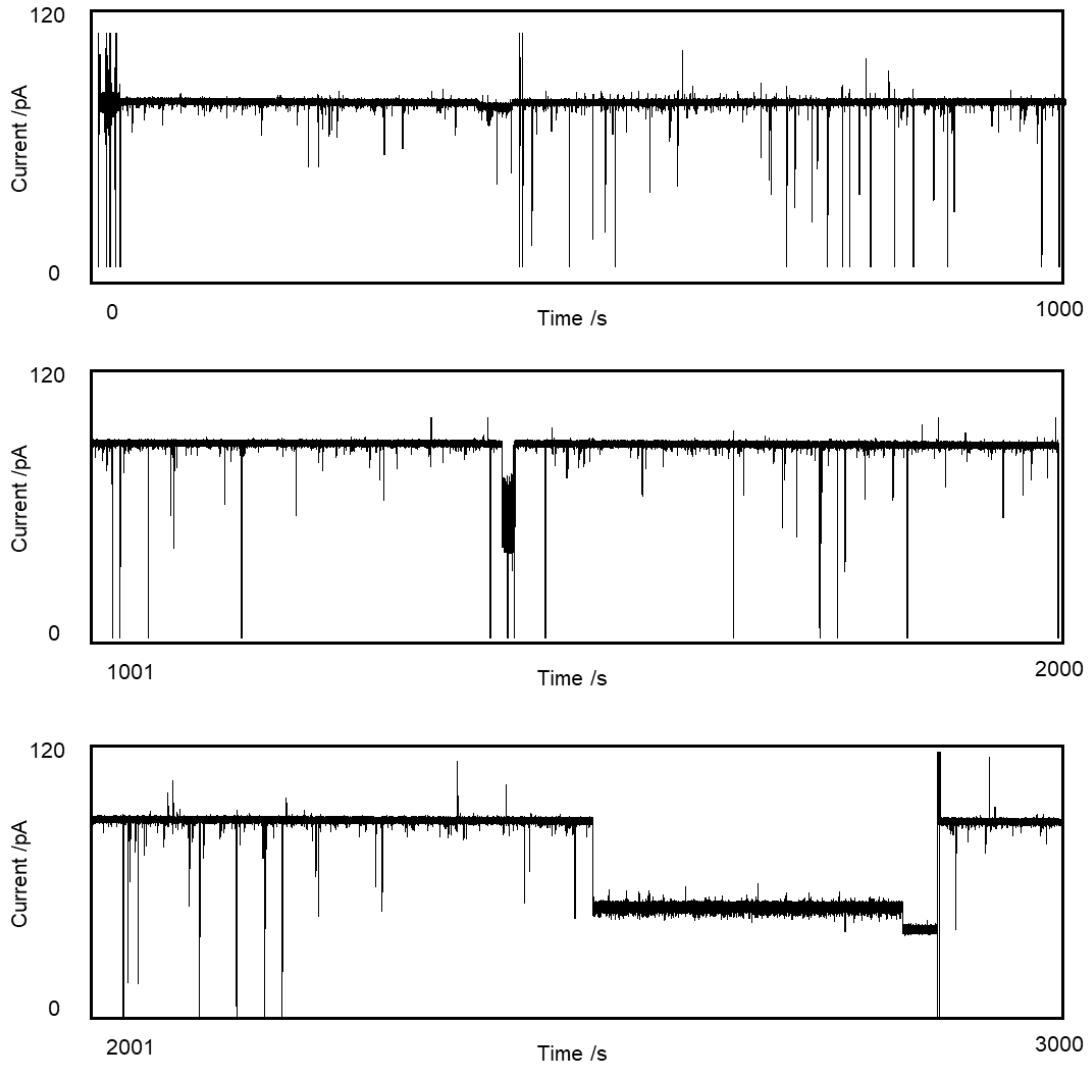

Figure 5.16: EDC (100 mM), sulfo-NHS (100 mM) and DMAP (0.01 mM) were mixed and left at room temperature for 20 minutes. The reaction mixture (30 µL) was added to the cis well of a nanopore cell and left for 1 hour. The system was under an applied potential of +100 mV. No modification was observed. Buffer 1 M KCl, 30 mM K_2HPO_4, pH 8. Voltage +100 mV. Bessel filter 100 Hz and output gain x50. Lowpass Bessel filter 300 Hz applied post-acquisition.

Channel characterisation is applied to confirm that successful modification has occurred (**Figure 5.17**). Using Clampfit, an incremental change in voltage is applied between +100 and -100 mV in 10 mV steps.

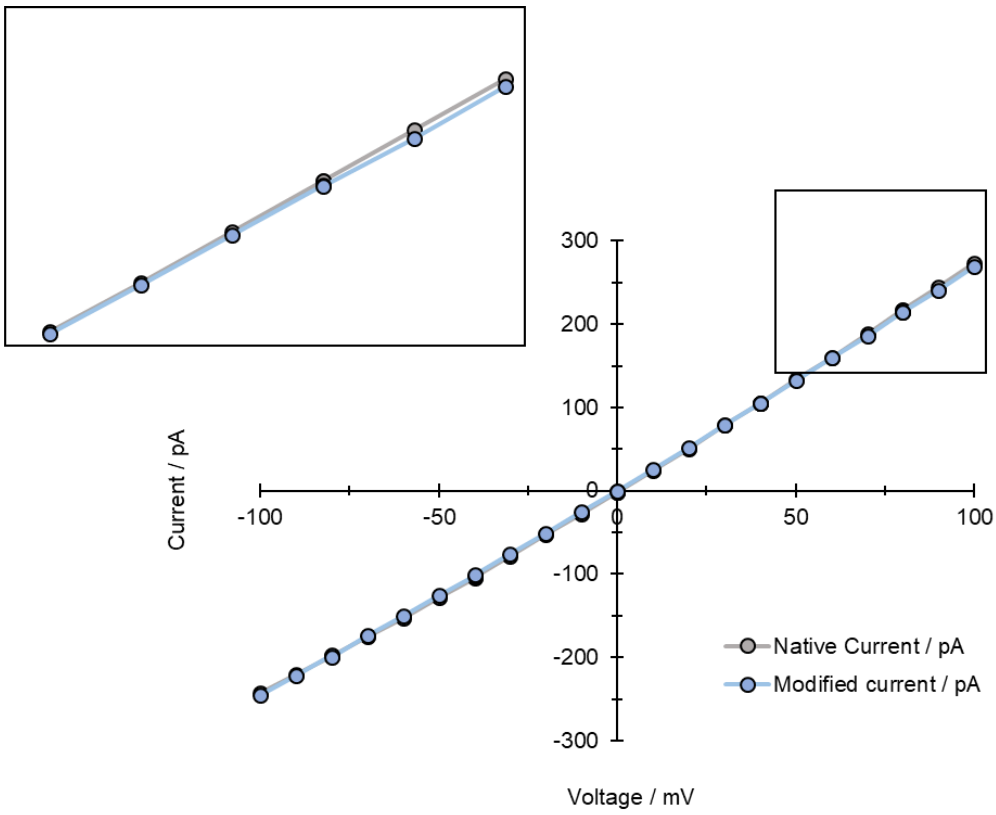

Figure 5.17: Characterisation trace for the modification of an α-HL channel with activated benzoic acid in a 3 M KCl buffered solution. A solution of benzoic acid (30 mM, water) was prepared. A separate solution of EDC (300 mM), sulfo-NHS (30 mM) and DMAP (0.3 mM) was prepared in water. The two solutions were mixed 1:1 to give a stock acid concentration of 15 mM. Voltage was varied in 10 mV increments between +100 and -100 mV. Buffer 3 M KCl, 30 mM, K_2HPO_4, pH 8. Lowpass Bessel filter 100 Hz and output gain x50.

Oxaziridine functionalisation of methionine

Compound **11** (1 µL, 100 mM) was added to the *cis* well of the pore. Within 30 s, an irreversible modification was observed. Successful modification was confirmed by a characterisation plot (**Figure 5.18B**).

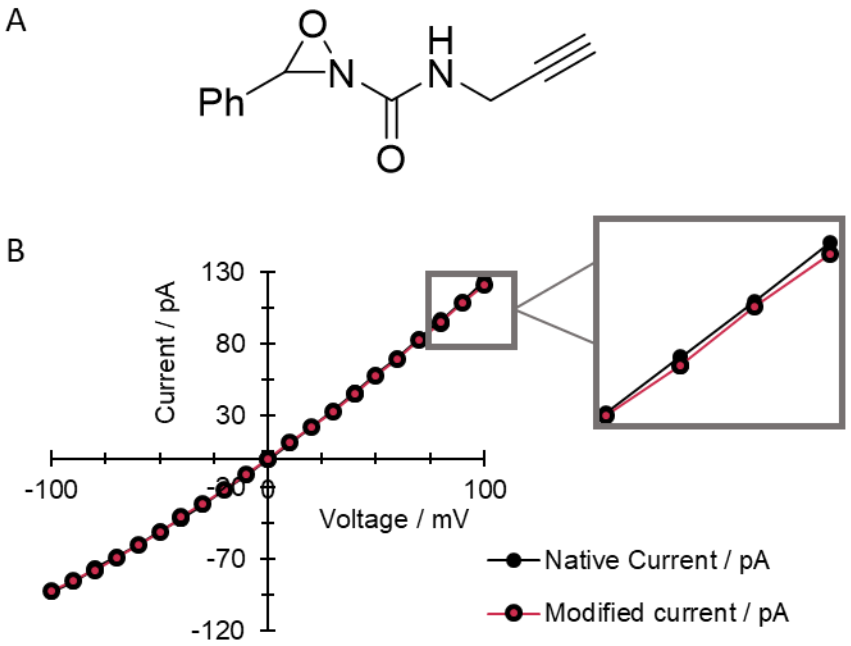

Figure 5.18: A) Structure of the alkyne terminated oxaziridine (compound **11**). B) Characterisation trace for the attachment of compound **11** reagent to the pore. Compound **11** (1 µL, 100 mM) was added to the *cis* well of the pore. Within 30 s, an irreversible modification was observed. Immediately, methionine (8 µL, 250 mM) was added to the *cis* well with mixing. Voltage was varied in 10 mV increments between +100 and -100 mV. Buffer 1 M KCl, 30 mM K_2HPO_4, pH 8. Voltage +100 mV. Lowpass Bessel filter 100 Hz and output gain x50.

Exploring in situ modification at tyrosine

A biphenyl sulfonyl fluoride (**Figure 5.19A**) was synthesised A solution of compound **14** (500 mM) was prepared in acetonitrile. 10 µL of this solution was added to the cis well under an applied potential (**Figure 5.19 B**).

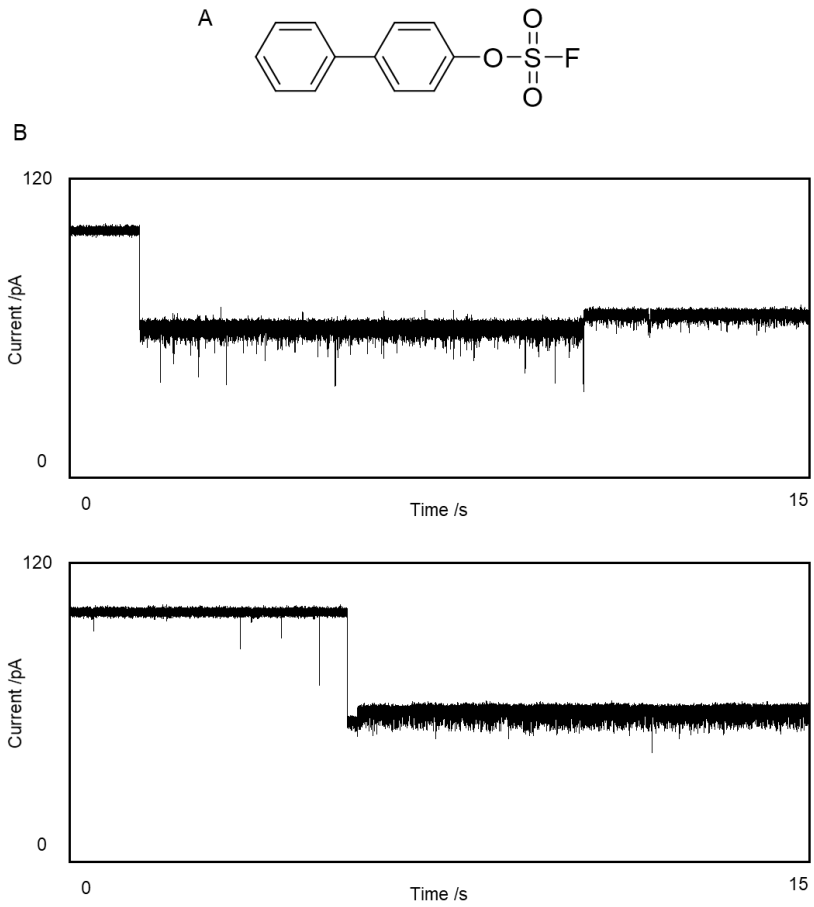

Figure 5.19: Two different SuFex modifications. A) Structure of the SuFEx reagent, compound **14**. B) A solution of compound **14** (500 mM) was prepared in acetonitrile. 10 µL of this solution was added to the *cis* well under an applied potential. On two separate occasions, a two-step irreversible modification was. However, the modification had poor reproducibility and the failed attachment attempts vastly outnumbered the successful. 1 M KCl, 30 mM K_2HPO_4, pH 8. Voltage +100 mV. Lowpass Bessel filter 100 Hz and output gain x50.

5.6 Transmembrane Molecular Machines

Membrane stability under UV exposure

To ensure that the UV exposure would not perturb the bilayer, the system was irradiated with UV light in the absence of any analyte. A circuit was constructed as outlined in **Section 5.3**. This was grounded to the inside of the faraday cage to ensure that there was no electrical interference. The system was irradiated with light and the noise compared to the trace under ambient conditions (**Figure 5.20**)

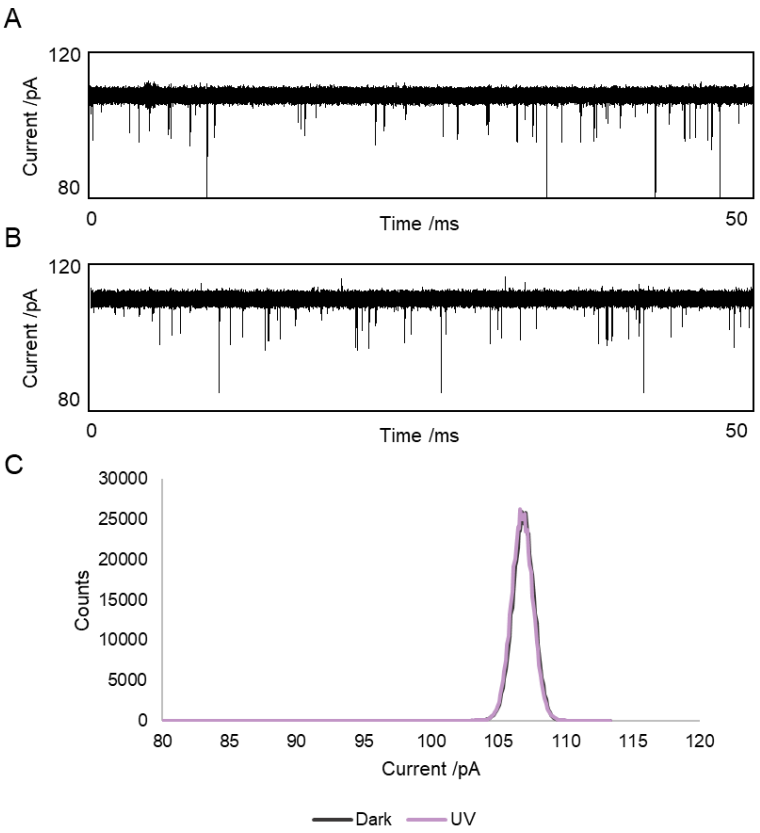

Figure 5.20: The stability of the membrane upon irradiation with UV light was accessed. A) current trace in the absence of light. B) Current trace upon the application of UV light (λ = 365 nm). C) All points histogram for the traces in the absence of light (grey) and in the presence of UV light (violet). They two traces overlap exactly, showing no perturbation of the signal noise by the use of the UV diode. Volume 600 µL. Buffer 1 M KCl, 30 mM K_2HPO_4, pH 8. Voltage +100 mV. Lowpass Bessel filter 100 Hz and output gain x50.

Transmembrane molecular Rotors

Attachment of compound 20 to the pore:

Compound **20** was attached to the pore following the standard procedure outlined in **Section 5.5** (**Figure 5.21**).

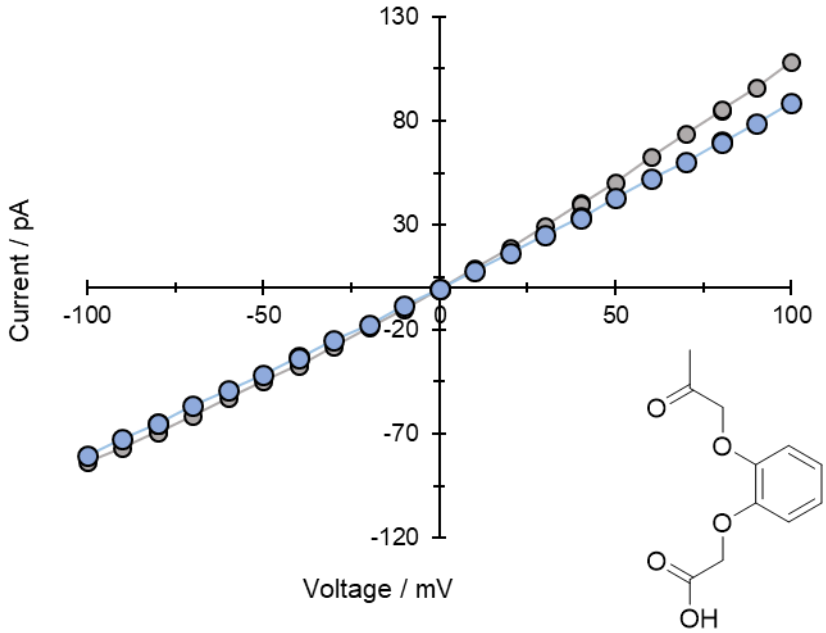

Figure 5.21: Characterisation trace for the atachment of [2-(2-oxopropoxy)phenoxy] acetic acid (compound **20**) to the pore. A solution of compound **20** (0.0936 M) was prepared in DMSO. A second solution of EDC (0.16 M), NHS (0.30 M) and DMAP (0.008 M) was prepared in DMSO. Both solutions were heated gently and perturbed with ultrasound in order to dissolve and disperse the solid. These solutions were mixed in a 1:1 v/v ratio and reacted for approximately 1 hour prior to addition to the nanopore. The buffered cell (1 M KCl, 30 mM KPi, pH 8) was set up as detailed previously, with an applied voltage of +100 mV. Once a pore had formed, the activated compound **20** solution was injected as close to the aperture as possible using a gel loading tip and a micro pipette. Approximately 500 s was allowed between subsequent additions. Additions were made until modification occurred. The modified pore was characterised.

Attachment of compound 21 to the pore:

Compound **21** was attached to the pore following the standard procedure outlined in **Section 5.5** (**Figure 5.22**)

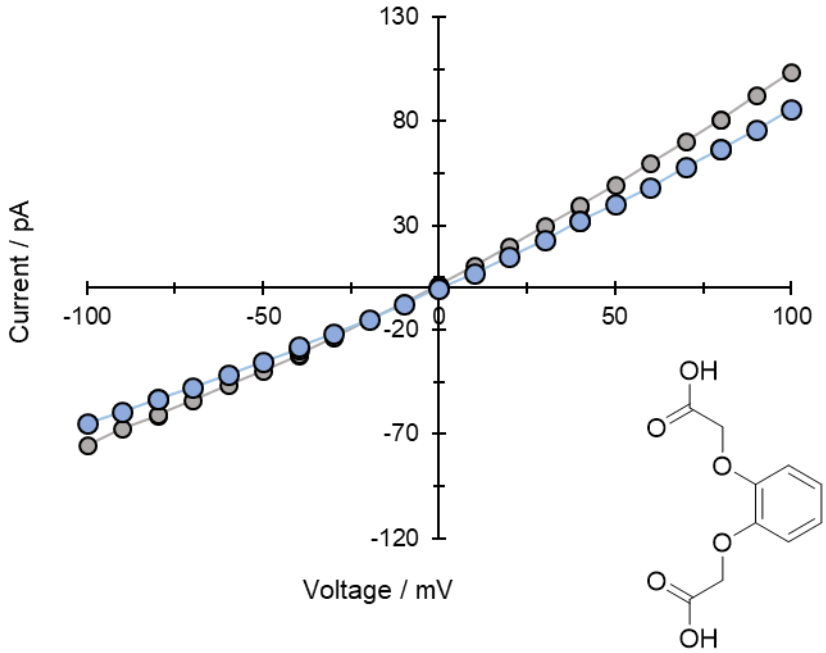

Figure 5.22: Characterisation trace for the attachment of the 2-[2-(2-hydroxy-2-oxoethoxy)phenoxy]acetic acid (compound **21**). Compound **21** (0.021 g, 92.8 µmol) was made into a solution of DMSO (1 mL). A second solution of EDC (0.0248 g), DMAP (0.0001 g) and sulfo-NHS (0.0345 g) was made into DMSO (1mL). Both solutions were heated gently and perturbed with ultrasound in order to dissolve and disperse the solid. The solutions were mixed in a 1:1 v/v ratio and left for between 30 minutes and 2 hours. The buffered cell (1 M KCl, 30 mM KPi, pH 8) was set up as detailed previously, with an applied voltage of +100 mV. Once a pore had formed, the activated compound **21** solution was injected as close to the aperture as possible using a gel loading tip and a micro pipette. Approximately 500 s was allowed between subsequent additions. Additions were made until modification occurred. The modified pore was characterised.

Molecular Pump

Exploration of Dibenzo-24-crown-8 binding events

A single channel was formed following standard procedure. Dibenzo-24-crown-8 solution (10 mM, acetonitrile) was added to the cis well without mixing (**Figure 5.23**).

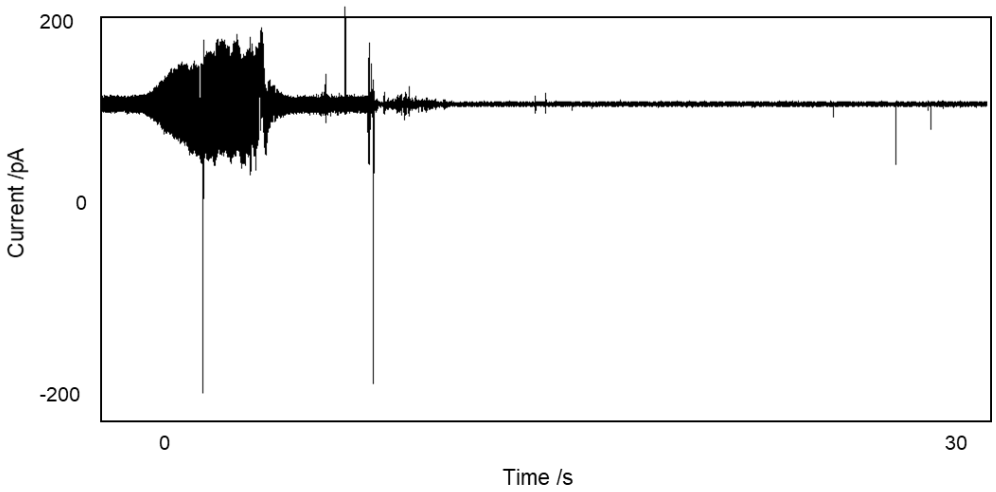

Figure 5.23: Dibenzo-24-crown-8 solution (10 mM, acetonitrile) was added to the *cis* well without mixing and no events were observed. Volume 600 µL. Buffer 1 M KCl, 30 mM K_2HPO_4, pH 8. Voltage +100 mV. Lowpass Bessel filter 100 kHz and output gain x50.

A channel was formed under standard procedure. Dibenzo-24-crown-8 solution (10 mM, acetonitrile) was added to the trans well with mixing (**Figure 5.24**).

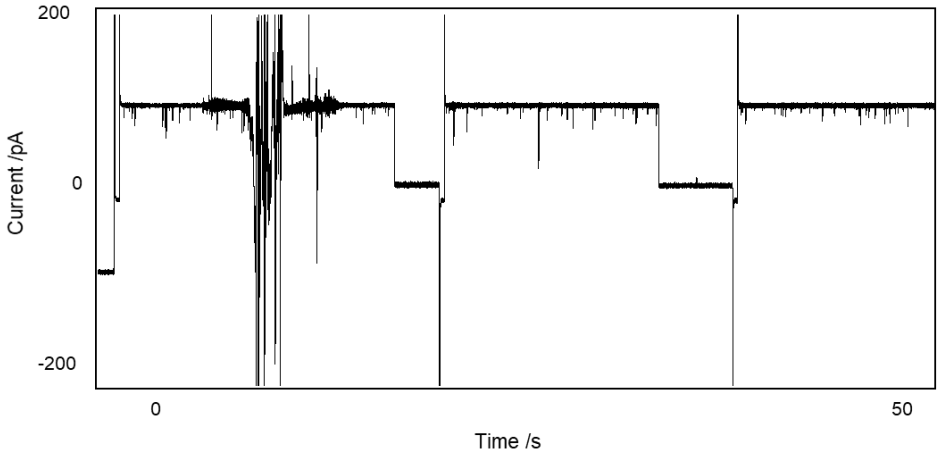

Figure 5.24: Dibenzo-24-crown-8 solution (10 mM, acetonitrile) was added to the *trans* well with mixing. No events were observed. Volume 600 µL. Buffer 1 M KCl, 30 mM K2HPO4, pH 8. Voltage +100 mV. Lowpass Bessel filter 100 kHz and output gain x50.

DNA threading

A channel was formed following standard procedure. A solution of PEG-DNA (10 µL of 10 mM stock) was added to the *cis* side without Dibenzo-24-crown-8 present (**Figure 5.25**).

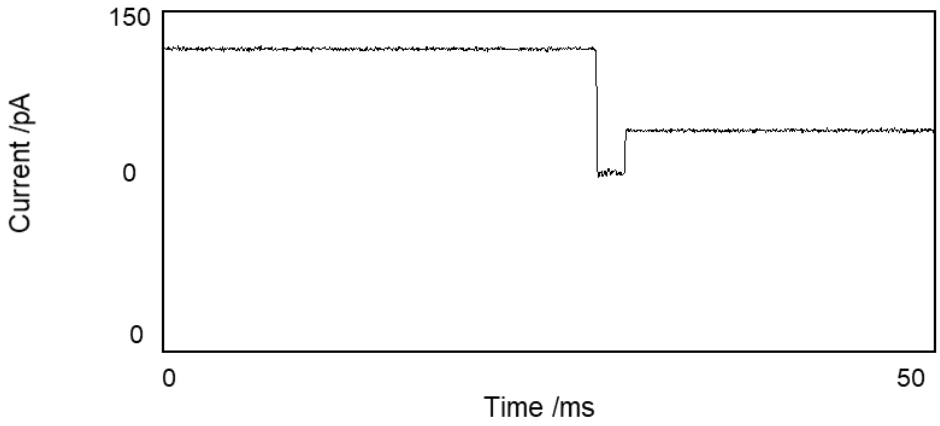

Figure 5.25: Addition of PEG-DNA 10 µL of 10 mM stock without Dibenzo-24-crown-8 present. Applied potential +100 mV. Volume 600 µL. Buffer 1 M KCl, 30 mM K2HPO4, pH 8. Voltage +100 mV. Lowpass Bessel filter 100 Hz and output gain x50.

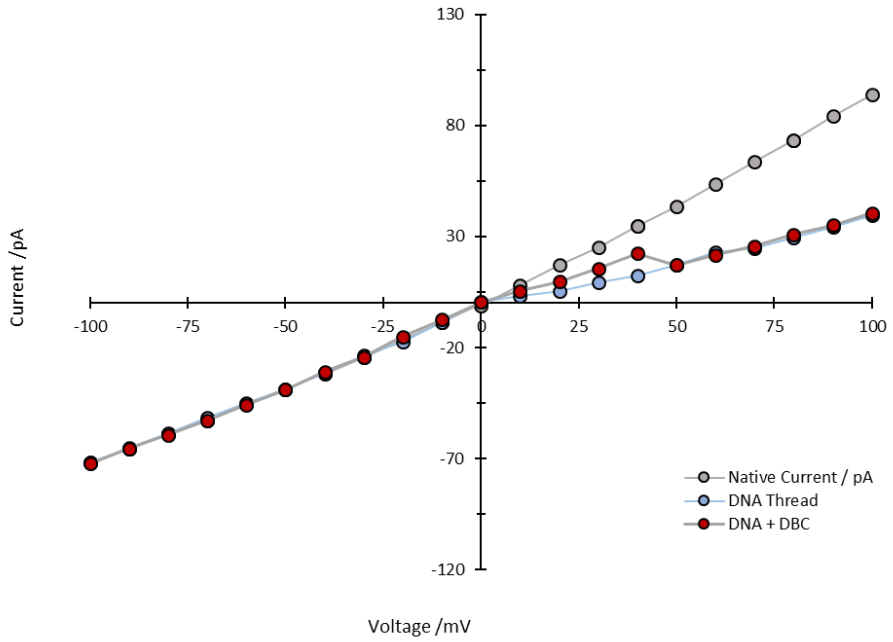

Figure 5.26: Characterisation trace showing the free pore (grey). Streptavidin-biotin DNA thread was added to the channel under an applied potential of +100 mV. Once trapping was achieved, the applied potential was decreased in 10 mV increments (blue). Under a positive applied potential, the thread was held in place. However, upon the inversion of the potential to the negative, the thread was ejected. Dibenzo-24-crown-8 (10 µL of 10 mM stock) was then added to the system. Multiple subsequent trapping events were then observed. When these were characterised, the same I/V sweep was observed (red).

5.7 Synthesis

Reagents were sourced from commercial vendors and used as received. Several chemicals were supplied by collaborators, as highlighted in the text. Unless otherwise stated, reactions were carried out under nitrogen, using the recycled ‘house’ supply. Where stated, dry and degassed solvents were used: these were procured from the School of Chemistry Solvent Purification Facility (SPF).

Analytical Thin Layer Chromatography (TLC) was conducted on aluminium sheets coated with silica gel 60F (Merk) and visualised using UV light (254 nm) or the appropriate stain, as stated in each procedure.

Mass spectrometry measurements were performed by a facility technician using the in house facilities at the University of Edinburgh. Samples were run using a Bruker miroTOF spectrometer. All samples were ionised via electrospray ionisation.

All NMR spectra were recorded in the School of Chemistry, University of Edinburgh. ^{1}H and ^{13}C spectra were recorded on an AVA500 Bruker spectrometer at room temperature. Timed experiments were recorded on a 500 MHz PRO500. Analysis was completed using MestReNova. All measurements were conducted by DCG using an auto sampler.

Synthesis of Compound 7

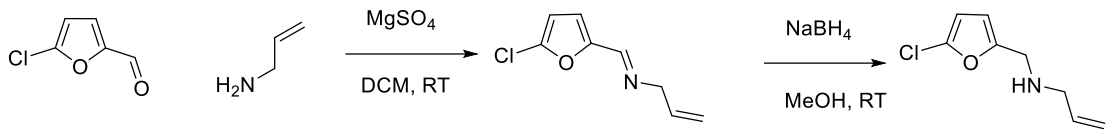

The reaction vessel was charged with $MgSO_4$ (2.5 g). The flask was evacuated and flushed with N_2 three times. Allylamine (480 mg, 8.4 mmol, 0.63 mL) and dry DCM (15 mL) were added via the septum. The resulting suspension was cooled to 0 ^oC on ice and stirred for 1 hour under nitrogen. 5-chloro-2-furaldehyde (1 g, 7.7 mmol) was dissolved in dry DCM (6 mL) and added via a septum. The solution was stirred on ice for a further 30 minutes, returned to room temperature and stirred overnight. $MgSO_4$ was removed by filtration and the solvent removed under reduced pressure. To yield a yellow oil.

The resulting oil was dissolved in dry MeOH (30 mL). The solution was chilled on ice with vigorous stirring, and $NaBH_4$ (195 g, 5.2 mmol) was added slowly. The solution was stirred on ice for a further 30 minutes, then returned to room temperature, and stirred under nitrogen overnight. The reaction mixture was quenched with water (100 mL), extracted with diethyl ether (3 x 60 mL) and washed with water (50 mL). The crude amine was purified by column chromatography (hexane:ethylacetate). Yield = 81% (6.2 mmol). Synthesis was conducted following literature procedure and observed characterisation was in agreement with literature values.[1]

^{1}H NMR (500 MHz, Chloroform-d) δ 6.18 – 6.14 (m, 1H), 6.05 (dd, J = 3.3, 1.3 Hz, 1H), 5.93 – 5.82 (m, 1H), 5.22 – 5.15 (m, 1H), 5.14 – 5.09 (m, 1H), 3.72 (s, 2H), 3.24 (dd, J = 6.0, 1.5 Hz, 2H), 1.87 (s, 1H).

^{13}C NMR (126 MHz, CDCl3) δ 153.34, 136.06, 135.34, 116.62, 109.50, 106.62, 51.18, 45.21.

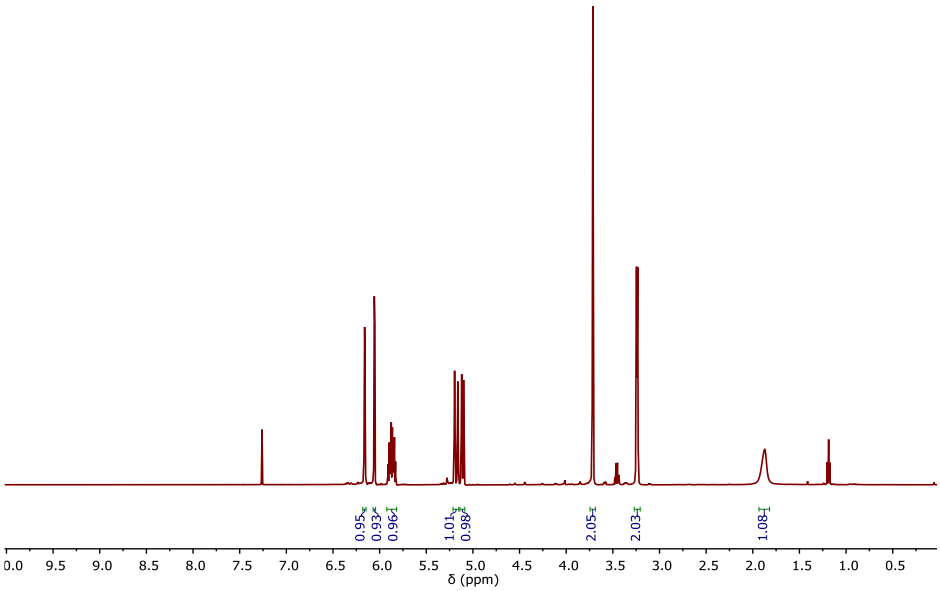

Figure 5.27: ^{1}H NMR spectrum of compound **7** in chloroform

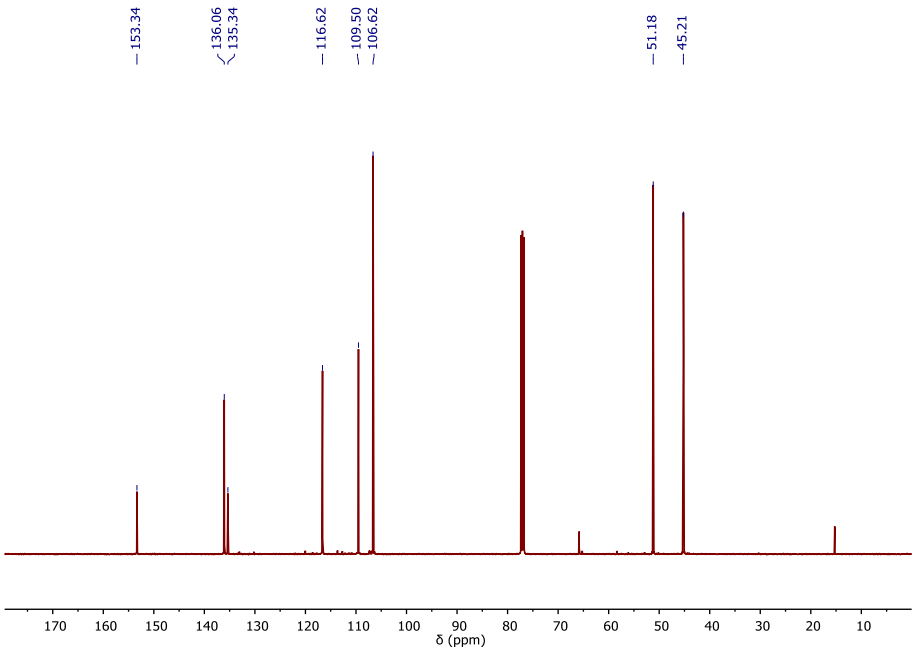

Figure 5.28: ^{13}C NMR spectrum of compound **7** in chloroform

Synthesis of Compound 9

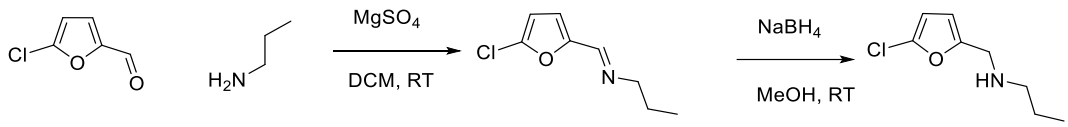

The reaction vessel was charged with $MgSO_4$ (2.5 g). The flask was evacuated and flushed with N_2 three times. Propylamine (495 mg, 8.4 mmol, 0.69 mL) and dry DCM (15 mL) were added via the septum. The resulting suspension was cooled to 0 ^oC on ice and stirred for 1 hour under nitrogen. 5-Chloro-2-furaldehyde (1 g, 7.7 mmol) was dissolved in dry DCM (6 mL) and added via a septum. The solution was stirred on ice for a further 30 minutes, returned to room temperature and stirred overnight. $MgSO_4$ was removed by filtration and the solvent removed under reduced pressure. To yield a yellow oil.

The resulting oil was dissolved in dry MeOH (30 mL). The solution was chilled on ice with vigorous stirring, and $NaBH_4$ (195 g, 5.2 mmol) was added slowly. The solution was stirred on ice for a further 30 minutes, then returned to room temperature, and stirred under nitrogen overnight. The reaction mixture was quenched with water (100 mL), extracted with diethyl ether (3 x 60 mL) and washed with water (50 mL). The crude amine was purified by column chromatography (hexane:ethylacetate). Yield = 76% (5.6 mmol). Synthesis was conducted following literature procedure and observed characterisation was in agreement with literature value.[1]

^{1}H NMR (500 MHz, Chloroform-d) δ 6.19 – 6.14 (m, 1H), 6.06 (d, J = 3.2 Hz, 1H), 3.72 (s, 2H), 2.60 – 2.53 (m, 1H), 1.87 (s, 1H), 1.58 – 1.45 (m, 1H), 1.19 (t, J = 7.4 Hz, 0H), 0.91 (td, J = 7.4, 0.9 Hz, 3H).

^{13}C NMR (126 MHz, CDCl3) δ 153.56, 135.25, 109.34, 106.61, 50.83, 46.09, 22.95, 11.70.

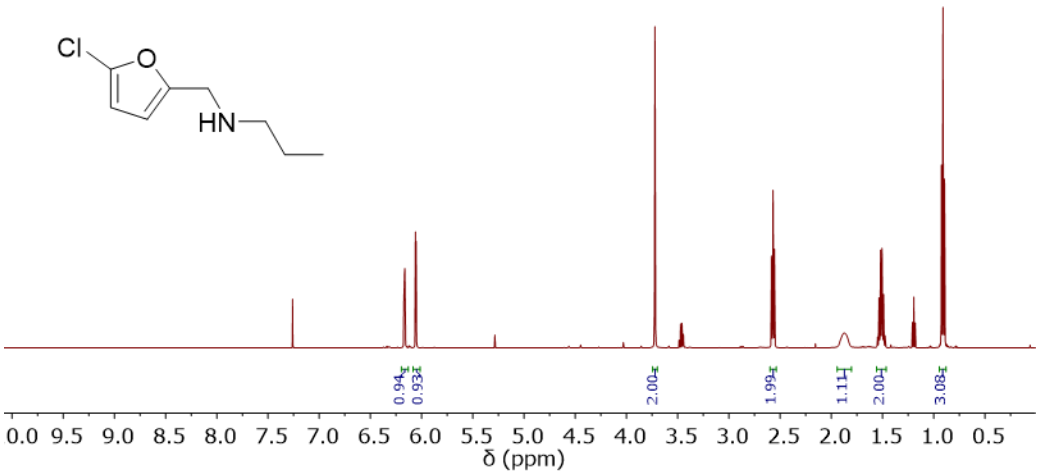

Figure 5.29: ^{1}H NMR spectrum of compound **9**

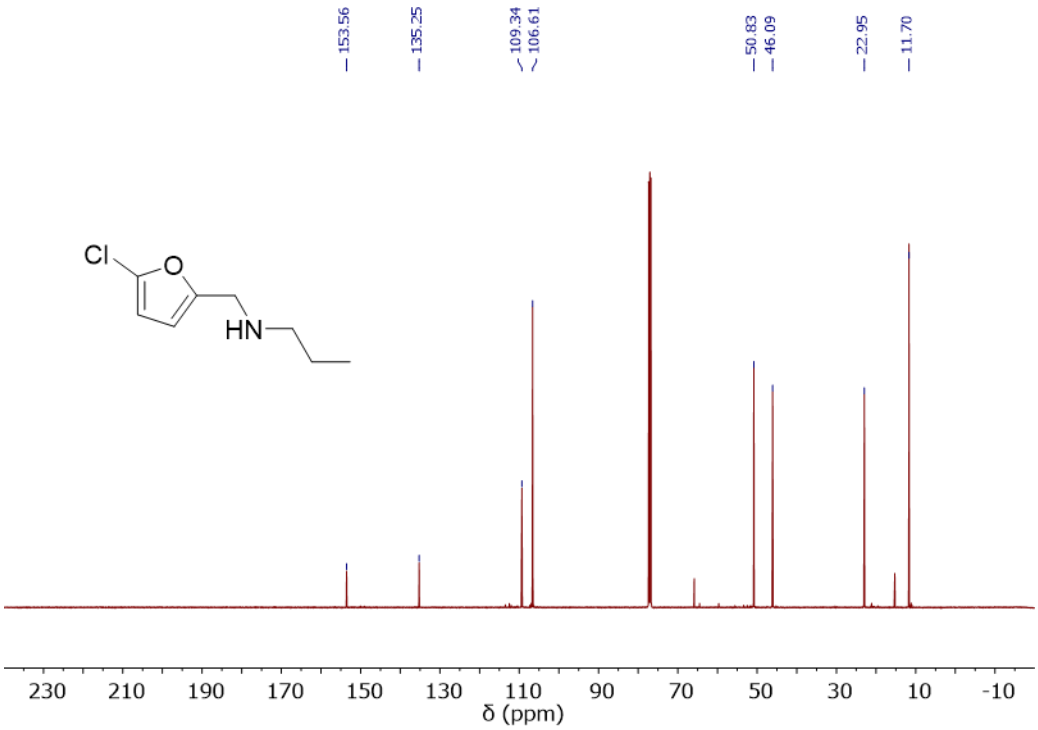

Figure 5.30: 13C NMR spectrum of compound 9

Synthesis of Compound 12

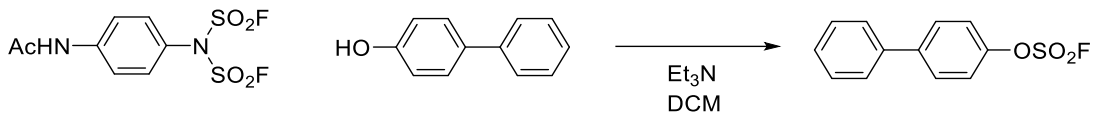

4-(Acetylamino)phenyl]imidodisulfuryl difluoride (AISF) (0.100 g, 0.314 mmol, 1.1 eq) and 4-phenyl phenol (0.048 g, 0.282 mmol, 1 eq.) were dissolved in dichloromethane (DCM) (5 mL). Triethylamine (0.063 g, 0.628 mmol, 2 eq.) in DCM (5 mL) was added dropwise to the solution. The solution was stirred continuously overnight at room temperature. The reaction mixture was concentrated under reduced pressure yielding a waxy solid. This was resuspended in a minimal volume of DCM, spiked with methanol and purified by column chromatography (10:1, hexane:ethyl acetate). Yield = 74% (0.21 mmol). Synthetic procedure was adapted from literature and observed characterisation was in agreement with literature value.[2-3]

^{1}H NMR (600 MHz, DMSO-d_6) δ 7.92 – 7.83 (m, 2H), 7.74 – 7.67 (m, 4H), 7.54 – 7.48 (m, 2H), 7.46 – 7.41 (m, 1H).

^{19}F NMR (471 MHz, Chloroform-d) δ 37.65 (s).

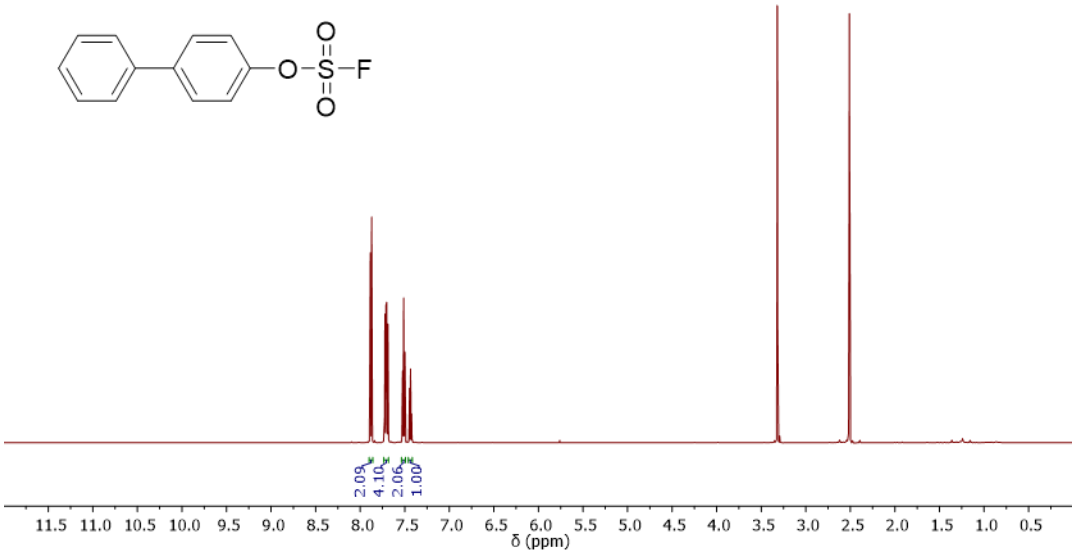

Figure 5.31: ^{1}H NMR (600 MHz, DMSO)

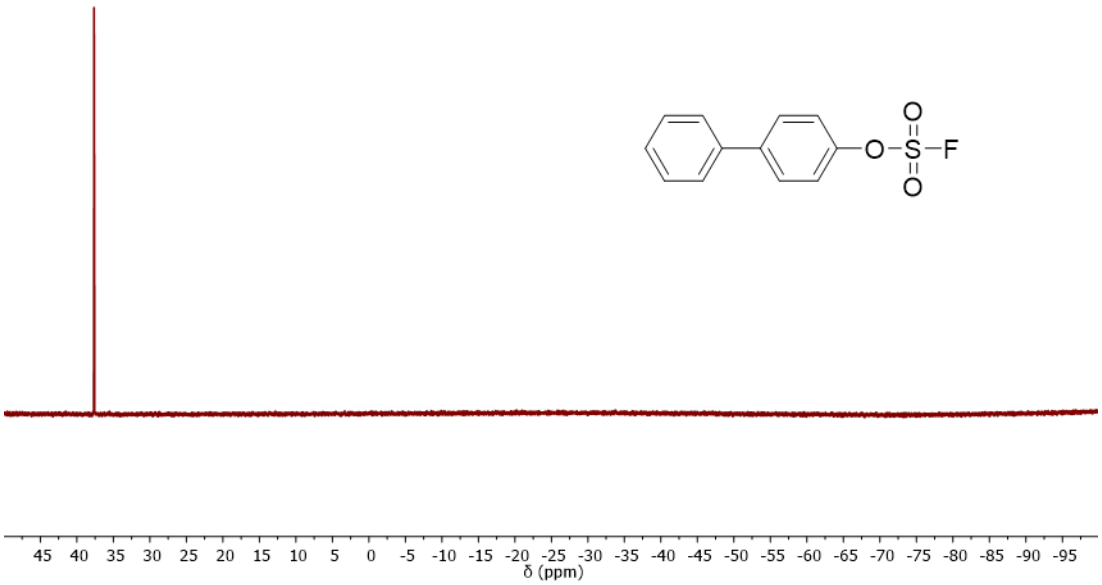

Figure 5.32 F NMR (471 MHz, CCl_4)

Synthesis of compound 30 via compound 29

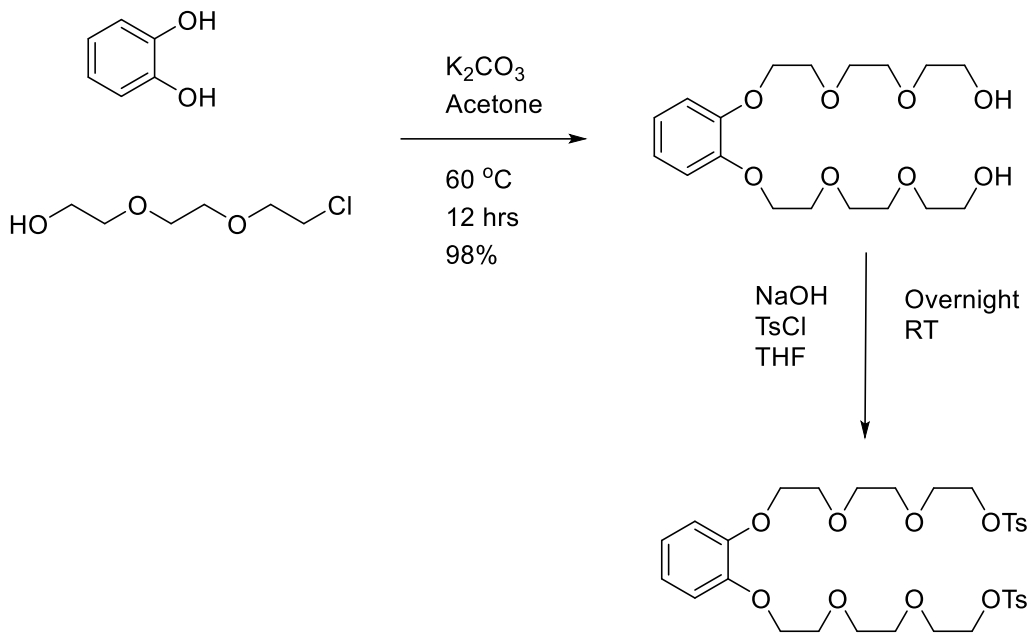

1,2-dihydroxybenzene (200 mg, 1.82 mmol), 2-[2-(2-chloroethoxy)ethoxy]ethanol (0.47 mL, 3.36 mmol) and potassium carbonate (1.00 g, 7.28 mmol) were mixed in acetone (40 mL). The mixture was heated under reflux at 60 °C overnight. The reaction mixture was cooled to RT and excess solid was removed under suction filtration. The filtrate was concentrated under reduced pressure to yield a reddish brown oil (0.6746 g, 1.8 mmol). Crude NMR showed that the synthesis was successful; however starting material was still present. Crude product was carried forward without purification as per the literature prep.[4] 2-[2-[2-[2-[2-[2-(2-hydroxyethoxy)ethoxy]ethoxy]phenoxy]ethoxy]ethoxy]ethanol (0.6746 g, 1.8 mol) was dissolved in NaCl solution (0.85 M, 20 mL). Tosyl chloride (0.641 g, 3.36 mmol) was dissolved in THF (10 mL) and added dropwise to the mixture with stirring. The reaction was stirred at room temperature overnight. THF was removed under reduced pressure and the aqueous layer was extracted using DCM (2 x 150 mL). The combined organic extracted were washed with water and dried over magnesium sulfate. The filtrate was concentrated under reduced pressure to yield a pale yellow oil. The oil was purified by column

chromatography (Hexane:ethyl acetate/1:3) to yield product (0.126 g, 0.185 mmol, 10 %). Characterisation was consistent with literature preparation.[5]

1H NMR (500 MHz, $CDCl_3$) δ 7.82 – 7.80 (m, 4H), 7.36 – 7.33 (m, 4H), 6.93 (s, 4H), 4.19 – 4.15 (m, 8H), 3.87 – 3.82 (m, 4H), 3.73 – 3.67 (m, 8H), 3.64 – 3.60 (m, 4H), 2.45 (s, 6H).

^{13}C NMR (126 MHz, $CDCl_3$) δ 148.97, 144.78, 133.02, 129.82, 127.97, 121.68, 114.91, 70.82, 70.76, 69.84, 69.27, 68.84, 68.72, 21.63.

Synthesis of compound 31

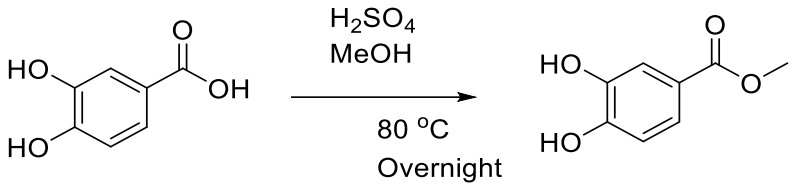

3,4-dihydroxubenzoic acid (0.5 g, 0.003 mol) was dissolved in methanol (50 mL). H_2S0_4 (2 M, 1 mL) was added dropwise to the solution. The reaction mixture was heated under reflux (80 ^oC) overnight. The mixture was quenched by adding water (10 mL) and the excess solvent was removed under reduced pressure. The product was dissolvent in DCM (150 mL) and washed brine (150 mL) and water (150 mL). The organic layer was dried over magnesium sulfate. The filtrate was concentrated under reduced pressure to yield product (0.1662 g, 33%).

^{1}H NMR: (500 MHz, DMSO) δ = 9.66 (s, 1H), 9.43 (s, 1H), 7.37 – 7.33 (m, 1H), 7.31 (dd, *J* = 8.3, 2.1 Hz, 1H), 6.80 (d, *J* = 8.2 Hz, 1H), 3.76 (s, 3H).

Synthesis of compound 31

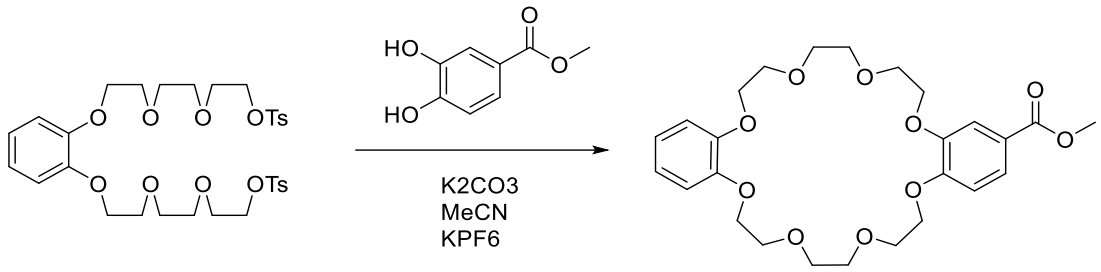

1,2-bis[2-[2-(2-tosylethoxy)ethoxy]ethoxy]benzene (0.1 g, 0.146 mmol), methyl-3,5-dihydroxybenzoate (0.0246 g, 0.146 mmol) and KPF_6 (0.0322 g, 0.175 mmol) were dissolved in acetonitrile (50 mL). The solution was degassed with nitrogen and the vessel wrapped in foil to exclude light. Potassium carbonate (0.081 g, 0.548 mmol) was added. The reaction mixture was heated under reflux (80 ^{o}C) under nitrogen for three days. The solution was filtered to remove excess solid and the filtrate concentrated under reduced pressure. The resulting solid was dissolved in ethyl acetate and passed through a pad of silica to removed inorganic ions. The filtrate was concentred under reduced pressure to yield the product, a waxy oil. Further purification was not carried out as the product was carried forward to the next step. Characterisation was consistent with literature preparation.[5]

^{1}H NMR (500 MHz, $CDCl_3$): δ = 7.64 (d, *J* = 8.4 Hz, 1H), 7.52 (s, 1H), 6.91 – 6.86 (m, 4H), 6.84 (s, 1H), 4.21 – 4.18 (m, 4H), 4.17 – 4.13 (m, 4H), 3.95 – 3.90 (m, 8H), 3.88 (s, 3H), 3.83 (d, *J* = 3.0 Hz, 8H).

Synthesis of 2-carboxy-dibenzo-24-crown-8 (compound **33**)

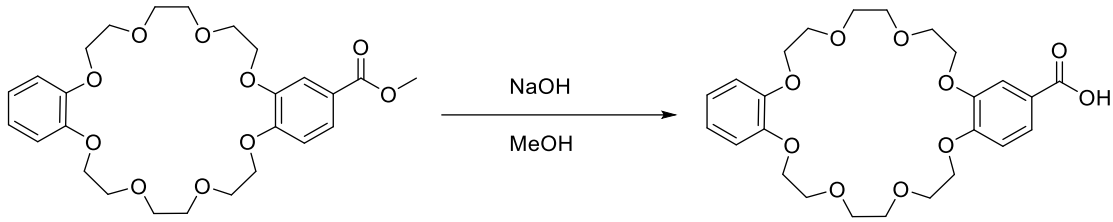

2-carboyl-dibenzo-24-crown-8 (0.056 g, 0.11 mmol) was dissolved in methanol (50 mL). Sodium hydroxide solution (2 M, 5 mL) was added dropwise and the reaction was heated under reflux for 4 hours. The reaction mixture was quenched with water (10 mL) and HCl (2M, 6 mL) was added until the mixture was acidic. The product was extracted into DCM (3 x 100 mL). The organic extracts were dried over magnesium sulfate and condensed under reduced pressure. The product was recrystallised from ethanol. Yield = 94% (0.1 mmol). Characterisation was consistent with the loss of the ester methyl peak from literature prep.[5]

^{1}H NMR (500 MHz, $CDCl_3$) δ = 7.70 (d, *J* = 8.3 Hz, 1H), δ = 7.56 (s, 1H), δ = 6.93 – 6.80 (m, 5H), δ = 4.20 (q, *J* = 4.5 Hz, 4H), δ = 4.17 – 4.13 (m, 4H), δ = 3.96 – 3.90 (m, 8H), δ = 3.83 (d, *J* = 4.1 Hz, 8H).

Mass Spec (ESI, positive ionisation): Peak expected 515.1888 – $[M+Na]^+$. Peak observed 515.1882

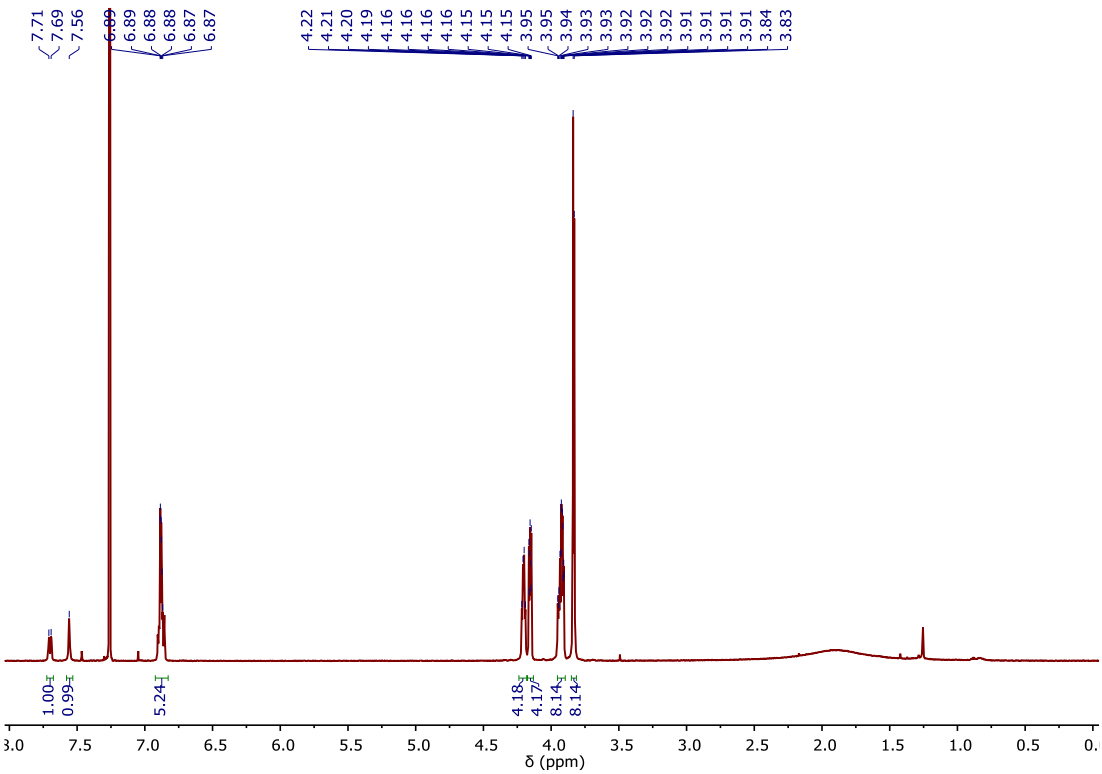
7.71
7.69
7.56
6.89
6.89
6.88
6.88
6.87
6.87
4.22
4.21
4.20
4.19
4.16
4.16
4.16
4.16
4.15
4.15
4.15
3.95
3.95
3.94
3.93
3.93
3.92
3.92
3.92
3.91
3.91
3.91
3.91
3.84
3.83
1.00
0.99
5.24
4.18
4.17
8.14
8.14
δ (ppm)

5.8 References

1. Jayasinghe, L.; Miles, G.; Bayley, H., Role of the Amino Latch of Staphylococcal α-Hemolysin in Pore Formation. *J. Biol. Chem.* **2006,** *281* (4), 2195-2204.

2. Palma, A.; Artelsmair, M.; Wu, G.; Lu, X.; Barrow, S. J.; Uddin, N.; Rosta, E.; Masson, E.; Scherman, O. A., Cucurbit[7]uril as a Supramolecular Artificial Enzyme for Diels–Alder Reactions. *Angew. Chem.* **2017,** *129* (49), 15894-15898.

Appendix A

Cucurbituril catalysis at the single molecule level

Contributions: work in this chapter has been completed in collaboration with Prof. Alberto Credi, University of Bologna and Prof. Nicolas Giuseppone, University of Strasbourg and Prof Ivan Aprahamian, Dartmouth College. Reagents were supplied for each collaborator as specified in the text. Unless otherwise stated, all experimental work discussed was completed by Dominic Cairns-Gibson.

Variable applied voltage with CB[7] in the pore

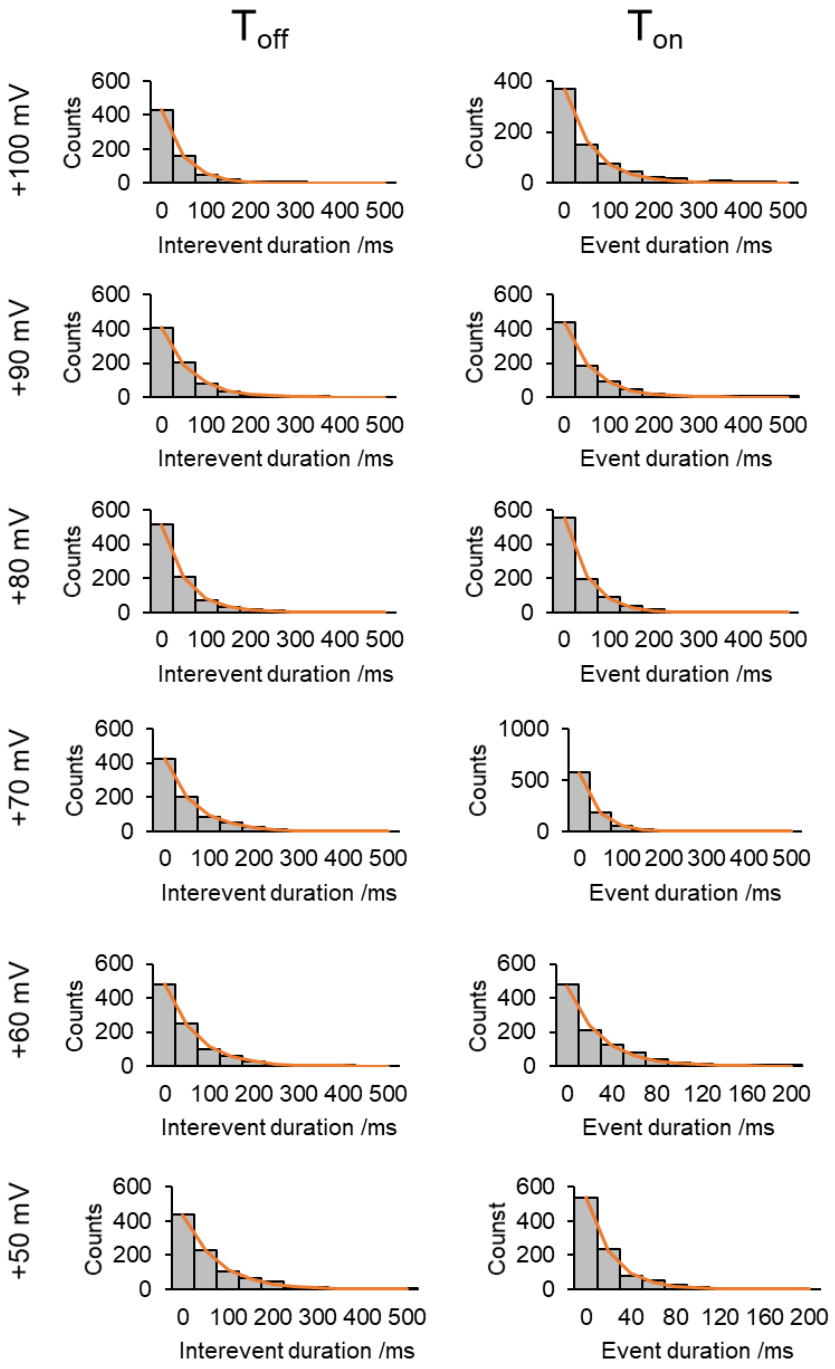

Figure A.1: Level frequency histograms of the binging events of CB[7] upon varying the voltage in 1 M KCl. CB[7] (10 µL of 10 mM stock) was added to the *trans* well. Levels were detected using threshold detection in Clampfit 10.7. 200 s of data was analysed for each applied voltage.

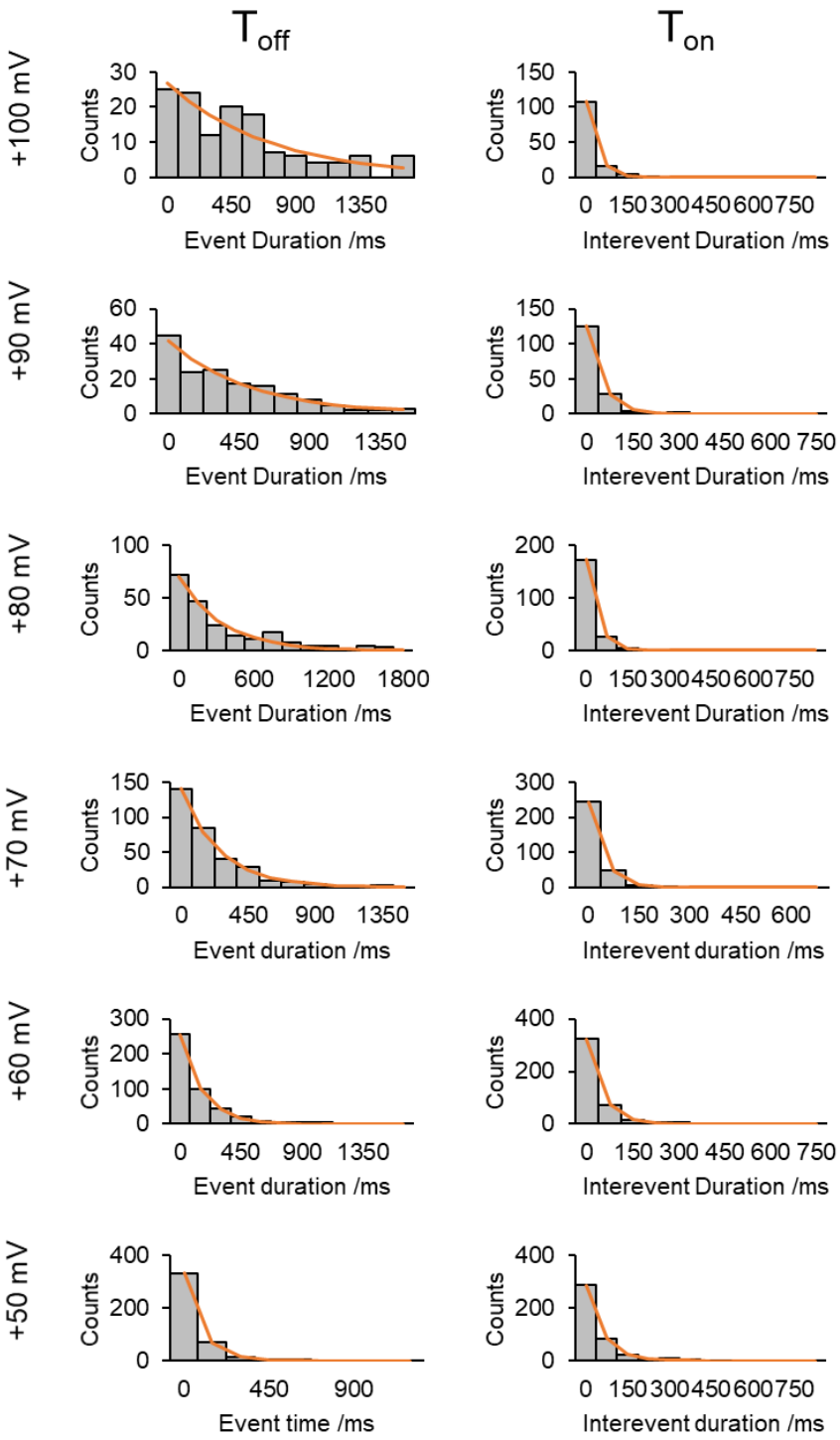

Figure A.2: Level frequency histograms of the binging events of CB[7] upon varying the voltage in 2 M KCl. CB[7] (10 µL of 10 mM stock) was added to the *trans* well. Levels were detected using threshold detection in Clampfit 10.7. 200 s of data was analysed for each applied voltage.

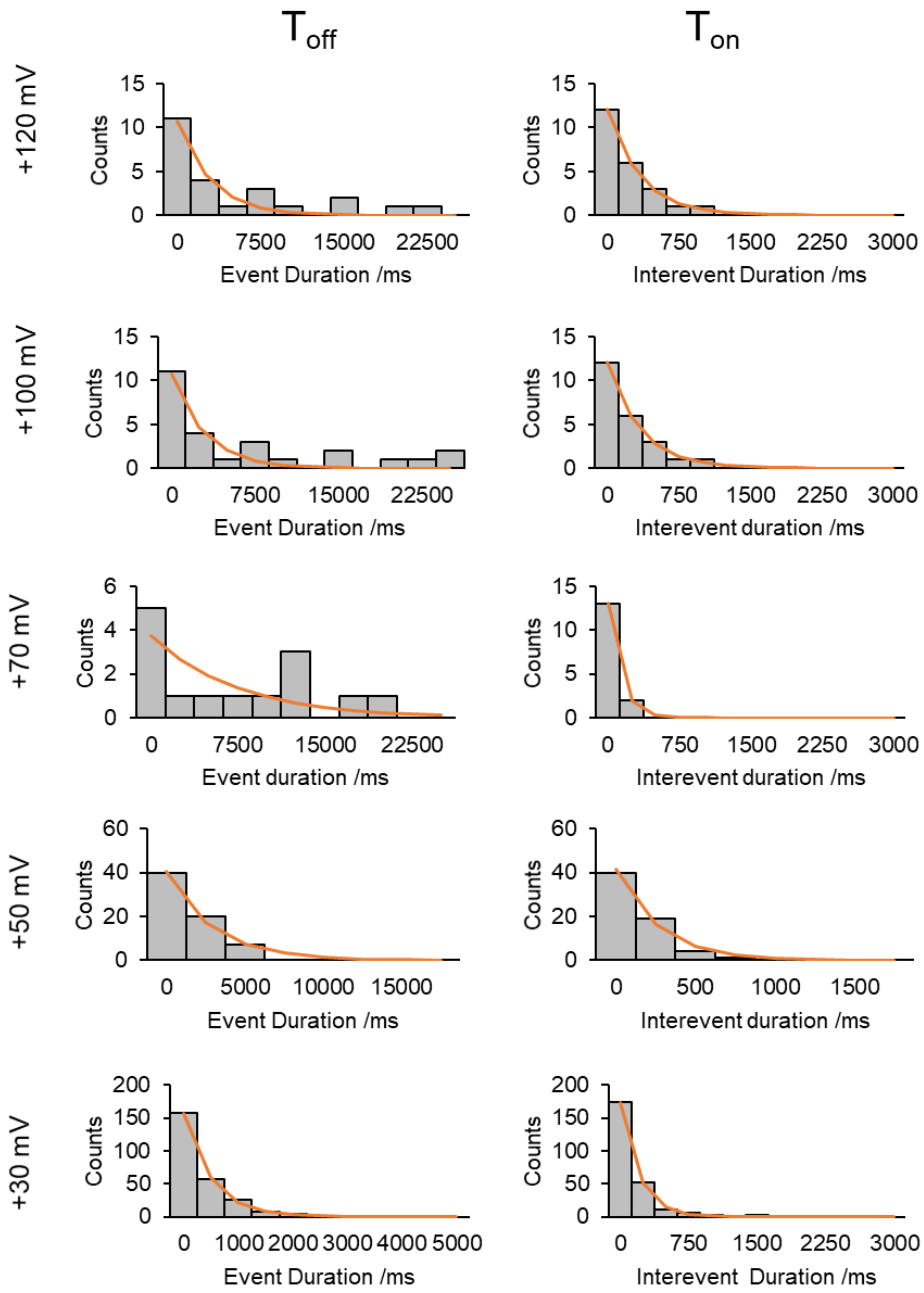

Figure A.3: Level frequency histograms of the binging events of CB[7] upon varying the voltage in 3 M KCl. CB[7] (10 µL of 10 mM stock) was added to the *trans* well. Levels were detected using threshold detection in Clampfit 10.7. 200 s of data was analysed for each applied voltage. Note that above +50 mV very few events were observed in this time frame leading

Concentration titration of CB[7]

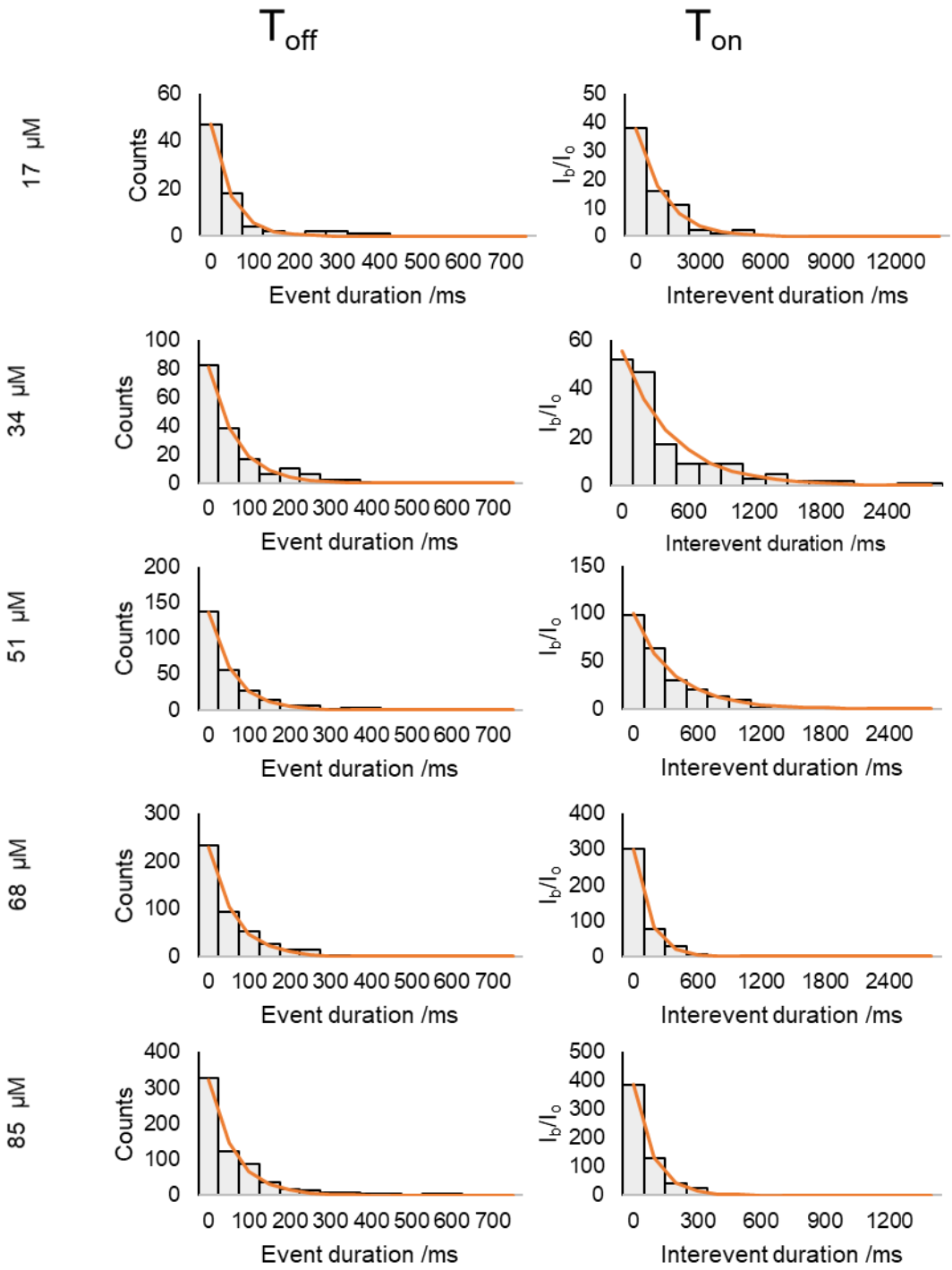

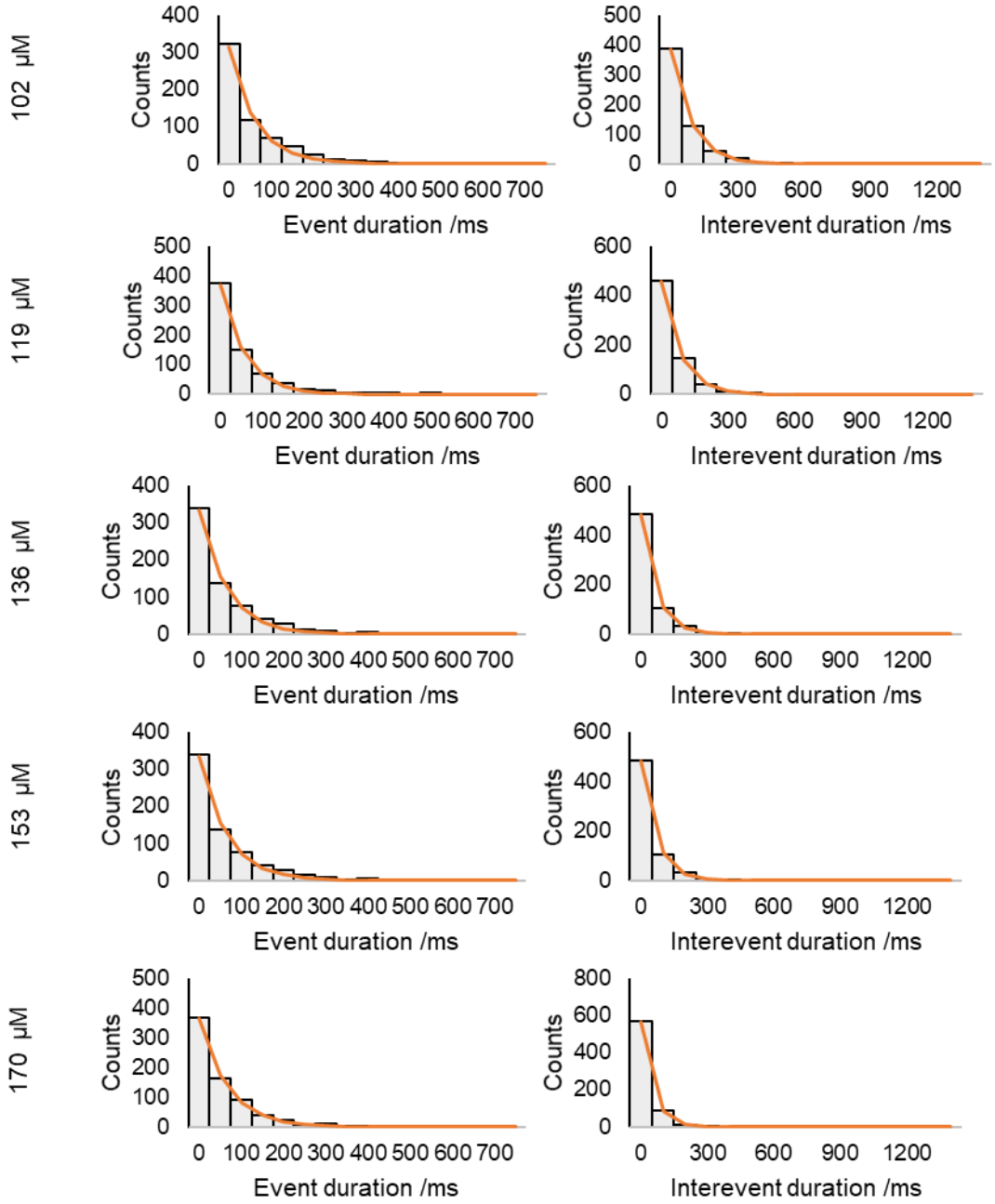

Figure A.4: Level frequency histograms for the concentration titration of CB[7] 1 M KCl buffer. A solution of CB[7] (10 mM) was prepared in KCl buffer. Using serial dilution, the concentration was reduced and an aliquot was added to give the desired final concentration. 1 M KCl, 30 mM K_2HPO_4, pH 8. Voltage +150 mV. Levels were detected using threshold detection in Clampfit 10.7. 200 s of data was analysed for each applied voltage.

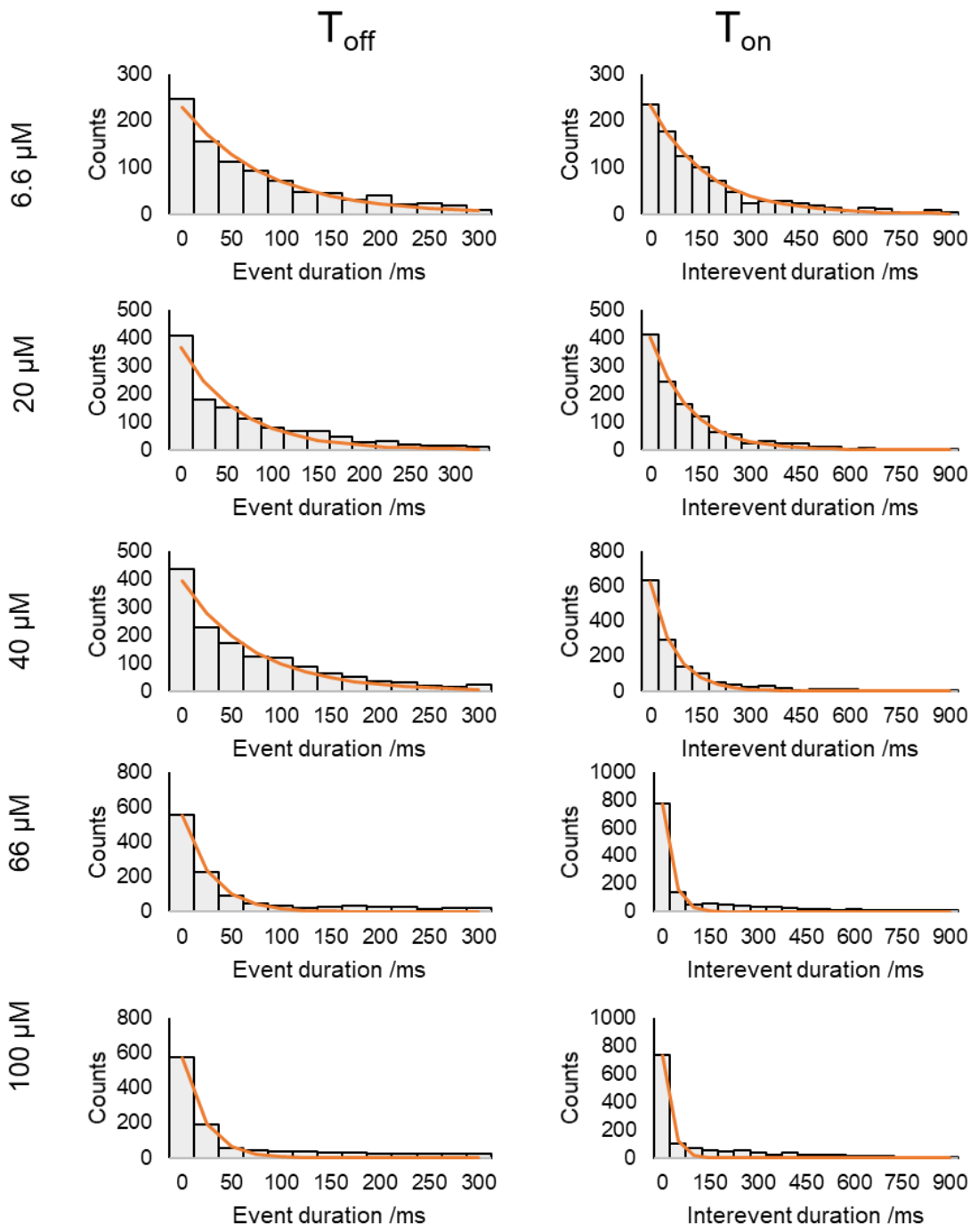

Figure A.5: Level frequency histograms for the concentration titration of CB[7] 2 M KCl buffer. A solution of CB[7] (10 mM) was prepared in KCl buffer. Using serial dilution, the concentration was reduced and an aliquot was added to give the desired final concentration. 1 M KCl, 30 mM K_2HPO_4, pH 8. Voltage +150 mV. Levels were detected using threshold detection in Clampfit 10.7. 200 s of data was analysed for each applied voltage.

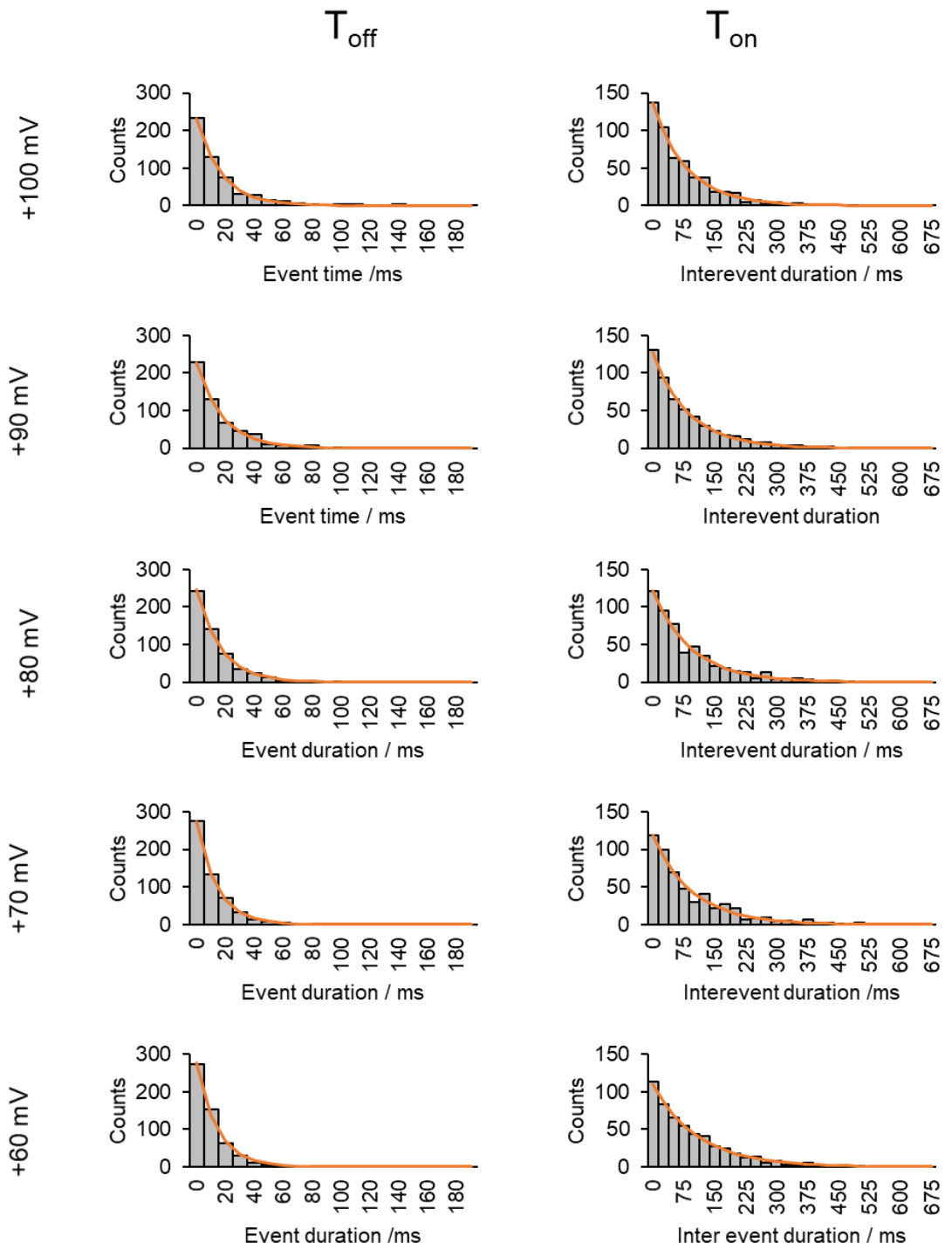
T off
T on
+100 mV
+90 mV
+80 mV
+70 mV
+60 mV
Counts
Event time /ms
Interevent duration / ms
Event time / ms
Interevent duration
Event duration / ms
Interevent duration / ms
Event duration / ms
Interevent duration /ms
Event duration /ms
Inter event duration / ms

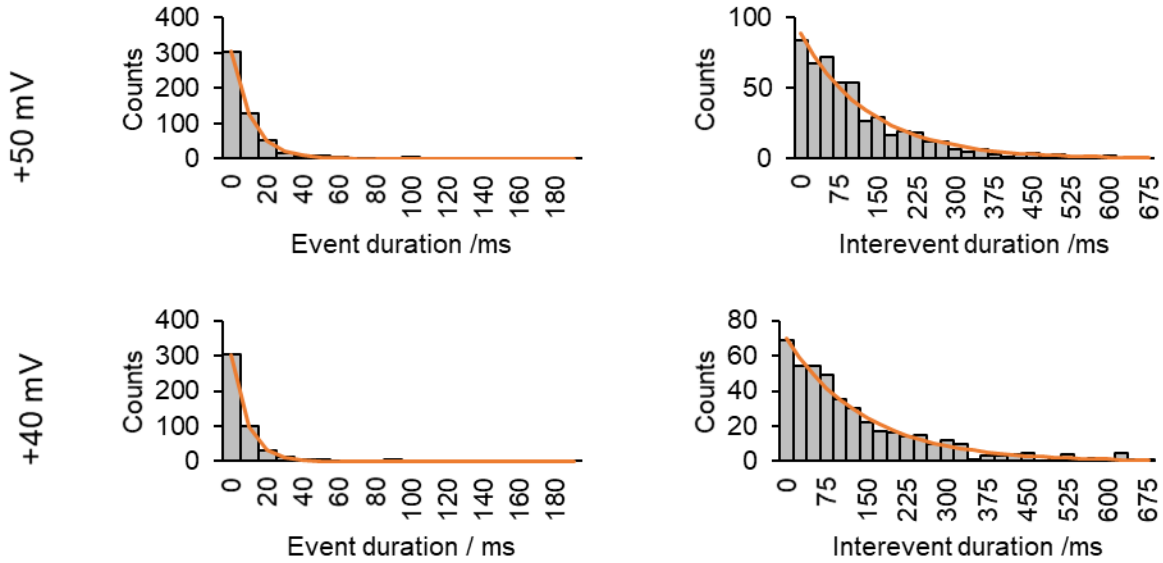

Figure A.6: Level frequency histograms of the binding events of CB[7] upon varying the voltage in 1 M CsCl. CB[7] (10 µL of 10 mM stock) was added to the *trans* well. Levels were detected using threshold detection in Clampfit 10.7. 200 s of data was analysed for each applied voltage.

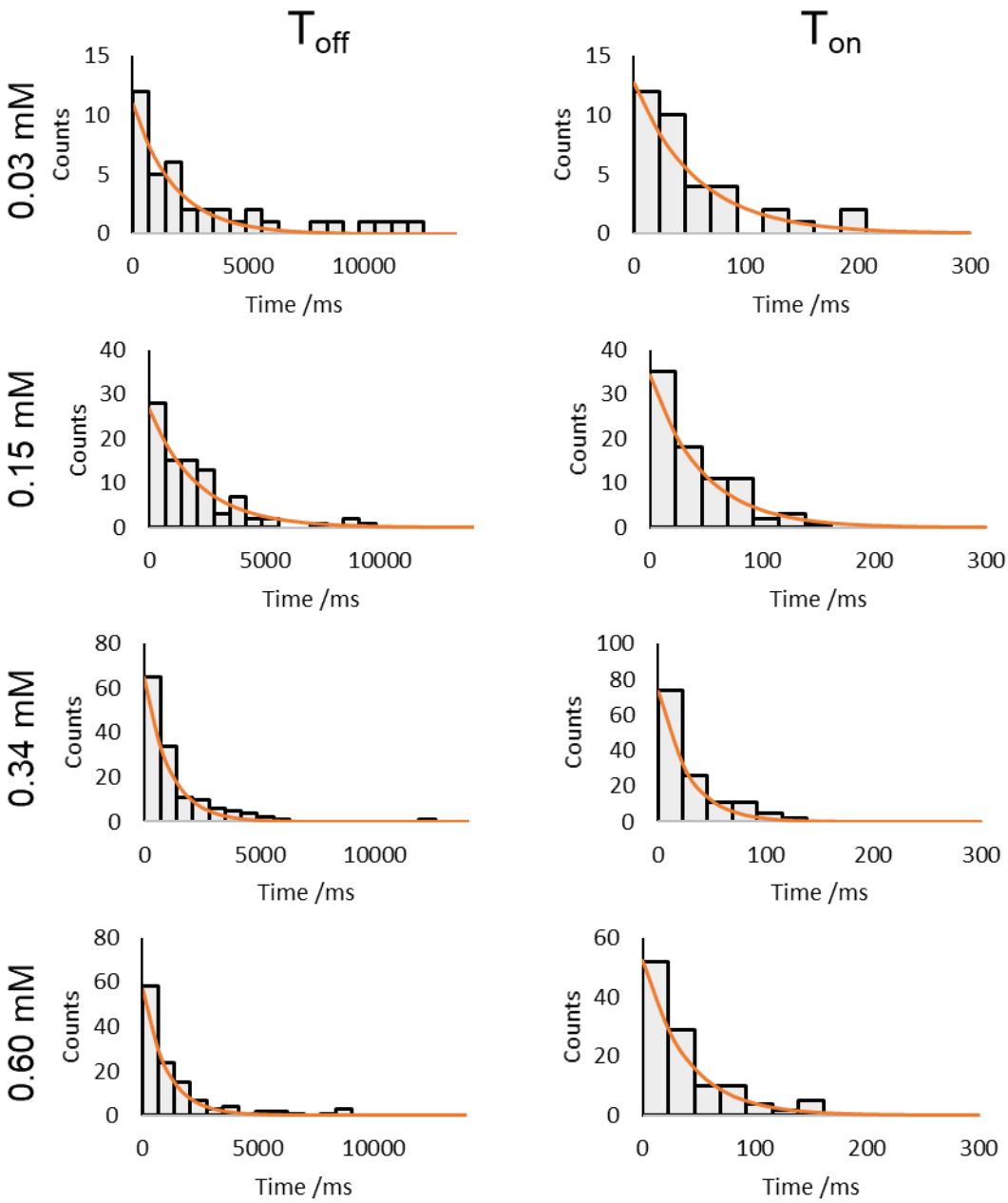
T off
T on
0.03 mM
0.15 mM
0.34 mM
0.60 mM
Counts
Time /ms
0
5000
10000
100
200
300

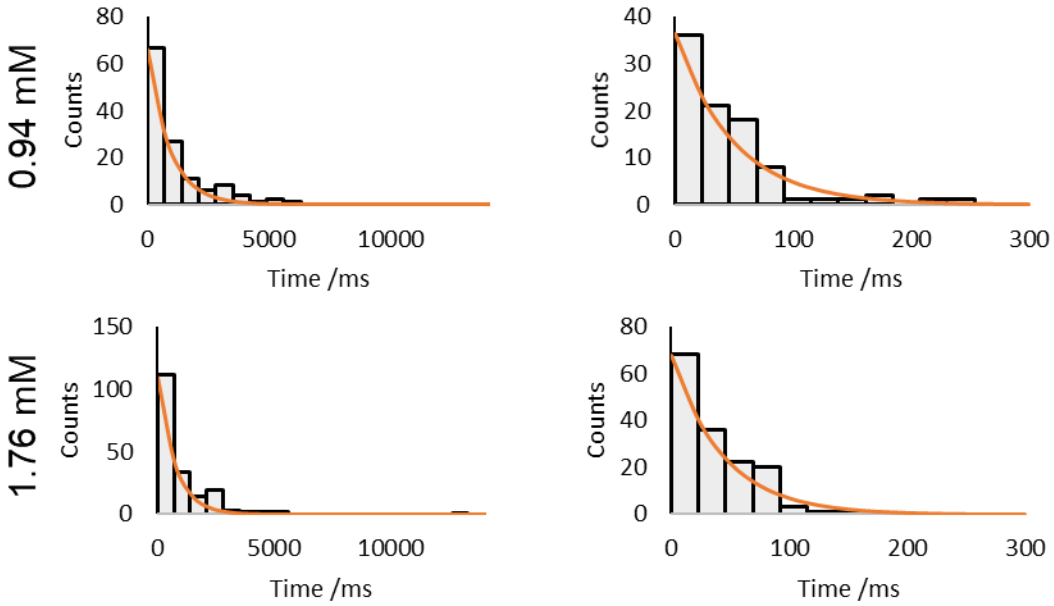

Figure A.7: Level frequency histograms of the binding events upon varying the concentration of ammonia (0.03 mM to 1.76 mM). CB[7] (10 µL of 10 mM stock) was added to the *trans* well. Ammonium hydroxide (33%) was diluted and added to the *trans* well to give the desired concentration. Levels were detected using threshold detection in Clampfit 10.7. 200 s of data was analysed for each applied voltage. Voltage +100 mV. 3 M KCl, 30 mM K_2HPO_4, pH 8.

Single molecule Diels-Alder observation

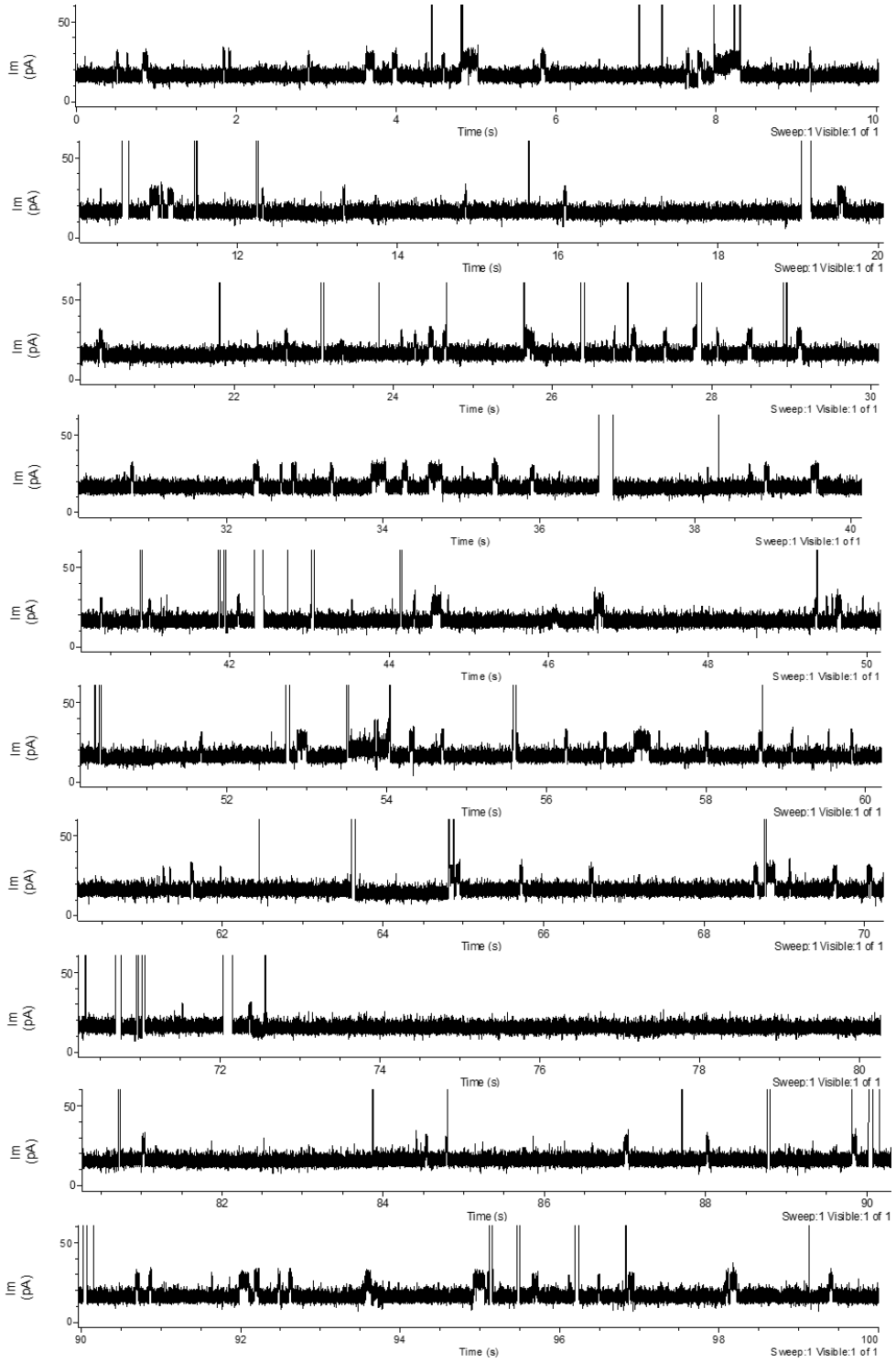

Figure A.8: Current trace of CB[7] (10 µL of 10 MM stock) in the pore. 2 M KCl, 30 mM K_2HPO_4, pH 8. Voltage +150 mV.

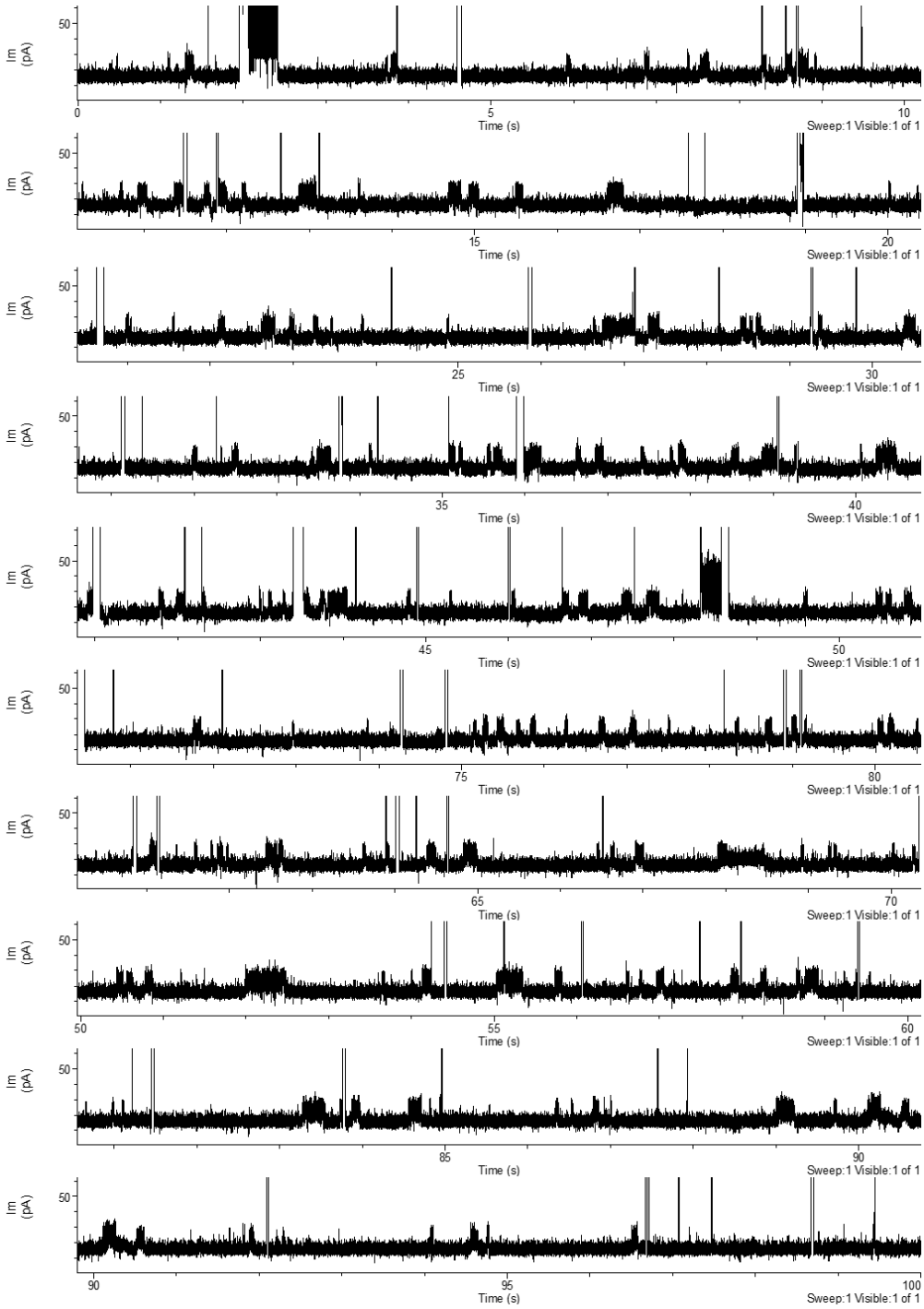

Figure A.9 Current trace of CB[7] (10 µL of 10 MM stock) in the pore in the presence of **compound 7** (10 µL of 10 MM stock). 2 M KCl, 30 mM K_2HPO_4, pH 8. Voltage +150 mV.

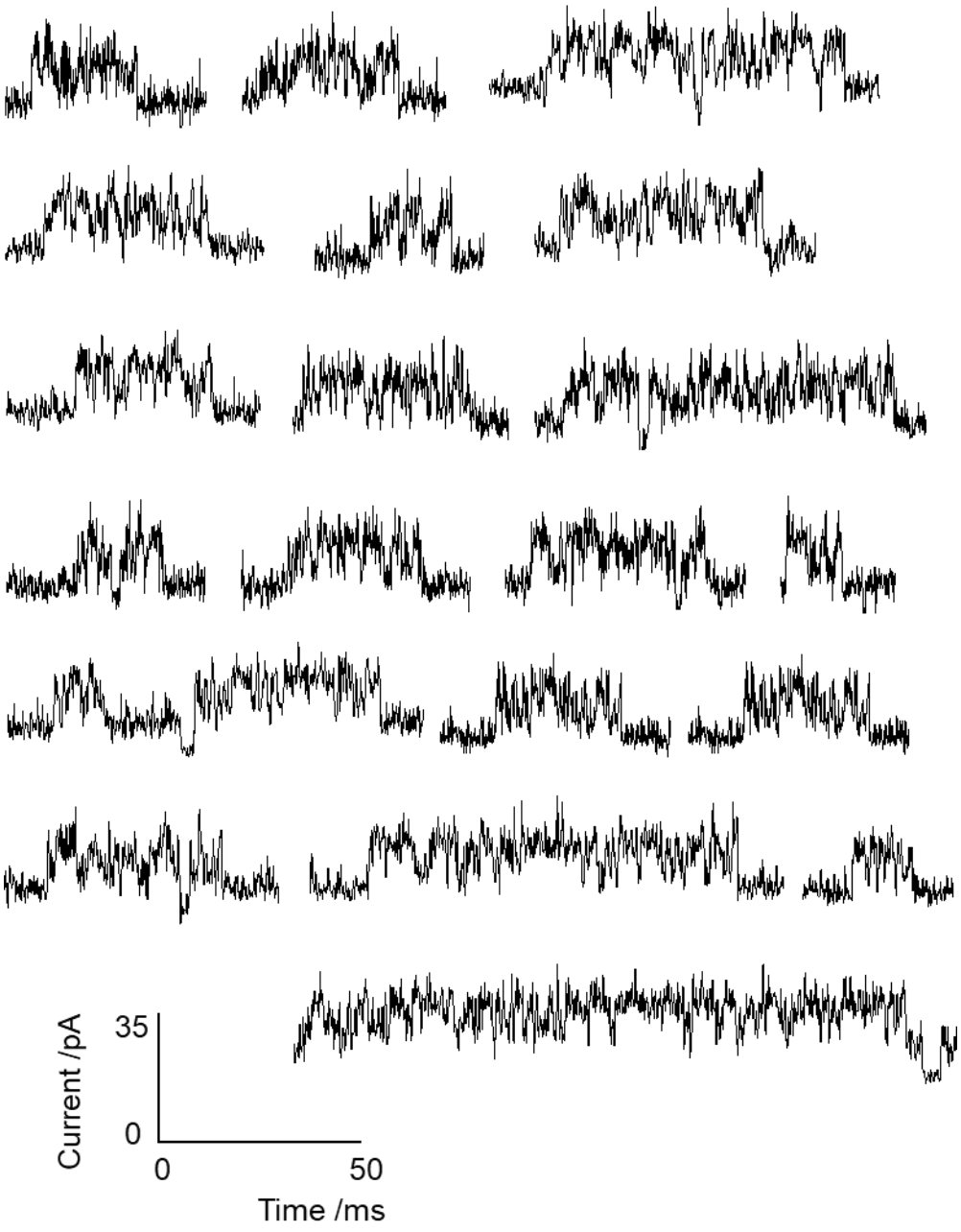

Figure A.10: Events observed upon the addition of CB[7] (10 mM) and compound **7** (10 mM) to the *trans* well of an α-HL nanopore. Scale bar for the axis is shown in the bottom left. Buffer 1 M KCl, 30 mM K2HPO4, pH 8. Voltage +100 mV. Lowpass Bessel filter 100 Hz and output gain x20.

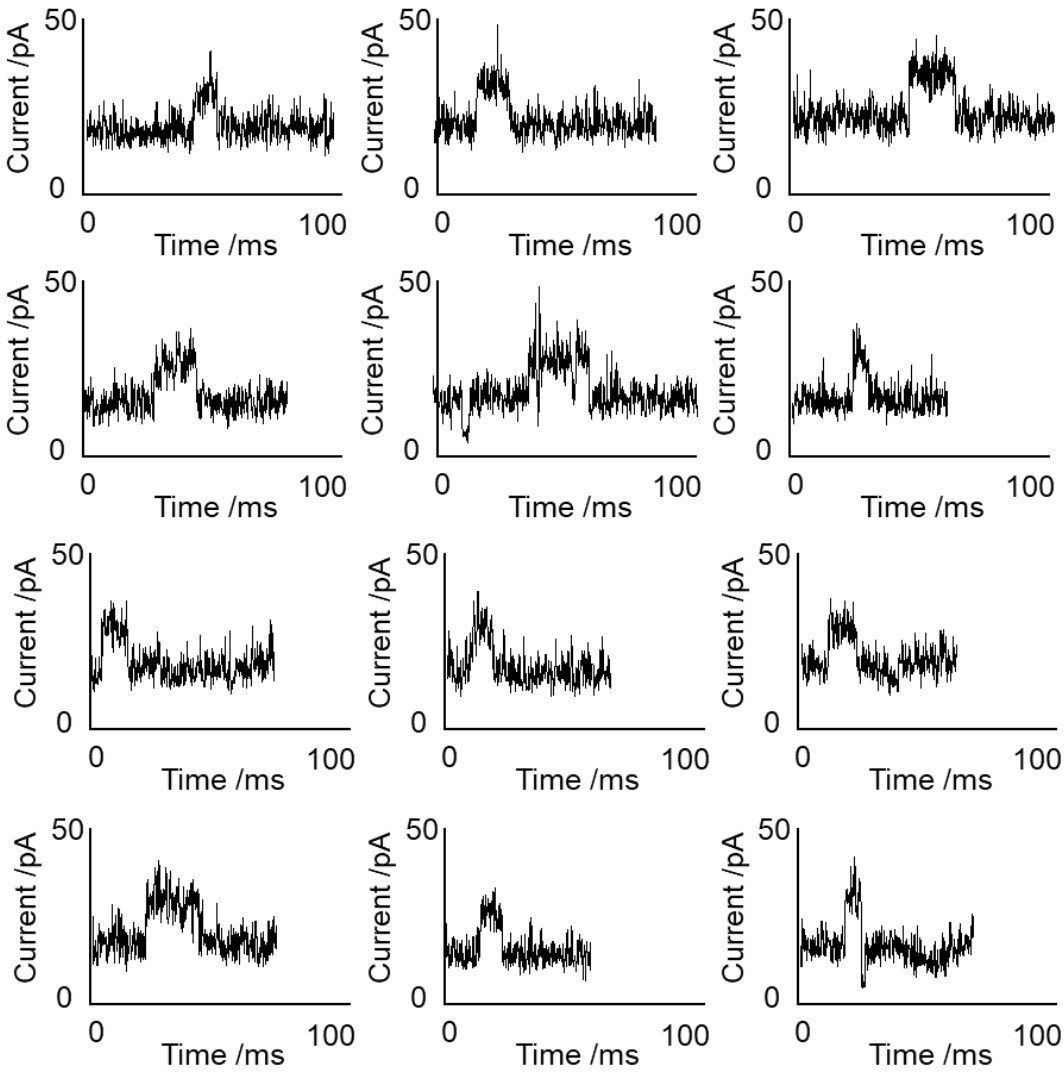

Figure A.11: Events observed upon the addition of CB[7] (10 mM) and compound **8** (10 mM) to the *trans* well of an α-HL nanopore. Buffer 1 M KCl, 30 mM K2HPO4, pH 8. Voltage +100 mV. Lowpass Bessel filter 100 Hz and output gain x20.

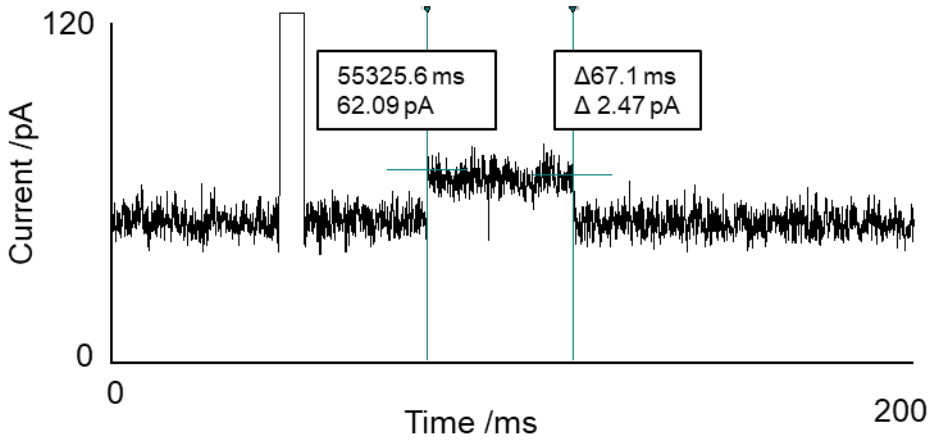

Figure A.12: Example of the positioning of cursors for all points histogram analysis of the upwards events

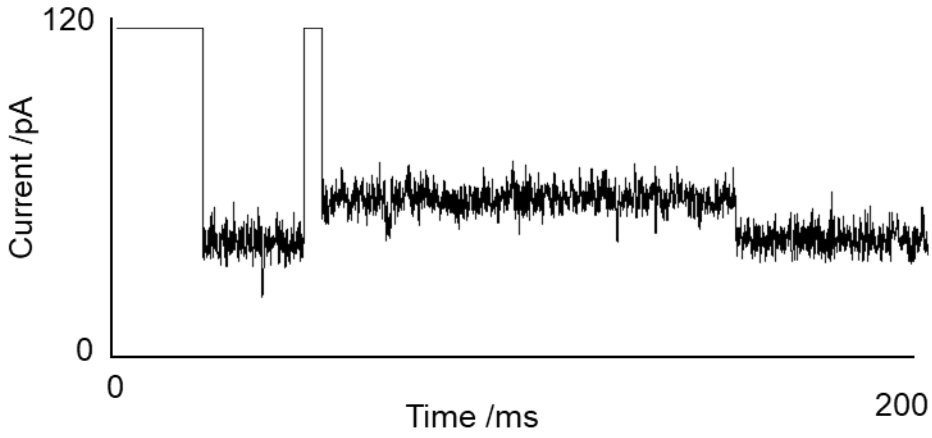

Figure A.13: Example of the excluded events for all points histogram analysis.

Appendix B

α-Hemolysin as a Framework for Transmembrane Molecular Machines

Observations of motors

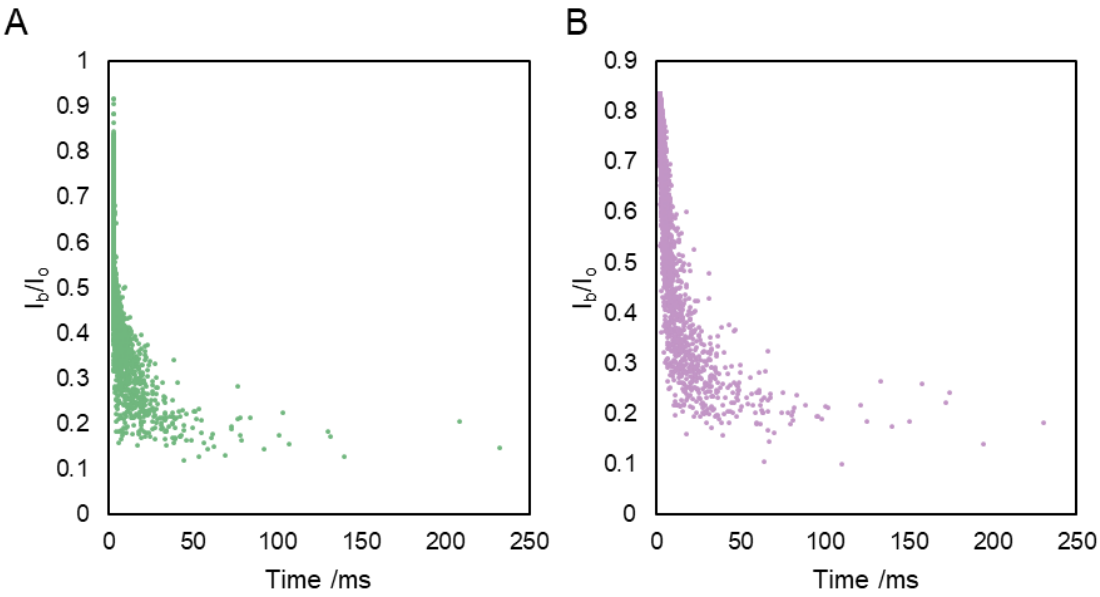

Figure B.1 A) Plot of the event duration against the I_b/I_o for the first attached level for compound **23** B) Plot of the event duration against the I_b/I_o for the second attached level for the bis-alkyne motor. Applied potential +100 mV. Volume 600 µL. Buffer 1 M KCl, 30 mM K_2HPO_4, pH 8. Voltage +100 mV. Lowpass Bessel filter 100 Hz and output gain x50.

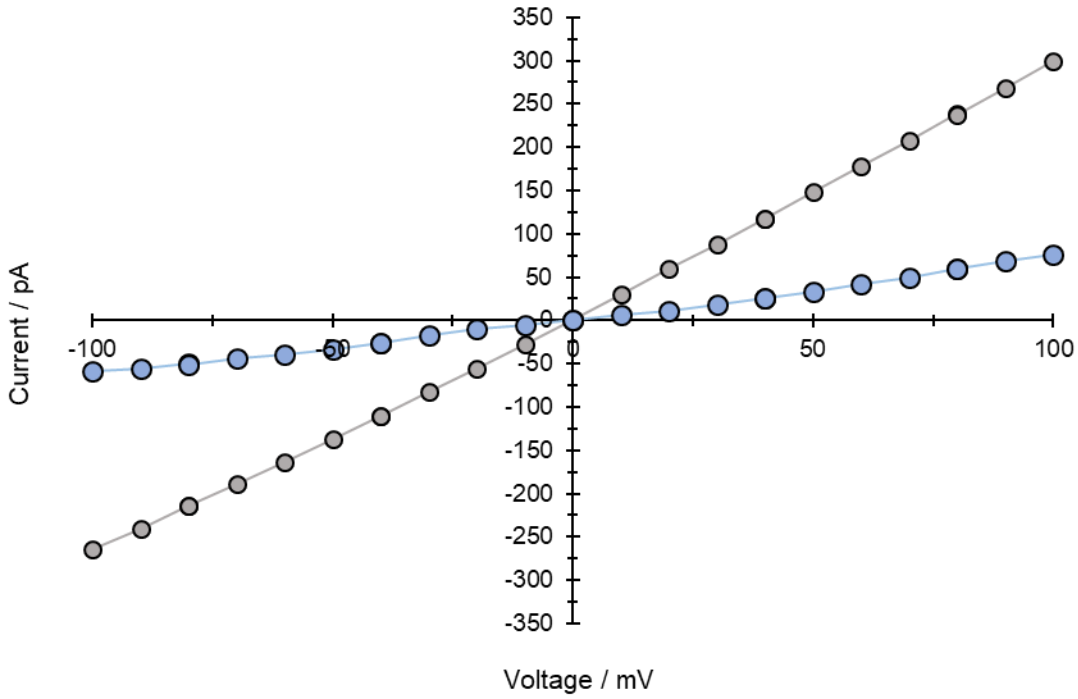

Figure B.2: Characterisation trace for the attachment of compound **23** in 3M KCl buffer.

References

1. Palma, A.; Artelsmair, M.; Wu, G.; Lu, X.; Barrow, S. J.; Uddin, N.; Rosta, E.; Masson, E.; Scherman, O. A., Cucurbit[7]uril as a Supramolecular Artificial Enzyme for Diels–Alder Reactions. *Angew. Chem.* **2017,** *129* (49), 15894-15898.

2. Domino, K.; Veryser, C.; Wahlqvist, B. A.; Gaardbo, C.; Neumann, K. T.; Daasbjerg, K.; De Borggraeve, W. M.; Skrydstrup, T., Direct Access to Aryl Bis(trifluoromethyl)carbinols from Aryl Bromides or Fluorosulfates: Palladium-Catalyzed Carbonylation. *Angew. Chem. Int. Ed.* **2018,** *57* (23), 6858-6862.

3. Chen, W.; Dong, J.; Plate, L.; Mortenson, D. E.; Brighty, G. J.; Li, S.; Liu, Y.; Galmozzi, A.; Lee, P. S.; Hulce, J. J.; Cravatt, B. F.; Saez, E.; Powers, E. T.; Wilson, I. A.; Sharpless, K. B.; Kelly, J. W., Arylfluorosulfates Inactivate Intracellular Lipid Binding Protein(s) through Chemoselective SuFEx Reaction with a Binding Site Tyr Residue. *J. Am. Chem. Soc.* **2016,** *138* (23), 7353-7364.

4. Zhao, Y.-L.; Liu, L.; Zhang, W.; Sue, C.-H.; Li, Q.; Miljanić, O. Š.; Yaghi, O. M.; Stoddart, J. F., Rigid-Strut-Containing Crown Ethers and [2]Catenanes for Incorporation into Metal–Organic Frameworks. *Chem. Eur. J.* **2009,** *15* (48), 13356-13380.

5. Wessels, H. R.; Gibson, H. W., Multi-gram syntheses of four crown ethers using K+ as templating agent. *Tetrahedron* **2016,** *72* (3), 396-399.